Georg Nußbaumer, BSc

In-situ block identification, assessment and visualisation for tunnelling using LiDAR and Block Theory – a case study of the Arzberg Raabstollen Adit, Austria

MASTER'S THESIS

to achieve the university degree of

Master of Science

Master's degree programme: Earth Sciences

submitted to

Graz University of Technology

Supervisor

Ao.Univ.-Prof. Dr. Qian LIU

Institute of Applied Geosciences

Graz, May 2016

AFFIDAVIT

I declare that I have authored this thesis independently, that I have not used other than the declared sources/resources, and that I have explicitly indicated all material which has been quoted either literally or by content from the sources used. The text document uploaded to TUGRAZonline is identical to the present master‘s thesis dissertation.

Date Signature

Abstract

Existing laser scan data for the Arzberg Raabstellen Adit were used for this master's thesis. The data were processed using the computer program RiSCAN PRO. Discontinuities were fitted into the relief model in order to create a fracture system model. The LiDAR 3D surface model provides in-situ geometrical parameters of discontinuities: position, orientation, size and spacing. Using Block Theory, potential key blocks are identified within the tunnel adit. These blocks are visualized in the 3-dimensional model. Using several DOS programs we were able to do volume calculations, failure mode analysis and further geometric visualisation of these removable blocks. This master's thesis shows a simplified method for identifying removable blocks by combining existing Block Theory and Terrestrial Laser Scan Data.

Zusammenfassung

Existierende Daten aus Laser-Scan-Untersuchungen des Arzberg Raabstollens wurden für diese Masterarbeit herangezogen. Die Daten wurden mit dem Computerprogramm RiSCAN PRO verarbeitet. Klüfte wurden in ein Reliefmodell ortsbezogen eingebaut und ein Kluftmodell wurde erstellt. Das 3D-LiDAR-Oberflächenmodell enthält ortsbezogene geometrische Parameter der Klüfte: Position, Orientierung, Größe und Abstand. Basierend auf Block Theory wurden potenziell instabile Blöcke im Tunnelbereich identifiziert und im 3-dimensionalen Modell visualisiert. Mit Hilfe von mehreren DOS Programmen war es möglich, Blockvolumen zu berechnen, Versagungsmodi zu analysieren und andere geometrische Visualisierungen der instabilen Blöcke herzustellen. Diese Masterarbeit zeigt eine vereinfachte Methode zur Identifizierung von instabilen Blöcken mit der Anwendung von Block Theory und terrestrischen Laserscandaten.

Acknowledgements

First and foremost I would like to thank Dr. Qian Liu for supervising this master’s thesis. I am grateful that you always took the time to answer my questions and helped me through any problems I had. I could not have asked for a better supervisor.

I would like to thank Dr. Dietmar Klammer and Anni Pendl who helped me countless times throughout my studies. Also, Peter Schreiber for all his computer support.

I would like to thank my family for their continuous support and patience.

Table of Contents

List of Figures

List of Tables

List of Equations

1 Introduction

Using remote sensing data from a terrestrial laser scan (TLS), a computer based 3D representation of geomorphology interacting with a fracture network is created. With the aid of data manipulation techniques enabled by the RiSCAN PRO software, the model is presented as close to “real life” as possible. Discontinuities are constructed into the surface model and are visualised in-situ. Previously failed blocks, defined by their discontinuities and free surfaces, are mapped out in-situ. The discontinuities that make up the blocks create a complex fracture network model. The in-situ failed blocks are reproduced using Block Theory software. First, the discontinuities and free surfaces of individual blocks are shown on stereonets which show their Joint Pyramid-Codes and surfaces on which they fail. Second, the individual blocks are visualised in 3D and then their volumes calculated. Lastly, the in-situ failed blocks are shown on the tunnel cross-section.

Several computer programs were used for this project. The laser scan data was processed using the software RiSCAN PRO, which shall be explained in greater detail. Computer programs based on Goodman and Shi’s Block Theory were utilised to plot blocks on stereonets, visualise blocks in 3D, calculate their volume and show blocks on the tunnel cross-section. Block Theory identifies potentially removable blocks based on orientation and spacing information of discontinuities.

For this study, complete laser scan data of the Raabstollen adit of the Arzberg in eastern Styria, Austria were used. Once processed, the laser scan model allows for rapid discontinuity identification and measurement without being present on site. Potentially dangerous and/or hard to reach discontinuity surfaces can be mapped with mm-accuracy.

2 The Advantages of LiDAR

Terrestrial laser scanning is a tool for acquiring spatial data. Combining a terrestrial laser scan with digital photography and RTK-GPS results in a Virtual Outcrop Model (VOM). In engineering geology, this VOM is a 3-dimensional representation of "geomorphology and rock mass properties, especially discontinuity geometries and the interaction between geomorphology and fracture pattern" (Liu, 2012). With the digital camera, true colour information can be added to the 3D point cloud data. Individual scans can be merged into a single point cloud which can be registered into a single coordinate system. The triangulation of surfaces meshes and the texturing with digital photographs allows for accurate and precise measurement of rock mass structure. Software such as RiSCAN PRO allows individuals to map complex fracture networks of outcrops and excavations.

2.1 Field Work

Where are you planning to scan and what do you hope to extract from the scan? An outcrop or section of tunnel are chosen to be scanned, using the least amount of scan positions one should attempt to get the maximum coverage of the area of interest. Accuracy and precision considerations must be made in regards to the scale of the problem. Are we interested in metre-scale stratification or mm to cm-scale foliations? The positions of your scan positions as well as reflectors must be known in the field in order to allow for the scans to be registered into a single point cloud. Another important consideration is lighting in regards to digital photography, which will be important once texturing the model. Once these issues have been solved, data can be acquired and many issues further along the workflow will be avoided.

2.1.1 Considerations in the Field

Prior to scanning, it is important to consider the number of scans necessary for full coverage of the study area (Figure 2.1), what resolution best fits the study's purpose and how precise/accurate must your point cloud data be. All scan positions will later be merged into a single point cloud, it is paramount that these scans cover the entire study area at a resolution that fits the proposed application. Stable locations for scanning must be selected and scan coordinates determined via RTK-GPS. There should be a clear line of sight between the scanner and target surface and should be positioned so that it is normal to the target surface. Is this not the case, the data set will contain range shadows or holes. Common targets for different scans will act as tie points between scans when merging into a single point cloud, so their positions must be determined as well. Low intersection angles between the laser beam and scanned surface should be avoided. After each scan, supplementary images should be acquired for later texturing of the Virtual Outcrop Model (VOM).

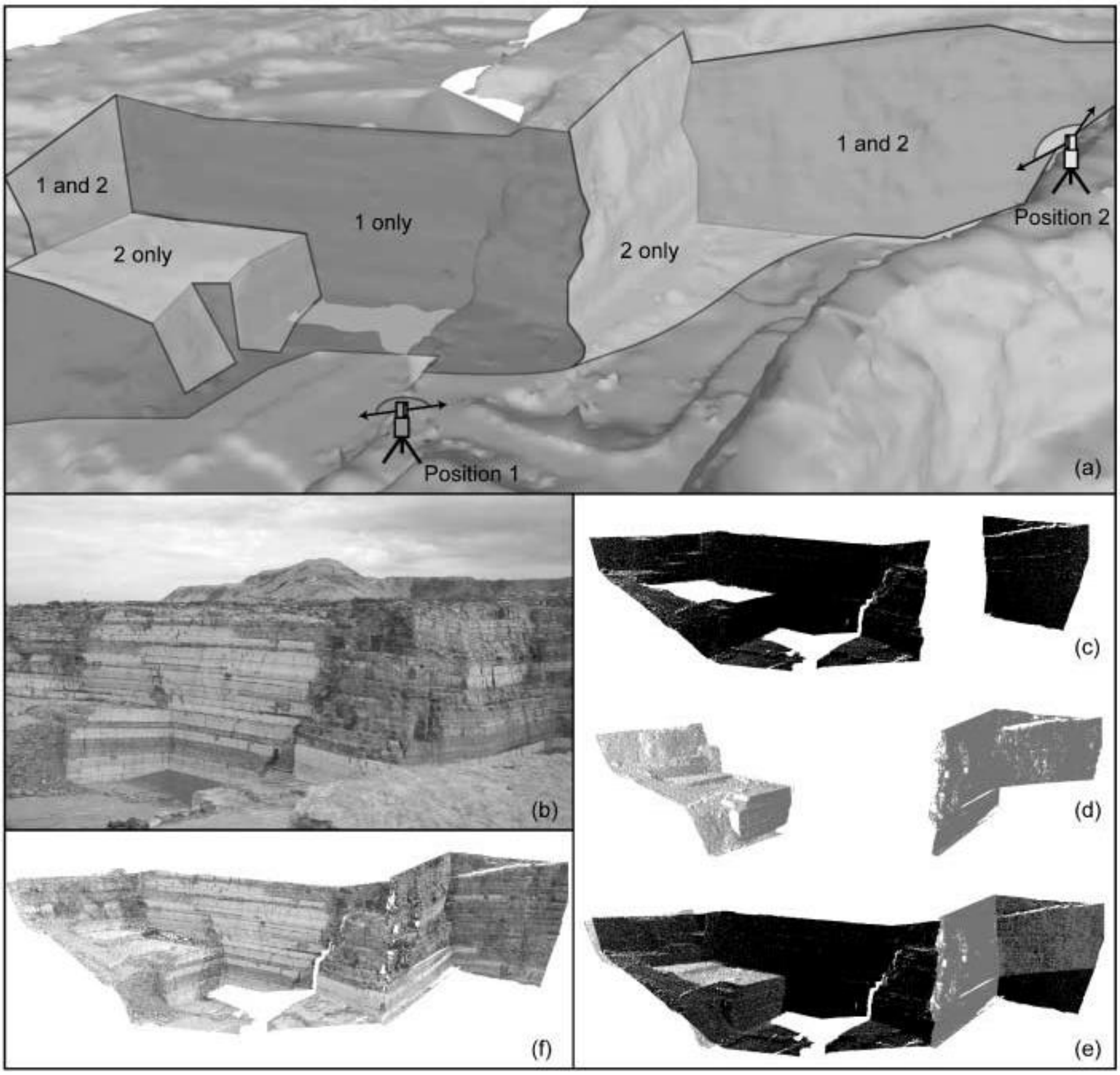

Figure 2.1: Number of scan positions vs. maximum area coverage (After Buckley, 2008)

2.1.2 Location-Dependent Specifications

The laser scan data for the Arzberg Raabstollen adit were acquired by Liu and Kieffer and the workflow is summarized in their paper *Digital tunnel mapping using terrestrial LiDAR - a case study* (Liu & Kieffer, 2012). The following is a summary of the location-dependent specifications that were selected based on the study location. The Raabstollen adit is a 30m long, east-west oriented section of the Arzberg silver-bearing lead zinc mineral deposit located in eastern Styria, Austria. The tunnel cross-section is shaped like an arc and has dimensions of approximately 2m x 2m. This portion of the Arzberg deposit is predominantly hosted in schists which have a chloritic overprint.

Based on these location specifications the following instrumentation was used and specifications selected. For data acquisition, a Riegl Model LMS-Z620 terrestrial laser scanner was used in conjunction with a tilt mount and high resolution digital camera mounted on a tripod. The specifications of the instrument are summarized in Table 2.1. The tilt mount increased the field of view so that the scans included the roof. In order to cover the entire field of interest, an angular resolution of 0.07 x 0.07 degrees was selected which gave a “survey point density of 3.66cm x 3.66cm at a distance of 30m.” Furthermore, 12 scan positions were needed to cover the 30m length of the study area which resulted in a 3D point cloud model with 54 million points. For each of the 12 scan positions, at least 3 retro-reflectors were surveyed so that they would act as tie points during the registration portion of the work flow. With these specifications, the tunnel geometry was surveyed with mm-accuracy.

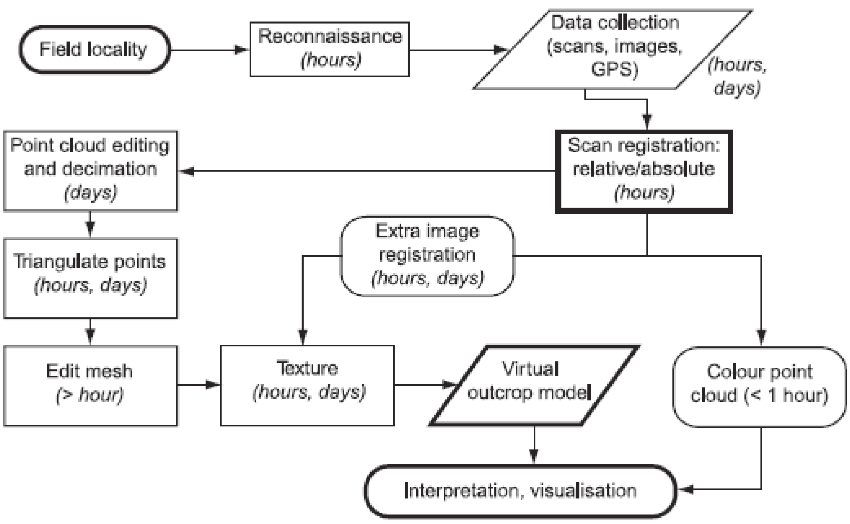

Figure 2.2 Typical workflow for TLS (After Buckley, 2008)

Scanner	Rigel 3D TLS LMS-Z620
Scan method	pulse based (time of flight)
Max. Scan distance (m) a target reflectivity of 90% a target reflectivity of 10%	 2000 750
Field of view (°)	360 (horizontal) × 80 (vertical)
Horizontal & vertical angle resolution (°)	0.004 × 0.004
Scanning speed	up to 11,000 meas./sec.
3D scan precision	10 mm (single shot in 100 m range) 5 mm (averaged in 100 m range)
High-resolution digital camera	Nikon D300, integrated & calibrated into scanner coordinate system
Inclination sensor & RTK-GPS	integrated

Table 2.1: Specifications of the Riegl 3D TLS LMS-Z620 (After Liu and Kieffer, 2012)

The zero-point of the sites coordinate system was designated on the adit invert where x = East, y = North and z = Up. Positions of the 12 scan positions and retro-reflectors were determined based on the coordinate's origin. Later, during the post-processing stage, the survey data were transformed into the local 3D coordinate system and oriented to geographic north.

During the data processing stage of the workflow (Figure 2.2), a few complications were encountered. Although the scans covered the entire span of the adit, portions of the point cloud data were denser than others. This was due to "large angles (approaching 90°) between the line-of-sight of the scanner and the normal direction of the excavation surface" (Liu and Kieffer, 2012). In order to remedy this issue, the registered point cloud data were triangulated resulting in a digital excavation surface model with uniform high resolution. Triangulation creates a mesh out of the point cloud data and is able to fill in gaps as well as connect points. Another problem that was encountered in post processing occurred while texturing the surface mesh with digital photographs. Lighting conditions in the adit made it difficult for the entire mesh to be coloured. Creating a laser scan without light is no issue; however, if one requires a textured mesh one must consider that far more images are required underground to accurately do so.

Terrestrial laser scanning is an invaluable tool for the mapping of 3D geomorphology especially in locations where physical measurements are restricted such as tunnels or cliff faces. Although a single laser scan takes on the order of 20 minutes to complete, the post-processing time can take weeks. In the near future, the standardisation and automation using algorithms of the post-processing steps will allow economical LiDAR mapping of tunnels during excavation (Liu & Kieffer, 2012).

2.1.3 Accuracy and Precision

"Terrestrial laser scanning, or lidar, is a recent innovation in spatial information data acquisition, which allows geological outcrops to be digitally captured with unprecedented resolution and accuracy" (Buckley et al., 2008). Accuracy and precision must be chosen based on the application and scale of the problem. Buckley et al. refer to this as the range: accuracy trade-off (Buckley et al., 2008). A lower powered laser has a lower range, but a stable shape beam, which allows for higher point accuracy. Buckley et al. further stress error propagation through the workflow. They site 3 possible sources of error: field-based, processing-based and image-based errors. Field-based errors reduce precision at the study area whether they be related to atmospheric visibility, terrain type or precision reduction due to greater range. Poor atmospheric visibility results in lower point precision. Surfaces that are oblique to scanning will contain lower point densities and should be considered prior to triangulation of data. Processing-based errors occur at some stage during the office workflow and will continue throughout the process. This may occur during triangulation when holes are filled resulting in deviation from the original point cloud. Image-based errors occur when images are not properly registered and so measurements taken in areas of interest will be inaccurate. It is therefore incredibly important to consider the possibilities of errors and to ensure that they do not propagate throughout the workflow.

2.2 Office Work

Before measurement and interpretation of Terrestrial Laser Scans (TLS) can begin, several steps must take place. Initially, the raw scan data must be registered so that data can be viewed as a whole. During this stage, reflectors act as tie points between scans and the individual scans are registered into a single coordinate system. Following the coarse registration, it is possible that common points between scans are offset. In order to remedy this, the Multi Station Adjustment plugin is used. Alignment of scan positions is calculated relative to other scans while one is fixed until the optimal alignment is reached. Triangulation then creates a surface out of the point cloud data and acts to join points and fill in voids. Once these steps are complete, the data can be textured with digital images to give a Virtual Outcrop Model (VOM). At this stage, polydata should be created to view areas of interest within the scans without overloading your system. Now the data can be measured and interpreted.

2.2.1 Coarse Registration

In order to register the point cloud data, a local coordinate system was defined; with a zero point oriented to geographical north and scaled (Figure 2.3). The 12 scan positions with known coordinates in the local coordinate system were merged together using common retro-reflectors based on the principle of back-sighting. In order to achieve an initial coarse registration, the following steps must take place. First, the coordinates of the 12 scans are imported. These coordinates can then be transformed from the Project Coordinate System (PCS) to a Global Coordinate System (GCS) using the calculate translation for POP matrix (Figure 2.4). For the purpose of this study, it was adequate to merge the scan positions into a single point cloud with the defined local coordinate system; however, for other applications a global coordinate system may be preferable. All tie point lists must be copied from the GLCS to the PRCS. The SOP Matrix from Scan Position 1 is then calculated and works the same for the remaining scan positions (Figure 2.5). At this point, the initial coarse registration is complete; however, comparing the different scan positions it is clear there is an offset of points (Figure 2.6). In order to correct this offset, the plugin “Multi Station Adjustment” is used.

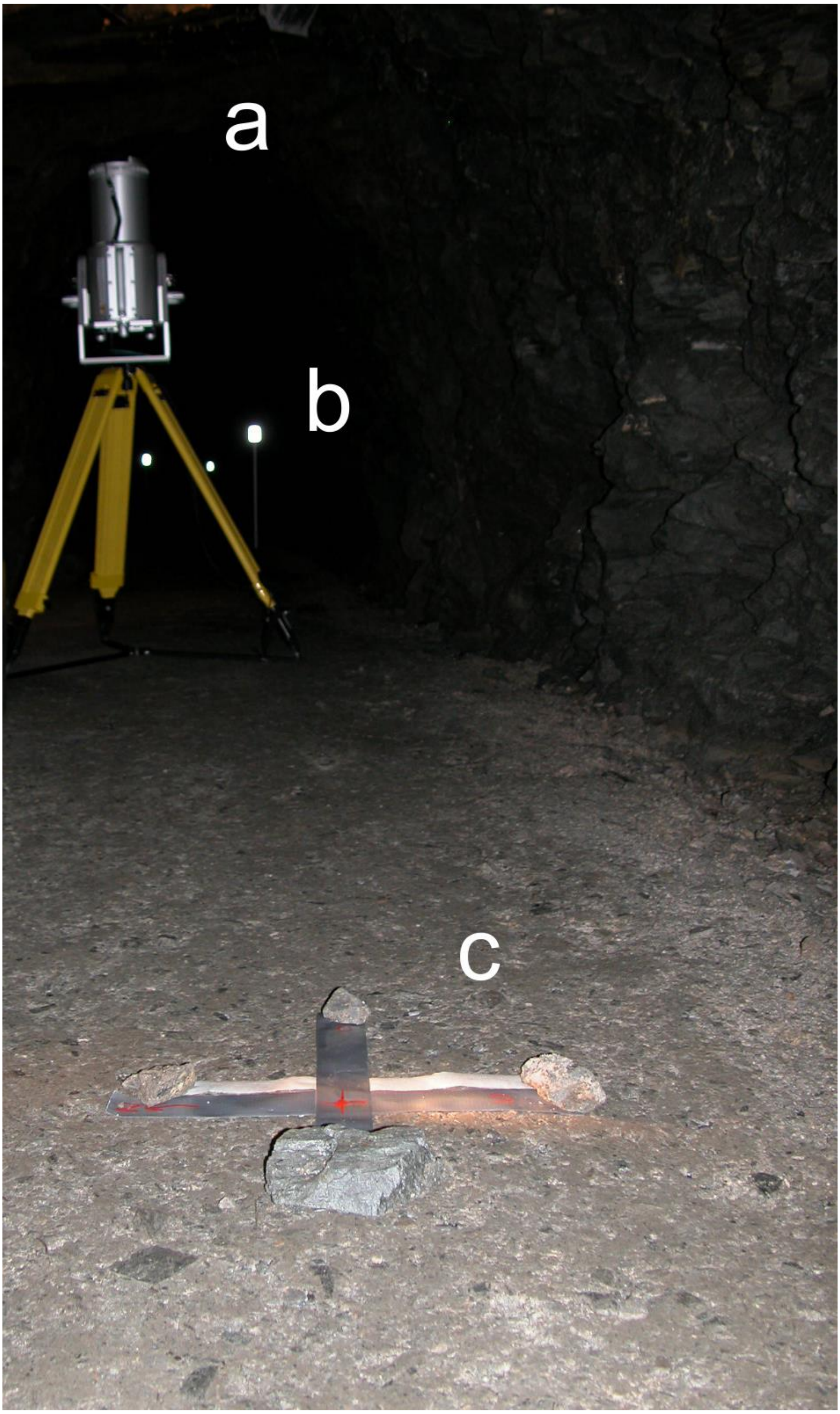

Figure 2.3: Setup during data acquisition: (a) laser scanner mounted on tripod (b) retro-reflectors (c) origin of local coordinate system oriented to geographical north (After Liu and Kieffer, 2012)

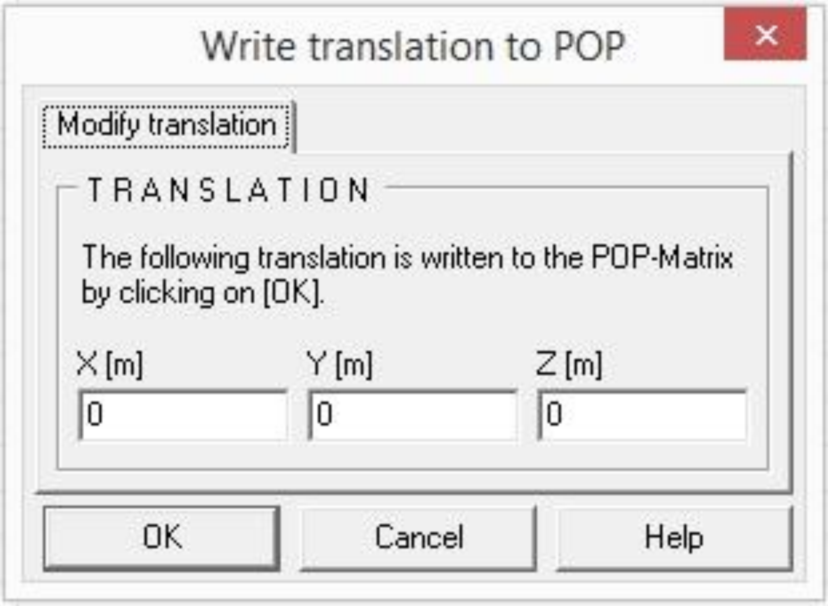

Figure 2.4: Write translation to POP window

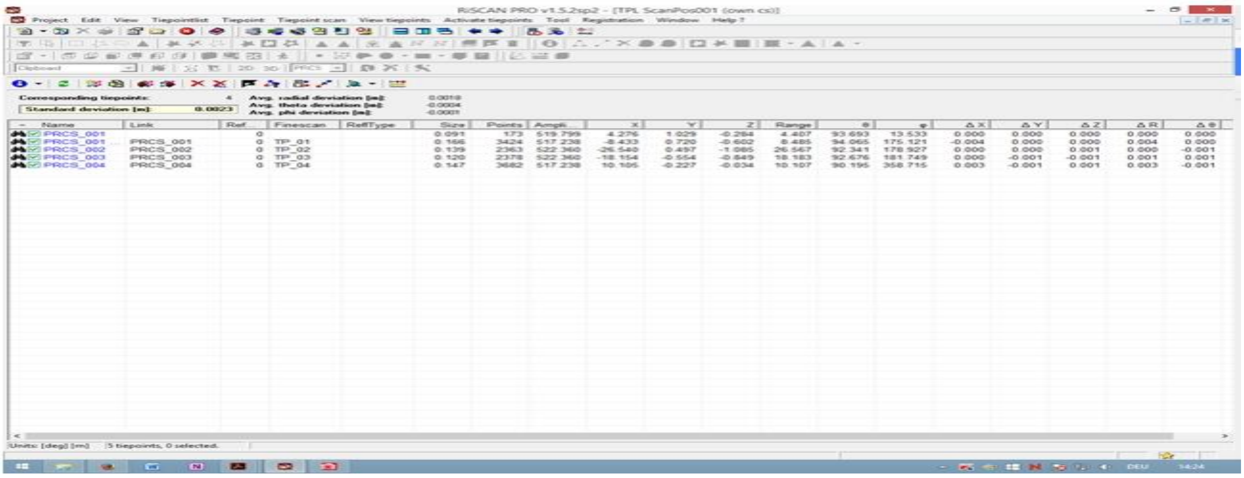

Figure 2.5: Calculate SOP Matrix window

2.2.2 Multi Station Adjustment (MSA)

The Multi Station Adjustment (MSA) plugin is used in order to get a better alignment of positions. The coarse registration in RiSCAN pro is based on tie points which correspond to the centre of reflective targets. Alignment errors may result due to suboptimal target reflector positioning, an unstable setup or general measurement errors. The MSA plugin optimises registration of the scan positions by changing their orientation and position multiple times in order to calculate the optimal alignment (RiSCAN PRO, 2015). Tie points, tie objects and polydata (= reduced point clouds) are used by the plugin to compare scan positions with each other.

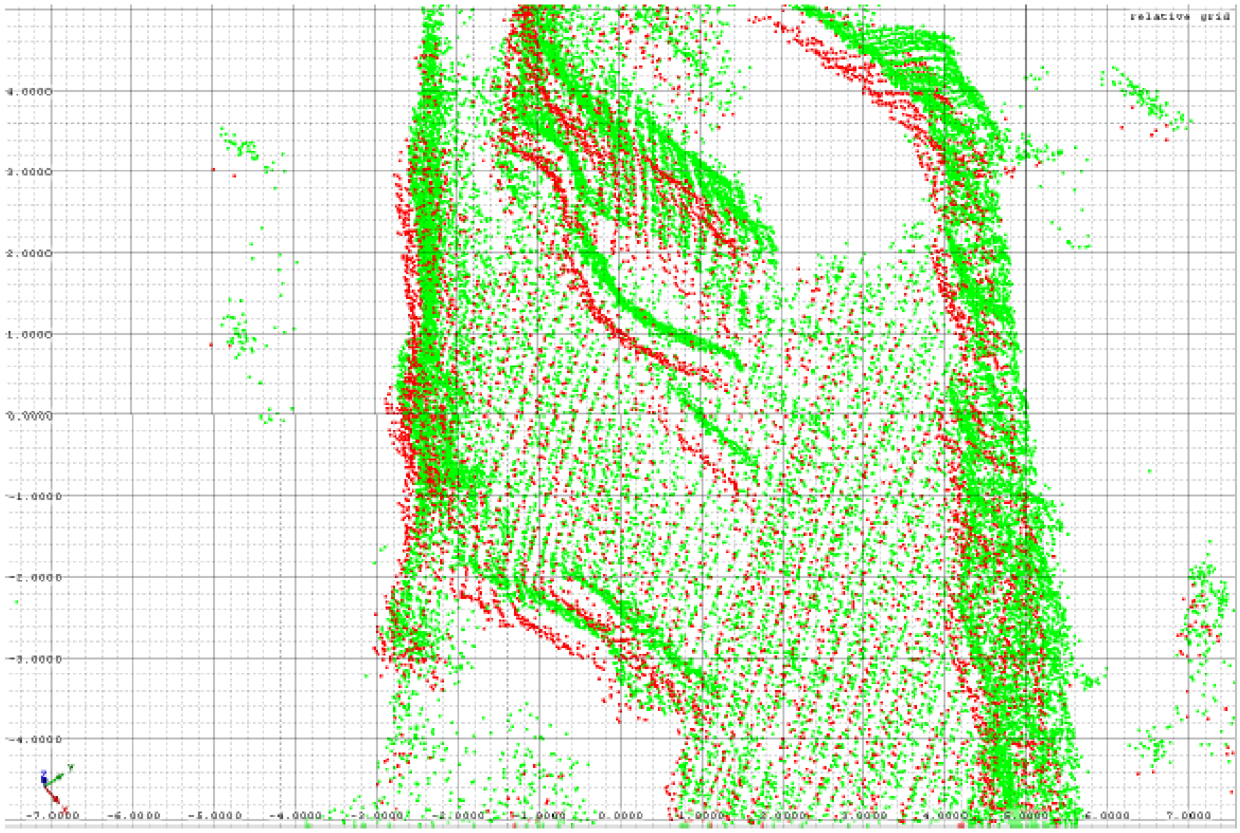

Figure 2.6: Offset of points between scan positions before Multi Station Adjustment

In order to make an adjustment one of the scan positions is fixed and acts as a reference for the other scan positions. For example, scan position 1 is fixed while positions 2 to 12 are aligned relative to it. The varying parameters are filled in and an analysis takes place. During the analysis, the standard deviation is calculated and points that belong to each other are searched for. By decreasing the parameter search radius, the standard deviation decreases. The “Statistics” window then shows these values (Figure 2.7). During this process there is no change of orientation or position of the scan positions. Once satisfied with the given statistics the “Calculate” button is selected and the positions are changed. The “Multi Station Adjustment” window shows the change of positions and orientations after adjusting (x, y, z), not actual positions or orientations (Figure 2.8). The result of the Multi Station Adjustment shows points that lie directly on top of one another (Figure 2.9). The registration is now complete and the data processing can begin.

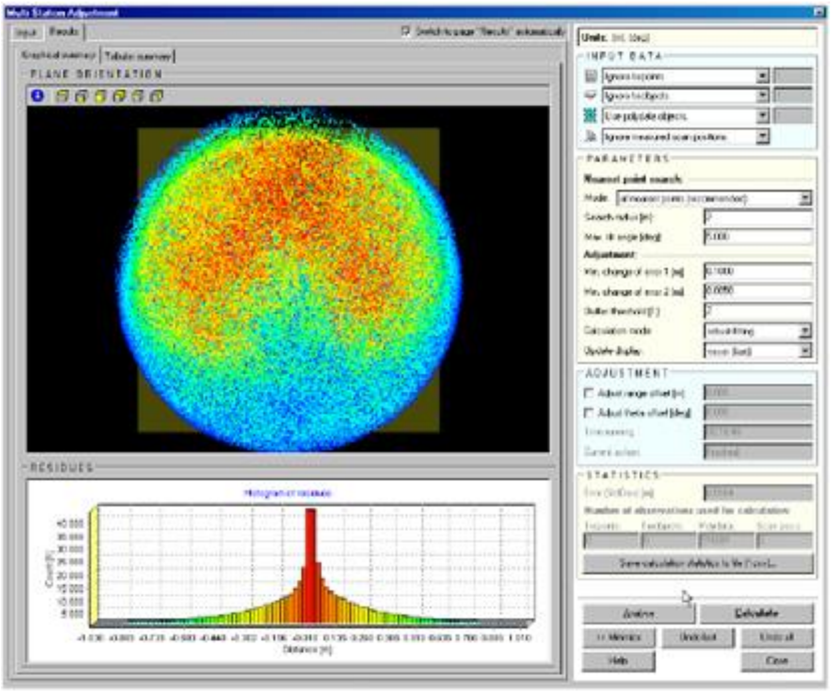

Figure 2.7: Statistics window in RiSCAN PRO

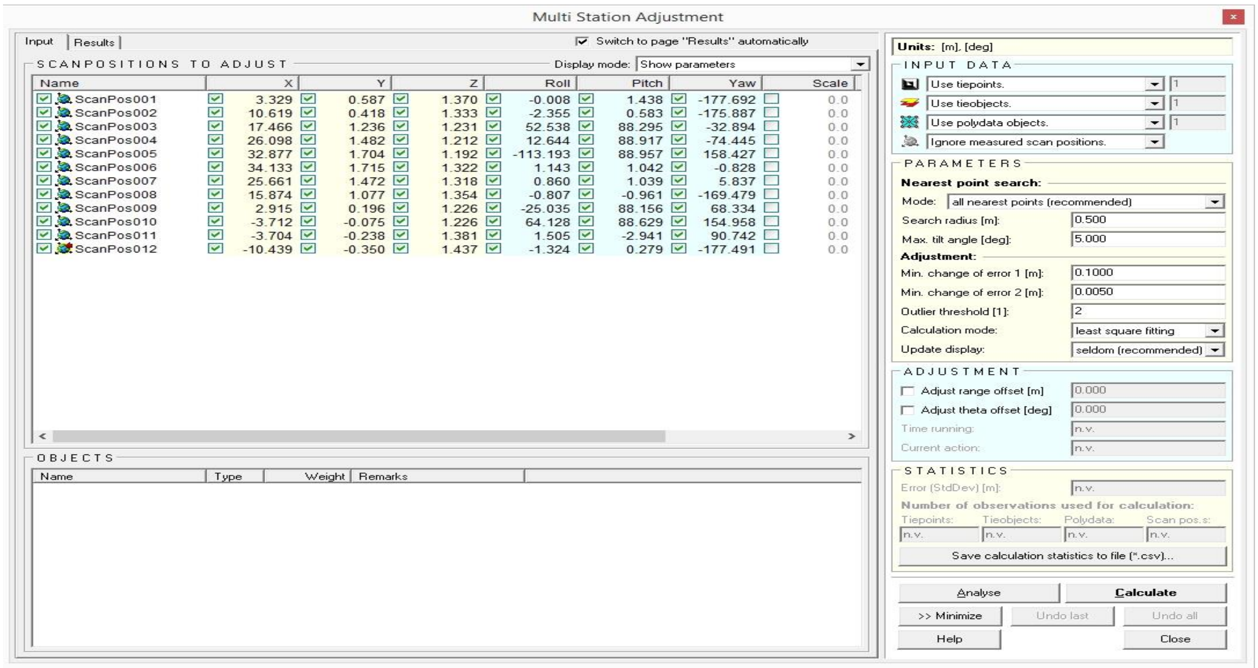

Figure 2.8: Multi Station Adjustment window of RiSAN PRO

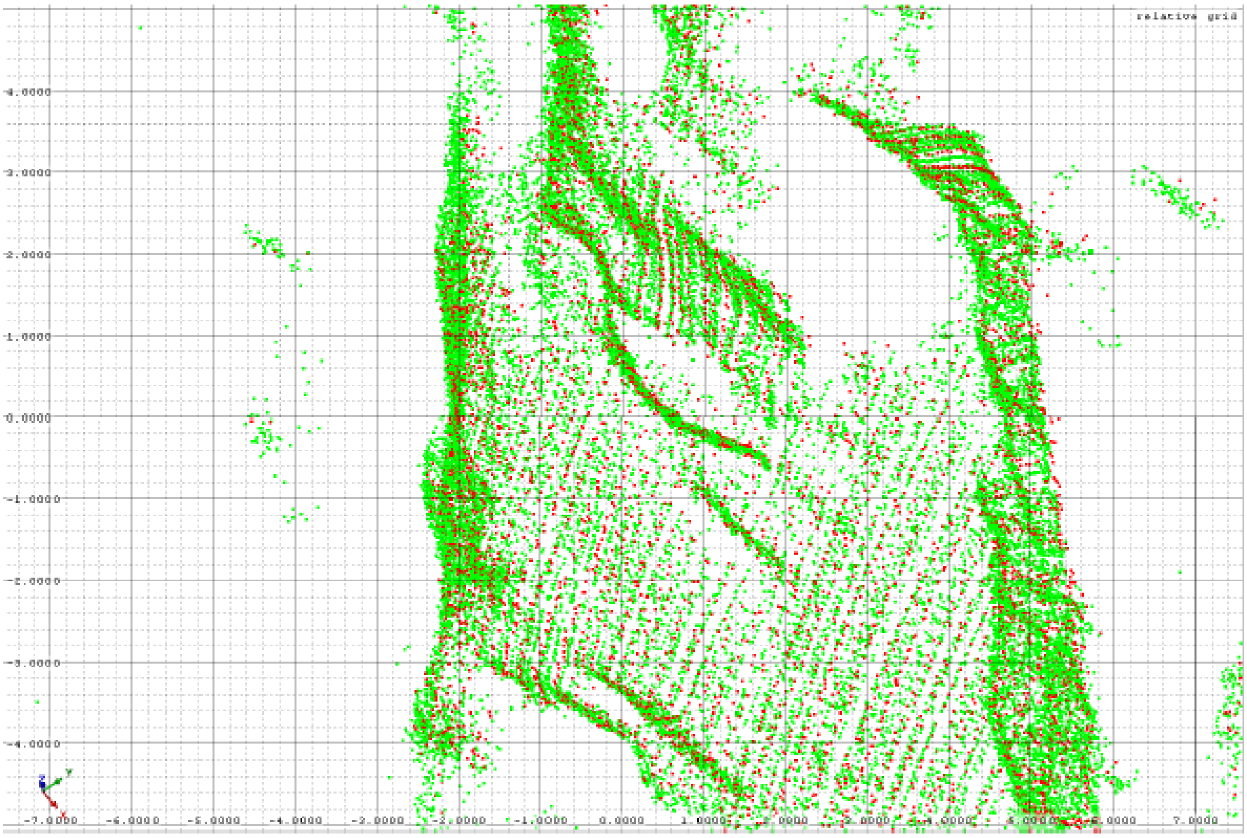

Figure 2.9: Result of MSA; common points of different scan positions lying on top of one another

2.2.3 Triangulation

Triangulation creates a mesh out of a point cloud. Using this operation points are joined and holes are filled. With triangulation, a point cloud is turned into a surface and the data points of the surface are connected with triangles. “Triangulated data (also called “mesh”) gives a better representation of the scanned object” (RiSCAN, 2005). As mentioned above, triangulation is invaluable in areas where point density is not uniform; however, needs to be implemented carefully so that later quantification of the geomorphology geometry remain accurate. Using RiSCAN PRO an octree filter was used to triangulate the Raabstollen adit data.

2.2.4 Creating Polydata

In order to analyse a larger data set it helps to be able to separate it into smaller areas. Looking at a tunnel for instance it helps to be able to view the roof and sidewalls separately and even to further split those areas into smaller sections.

These reduced areas are called polydata and represent a smaller point cloud of data. The steps below show how one would go about creating polydata. Using the selection mode tool the area of interest is selected. The “create new polydata” object is selected and the new polydata is then located in the project manager window under views where the polydata can be renamed. Depending on the specifications of the computer one is using, the system can often be overwhelmed by the sheer size of the point cloud data one is working with. The creation of polydata is a simple and fast way to look at specific areas efficiently.

2.2.5 3D TLS VS. Grid-Based DEM

Terrestrial laser scans require a georeferenced 3D Cartesian coordinate system with X = E (East), Y = N (North), Z = up. This is different than a grid-based Digital Elevation Model (see Figure 2.10) which is actually 2.5D since for each x, y position only a single z coordinate is allowed. This makes it ineffective in terms of describing 3D rock blocks: overhanging rock blocks and fractures or almost vertical rock faces. True 3D point clouds allow multiple height values for single x, y positions. “The given grid-based DEM is not appropriate for modelling 3D rock structure” (Liu & Kaufmann, 2015). Careful consideration should therefore be taken when using aerial laser data.

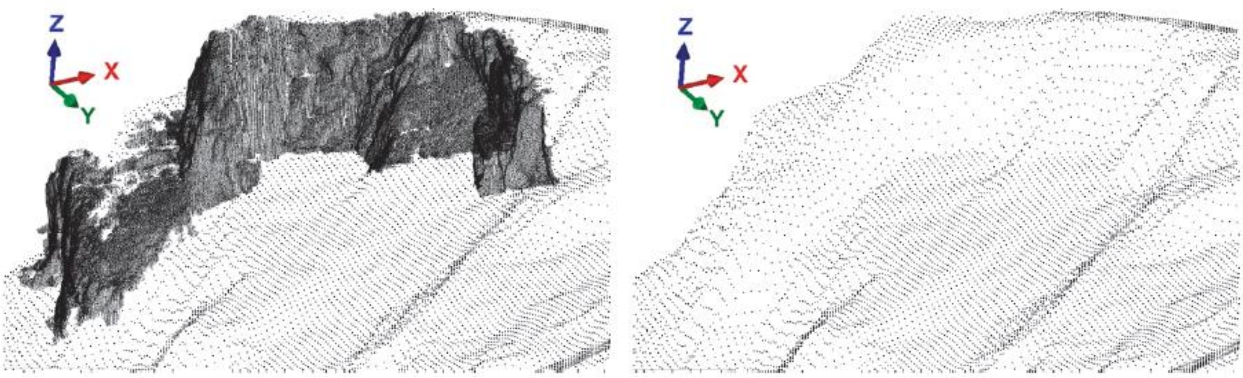

Figure 2.10: (A) 3D TLS points embedded in ALS DEM (B) grid-based DEM (After Liu & Kaufmann, 2015)

2.2.6 Automatic Mapping of Discontinuities

Automation of fracture set identification with similar dip and dip directions using Liu and Kaufmann's HSV-coloured 3D rock structure algorithm make discontinuity classification less time consuming (Liu & Kaufmann, 2015). For this principle, a unique HSV-colour was assigned to each orientation of 1 degree resolution for both dip and dip direction. Hue is linked to the dip direction of the normal of a fracture/rock face (=pure colour). The saturation or whiteness is linked to the dip of the normal. For fracture/rock faces that are vertical, whose normal has a dip of 0 degrees, saturation is equal to 1 and for horizontal faces, whose normal dip 90 degrees, saturation is equal to 0. The lightness value V describes darkness (0 = black, 1 = white). In the model, a consistent lightness of 0.75 has been applied. To put it simply, each unique fracture orientation is assigned its own colour and those become darker as the dip angle increases (Figure 2.11). This algorithm has the potential to automatically assign fracture set orientations for rock masses of interest and would make the data processing portion of TLS less time consuming.

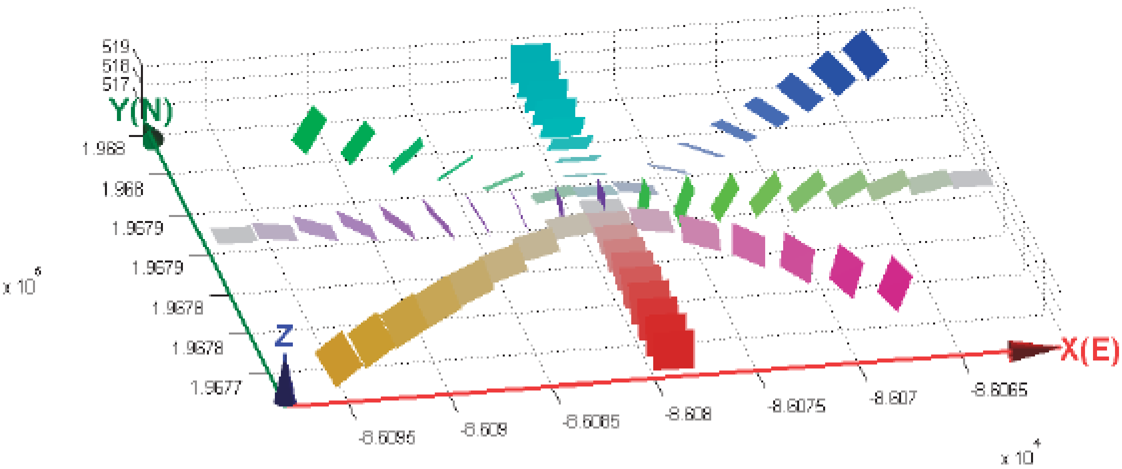

Figure 2.11: HSV-coloured fractures for geometrical representation (After Liu & Kaufmann, 2015)

3 Methods for the Determination of Block Size in Underground Excavations

"The in-situ block size of the rock mass may be the single most important parameter influencing the strength and stability of engineering openings" (Liu, 2012). Block Theory is a system to describe potentially removable blocks in excavations and on slopes. From fracture set and free space orientations, fracture spacing's and friction angles, Block Theory is able to identify removable blocks and the stability measures necessary to keep them in place. Block Theory is also able to produce the size of individual blocks which is connected to the degree of jointing within in a rock mass. Previous methods for describing rock masses looked at the degree of jointing or block size as a portion of the quality of a rock mass. Instead of looking at individual blocks like Block Theory, previous attempts to quantify rock mass quality took many other factors into consideration including but not limited to joint roughness, joint alteration, groundwater condition, rock strength, etc. to describe overall rock mass behaviour. In engineering geology, rock mass characterisation methods have one thing in common: they all attempt to give insight into rock mass behaviour as a result of anthropogenic or natural forces that act on them. The following chapter goes into further details about these methods.

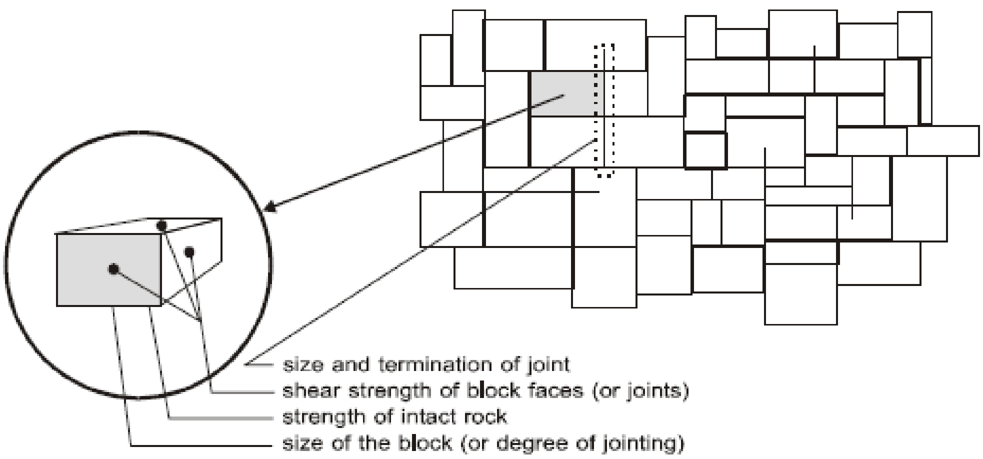

Figure 3.1: Rock mass parameters (After Palmström, 1995)

3.1 Rock Quality Designation

As a geologist, measuring rock blocks is especially difficult since there are only one-dimensional scanlines and drill holes or two-dimensional outcrops available to quantify them. In 1967, Deere et al. created a method for the description of the degree of jointing specifically for core logging. Rock Quality Designation (RQD) is equal to the sum of intact core pieces larger than 10cm divided by the length of the core run given as a percentage (see Figure 3.2). Though it was developed for drill core logs, it can also be attained using a scanline.

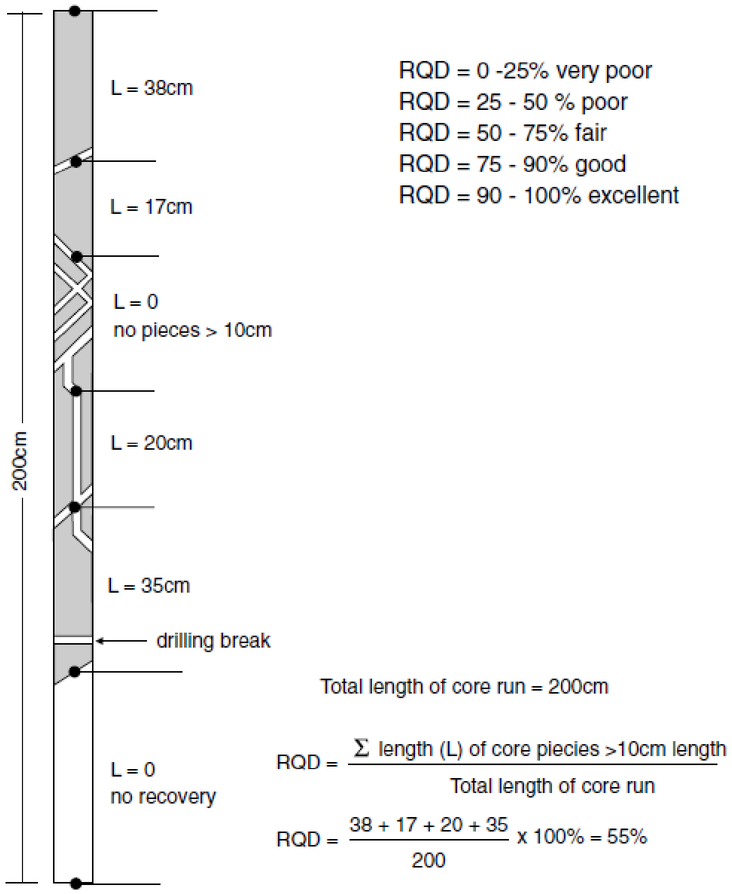

Figure 3.2: Procedure to measure and calculate RQD (After Deere et al., 1967)

RQD is sensitive to sampling directions where block shapes are anisotropic, on the other hand it is insensitive to large and small block size distributions (Figures 3.3 and 3.4). RQD makes up a portion for Bieniawski's Rock Mass Rating and Barton et al.'s Q-System to be discussed in greater detail below. Unlike Deere et al., Pamström took an index approach to look at fracture density and block size.

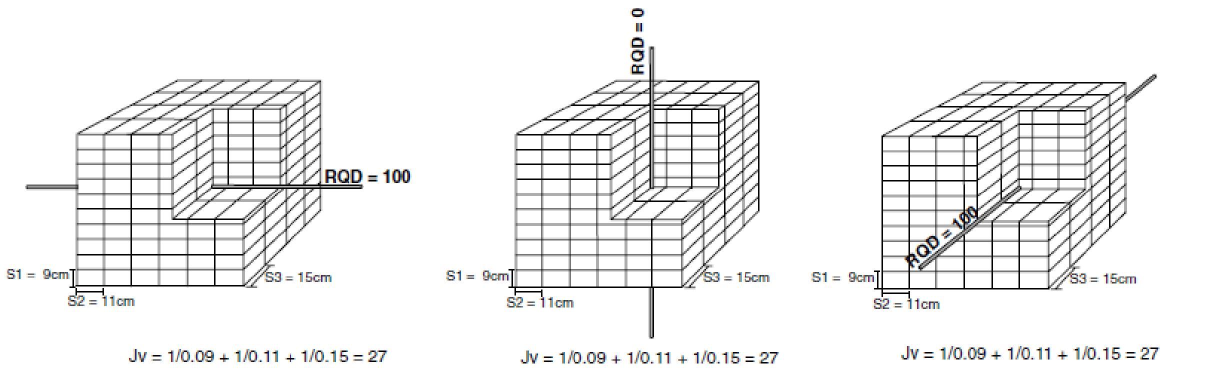

Figure 3.3: RQD sensitive to sampling/drilling direction (After Deere et al., 1989)

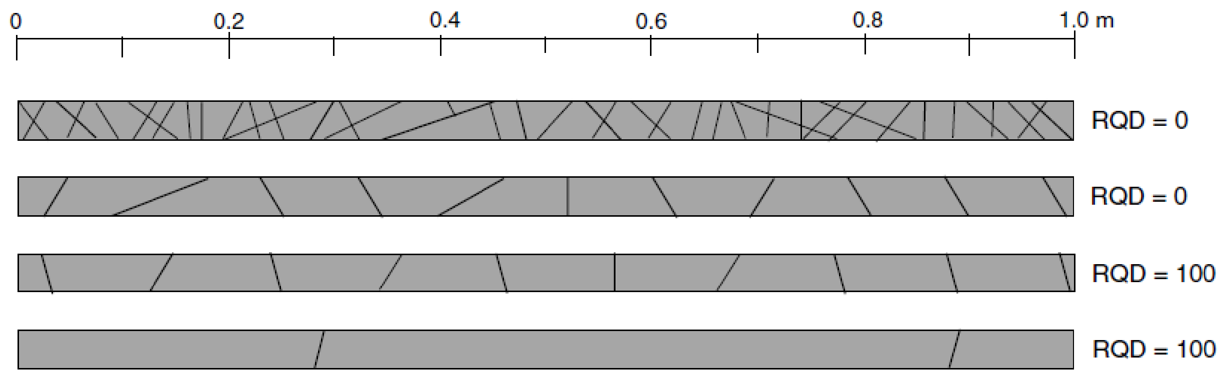

Figure 3.4: RQD values for different joint spacings (After Palström, 1995)

3.2 Volumetric Joint Count and Block Size

Palmström came up with an index approach to quantify the density of joints or Volumetric Joint Count (J_v) and block size (V_b). The volumetric joint count is given by Equation 3.1 and is equal to the number of fractures that intersect a cubic metre of rock. It also takes into account the effect of random fractures which is given by N_r. Block size, V_b, is given by Equation 3.2 and is a function of the block shape factor β, the volumetric joint count J_v and the angles between fractures γ which are shown in Figure 3.5. More rigorous approaches exist as well which consider impersistent fracture sets. Figure 3.6 shows that both volumetric joint count and block volume cover a wider range of jointing in comparison to Rock Quality Designation. RQD has a value of 0 for distances between joints less than 10cm and 100 for distances between joints equal to or greater than 10cm. Figure 3.7 shows the correlation between volumetric joint count (J_v) and block size (V_b) as well as block form.

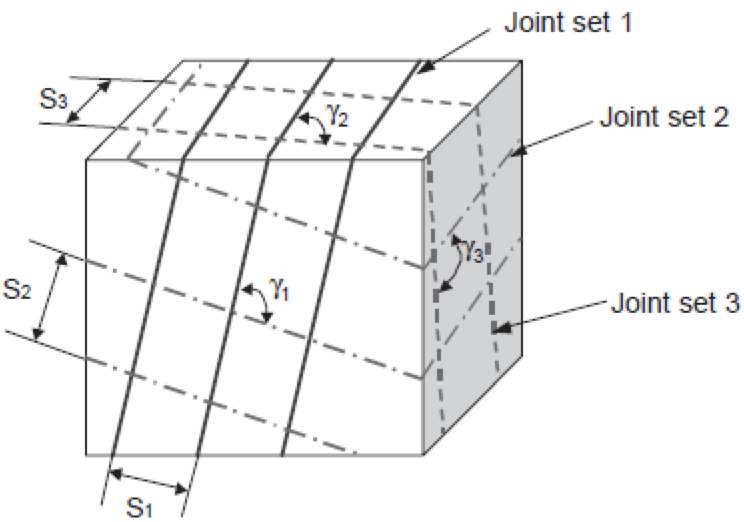

Figure 3.5: Joint spacing's (S) and angles between joint sets (γ) (After Liu, 2012)

(Equation 3.1) $J_v = 1/S_1 + 1/S_2 + 1/S_3 + \ldots 1/S_n + Nr/(5\sqrt{A})$

Where S = average spacing for fracture sets

N_r = number of random fractures in the actual location

A = the area in m²

(Equation 3.2) $V_b = \beta * Jv^{-3} * 1/\sin\gamma_1 * \sin\gamma_2 * \sin\gamma_3$

Where block shape factor $\beta = (\alpha_2 + \alpha_2 * \alpha_3 + \alpha_3)^3/(\alpha_2 * \alpha_3)^2$

($\alpha_2 = S_2/S_1$ and $\alpha_3 = S_3/S_1$)

γ = angles between fractures

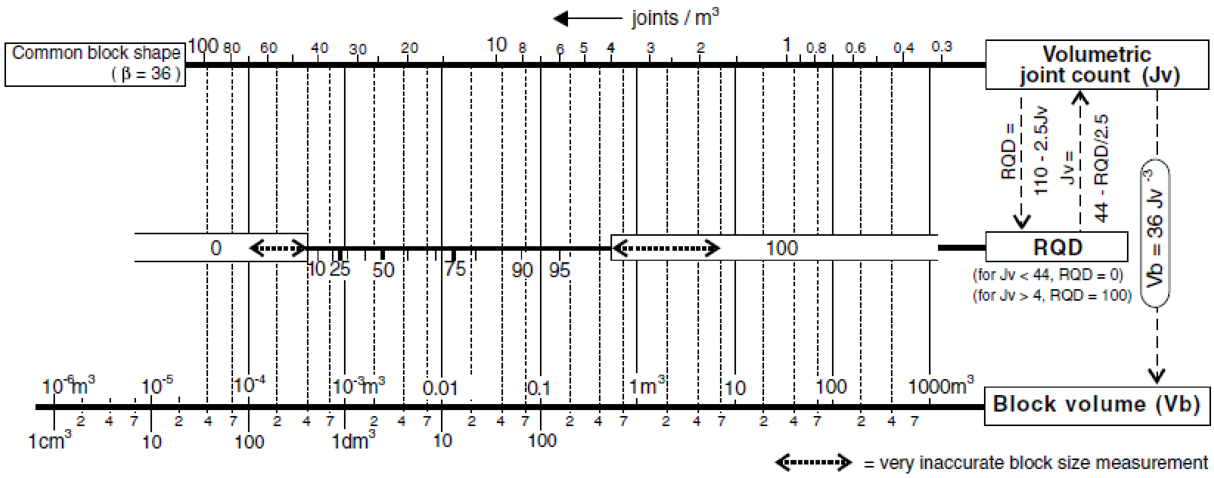

Figure 3.6: Block volume (Vb) and volumetric joint count (Jv) cover a larger range of jointing than RQD (After Liu, 2012)

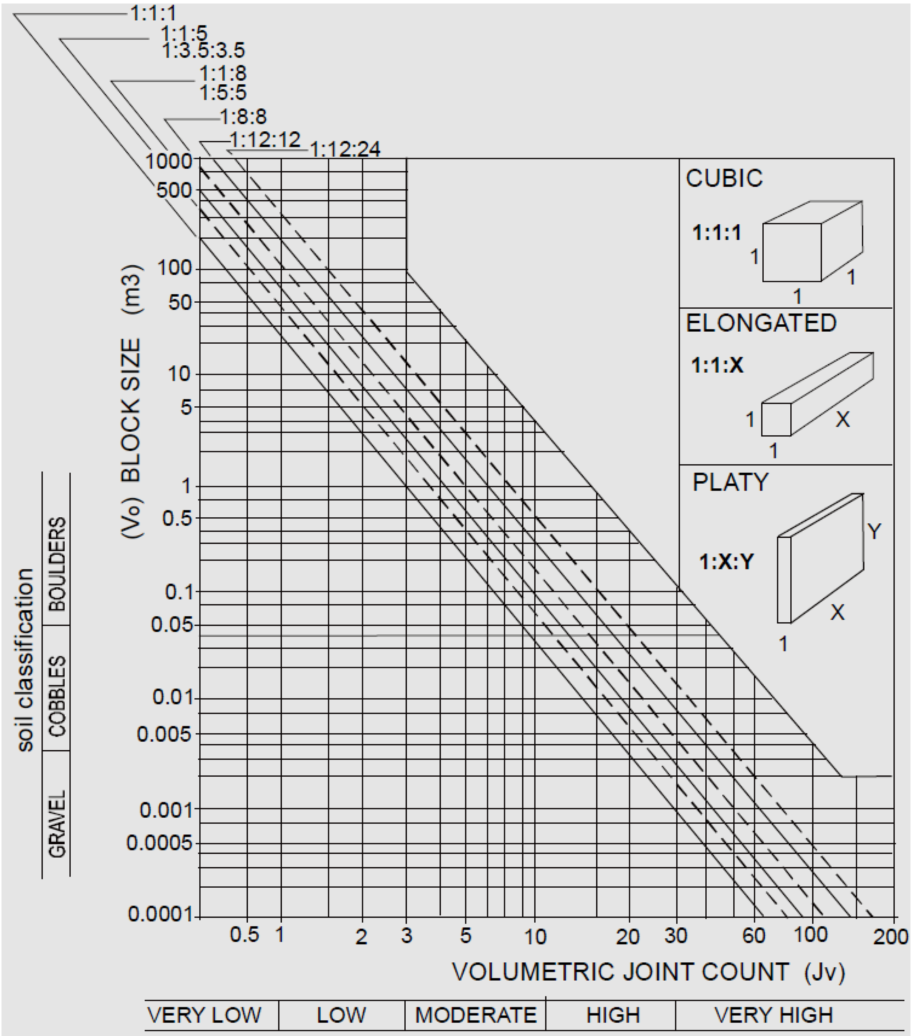

Figure 3.7: Correlation between volumetric joint count (J_v) and block size (V_b) (After Liu, 2012)

3.3 Rock Mass Rating and Q-System

Two approaches exist for the classification of rock masses which consider Deere et al.'s Rock Quality Designation (RQD). Bieniawski's Rock Mass Rating (RMR) was developed based on his experiences in shallow mining tunnels in sedimentary rocks. In a unit with homogeneous geological structure, the following six parameters are determined and then rated: uniaxial compressive strength, rock quality designation, joint spacing, joint condition, groundwater condition and joint orientation. The RMR rating assigns values to each parameter and is equal to the algebraic sum of these values once adjusted for the orientation of discontinuities. For this classification system, the rock mass is separated into various structural areas and rated separately. A change in rock type or the presence of a fault would indicate a change in structural area. Table 3.1 shows the ratings for the individual parameters of the RMR classification and Table 3.2 shows the individual rock mass classes and guidelines for the excavation and support of a rock tunnel with a span of 10m. The applications of RMR cover the stand-up times for arched roofs to the in-situ modulus of deformation. The second classification system which takes into account RQD is the Q-System which was developed at the Norwegian Geotechnical Institute (NGI) in 1974 by Barton et al. The Q-System is used to describe rock masses with respect to the stability of underground openings in hard and jointed rocks. Its value is based on the estimation of six rock mass parameters which can be separated into 3 components: degree of jointing (RQD/J_n), joint friction (J_r/J_a) and active stress (J_w/SRF). Equation 3.3 shows how to calculate for Q. The values for the individual parameters are meant to be determined in the field using tables which contain numerical values for each situation (see NGI, 2013). Figure 3.8 shows necessary support measures for an underground opening based on Q-values. The limitations of the RMR and Q-Systems mostly relate to the shortcomings of RQD which were discussed above.

A. CLASSIFICATION PARAMETERS AND THEIR RATINGS							
	Parameter		Range of values				
1	Strength of intact rock material	Point-load strength index	>10 MPa	4 - 10 MPa	2 - 4 MPa	1 - 2 MPa	For this low range - uniaxial compressive test is preferred
		Uniaxial comp. strength	>250 MPa	100 - 250 MPa	50 - 100 MPa	25 - 50 MPa	5 - 25 MPa 1 - 5 MPa < 1 MPa
	Rating		15	12	7	4	2 1 0
2	Drill core Quality *RQD*		90% - 100%	75% - 90%	50% - 75%	25% - 50%	< 25%
	Rating		20	17	13	8	3
3	Spacing of discontinuities		> 2 m	0.6 - 2 . m	200 - 600 mm	60 - 200 mm	< 60 mm
	Rating		20	15	10	8	5
4	Condition of discontinuities (See E)		Very rough surfaces Not continuous No separation Unweathered wall rock	Slightly rough surfaces Separation < 1 mm Slightly weathered walls	Slightly rough surfaces Separation < 1 mm Highly weathered walls	Slickensided surfaces or Gouge < 5 mm thick or Separation 1-5 mm Continuous	Soft gouge >5 mm thick or Separation > 5 mm Continuous
	Rating		30	25	20	10	0
5	Ground water	Inflow per 10 m tunnel length (l/m)	None	< 10	10 - 25	25 - 125	> 125
		(Joint water press)/ (Major principal σ)	0	< 0.1	0.1, - 0.2	0.2 - 0.5	> 0.5
		General conditions	Completely dry	Damp	Wet	Dripping	Flowing
	Rating		15	10	7	4	0

B. RATING ADJUSTMENT FOR DISCONTINUITY ORIENTATIONS (See F)						
Strike and dip orientations		Very favourable	Favourable	Fair	Unfavourable	Very Unfavourable
Ratings	Tunnels & mines	0	-2	-5	-10	-12
	Foundations	0	-2	-7	-15	-25
	Slopes	0	-5	-25	-50	

C. ROCK MASS CLASSES DETERMINED FROM TOTAL RATINGS					
Rating	100 ← 81	80 ← 61	60 ← 41	40 ← 21	< 21
Class number	I	II	III	IV	V
Description	Very good rock	Good rock	Fair rock	Poor rock	Very poor rock

D. MEANING OF ROCK CLASSES					
Class number	I	II	III	IV	V
Average stand-up time	20 yrs for 15 m span	1 year for 10 m span	1 week for 5 m span	10 hrs for 2.5 m span	30 min for 1 m span
Cohesion of rock mass (kPa)	> 400	300 - 400	200 - 300	100 - 200	< 100
Friction angle of rock mass (deg)	> 45	35 - 45	25 - 35	15 - 25	< 15

E. GUIDELINES FOR CLASSIFICATION OF DISCONTINUITY conditions					
Discontinuity length (persistence) Rating	< 1 m 6	1 - 3 m 4	3 - 10 m 2	10 - 20 m 1	> 20 m 0
Separation (aperture) Rating	None 6	< 0.1 mm 5	0.1 - 1.0 mm 4	1 - 5 mm 1	> 5 mm 0
Roughness Rating	Very rough 6	Rough 5	Slightly rough 3	Smooth 1	Slickensided 0
Infilling (gouge) Rating	None 6	Hard filling < 5 mm 4	Hard filling > 5 mm 2	Soft filling < 5 mm 2	Soft filling > 5 mm 0
Weathering Ratings	Unweathered 6	Slightly weathered 5	Moderately weathered 3	Highly weathered 1	Decomposed 0

F. EFFECT OF DISCONTINUITY STRIKE AND DIP ORIENTATION IN TUNNELLING**			
Strike perpendicular to tunnel axis		Strike parallel to tunnel axis	
Drive with dip - Dip 45 - 90°	Drive with dip - Dip 20 - 45°	Dip 45 - 90°	Dip 20 - 45°
Very favourable	Favourable	Very unfavourable	Fair
Drive against dip - Dip 45-90°	Drive against dip - Dip 20-45°	Dip 0-20 - Irrespective of strike°	
Fair	Unfavourable	Fair	

Table 3.1: Rock Mass Rating (After Bieniawski, 1989)

Rock mass class	Excavation	Rock bolts (20 mm diameter, fully grouted)	Shotcrete	Steel sets
I - Very good rock *RMR*: 81-100	Full face, 3 m advance.	Generally no support required except spot bolting.		
II - Good rock *RMR*: 61-80	Full face , 1-1.5 m advance. Complete support 20 m from face.	Locally, bolts in crown 3 m long, spaced 2.5 m with occasional wire mesh.	50 mm in crown where required.	None.
III - Fair rock *RMR*: 41-60	Top heading and bench 1.5-3 m advance in top heading. Commence support after each blast. Complete support 10 m from face.	Systematic bolts 4 m long, spaced 1.5 - 2 m in crown and walls with wire mesh in crown.	50-100 mm in crown and 30 mm in sides.	None.
IV - Poor rock *RMR*: 21-40	Top heading and bench 1.0-1.5 m advance in top heading. Install support concurrently with excavation, 10 m from face.	Systematic bolts 4-5 m long, spaced 1-1.5 m in crown and walls with wire mesh.	100-150 mm in crown and 100 mm in sides.	Light to medium ribs spaced 1.5 m where required.
V – Very poor rock *RMR*: < 20	Multiple drifts 0.5-1.5 m advance in top heading. Install support concurrently with excavation. Shotcrete as soon as possible after blasting.	Systematic bolts 5-6 m long, spaced 1-1.5 m in crown and walls with wire mesh. Bolt invert.	150-200 mm in crown, 150 mm in sides, and 50 mm on face.	Medium to heavy ribs spaced 0.75 m with steel lagging and forepoling if required. Close invert.

Table 3.2: Rock mass classes of the RMR system for rock tunnels with a 10m span (After Bieniawski, 1989)

(Equation 3.3) $Q = RQD/J_n \times J_r/J_a \times J_w/SRF$

Where RQD = Rock Quality Designation

J_n = Number of joint sets

J_r = Joint roughness number

J_a = Joint alteration number

J_w = Joint water reduction factor

SRF = Stress Reduction Factor

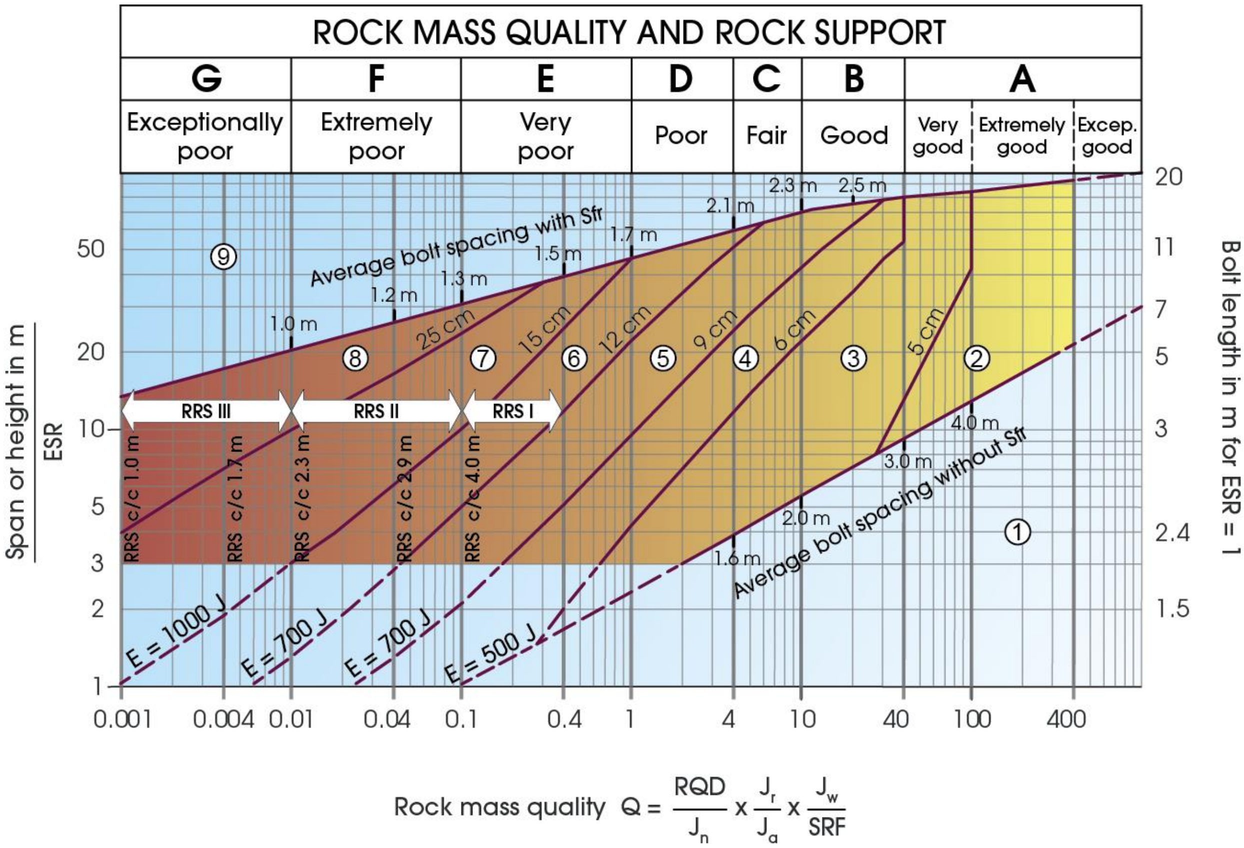

Figure 3.8: Necessary support for underground openings based on Q-values (After Liu, 2012)

3.4 Rock Mass Index

The Rock Mass Index (RMi) was created by Arild Palmstrøm in order to characterize rock mass strength as a construction material. Equation 3.4 shows how to calculate RMi which is the product of the uniaxial rock strength and the jointing parameter. The presence of discontinuities in a rock mass have the tendency to reduce the rocks inherent strength which this system takes into account. The joint roughness factor (jR) is equal to the product of joint smoothness (j_S) and joint waviness (j_W), both of which can be measured directly in the field and then rated. The applications of RMi are far reaching in rock engineering including fragmentation and blasting, stability and rock support assessments and TBM progress evaluations. The RMi can also be input into existing classification systems and into rock mechanics models and calculations (see Figure 3.9).

(Equation 3.4) $RMi = q_c * J_p$

Where q_c = uniaxial compressive strength of intact rock material [MPa]

J_p = jointing parameter

$= 0.2 * \sqrt{jC} * V_b^D$

$D = 0.37 * jC^{-0.2}$

$jC = jR/jA * jL$

Where jC = joint condition factor

V_b = block size

jR = joint roughness factor

jA = joint alteration factor

jL = joint size factor

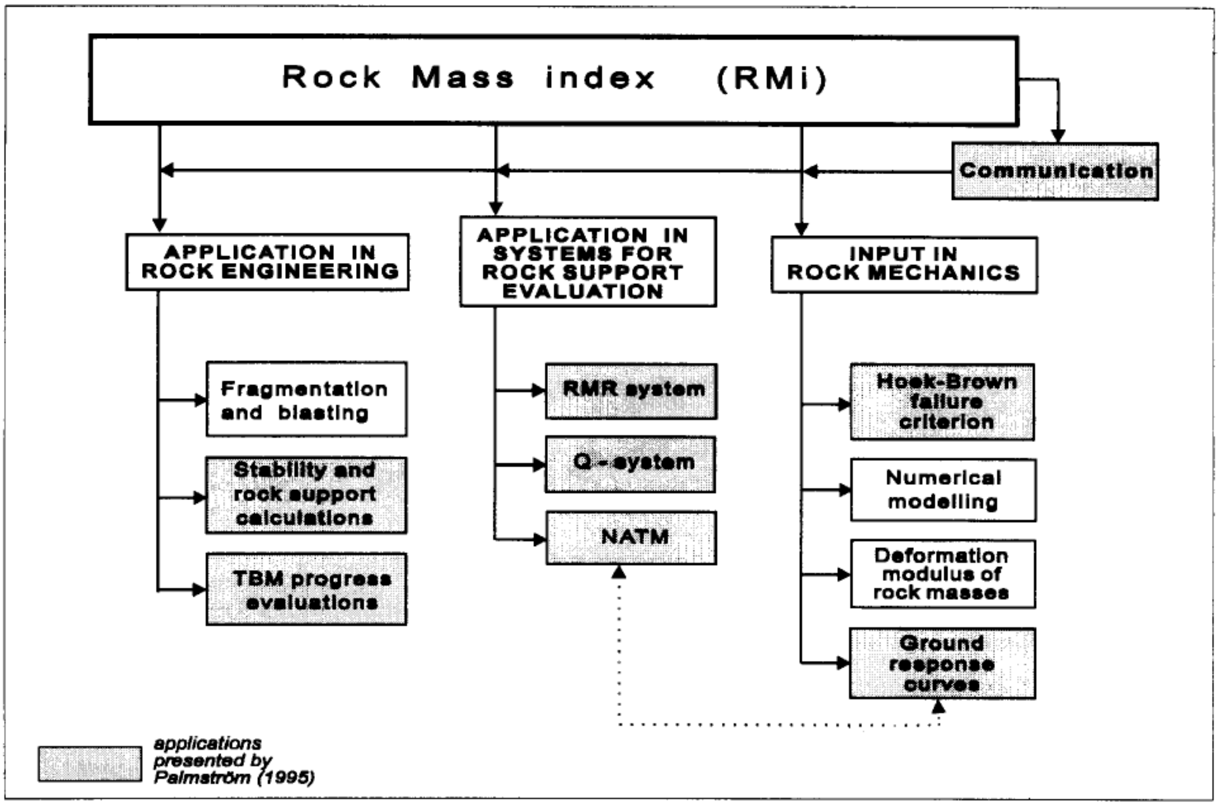

Figure 3.9: Applications of RMi

(After Palmstrøm, 1995)

3.5 Geological Strength Index

The Geological Strength Index (GSI) was created by Hoek and Brown in 1995 to classify both hard and weak rock masses. The GSI is unique in that it allows for the classification of a rock mass via a GSI chart (see Figure 3.10). According to Hoek, the GSI was meant to act as a replacement for the RMR which was inferior at describing poor quality rock masses and is based more on geological observations rather than numbers (Martin, 2002). The GSI chart was later quantified by Cai et al. in 2004 by incorporating block size (Vb) and the joint condition factor (Jc) which were both included in Palmstrøm's RMi system. Although the GSI system is very easy to use, its limitation is that it assumes the rock mass to be isotropic. "The GSI was designed primarily to be used as a tool to estimate the parameters in the Hoek-Brown strength criterion for rock masses, and deformability and strength of rock mass using relationship modified from other classification systems (Hoek et al., 2002 in Abbas et al., 2016).

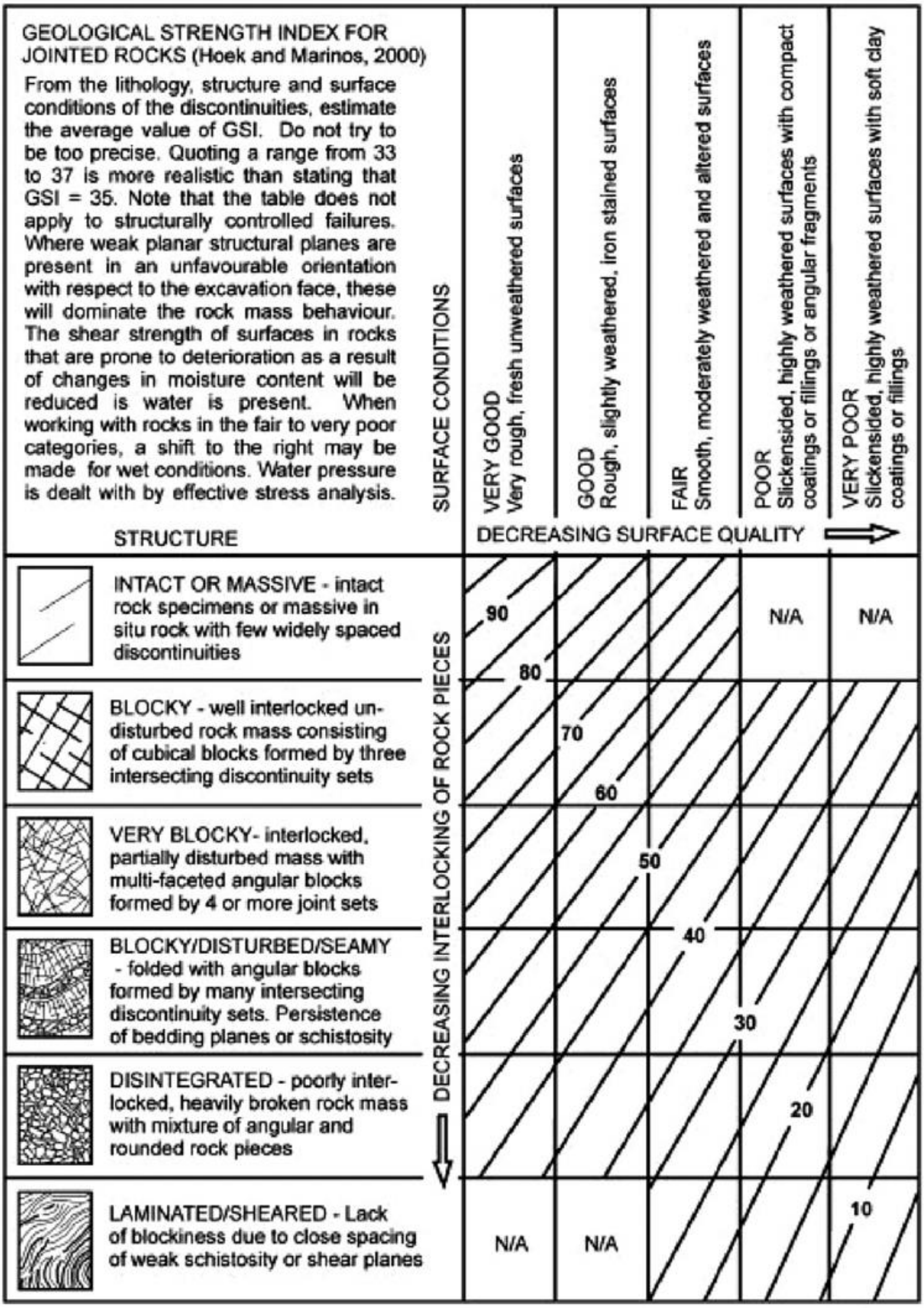

Figure 3.10: Geological Strength Index chart

(After Hoek et al., 1995)

3.6 Block Theory

The following section will discuss Block Theory in greater detail.

3.6.1 Discontinuity Controlled Failure

If a slope meets the kinematic test for sliding and is steeper than the friction angle, in theory it should fail, but it usually does not. This is because there is no block form (Figure 3.11). In order to form a removable block the number of joint surfaces and free surfaces must total at least four. This can be a combination of two joints and two free surfaces, three joints and one free surface or one joint and three free surfaces (Figure 3.12). Furthermore, it must daylight.

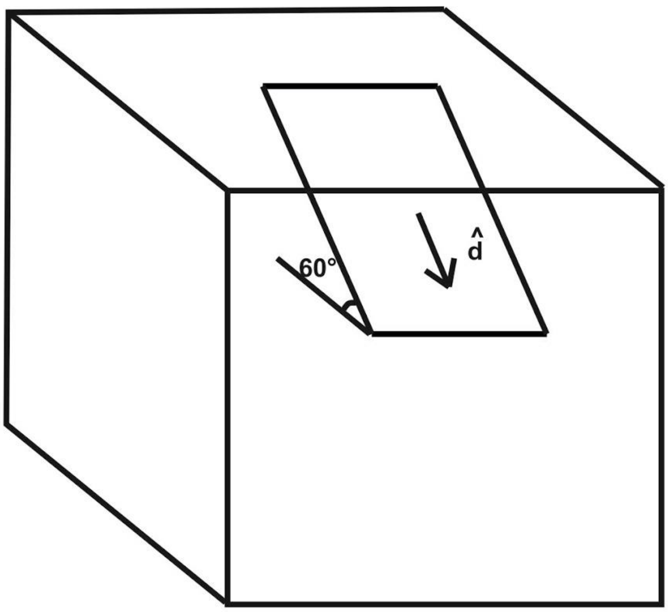

^

Figure 3.11: vector d = (dip direction, dip magnitude)

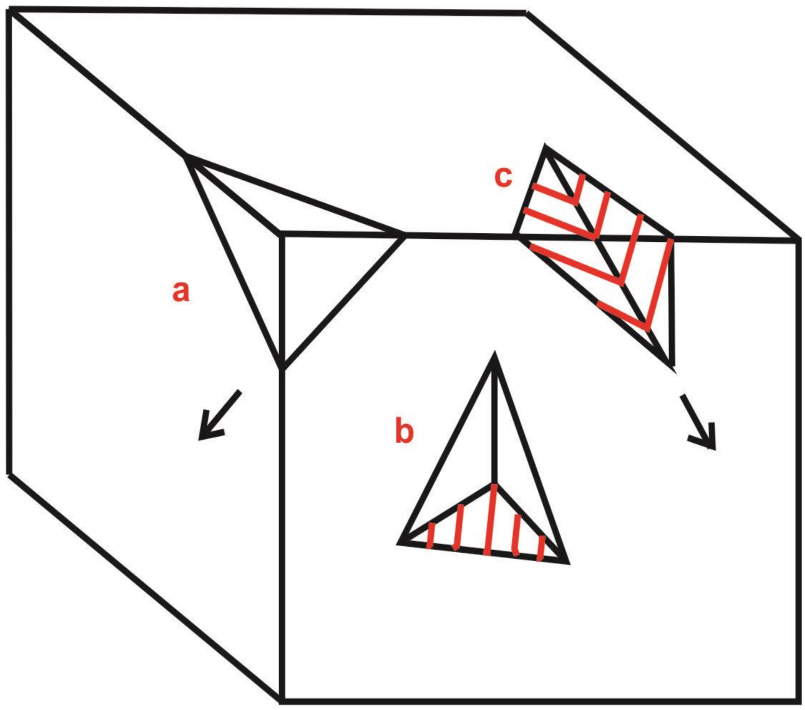

Figure 3.12: a - 1 Joint Surface + 3 Free Surfaces = 4;

b - 3 Joint Surfaces + 1 Free Surface = 4; c - 2 Joint Surfaces + 2 Free Surfaces = 4

(After Goodman, 1989)

3.6.2 Block Types

Block Theory identifies six block types which are separated into non-removable blocks and removable blocks. Non-removable blocks include joint blocks which have no intersection with the free surface, infinite blocks have no end and tapered blocks are tapered closed (Figure 3.13). Removable blocks consist of safe removable blocks which are stable even without friction, potential key blocks whose safety are provided by joint friction and key blocks which will fail if isolated (Figure 3.14). Block Theory identifies these removable blocks based on a kinematic test. Figure 3.15 shows the 5 block types as they appear on the cross-section of a tunnel opening.

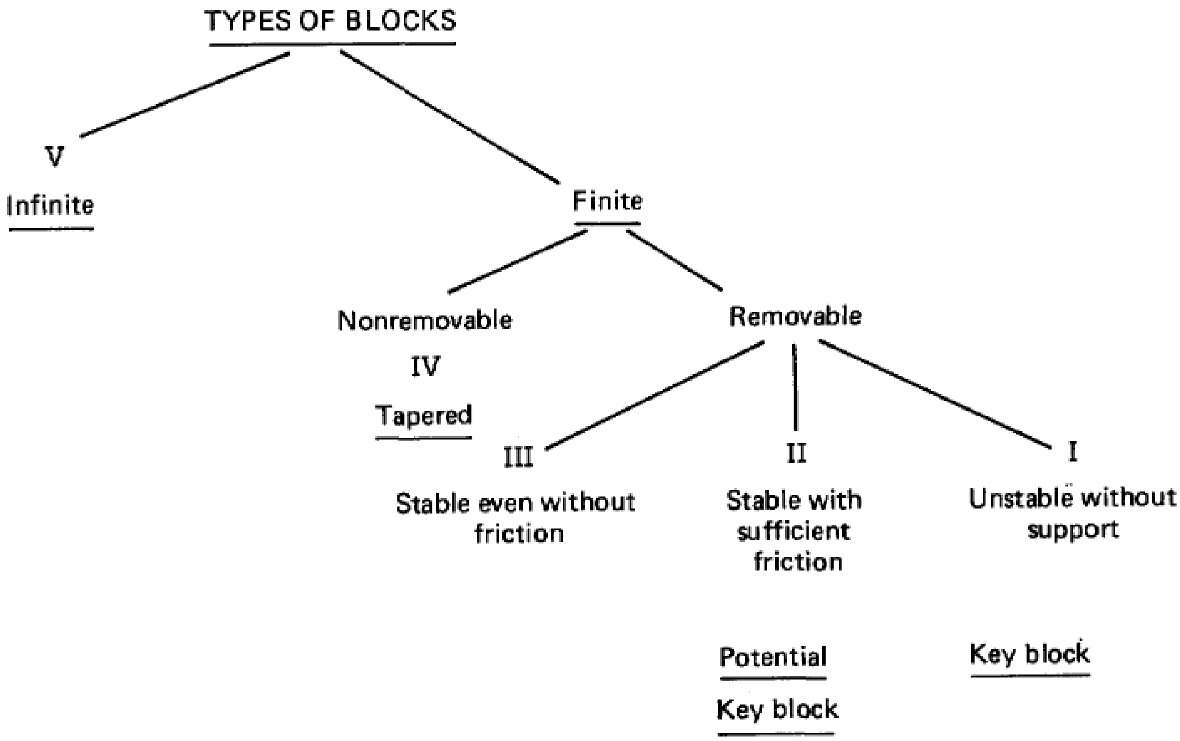

Figure 3.13: Types of Blocks (After Goodman and Shi, 1985)

Non-removable Blocks

VI – Joint Block (no intersection with free surface)

V – Infinite Block (no end)

IV – Tapered Block

Removable Blocks

III – Safe Removable Block (stable even without friction)

II – Potential Key Block (safety provided by joint friction)

I – Key Block (will fail if isolated)

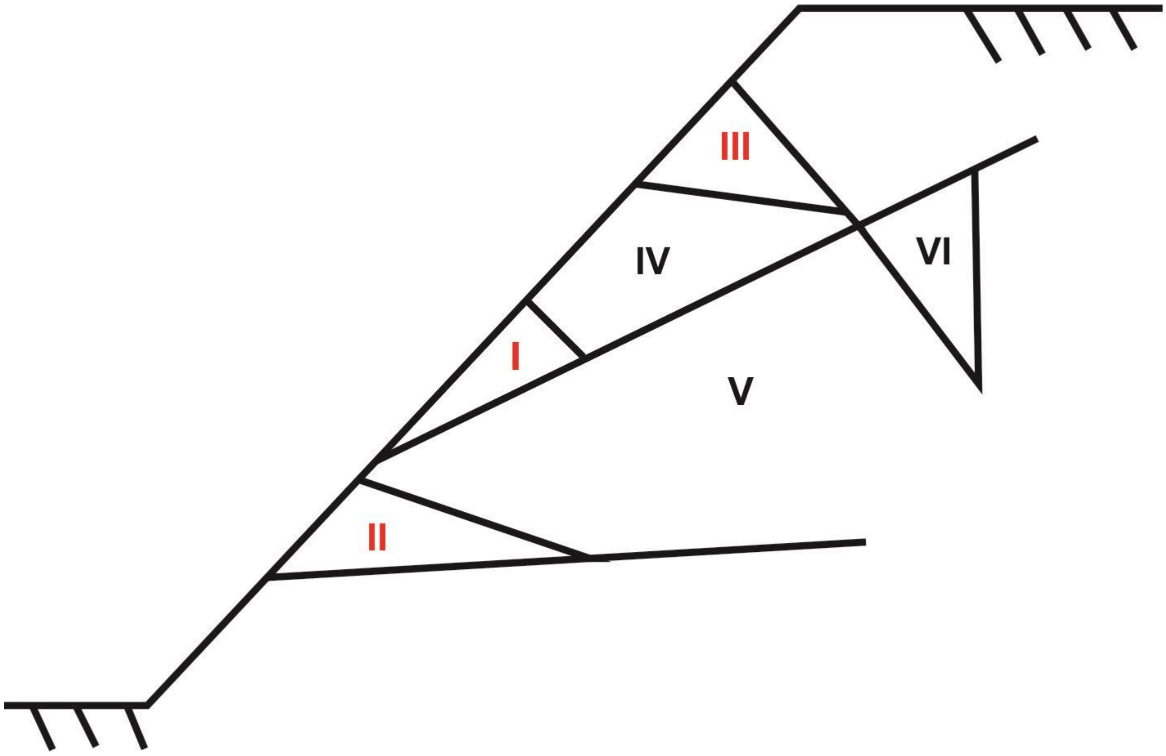

Figure 3.14: Block Types (After Liu, 2012)

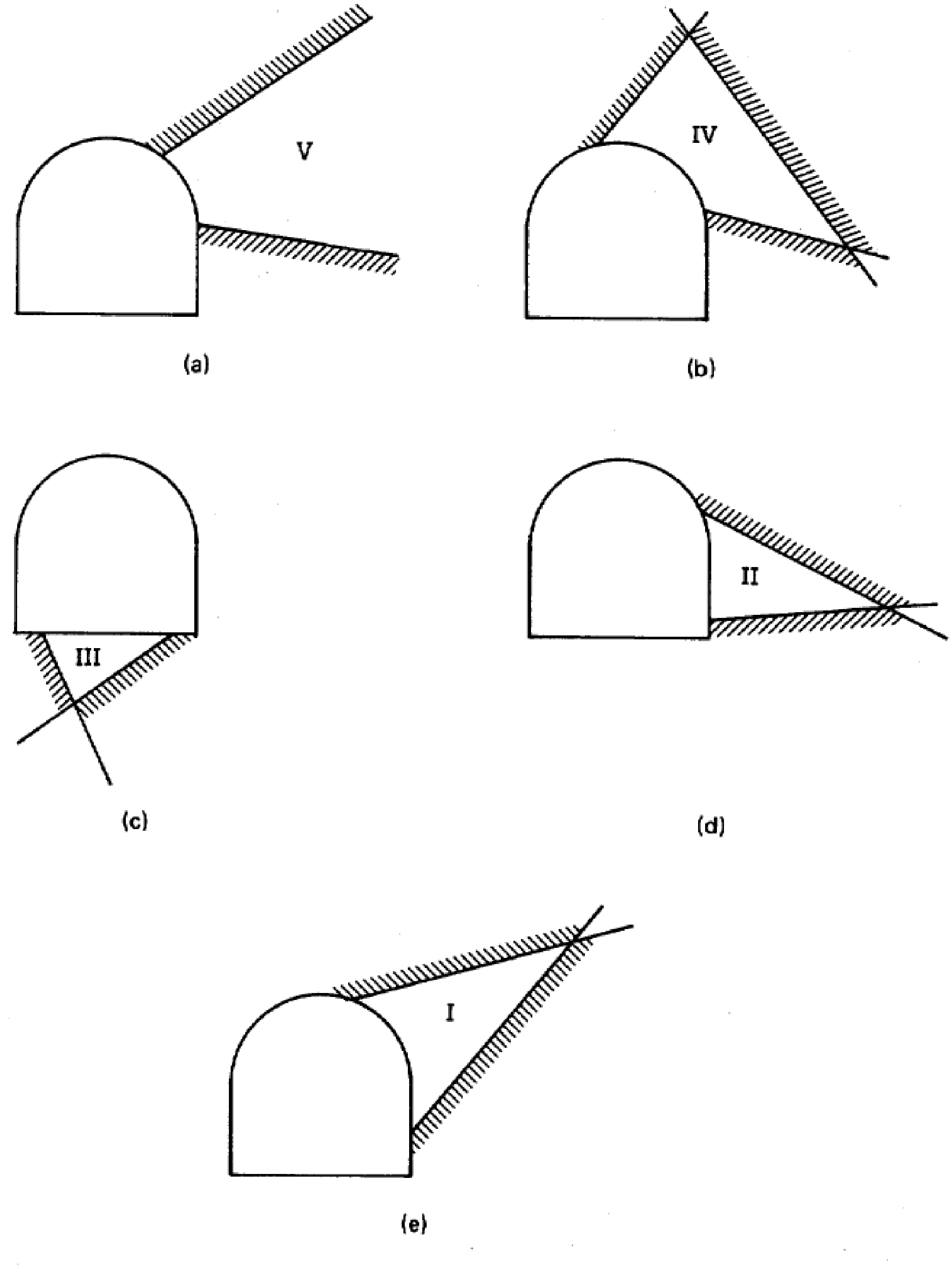

Figure 3.15: Types of Blocks: (a) infinite; (b) tapered; (c) stable; (d) potential key block; (e) key block

(After Goodman and Shi, 1985)

3.6.3 Shi's Theorem

According to Shi's Theorem, a block is removable if and only if there is no intersection of the Excavation Pyramid (EP) with respect to the Joint Pyramid (JP) or in the Space Pyramid (SP) (Goodman and Shi, 1985). In other words, the JP is totally within the SP. The Space Pyramid (SP) represents rock and the Excavation Pyramid (EP) free space such as a slope or excavation surface (Figure 3.15). Block Theory also requires several assumptions in order to work.

3.6.4 Assumptions of Block Theory

The assumptions of Block Theory are as follows (Goodman and Shi, 1985). 1, all joint surfaces are planar. 2, joint surfaces are continuous and do not terminate within the study area. 3, the system of joints is rigid therefore block deformation and distortion are negligible. 4, the orientation of joint sets and free surfaces must be determined as input parameters (Goodman and Shi, 1985). These planes can be shown graphically as great circles on a whole sphere stereographic projection (Figure 3.16).

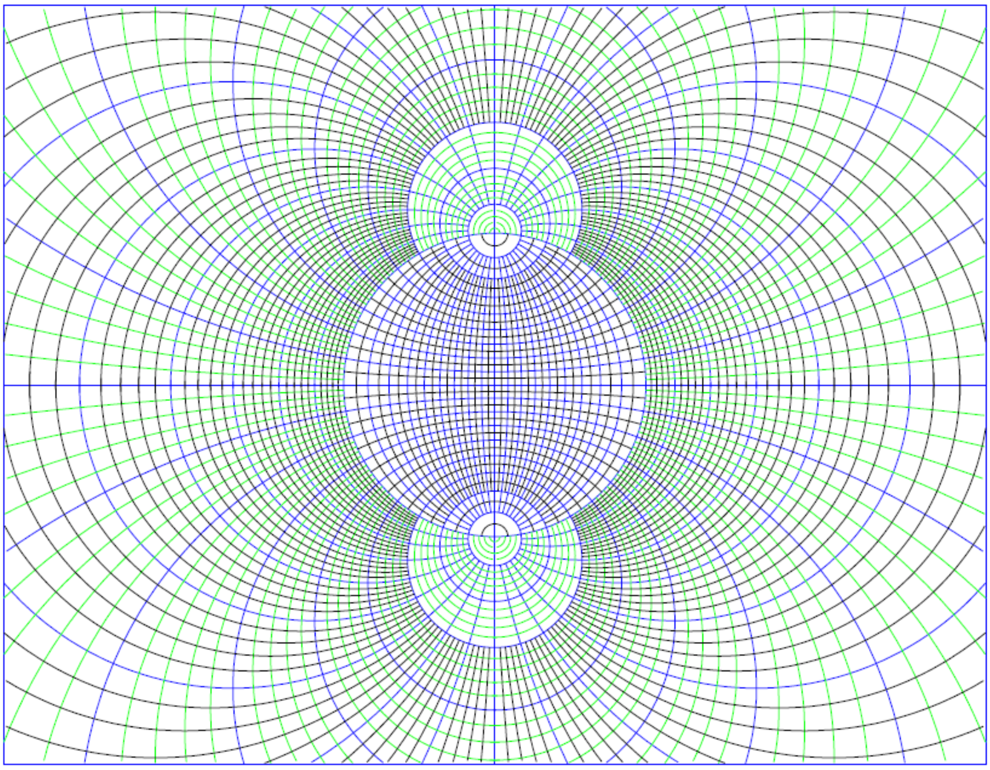

Figure 3.16: A stereonet of whole sphere projection (After Liu, 2012)

3.6.5 Block Theory Terminology

Joint Pyramid (JP) - A block formed by the intersections of joints, not including a free surface.

Excavation Pyramid (EP) - Represents rock side

Space Pyramid (SP) - Represents free space

Block Pyramid (BP) - A block formed by the intersections of joints and exposed to a free surface.

BP = JP ∩ EP; BP is the intersection of the JP with the EP for a given block

JP ∩ EP = ø; A block is finite if the block pyramid is empty

SP = ~EP; SP is complementary to EP

JP ⊂ SP; A BP block is only finite if its JP lies entirely within the SP

3.6.6 Removability of Blocks

Based on Block Theory's assumptions the following questions can be answered: how many 3-dimensional rock blocks are removable, what volume do these blocks have and what is their failure mode (Liu, 2012). The following equations show the correlation between the number of joint sets n and the Joint Pyramids JP on a stereographic projection. The number of JPs is given by Equation 3.5: given 4 joint sets there are 16 JPs. Equation 3.6 gives the amount of infinite or non-empty JPs, those which are not completely closed: for 4 joint sets there are 14 infinite JPs. Of these infinite JPs, 8 intersect the free plane EP (Equation 3.7) and 6 do not intersect the EP (Equation 3.8). Removable finite blocks BPs are given by Equation 3.9: for 4 joint sets there are 3 non-empty JPs which do not intersect an EP. The combination of these non-empty or infinite JPs with EP (=BP) represent block types I, II and III or potential removable blocks. Non-empty and non-removable JPs are given by Equation 3.10 and tapered empty JPs by Equation 3.11.

(Equation 3.5) 2^n

(Equation 3.6) $N_R = n^2 - n + 2$

(Equation 3.7) $2n$

(Equation 3.8) $n^2 - 3n + 2 = (n^2 - n + 2) - 2n$

(Equation 3.9)	$(n^2 - 3n + 2)/2$
(Equation 3.10)	$(n^2 - n + 2) - (n^2 -3n + 2)/2 = (n^2 + n + 2)/2$
(Equation 3.11)	$N_T = 2^n - (n^2 - n + 2)$

3.6.7 Block Codes

Block Theory uses both graphical and analytical means to identify removable blocks. These means are stereographic projection and vector methods (Liu, 2012). In order to identify where these removable blocks lie in space, the concept of half-space is very important. Using lower hemisphere stereographic projection “0” indicates the area above a plane and “1” indicates the area below a plane. If we consider a block with 4 planes with the half-space code 1010, it corresponds to a block in space below plane 1, above plane 2, below plane 3 and above plane 4. Using whole sphere projection, we use the description of half-space via the upper focal point. This means that the area within a plane is the lower half space and the area outside a plane is the upper half space. A block is defined by the intersection of its planes which are the upper or lower-spaces depending on perspective. Both the codes of the Joint Pyramids (JPs) and the Excavation Pyramids (EPs) must be considered when dealing with removable blocks or Block Pyramids:

3.7 Computer Programs

The following computer programs were reprogrammed by Dr. Qian Liu based on the original programs of Block Theory. With basic input parameters including but not limited to fracture set orientations, free plane orientations and fracture set spacing, the programs output visualisation and identification information. These include stereographic projection of fracture sets, joint pyramid codes, block visualisation, calculation of block volume, sliding and failure modes and key blocks in tunnels. The programs are described below in greater detail.

3.7.1 B02HPGL.EXE

B02HPGL.EXE uses the orientation data, dip and dip direction, of fracture sets and excavation planes to create a whole sphere stereographic projection of the input data. Fracture sets are represented as solid great circles, free surfaces as dashed great circles and the reference circle in red. The combination of three or more joint planes and a free surface create curved polygons that are the stereographic projection of a Joint Pyramid. The first output stereonet plot contains these Joint Pyramids and their JP codes which are labelled within each polygon. The second output plot shows potential removable blocks and their sliding mode where tick marks represent the sliding direction and numbers the kinematic modes.

3.7.2 B03HPGL.EXE

B03HPGL.EXE uses the orientation data of fracture sets, excavation planes as well as spacing data for these planes to visualize removable blocks in 3 dimensions and calculate block volume. The program will create the visualisation of a fracture block, a removable block or a tapered block depending on the input block digits. According to Block Theory, only Joint Pyramids completely within the free surface or here dashed great circles are potential removable blocks.

3.7.3 B10HPGL.EXE

B10HPGL.EXE uses the orientation data of fracture sets and orientation surfaces as well as the friction angle of these planes to determine sliding direction, mode and force for each Joint Pyramid. The program output consists of 6 tables where tables 5 and 6 provide information on removable Joint Pyramids. Within Table 5 a “1” means that the Joint Pyramid is removable with respect to the free plane and a “0” means it is not removable. Furthermore Joint Pyramids are separated into Type I, II and III which correspond to a positive sliding force, a negative sliding force and no failure mode respectively.

3.7.4 B25HPGL.EXE

B25HPGL.EXE uses the orientation data of fracture sets and the cross-sectional tunnel geometry, orientation and shape, to output key or removable blocks in order to determine tunnel support. The form of the tunnel can be chosen from a list. The program visualises the relative position of removable blocks on the curved tunnel shape. It operates under the assumption that gravity is the only force. The output is a visualisation of the removable block with the curved free surface as well as the position of that block within the tunnel cross-section.

3.7.5 B29HPGL.EXE

B29HPGL.EXE is to be used in combination with B25HPGL.EXE and operates under the same assumption: that gravity is the only force. It uses the fracture set orientations, tunnel orientation and tunnel shape to output a stereographic projection of all possible Joint Pyramids on the tunnel cross-section. The graphic shows the possible removable blocks on the two dimensional tunnel cross-section within the stereographic projection areas. Blocks are drawn in maximum size in order to aid in the assessment of support measures.

4 Procedure

The following section summarises the procedure of this study.

4.1 Point Cloud Model of the Arzberg Raabstollen Adit

The post-processing stage of the workflow commenced with the registered point cloud model of the Arzberg Raabstollen adit. The 12 scan positions have been merged into a single point cloud, registered within the local coordinate system and textured with digital images to add true colour (Figure 4.1). In order to merge the scans, the retro-reflectors acted as tie points between scan positions. The coarse registration and Multi-Station Adjustment (MSA), discussed in further detail in sections 2.2.1 and 2.2.2, resulted in a very high matching quality of the tie point retro-reflectors. This can be seen in the range of the standard deviation of the tie point positions 0.017 – 0.007m which has a mean of 0.0035m. In Figure 4.2, it is evident that although the 12 scans covered the extent of the adit, there are areas with lower point density.

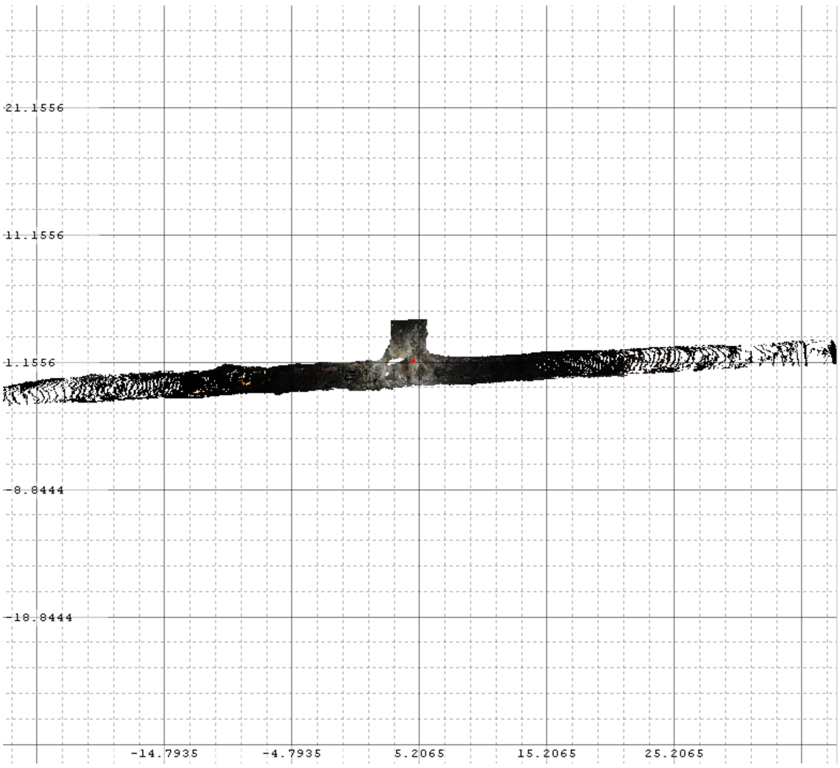

Figure 4.1: True colour 3D LiDAR point cloud model of the Raabstollen adit, plan view (Liu and Kieffer, 2012)

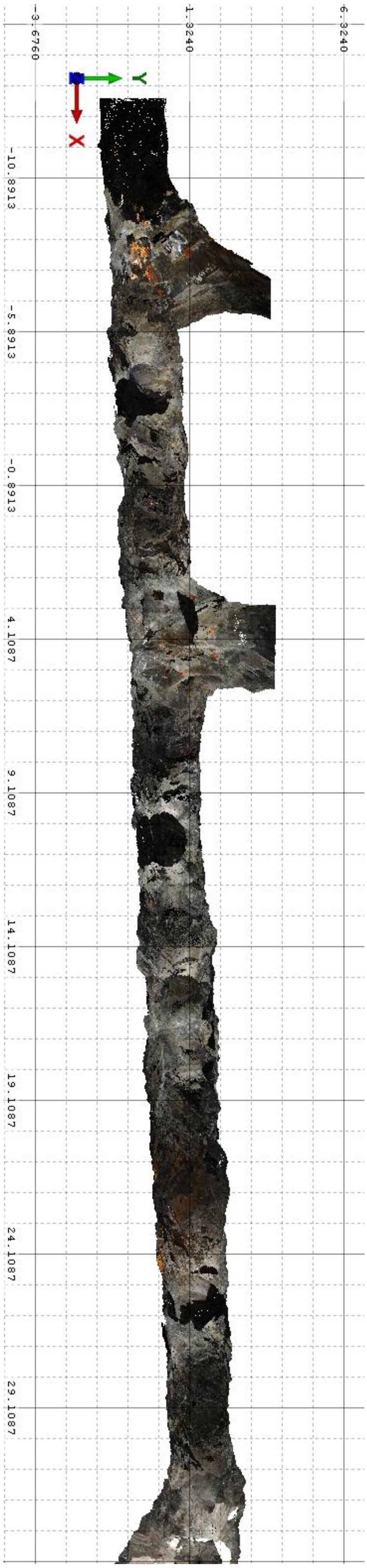

Figure 4.2: 12 scan positions merged as single point cloud in local coordinate system (After Liu and Kieffer, 2012)

In order to achieve accurate and precise structural measurements of fractures, the surface model needs to have uniform resolution. Triangulation creates a mesh out of the point cloud and results in surface models with uniform resolution. The cause of lower point density was discussed in further detail in section 2.2.3. Figures 4.9 through 4.12 show the result of triangulation: water-tight terrain models of the excavation surfaces.

Figures 4.3 through 4.8 are textured point clouds and meshes which clearly show fault zones, overbreaks, rock bolts holding schistosity and joints as well as removed rock wedges. Texturing of the model allows for simple identification of structural geometries and the scaled and oriented model makes measurement of these elements straightforward. In this study, removed rock wedges were identified in the model, such as in Figure 4.7, and the surfaces making up these wedges were constructed and subsequently measured. The orientation and spacing information of fractures, both gathered from the LiDAR model, allowed for the reconstruction, visualisation and volume calculations of the removed wedges/blocks.

What makes LiDAR preferential for tunnelling applications rather than photogrammetry? Foremost, laser scanning requires no light. The active and continuous collection of data with high accuracy and precision. And the ability to confidently add a quantitative element to rock mass structure.

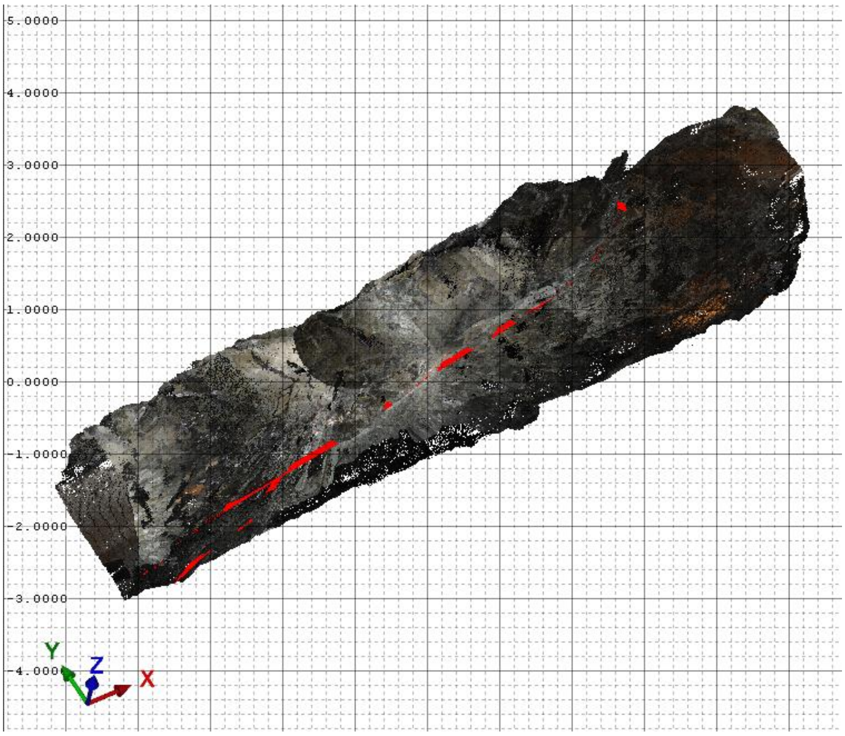

Figure 4.3: LiDAR model of the fault zone (red), viewed from above (After Liu and Kieffer, 2012)

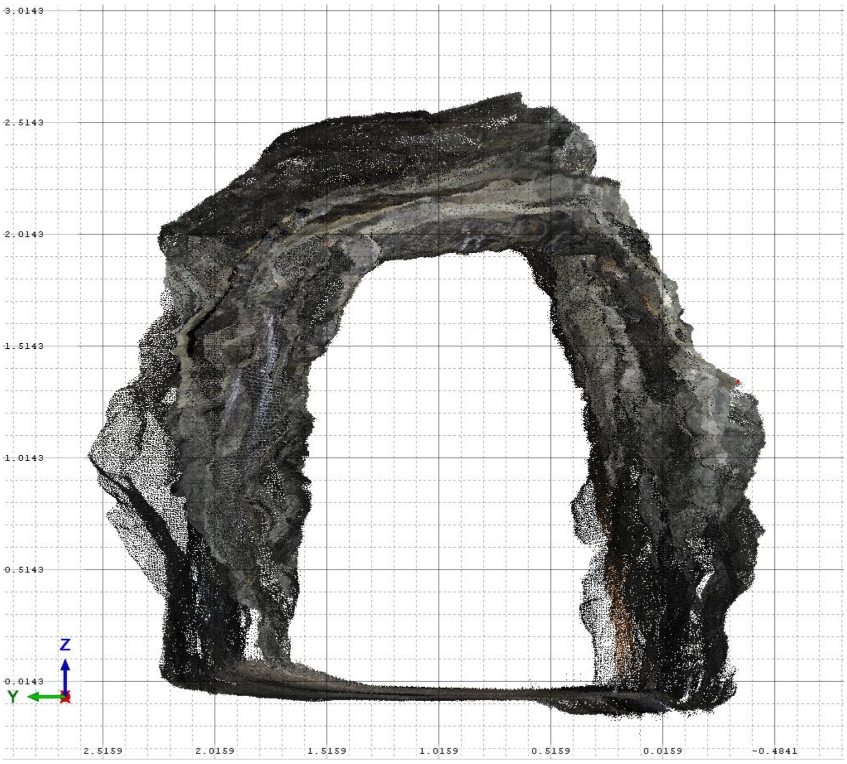

Figure 4.4: Overbreak due to fault zone, view to the east (After Liu and Kieffer, 2012)

Figure 4.5: Screenshot of 3D LiDAR point cloud model: rock bolts stabilising schistosity and joints, view to the east (After Liu and Kieffer, 2012)

Figure 4.6: Screenshot of 3D LiDAR point cloud model: overbreaks due to fault zone, view to the east (After Liu and Kieffer, 2012)

Figure 4.7: Screenshot of 3D LiDAR point cloud model: removed rock wedge right of reflector, view to the west (After Liu and Kieffer, 2012)

Figure 4.8: 3D textured mesh of fault zone, view to the east (After Liu and Kieffer, 2012)

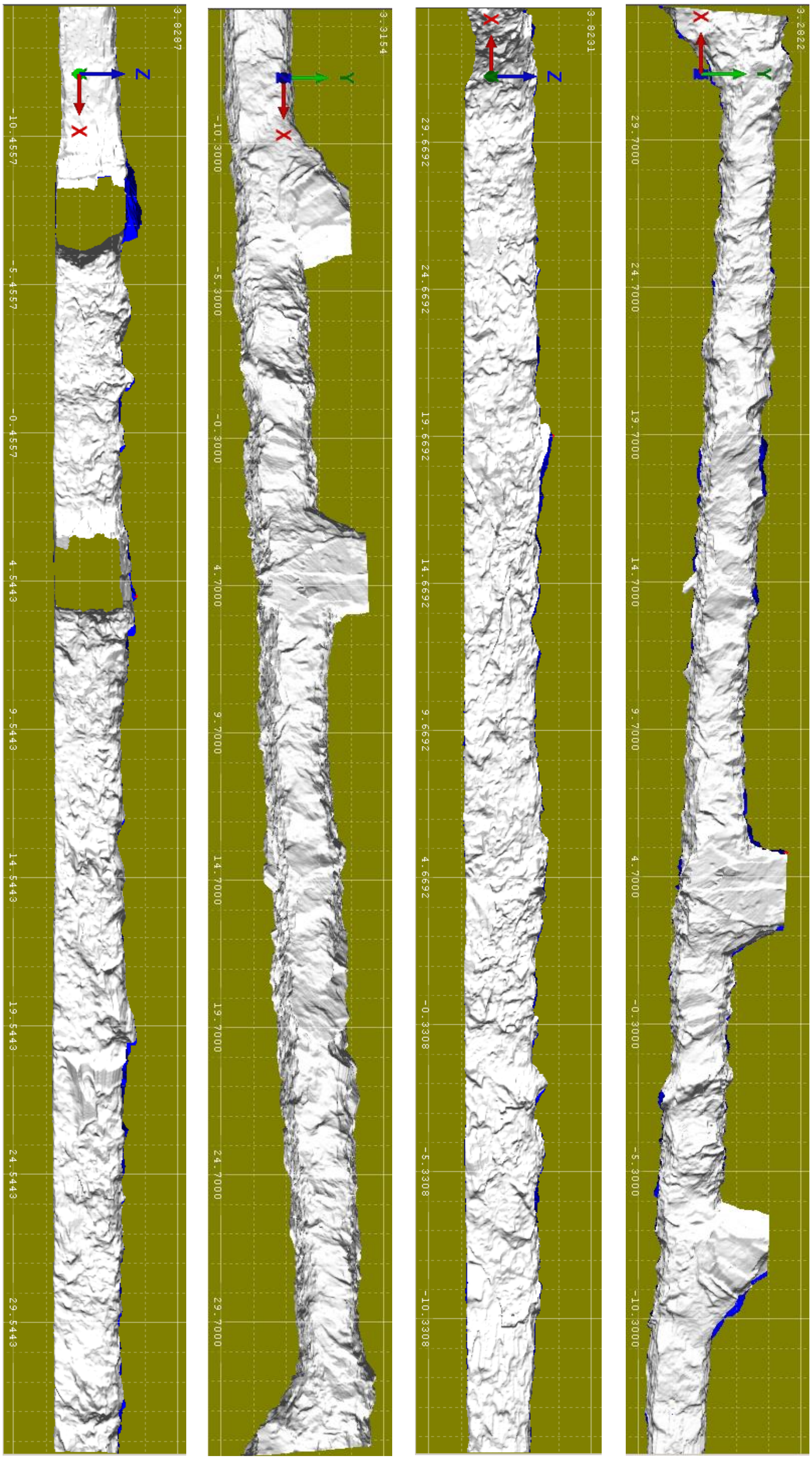

Figures 4.9 – 4.12: Terrain models of the excavation surfaces: first (left to right) side view of the north wall from inside, second plan view of the whole surface model, third side view of the south wall from inside and fourth bottom view towards roof (After Liu and Kieffer, 2012)

4.2 Creating Original 81 Blocks

The first part of the procedure in RiSCAN PRO involved the creation of 81 blocks. Initially, the discontinuities making up each block were constructed. Once constructed, the spacing's of the individual discontinuities were measured. The blocks were then defined by their Block Pyramid Codes. Each block was then visualized and its volume calculated using B03HPGL.EXE.

4.2.1 Constructing Discontinuities

RiSCAN PRO allows for the construction of discontinuities by selecting a plane which has a nearly homogeneous orientation. Once an area has been selected one can rename the plane, change its size, modify its location/orientation in space and simply look at the info window to get orientation data for that plane. Using this feature, planes of similar orientation (dip and dip direction) can be placed into groups by colour coding them. Planes making up a single removable block can be named accordingly. The following steps show how to construct such a plane: from selection mode (Figure 4.13), to creating a new plane object (Figure 4.14) to modifying orientation and position (Figure 4.15).

1. Press Selection Mode - Select the plane of interest

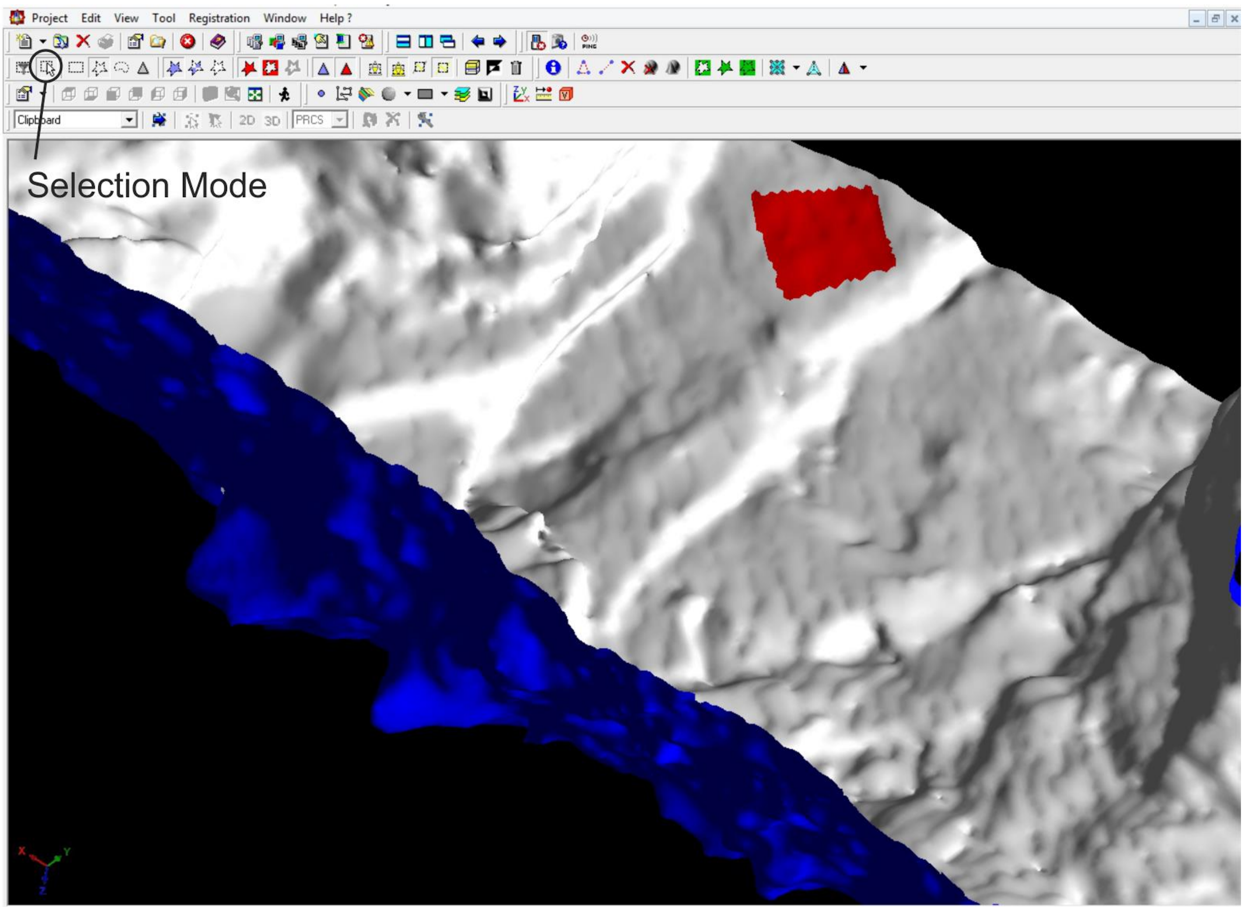

Figure 4.13: Selection Mode

2. Press Create new plane object - Scroll down to from selected area (limited)

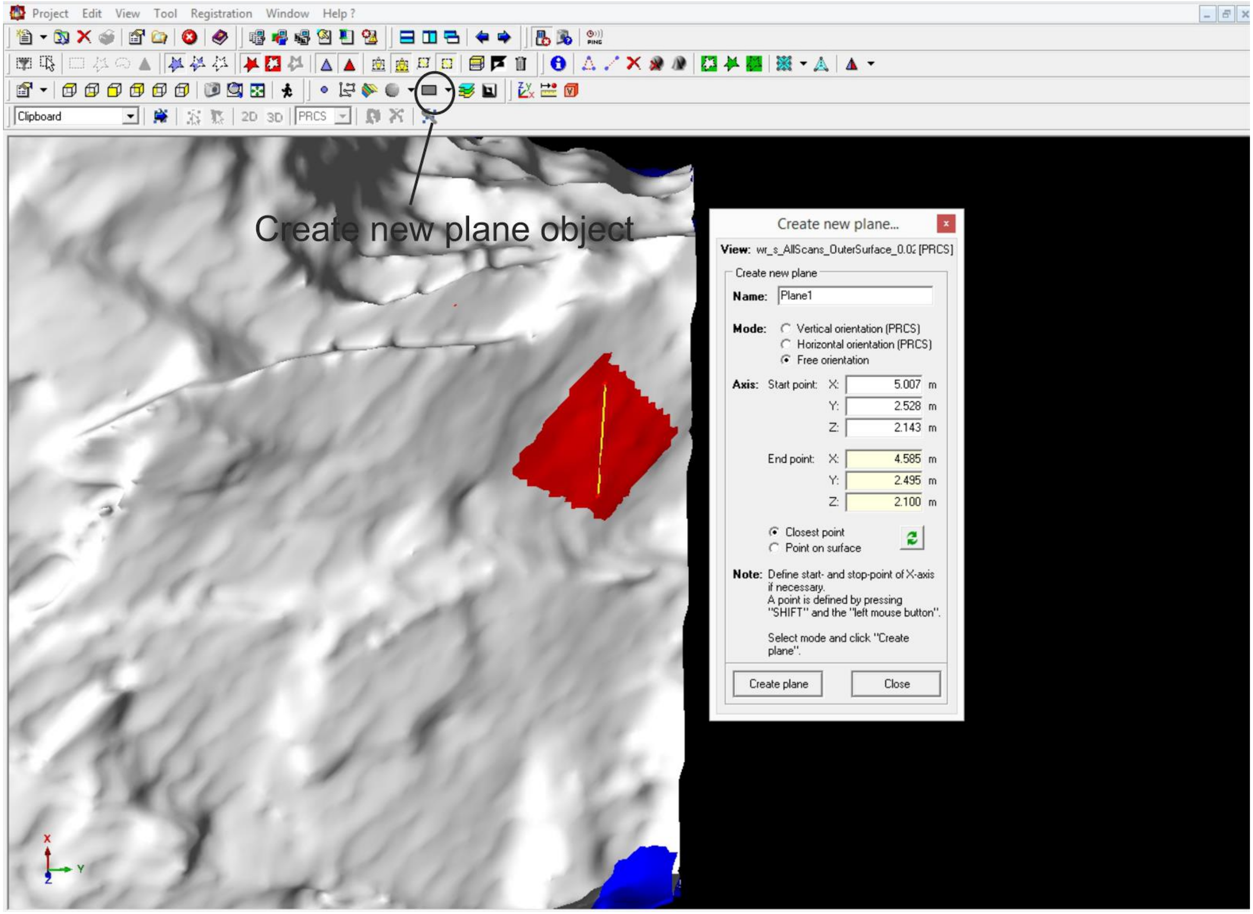

Figure 4.14: Create new plane object from select area limited

3. Select start- and end-points - Hold down the Shift key and select start- and end-points then click create plane. The new plane is visible in the Object Inspector window. Rename new plane.

By right clicking the plane in the Object Inspector window the position and orientation of the plane can be changed. The steps are listed below.

1. Select Modify orientation and position
2. Select between translate and rotate
3. Click on x-, y- or z-axis to move - Change offset values depending on direction of movement (positive or negative) along axis and value depending on magnitude of displacement or rotation.

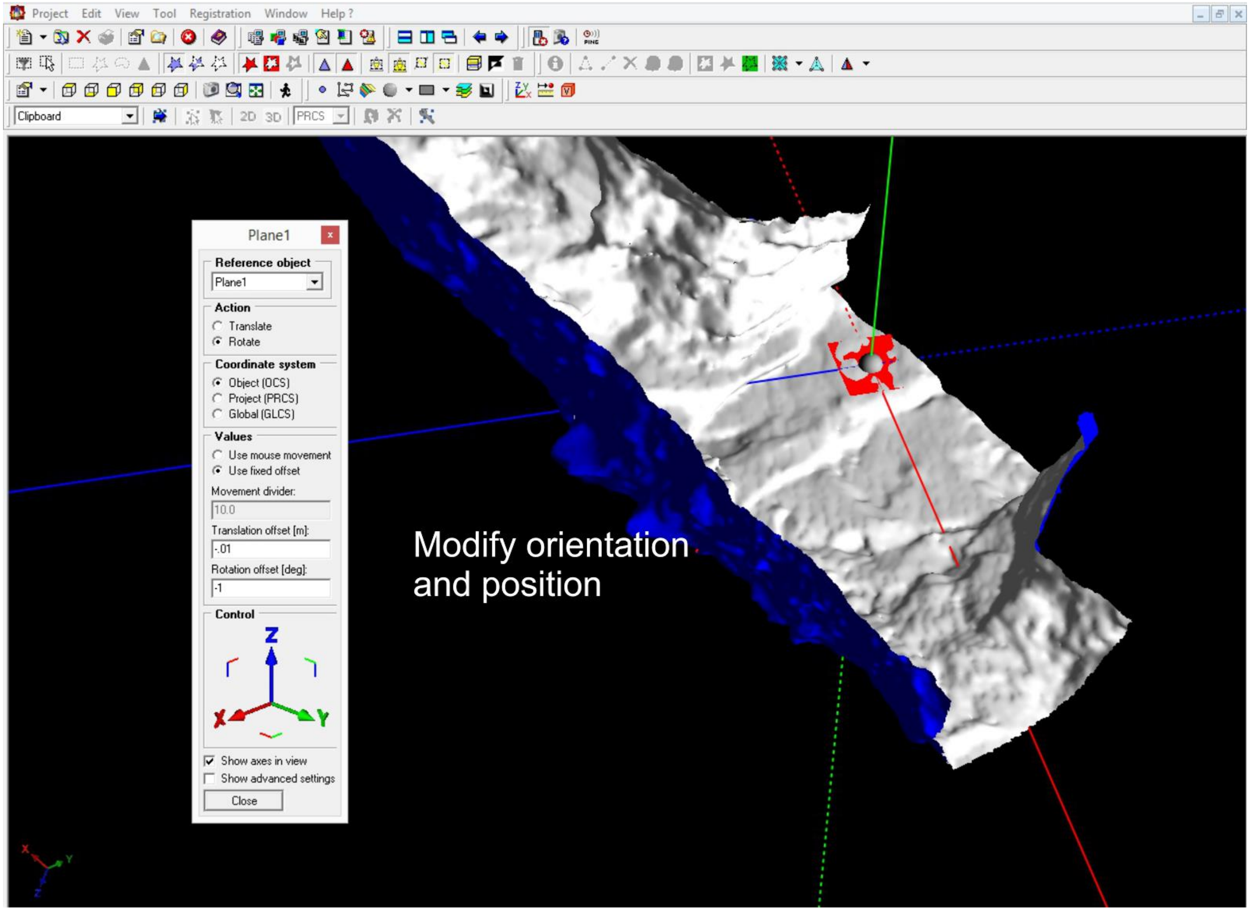

Figure 4.15: Modify orientation and position

Select the plane of interest and information about that plane are listed in the Info window. Information includes the area of the plane, dip angle, dip direction, etc.

4.2.2 Measuring Spacing of Discontinuities

RiSCAN PRO allows you to measure the distance between two points or the distance between a point and a plane. When doing so it is important that the orthogonal camera mode is selected so that the true distance is measured. In order to measure the spacing's of individual discontinuities of a block, the distance from point to plane is selected. The normal distance of the plane to the farthest point on the opposite side of the block constitutes the spacing of that plane. Figure 4.16 below shows the spacing measured for the light green discontinuity from its normal to the opposite side of the block and the spacing measured from the dark green discontinuity from its normal to the free surface of the block which has been removed in order to see inside the block. Using this method, spacing's for discontinuities of individual blocks were measured.

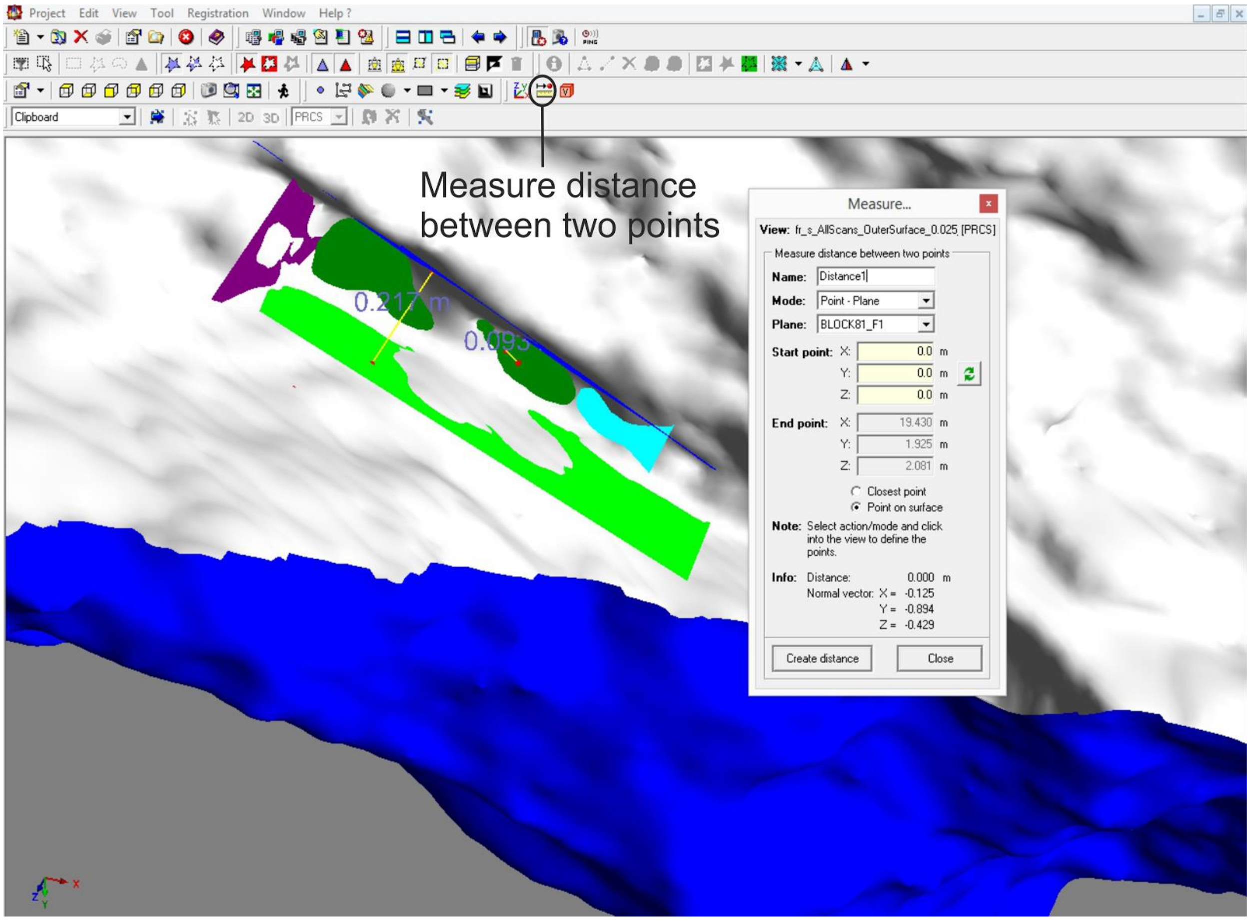

Figure 4.16: Measure distance between two points

4.2.3 Determining Block Pyramid Codes for Blocks

Block Pyramid Codes or BP-Codes for individual blocks were determined after all discontinuities of a block had been mapped out and their discontinuity spacing's measured. BP-Codes are made up of Joint Pyramid Codes and Excavation Pyramid Codes where the former represents the discontinuities that make up the block and the latter the free surface. In this study we are working with a lower hemisphere stereographic projection where a "0" represents the upper half space of a plane and a "1" the lower half space of a plane. Block 53 in Figure 4.17 below is shown as an example of how the BP-Code was determined. Block 53, which is made up of 5 discontinuities and 1 free surface has a BP-Code of 6 digits.

Block 53 has the following JP-Code:

- Block 53 is in the lower half space of Discontinuity 1 (yellow) → 1
- Block 53 is in the lower half space of Discontinuity 2 (black) → 1
- Block 53 is in the upper half space of Discontinuity 3 (green) → 0

- Block 53 is in the lower half space of Discontinuity 4 (red) → 1
- Block 53 is in the upper half space of Discontinuity 5 (blue) → 0

Therefore Block 53 has the following JP-Code, 11010.

Block 53 has the following EP-Code:

- Block 53 is in the upper half space of the Free Surface (not shown) → 0

Therefore Block 53 has the following BP-Code, 11010 0.

Each of the 81 modelled blocks were designated a half space code. Now that all modelled blocks have orientation data for their discontinuities as well as spacing and half space codes, their volumes were calculated using B03HPGL.EXE.

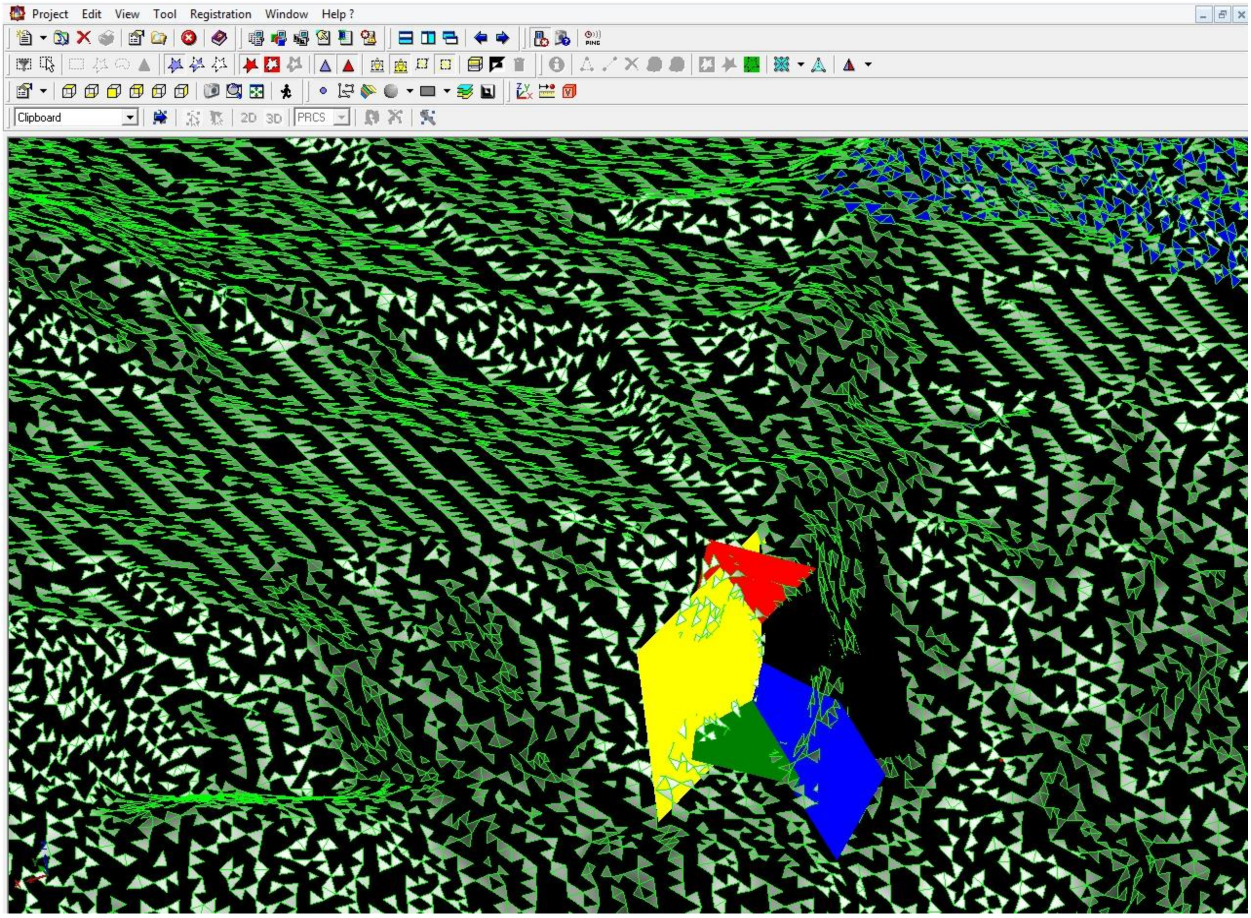

Figure 4.17: Block 53

4.2.4 Visualization and Volume Calculation

Using the B03HPGL.EXE program developed by Dr. Liu, we were able to calculate the volume and visualize each of the blocks. By inputting the orientation and spacing data for the discontinuities and free surface, the program outputs the volume and form of each block. The program also allows you to select the view at which the block will be displayed. This orientation is called the "projective orientation vector" and can be calculated with the following equations (Equations 4.1, 4.2 and 4.3) and is illustrated in Figure 4.18:

(Equation 4.1) X(East): $A = \sin\alpha \sin\beta$

(Equation 4.2) Y(North): $B = \sin\alpha \cos\beta$

(Equation 4.3) Z(Up): $C = \cos\alpha$

Where α is the dip and β is the dip direction

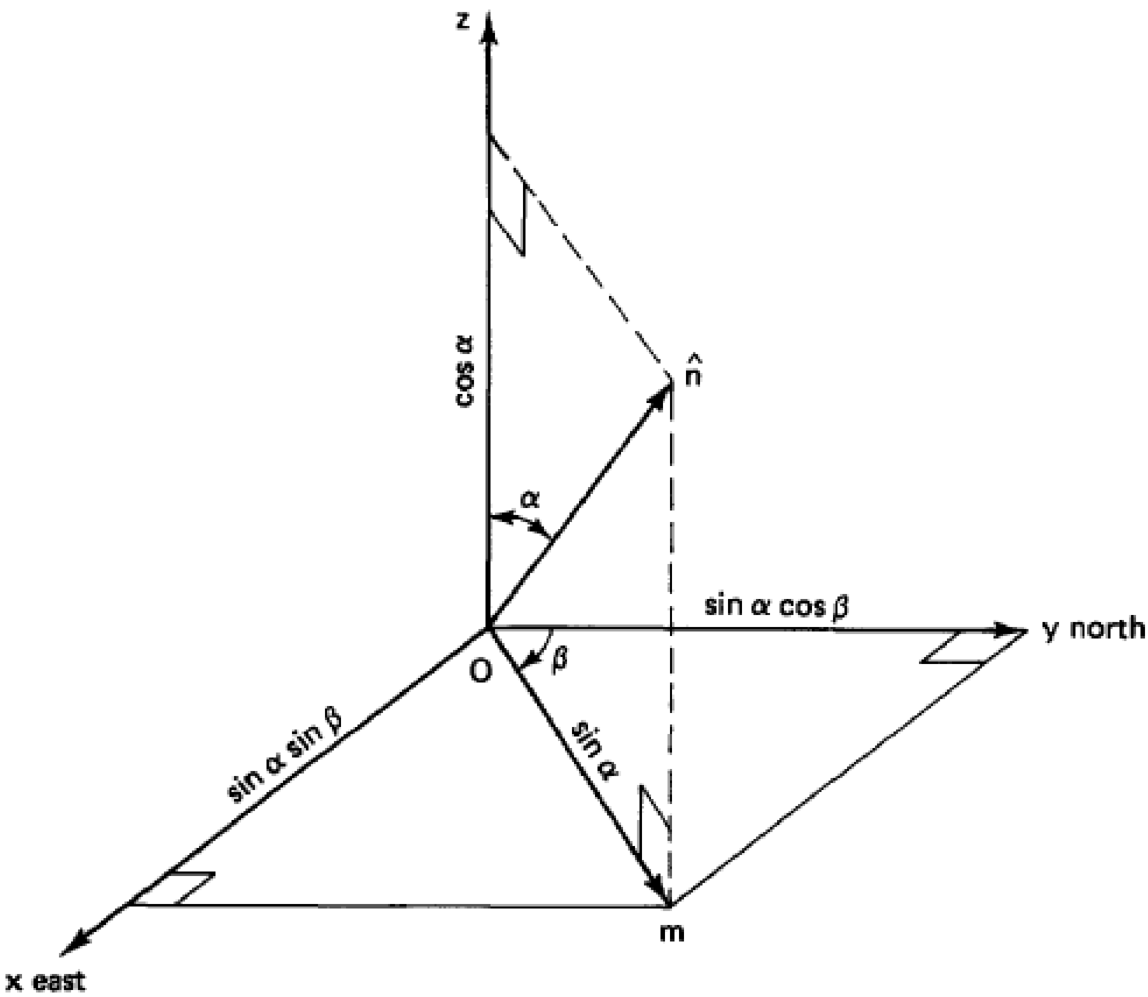

Figure 4.18: Coordinate system to calculate "projective orientation vector" (After Goodman and Shi, 1985)

Figure 4.19 shows the volume and form of Block 53 as output by B03HPGL.EXE.

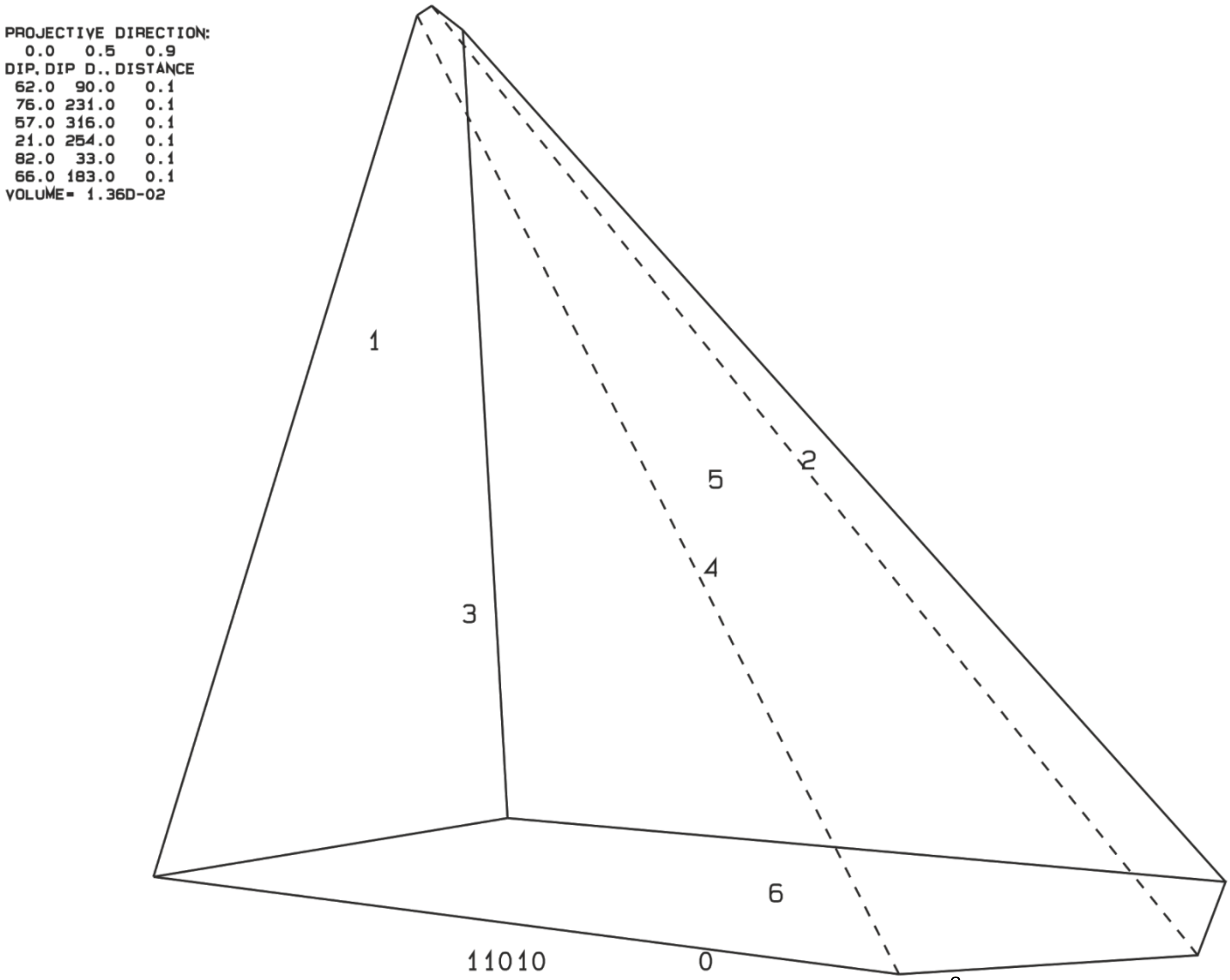

Figure 4.19: Block 53 form and volume; 0.0136m^3

4.3 Testing the Reproducibility of Modelled Blocks

In summary, 81 failed blocks have been modelled into the Arzberg laser scan model using the software RiSCAN PRO. For each block, the orientations of their discontinuities and free surfaces and their spacing's have been determined in RiSCAN PRO. Once constructed, the BP-Codes for each block were determined. The following steps in the procedure test the reproducibility of these blocks using Block Theory. In order to do so the Arzberg tunnel was divided into a smaller roof section located in the west of the tunnel designated Area 1 (Figure 4.20).

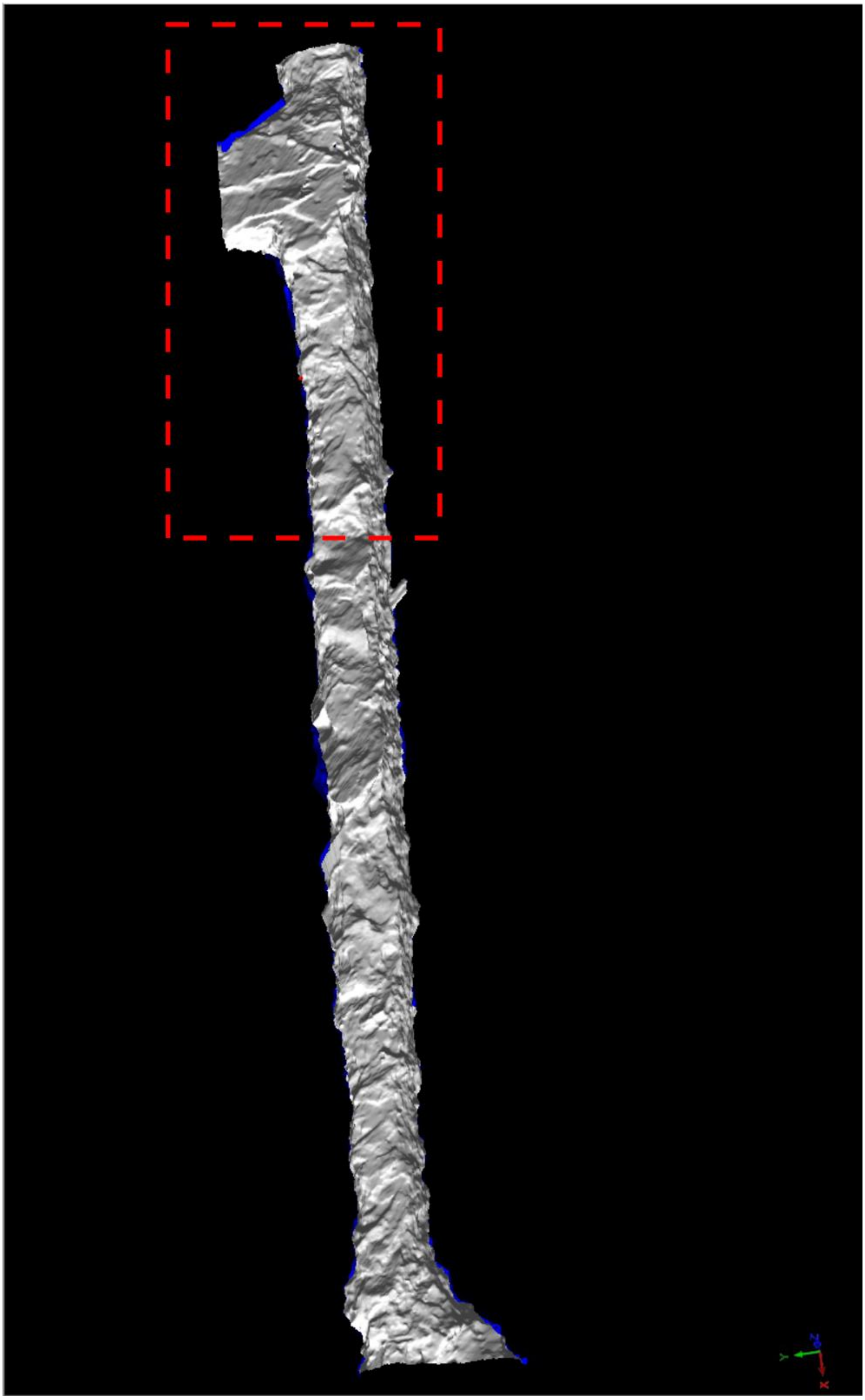

Figure 4.20: Location of Area 1 on Arzberg roof

4.3.1 Creating Joint Sets

Area 1 contains 16 of the 81 modelled blocks. The 16 blocks were removed from the model and typical discontinuities were created throughout the area. Discontinuities of similar orientation were colour-coded and placed into sets. Furthermore, the sets were broken down into various types: joints, foliation surfaces, fault zones, slickenslides, etc. Figure 4.21 shows Area 1 with the original 16 blocks. Figure 4.22 shows Area 1 with all the constructed discontinuities split into sets. Each colour represents a different set. For each set, at least 20 planes were constructed and their orientation data were plotted on stereonets using software called Dips and their average orientations were calculated. Table 4.1 shows the resulting orientation data for the 5 typical sets within Area 1. Figures 4.23 through 4.27 show density clusters of individual joint sets with great circles showing the unweighted average orientation of each set.

Joint Set	Colour	Dip	Dip Direction	Spacing [m]
J1	Green	40	321	0.24
F1	Red	8	322	0.05
J2	Yellow	68	101	0.53
J3	Black	56	225	0.31
J4	Blue	55	42	0.32

Table 4.1: Average orientation and spacing of 5 discontinuity sets of Area 1

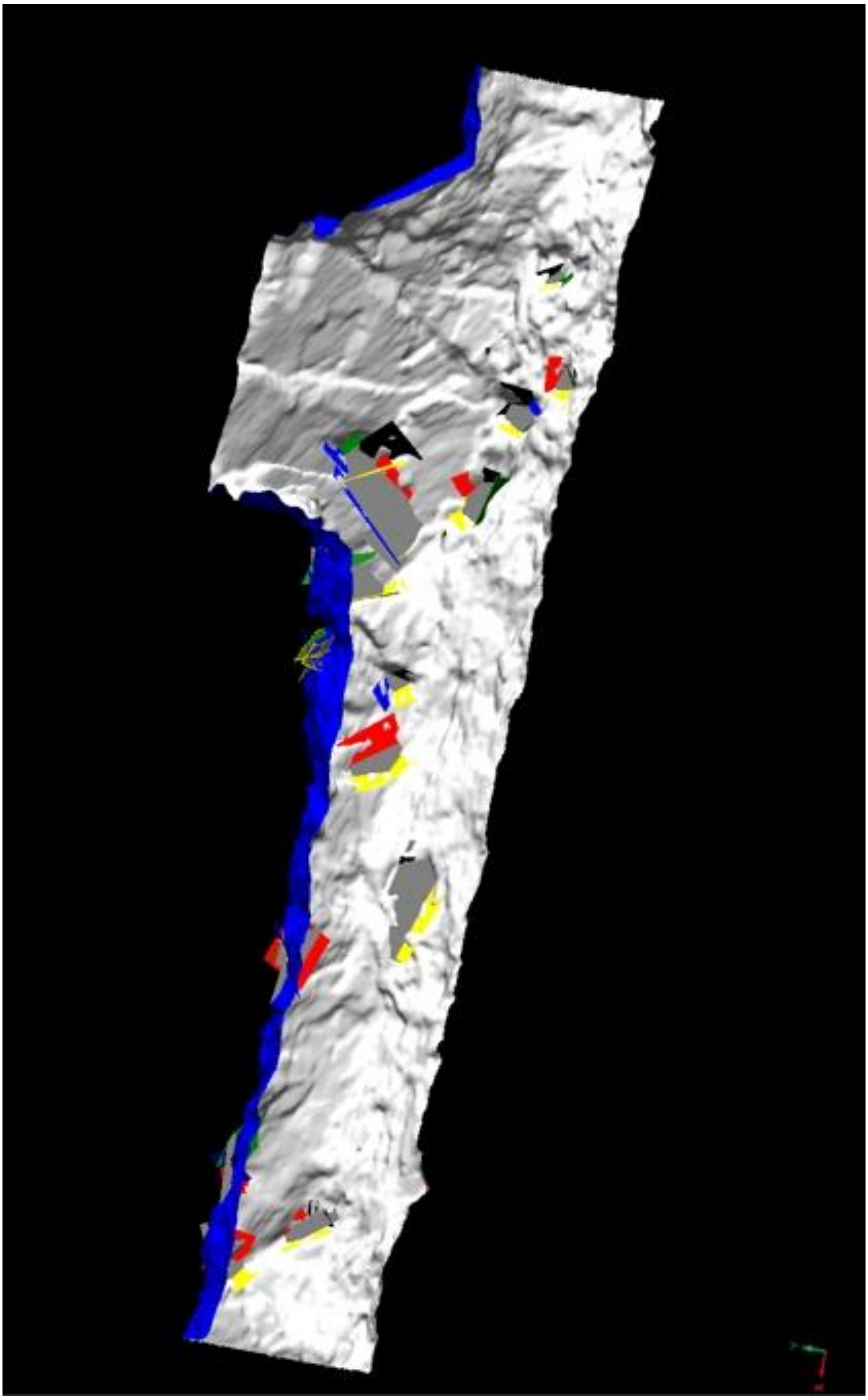

Figure 4.21: Area 1 with original 16 modelled blocks

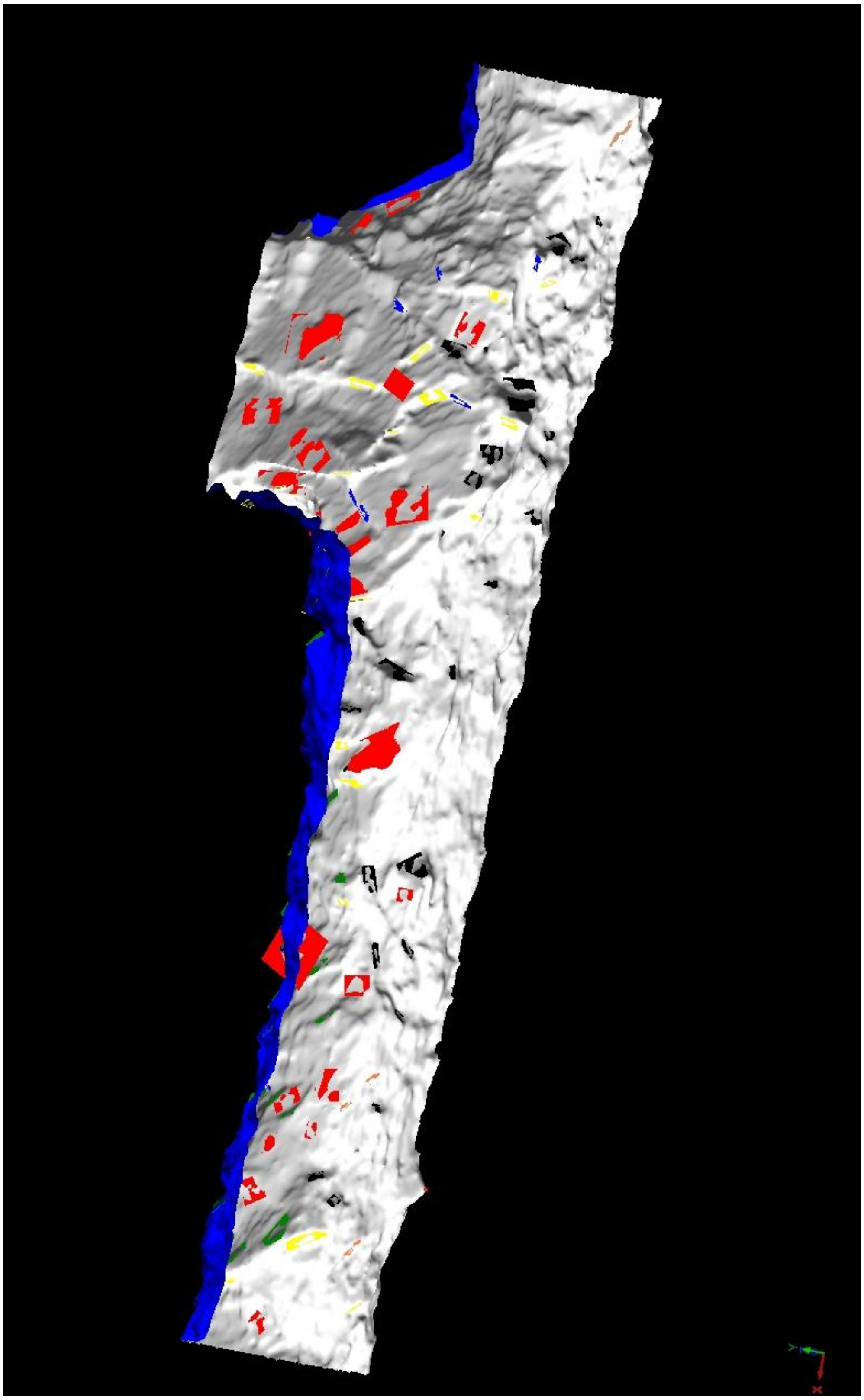

Figure 4.22: Area 1 with 5 modelled joint sets (J1: green, F1: red, J2: yellow, J3: black, J4: blue)

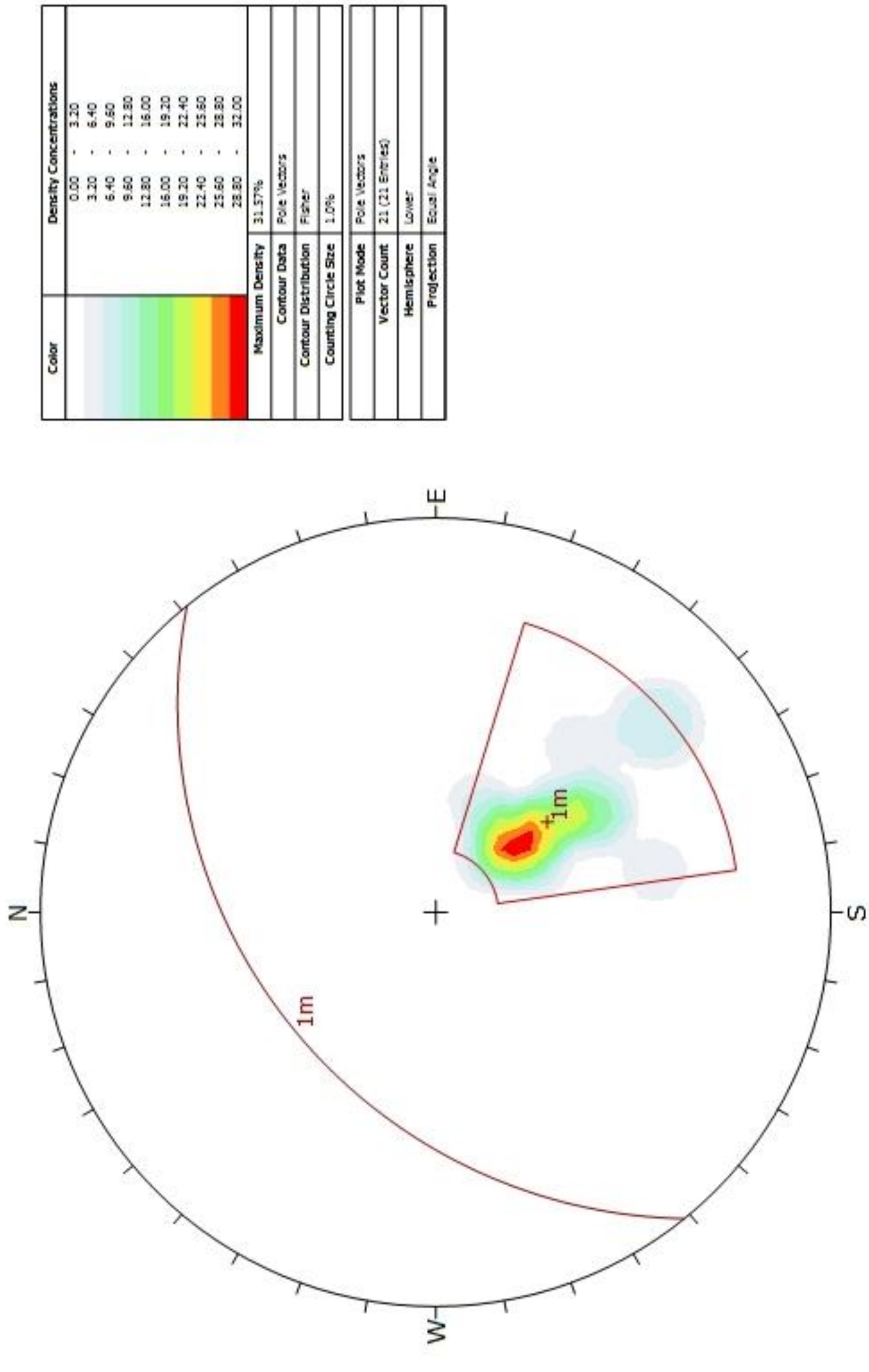

Figure 4.23: Average orientation of Joint Set 1; 40/321 (green)

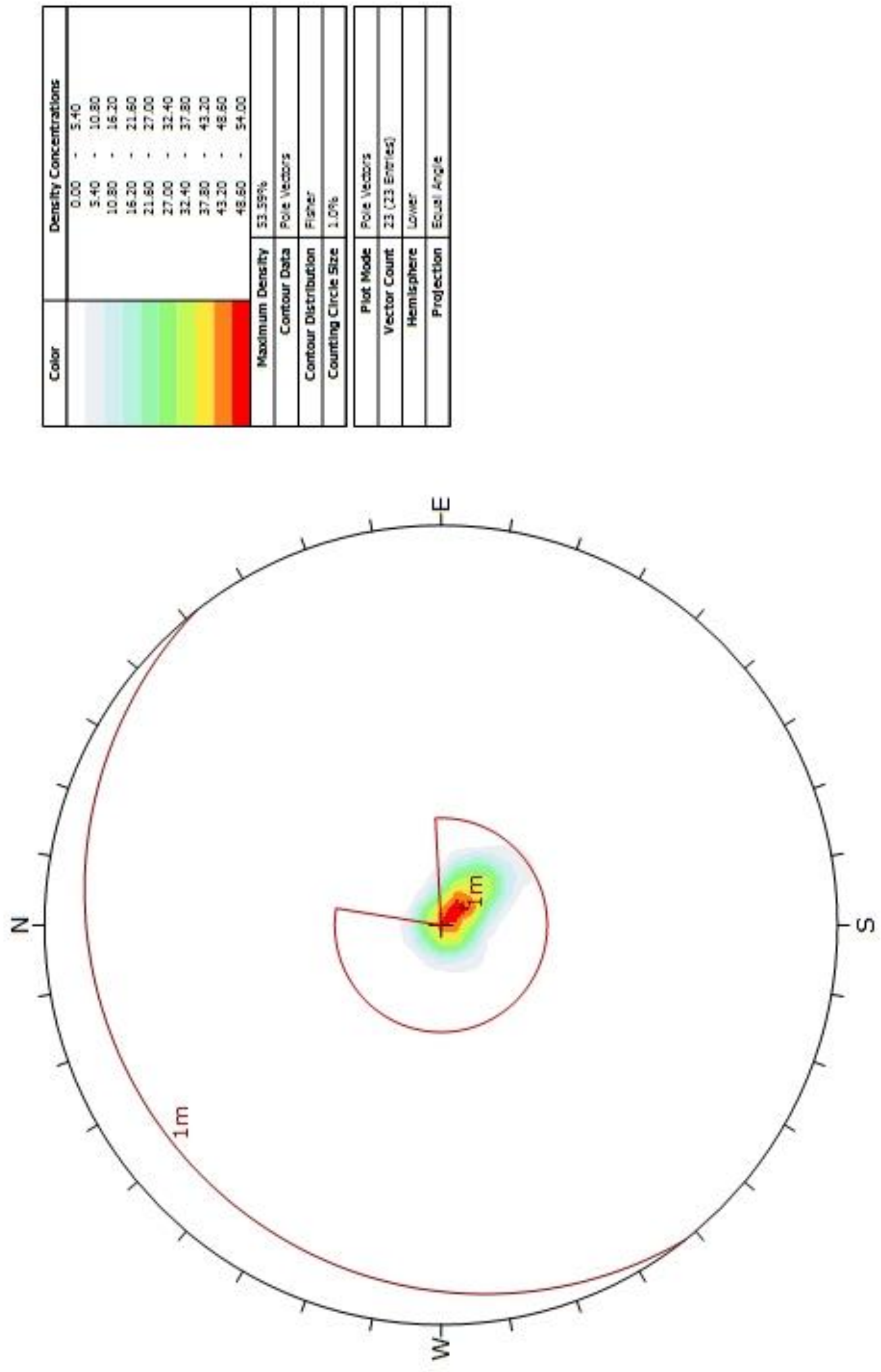

Figure 4.24: Average orientation of Foliation Set 1; 8/322 (red)

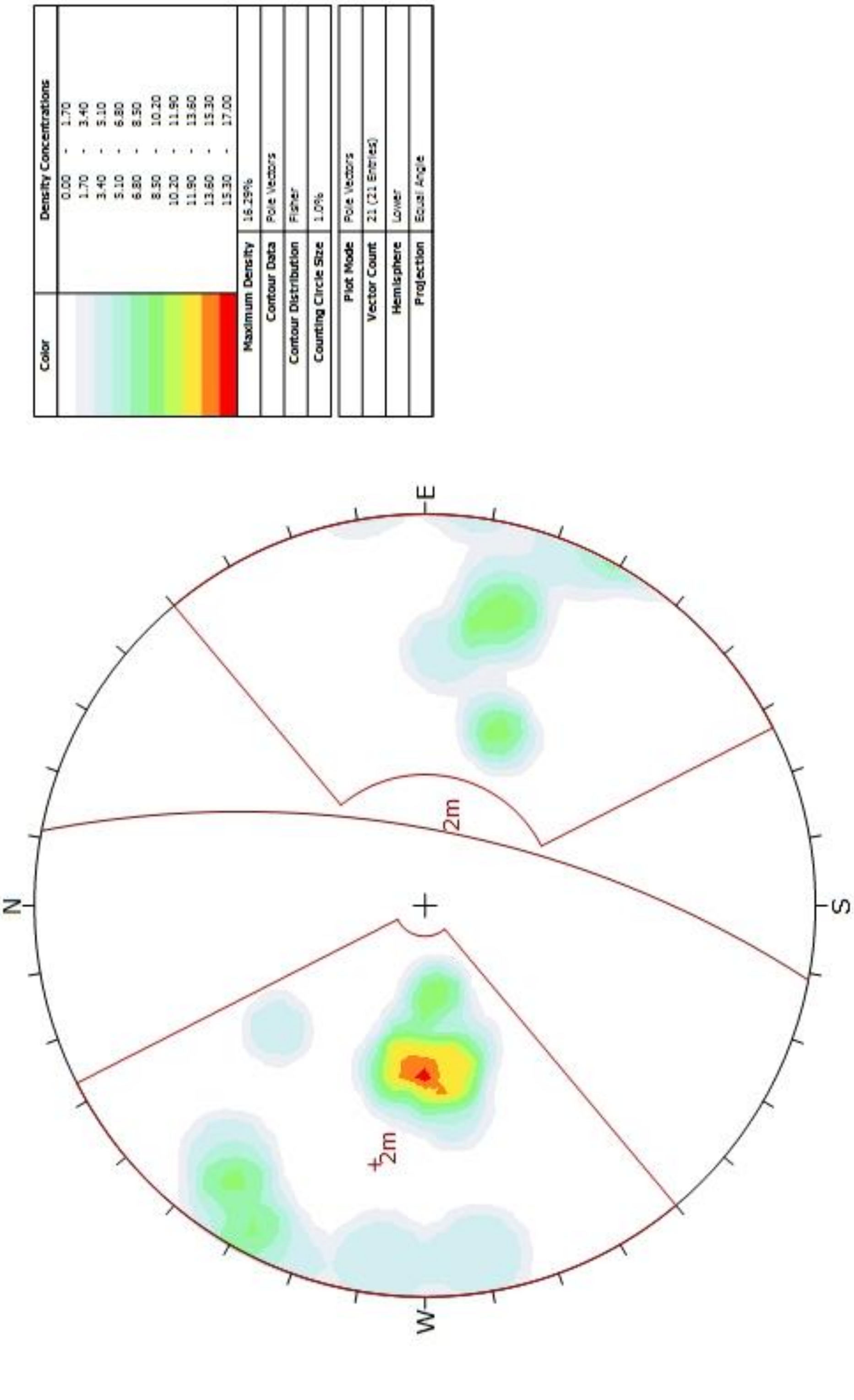

Figure 4.25: Average orientation of Joint Set 2; 68/101 (yellow)

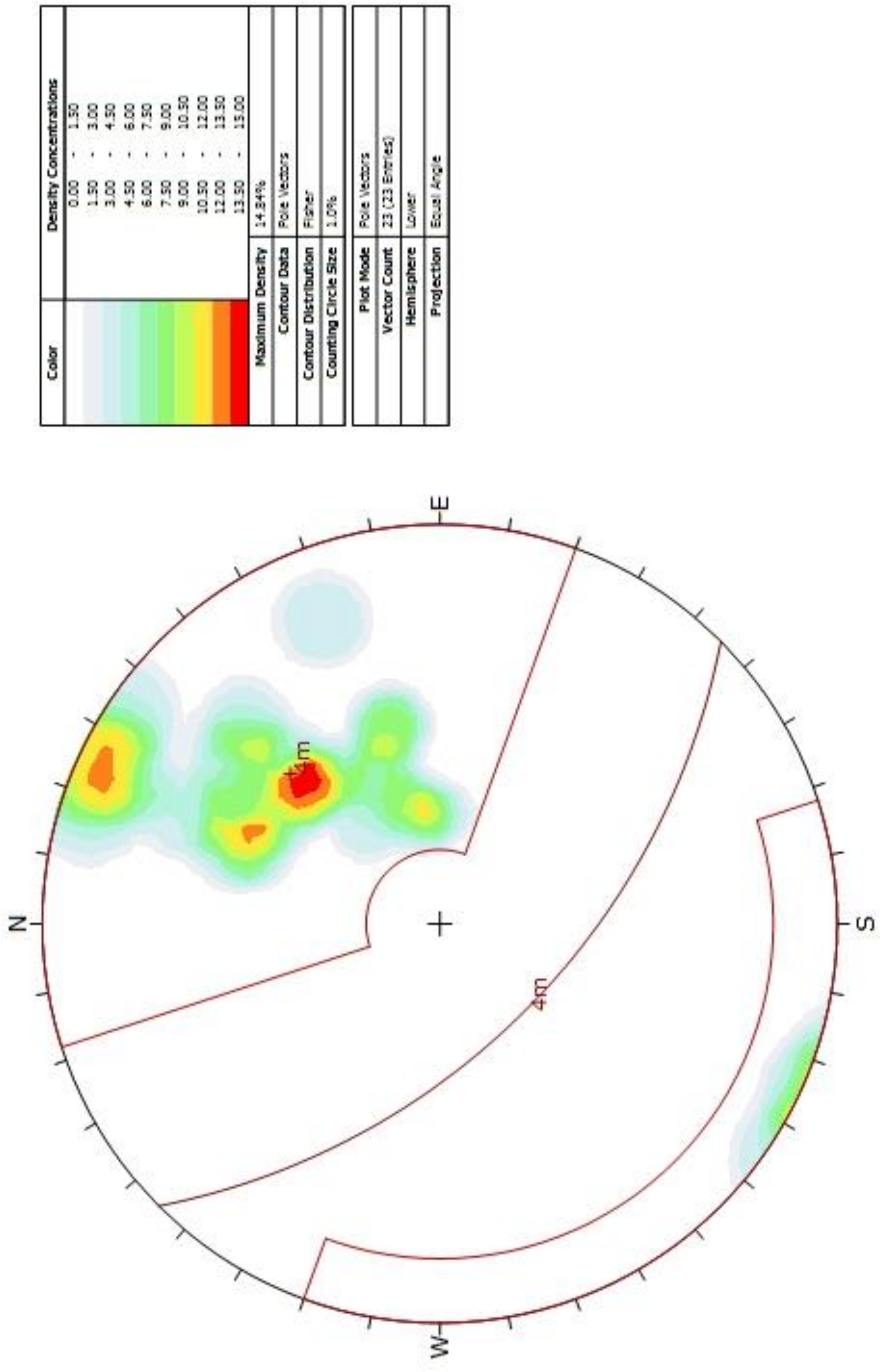

Figure 4.26: Average orientation of Joint Set 3; 56/225 (black)

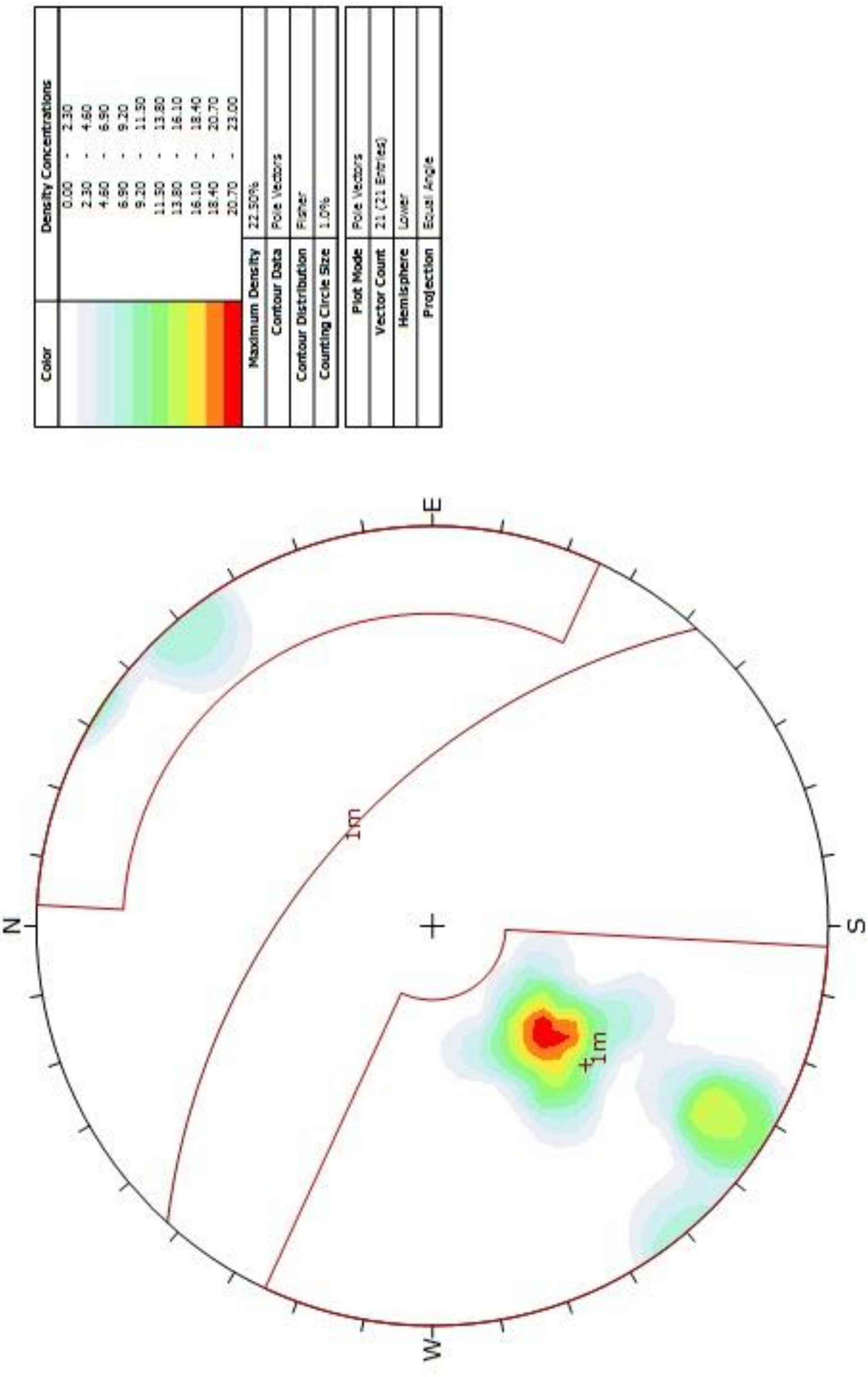

Figure 4.27: Average orientation of Joint Set 4; 55/42 (blue)

4.3.2 Calculating Joint Spacing

Using a virtual scanline with known orientation, the spacing's of each individual set were calculated. The scanline was created by measuring the distance from the start of Area 1 to the end in the direction the tunnel was excavated (00/090). Since the scanline orientation was not normal to the joint sets, the following calculations were made to get the normal spacing. The mean spacing of the scanline ($\bar{d}_s$) was calculated by dividing the length of the scanline by the number of times a given set crossed that scanline (Equation 4.4). Then by knowing the orientation of the scanline (dip = α_s and dip direction β_s) and the normal orientation of each of the sets (normal dip = α_n and normal dip direction = β_n) $\cos\delta$ can be calculated for each set (Equation 4.5). The solution from Equation 4.4 multiplied by the solution from Equation 4.5 gives the normal spacing of each of the joint sets (Equation 4.6).

(Equation 4.4) $\bar{d}_s = \sum_{i=1}^{n} d_i/n$

(Equation 4.5) $\cos\delta = |cos(\alpha_s - \alpha_n) * cos\beta_s * cos\beta_n + sin\beta_s * sin\beta_n|$

(Equation 4.6) $\bar{d}_n = \bar{d}_s * \cos\delta$

4.3.3 Matching Previously Mapped Blocks to Joint Sets for Reconstruction

For each of the 16 blocks of Area 1, there are discontinuity orientations that have to fit the 5 discontinuity sets. Blocks with greater than 5 discontinuities were eliminated which leaves 14 possible blocks to be reproduced. A further 6 blocks were eliminated due to repetition of joint sets; meaning that there were at least two discontinuities that could fit into a single discontinuity set. So 8 blocks remain with 3 and 4 discontinuity sets that fit the Area 1 established discontinuity sets. Table 4.2 shows the block number, its corresponding BP-Code and the joint sets that make up the code.

Digitally Identified in-situ blocks with LiDAR surface model			Reproducible after Block Theory
Block No.	**BP-Code**	**Joints**	**Reproducible**
8	111 0	J4 J1 F1	Yes
9	101 0	F1 J1 J3	Yes
10	1111 0	J2 **J3** F1 **J3**	No
32	1111 0	F1 J1 J2 J4	Yes
53	11010 0	J2 **J3** J1 **J3** J4	No
54	101111 0	**J2** J1 **J3** F1 **J3** **J2**	No
55	1100 0	J4 J1 **J2** **J2**	No
56	110111 0	J4 F1 J1 **J2** **J2** **J2**	No
57	111 0	F1 J4 J2	Yes
58	101 0	J2 J3 F1	Yes
59	111 0	**J2** **J2** F1	No
60	11001 0	**J1** F1 J4 J3 **J1**	No
61	0111 0	J2 J4 J1 J3	Yes
62	110 0	J2 J3 J1	Yes
64	111 0	J2 J3 J4	Yes
65	1111 0	**J2** J4 F1 **J2**	No

Table 4.2: Reproducibility of 16 blocks based on number of joints and repetition of joint sets

Blocks which are made up of 5 joints or less and which do not have two or more joints with similar joint orientations were designated reproducible. These 8 blocks were plotted on stereonets using B02HPGL.EXE and plotted on the cross-section of the tunnel using B29HPGL.EXE. Furthermore, their forms were visualized and their volumes calculated using B03HPGL.EXE. The following figures show the outputs of these blocks using the above mentioned programs.

5 Results

The following section summarises the results of this study.

5.1 Blocks of Area 1

Below are the original 16 in-situ blocks of Area 1. Their orientations and spacing’s were measured in-situ in RiSCAN PRO. Once their Block Pyramid (BP) code was determined, they were visualised in 3-dimensions and their volume calculated. Figures 5.1 through 5.16 below show the form and volume of the 16 blocks located in Area 1. The corresponding tables for each block show their in-situ discontinuity orientations, spacing’s, BP-codes and volume.

5.1.1 Block 8

Joint No.	Dip	Dip Direction	Spacing [m]	BP-Code	Volume [m³]
1	70	33	0.29	111 0	0.0423
2	64	313	0.32		
3	7	340	0.24		
4	37	337	0.10		

Table 5.1: Block 8 discontinuity orientations and spacing's, BP-code and volume

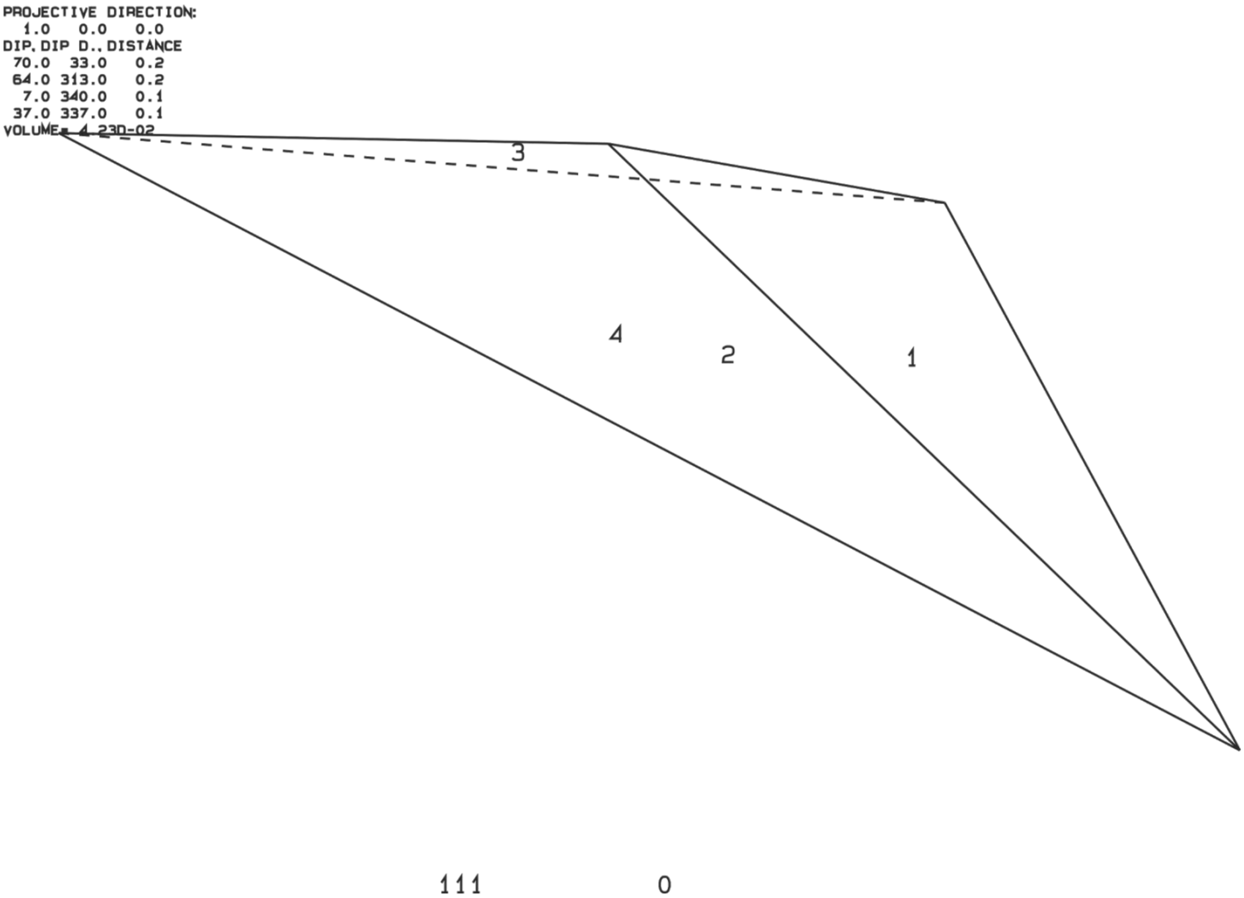

Figure 5.1: Block 8 form and volume original

5.1.2 Block 9

Joint No.	Dip	Dip Direction	Spacing [m]	BP-Code	Volume [m³]
1	4	139	0.20	101 0	0.0406
2	64	313	0.23		
3	32	228	0.25		
4	34	182	0.10		

Table 5.2: Block 9 discontinuity orientations and spacing's, BP-code and volume

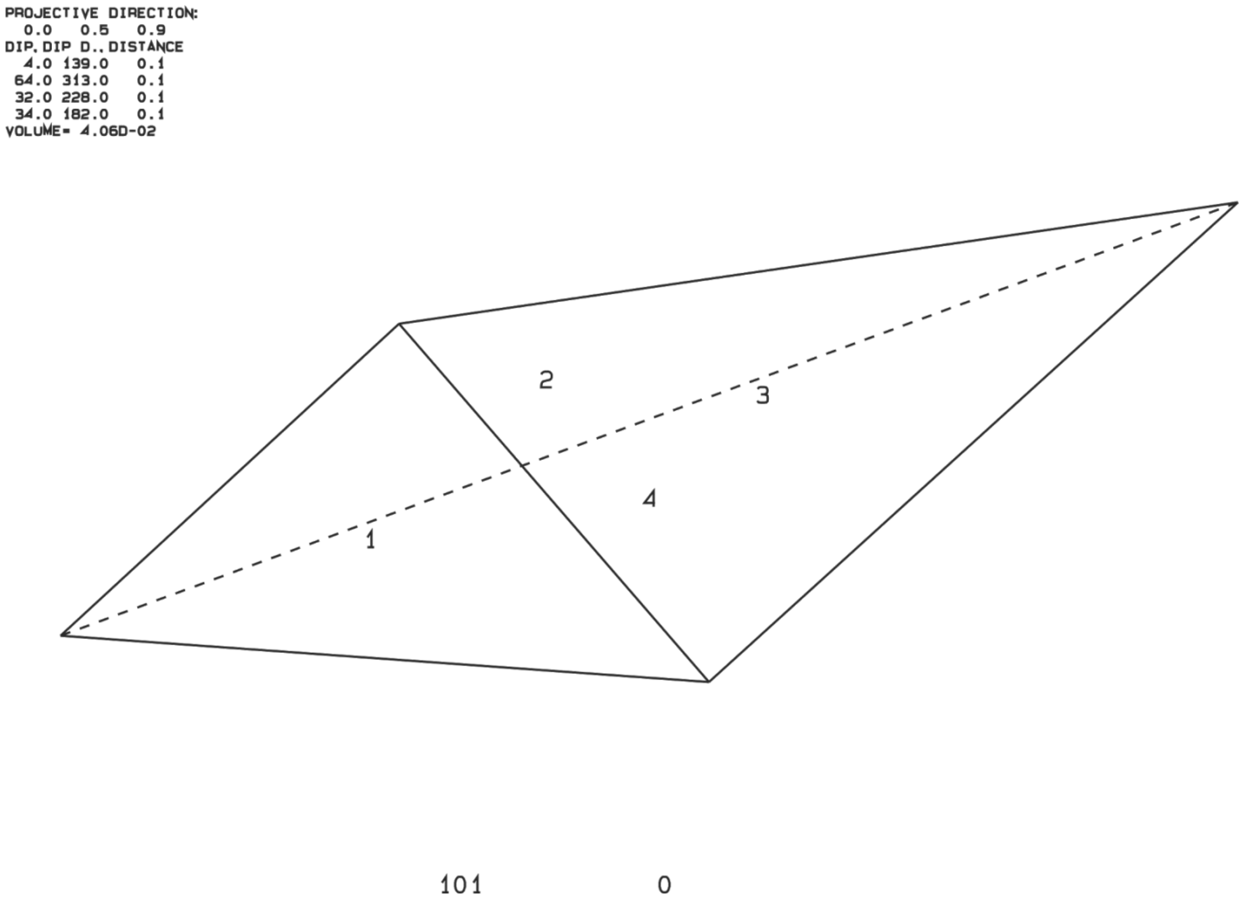

Figure 5.2: Block 9 form and volume original

5.1.3 Block 10

Joint No.	Dip	Dip Direction	Spacing [m]	BP-Code	Volume [m³]
1	80	127	0.16	1111 0	0.0123
2	62	199	0.22		
3	13	265	0.19		
4	43	211	0.16		
5	42	170	0.09		

Table 5.3: Block 10 discontinuity orientations and spacing's, BP-code and volume

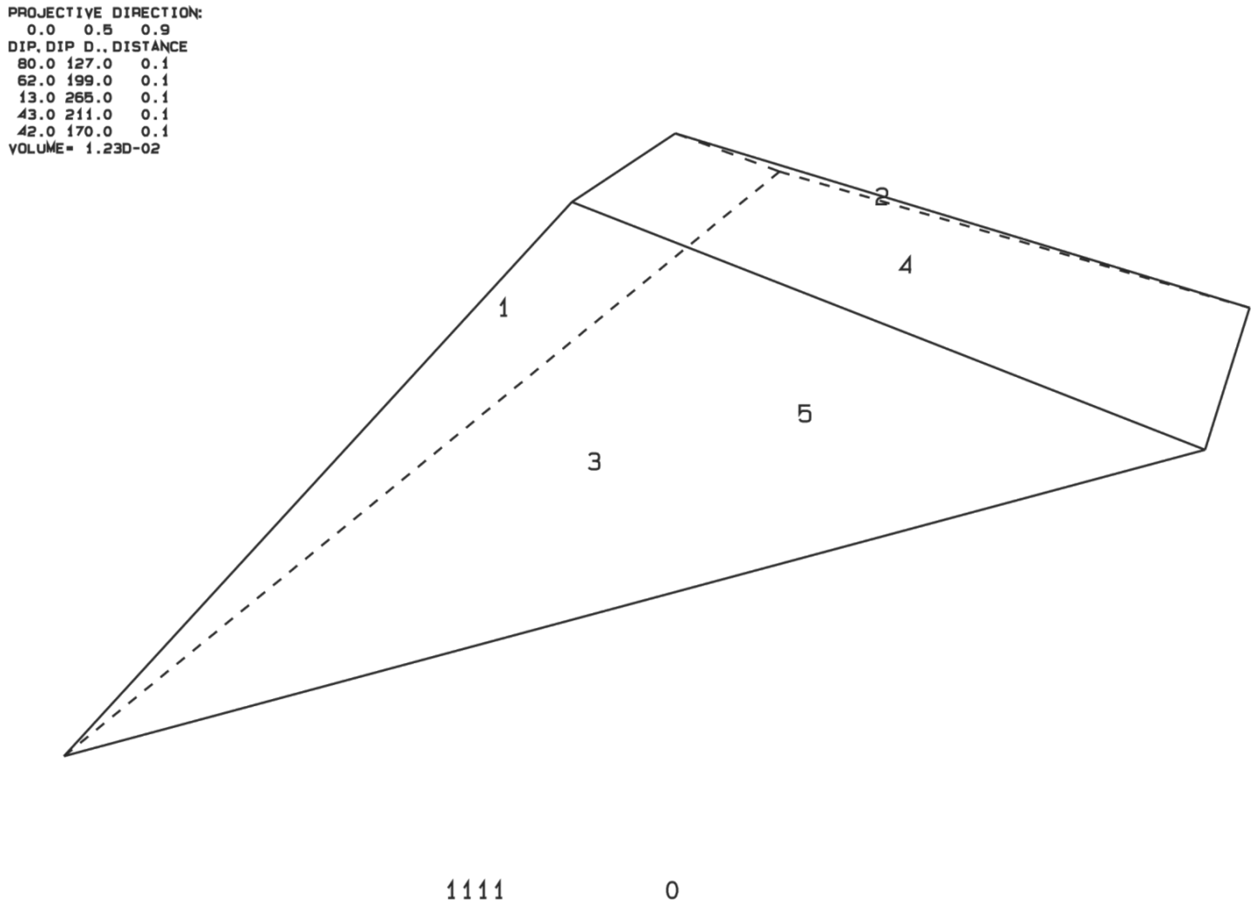

Figure 5.3: Block 10 form and volume original

5.1.4 Block 32

Joint No.	Dip	Dip Direction	Spacing [m]	BP-Code	Volume [m³]
1	7	332	0.18	1111 0	0.0106
2	65	311	0.21		
3	68	33	0.26		
4	35	27	0.11		
5	36	357	0.05		

Table 5.4: Block 32 discontinuity orientations and spacing's, BP-code and volume

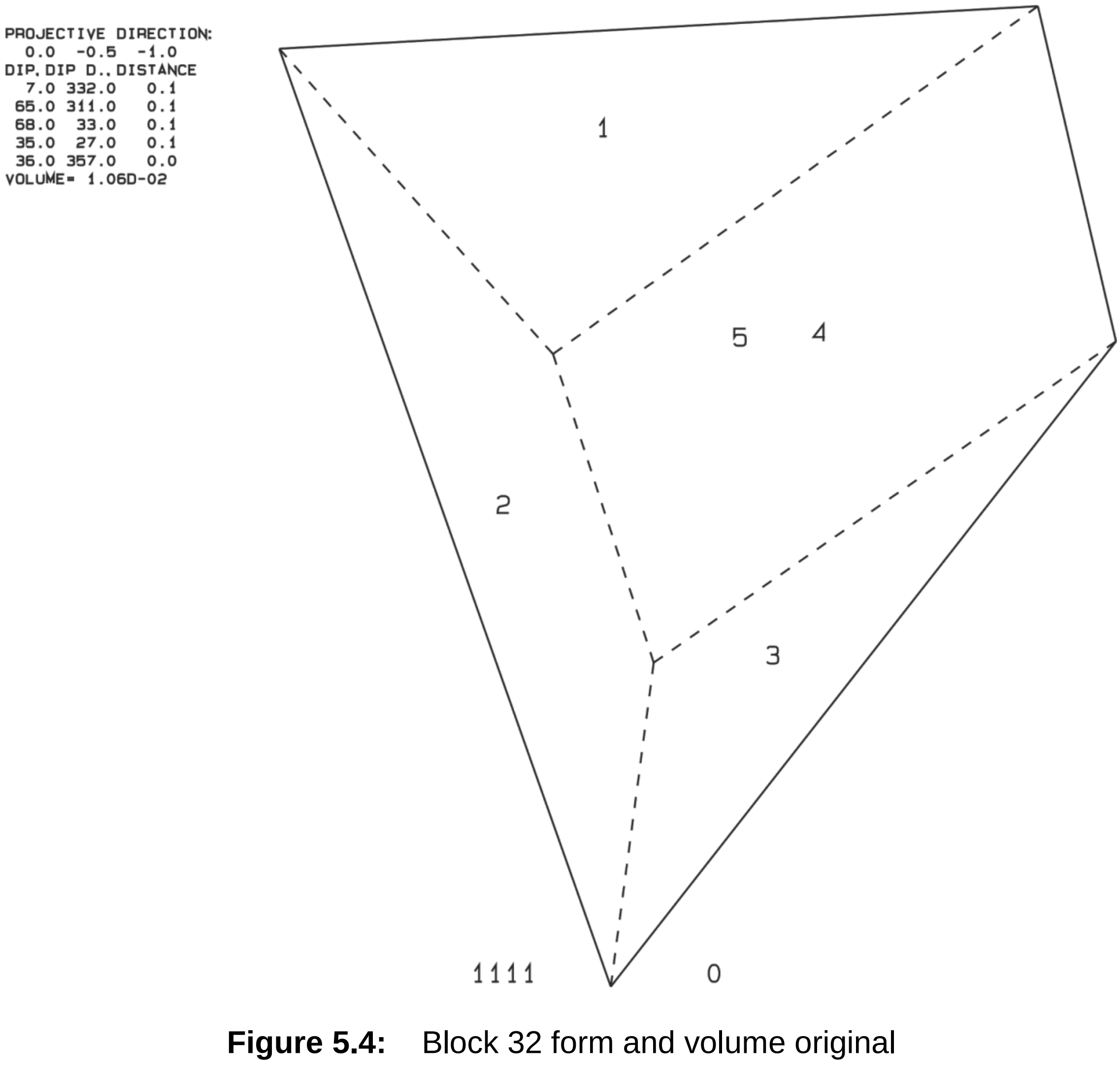

Figure 5.4: Block 32 form and volume original

5.1.5 Block 53

Joint No.	Dip	Dip Direction	Spacing [m]	BP-Code	Volume [m³]
1	62	90	0.26	11010 0	0.0136
2	76	231	0.16		
3	57	316	0.28		
4	21	254	0.19		
5	82	33	0.22		
6	66	183	0.18		

Table 5.5: Block 53 discontinuity orientations and spacing's, BP-code and volume

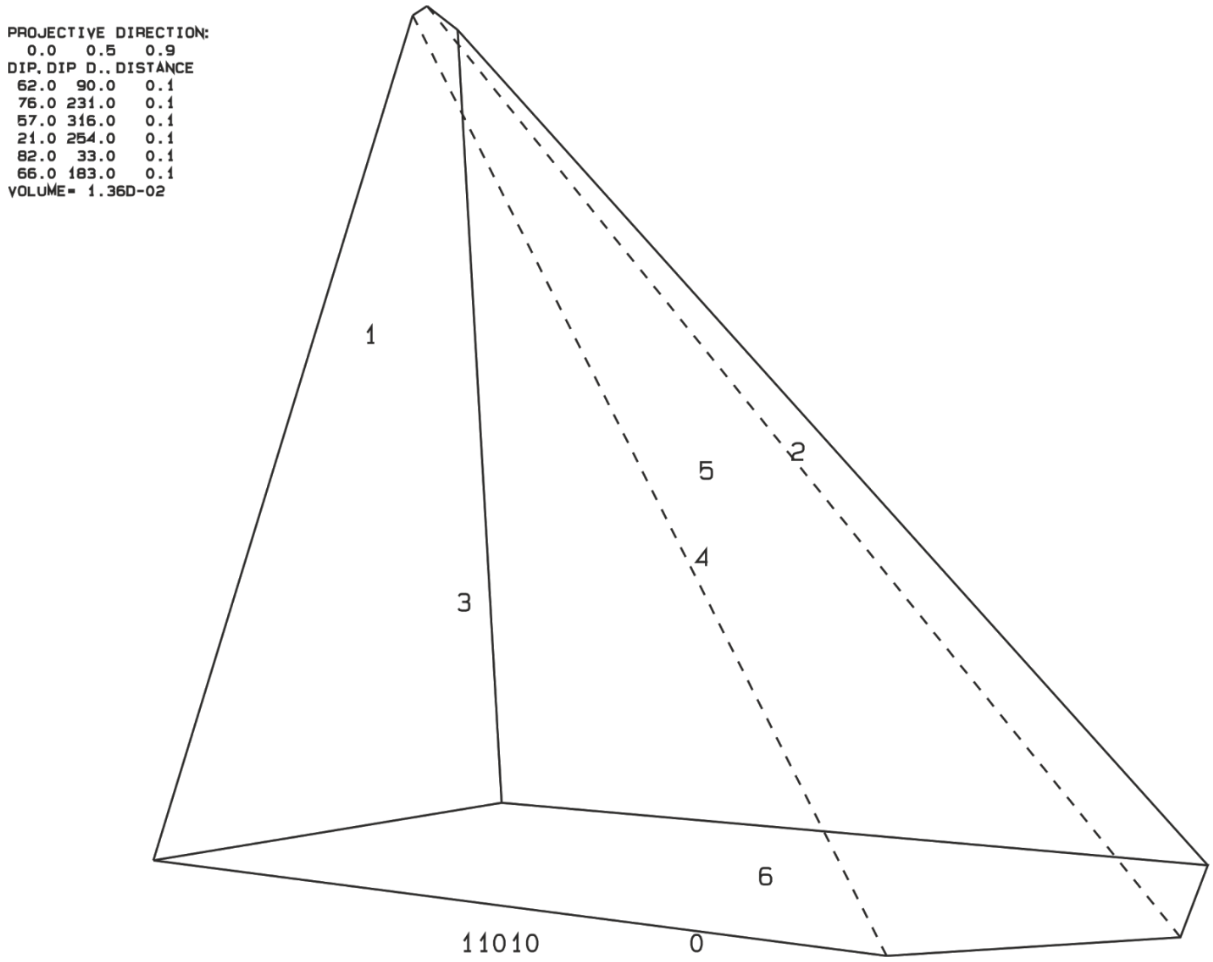

Figure 5.5: Block 53 form and volume original

5.1.6 Block 54

Joint No.	Dip	Dip Direction	Spacing [m]	BP-Code	Volume [m³]
1	57	100	0.38	101111 0	0.0201
2	30	326	0.34		
3	50	227	0.23		
4	15	265	0.30		
5	45	178	0.12		
6	31	140	0.09		
7	55	153	0.16		

Table 5.6: Block 54 discontinuity orientations and spacing's, BP-code and volume

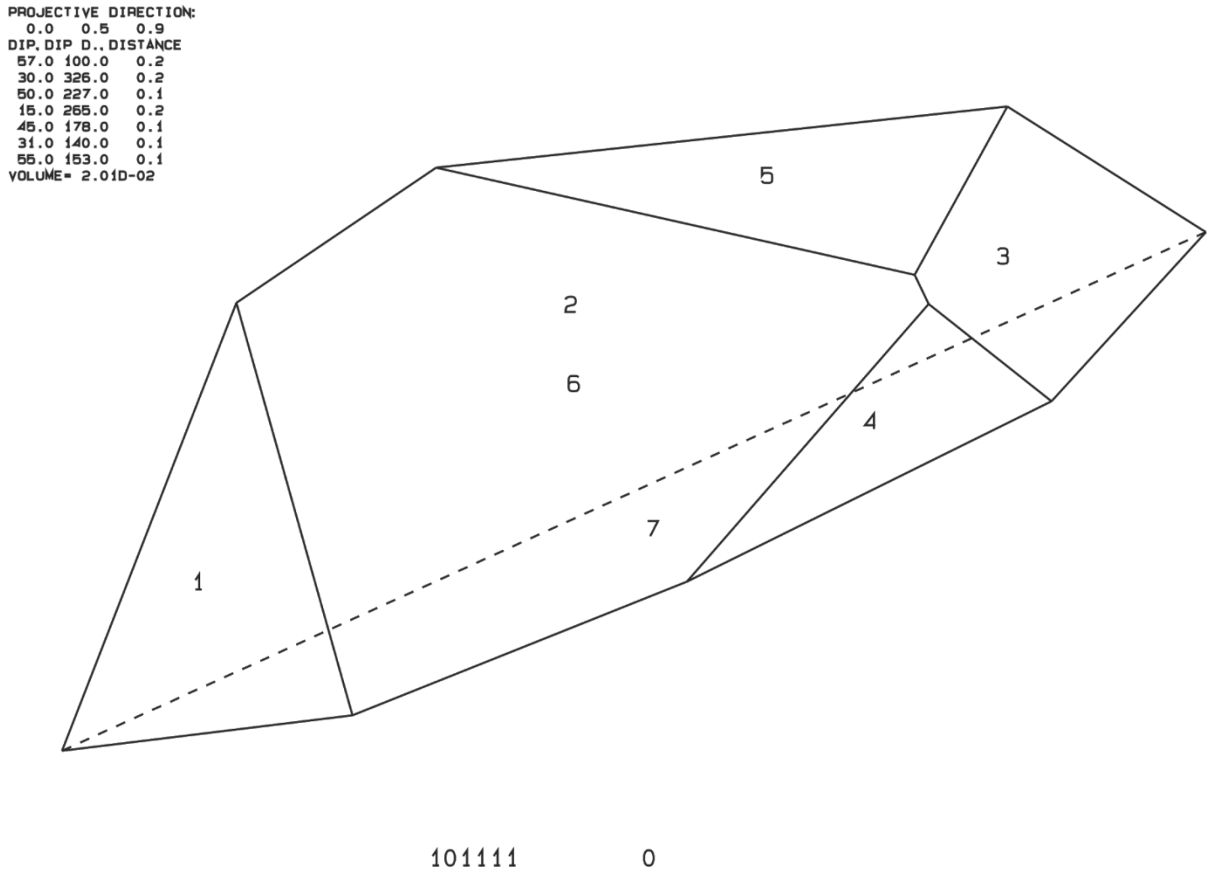

Figure 5.6: Block 54 form and volume original

5.1.7 Block 55

Joint No.	Dip	Dip Direction	Spacing [m]	BP-Code	Volume [m³]
1	61	21	0.22	1100 0	0.0108
2	28	292	0.30		
3	52	118	0.19		
4	88	127	0.12		
5	67	329	0.08		

Table 5.7: Block 55 discontinuity orientations and spacing's, BP-code and volume

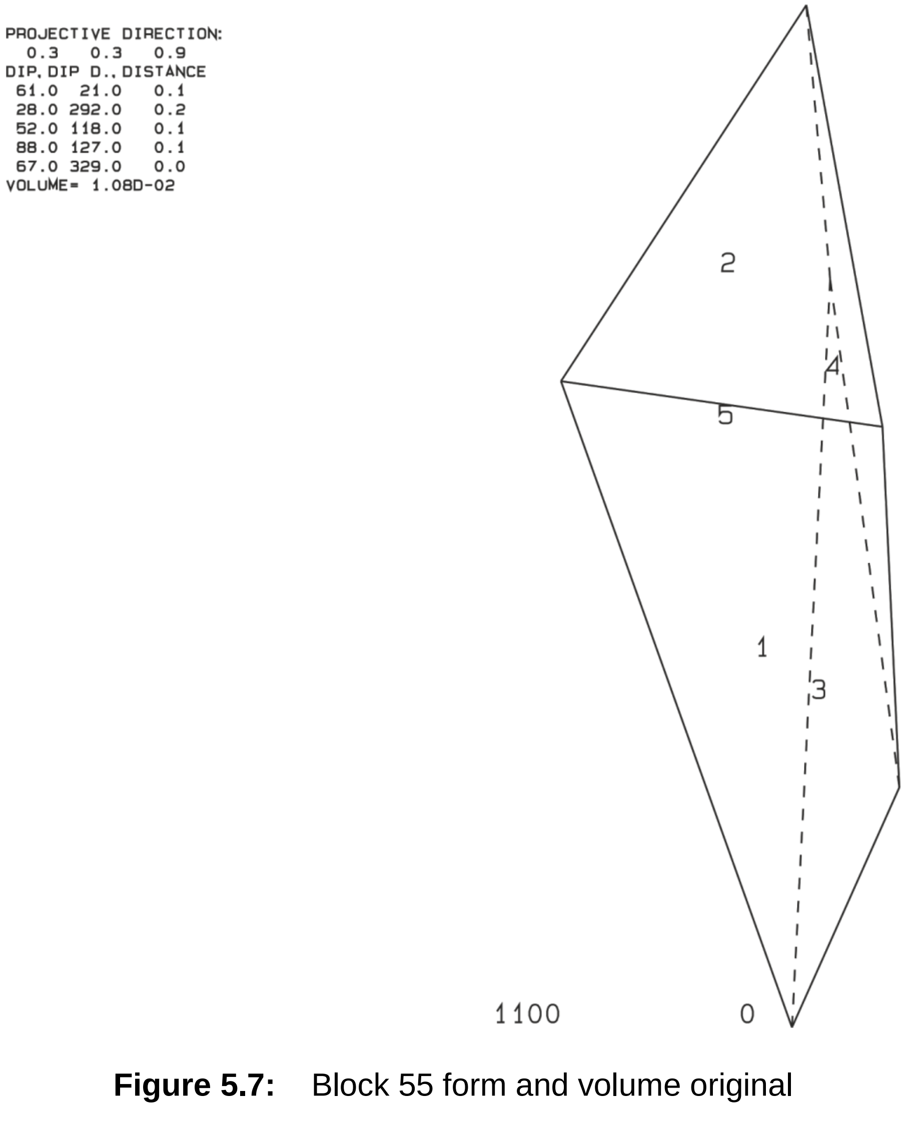

Figure 5.7: Block 55 form and volume original

5.1.8 Block 56

Joint No.	Dip	Dip Direction	Spacing [m]	BP-Code	Volume [m³]
1	46	44	0.31	110111 0	0.0163
2	6	333	0.18		
3	36	300	0.28		
4	46	103	0.19		
5	67	289	0.37		
6	61	153	0.12		
7	16	43	0.06		

Table 5.8: Block 56 discontinuity orientations and spacing's, BP-code and volume

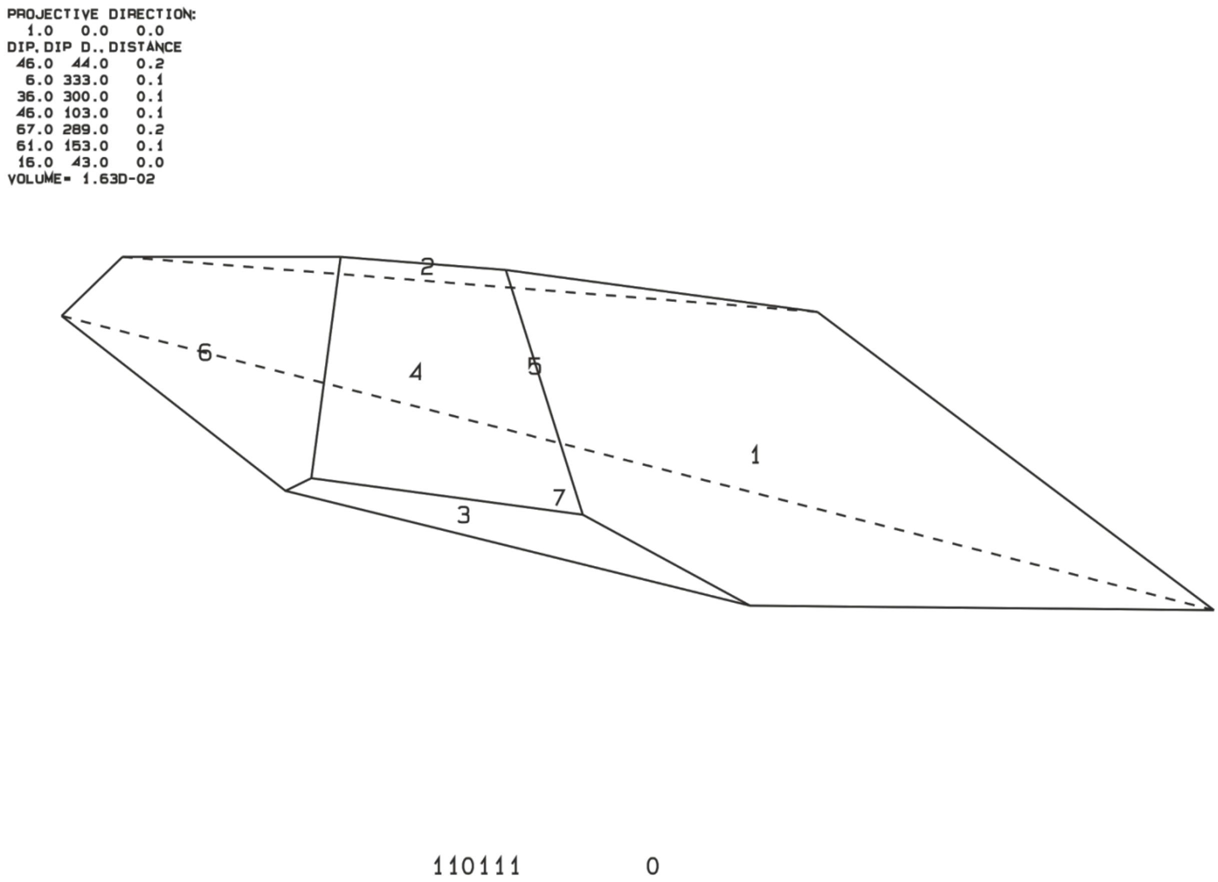

Figure 5.8: Block 56 form and volume original

5.1.9 Block 57

Joint No.	Dip	Dip Direction	Spacing [m]	BP-Code	Volume [m³]
1	24	310	0.20	111 0	0.0128
2	46	45	0.12		
3	43	106	0.20		
4	21	45	0.05		

Table 5.9: Block 57 discontinuity orientations and spacing’s, BP-code and volume

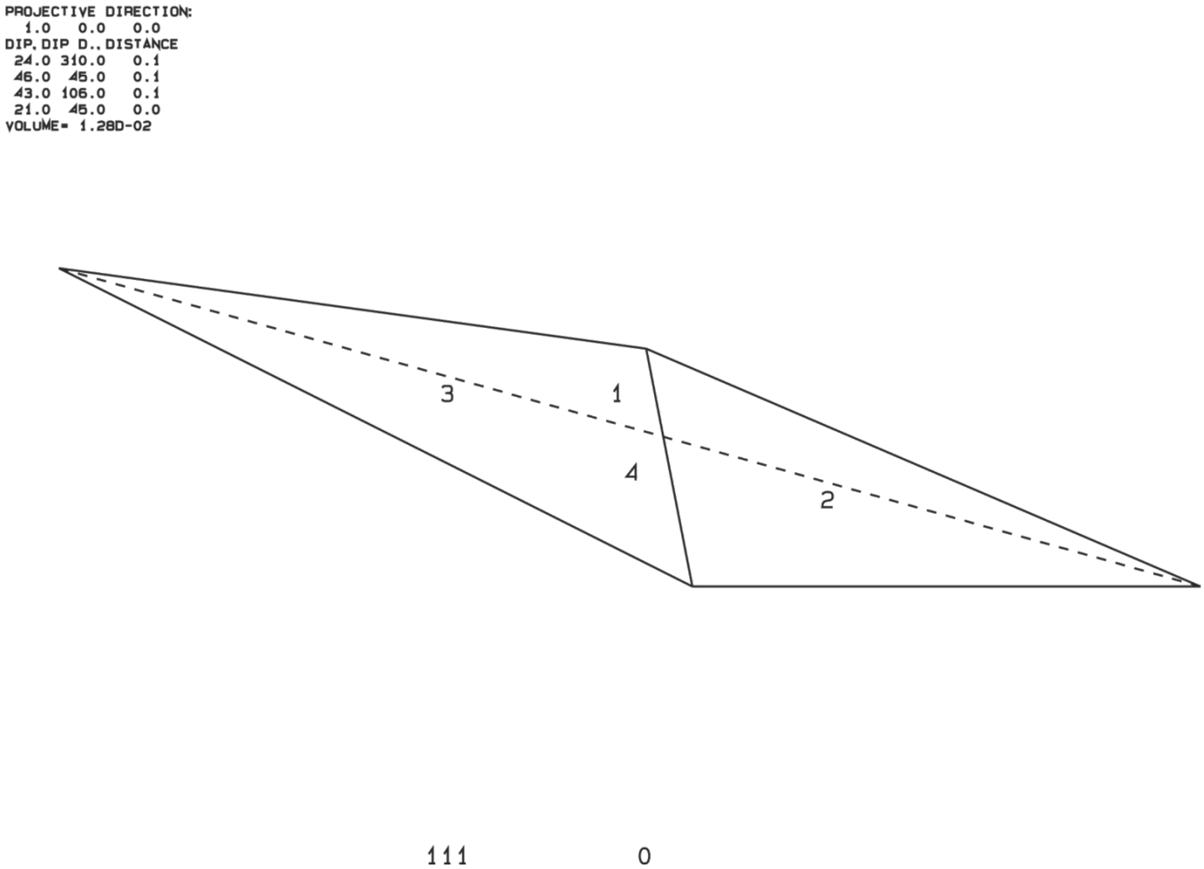

Figure 5.9: Block 57 form and volume original

5.1.10 Block 58

Joint No.	Dip	Dip Direction	Spacing [m]	BP-Code	Volume [m³]
1	82	150	0.10	101 0	0.00371
2	76	19	0.14		
3	28	229	0.20		
4	76	179	0.04		

Table 5.10: Block 58 discontinuity orientations and spacing’s, BP-code and volume

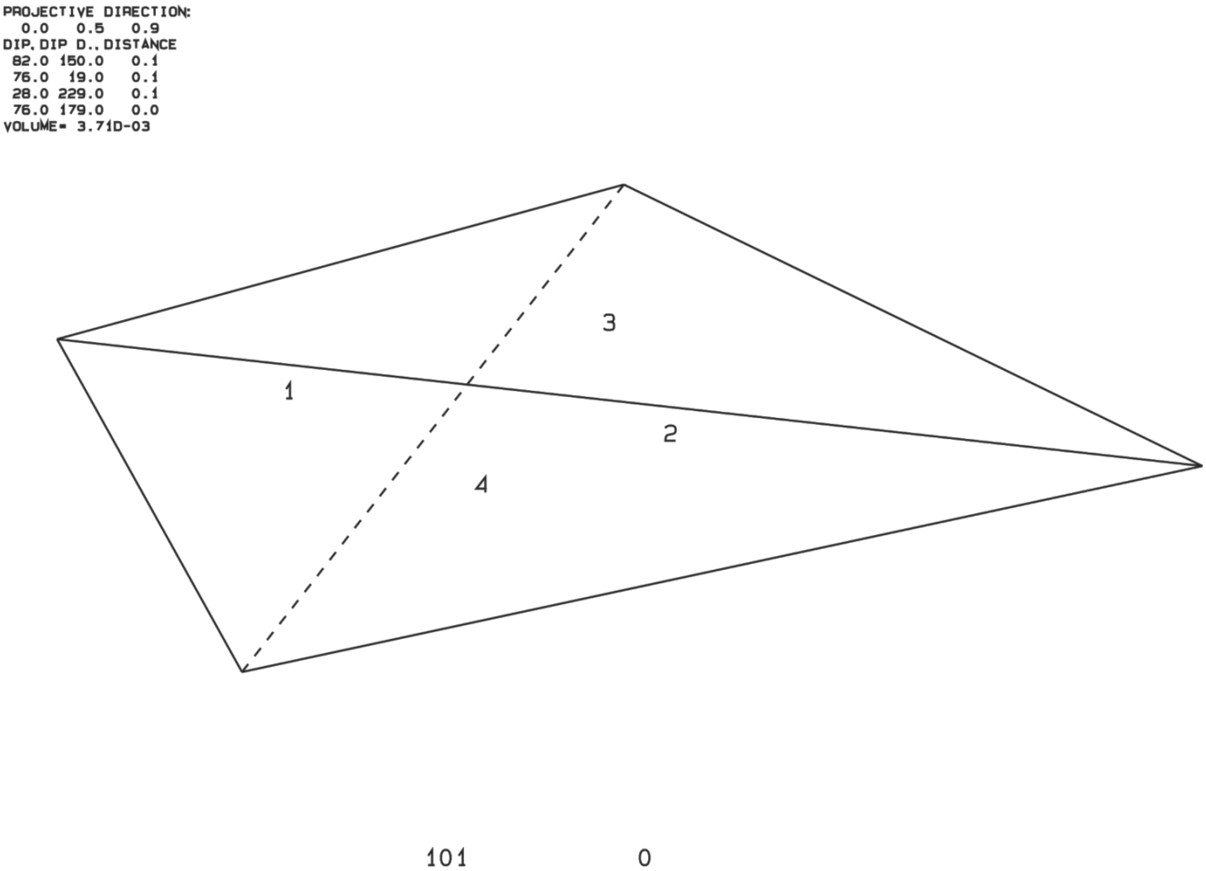

Figure 5.10: Block 58 form and volume original

5.1.11 Block 59

Joint No.	Dip	Dip Direction	Spacing [m]	BP-Code	Volume [m³]
1	59	143	0.30	111 0	0.0134
2	30	100	0.11		
3	5	0	0.05		
4	7	78	0.02		

Table 5.11: Block 59 discontinuity orientations and spacing's, BP-code and volume

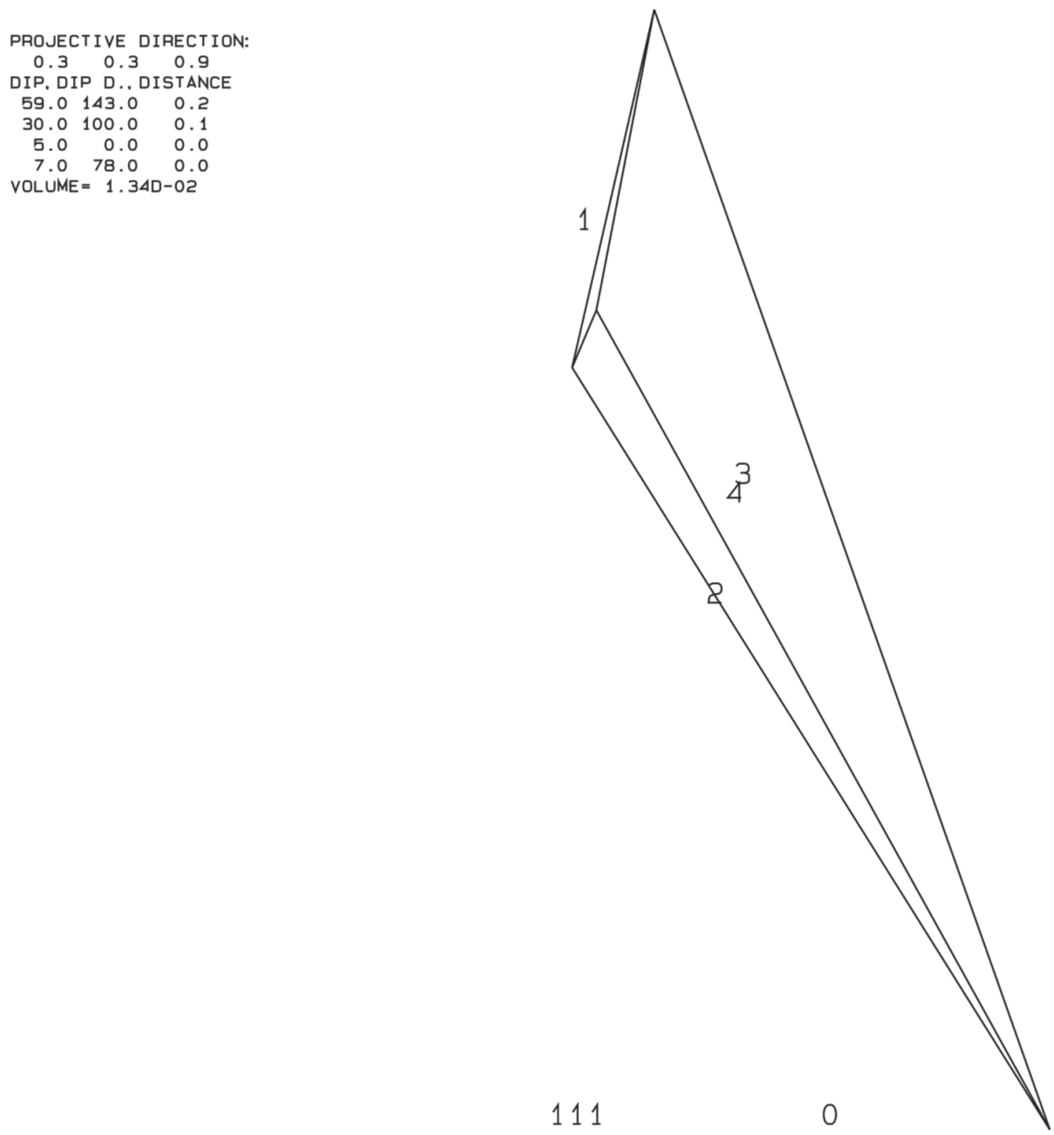

Figure 5.11: Block 59 form and volume original

5.1.12 Block 60

Joint No.	Dip	Dip Direction	Spacing [m]	BP-Code	Volume [m³]
1	48	320	0.19	11001 0	0.0159
2	19	49	0.21		
3	88	50	0.41		
4	82	186	0.31		
5	25	320	0.19		
6	44	355	0.04		

Table 5.12: Block 60 discontinuity orientations and spacing's, BP-code and volume

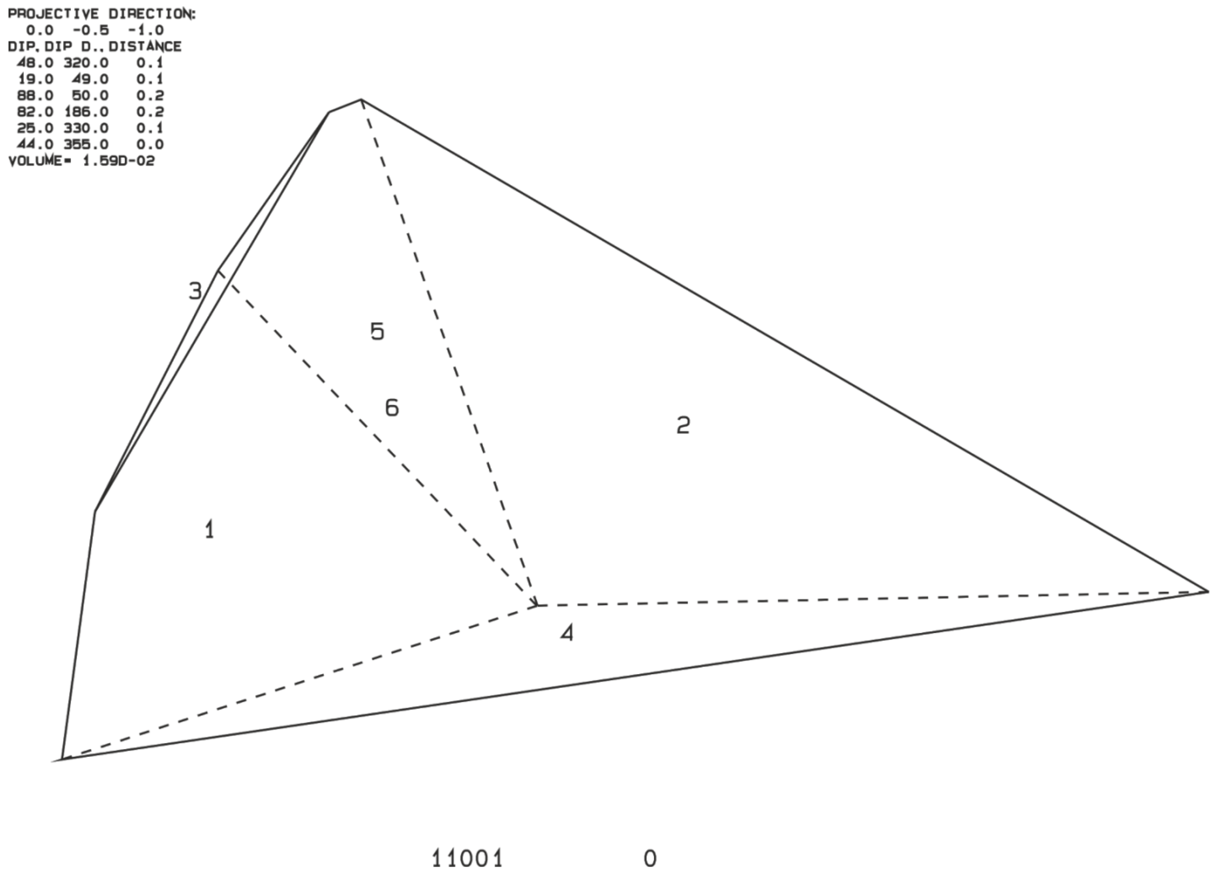

Figure 5.12: Block 60 form and volume original

5.1.13 Block 61

Joint No.	Dip	Dip Direction	Spacing [m]	BP-Code	Volume [m³]
1	82	296	0.24	0111 0	0.00989
2	25	20	0.20		
3	24	291	0.16		
4	32	254	0.11		
5	4	277	0.06		

Table 5.13: Block 61 discontinuity orientations and spacing’s, BP-code and volume

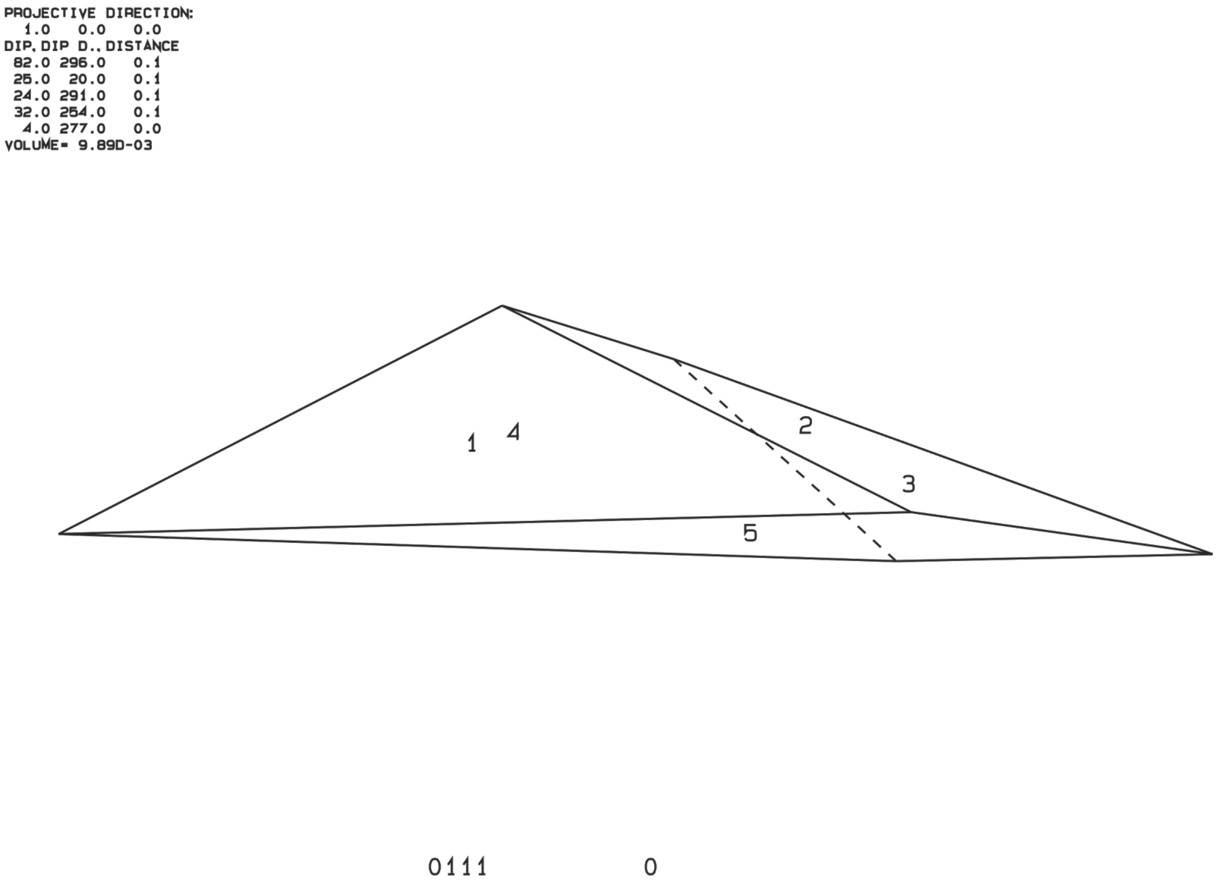

Figure 5.13: Block 61 form and volume original

5.1.14 Block 62

Joint No.	Dip	Dip Direction	Spacing [m]	BP-Code	Volume [m³]
1	83	124	0.08	110 0	0.00579
2	36	191	0.13		
3	86	332	0.08		
4	55	163	0.03		

Table 5.14: Block 8 discontinuity orientations and spacing’s, BP-code and volume

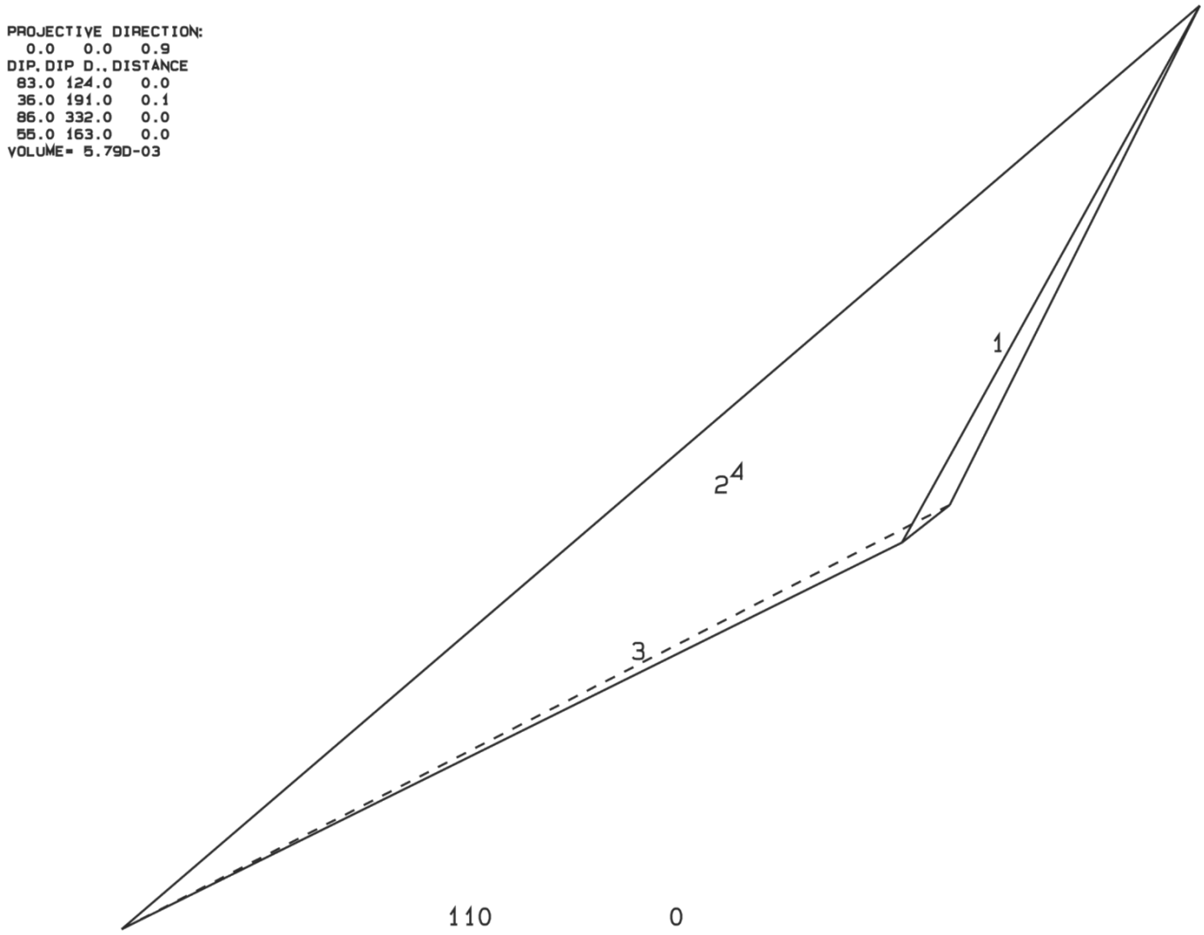

Figure 5.14: Block 62 form and volume original

5.1.15 Block 64

Joint No.	Dip	Dip Direction	Spacing [m]	BP-Code	Volume [m³]
1	27	147	0.09	111 0	0.0123
2	48	256	0.13		
3	22	33	0.09		
4	9	236	0.14		

Table 5.15: Block 64 discontinuity orientations and spacing’s, BP-code and volume

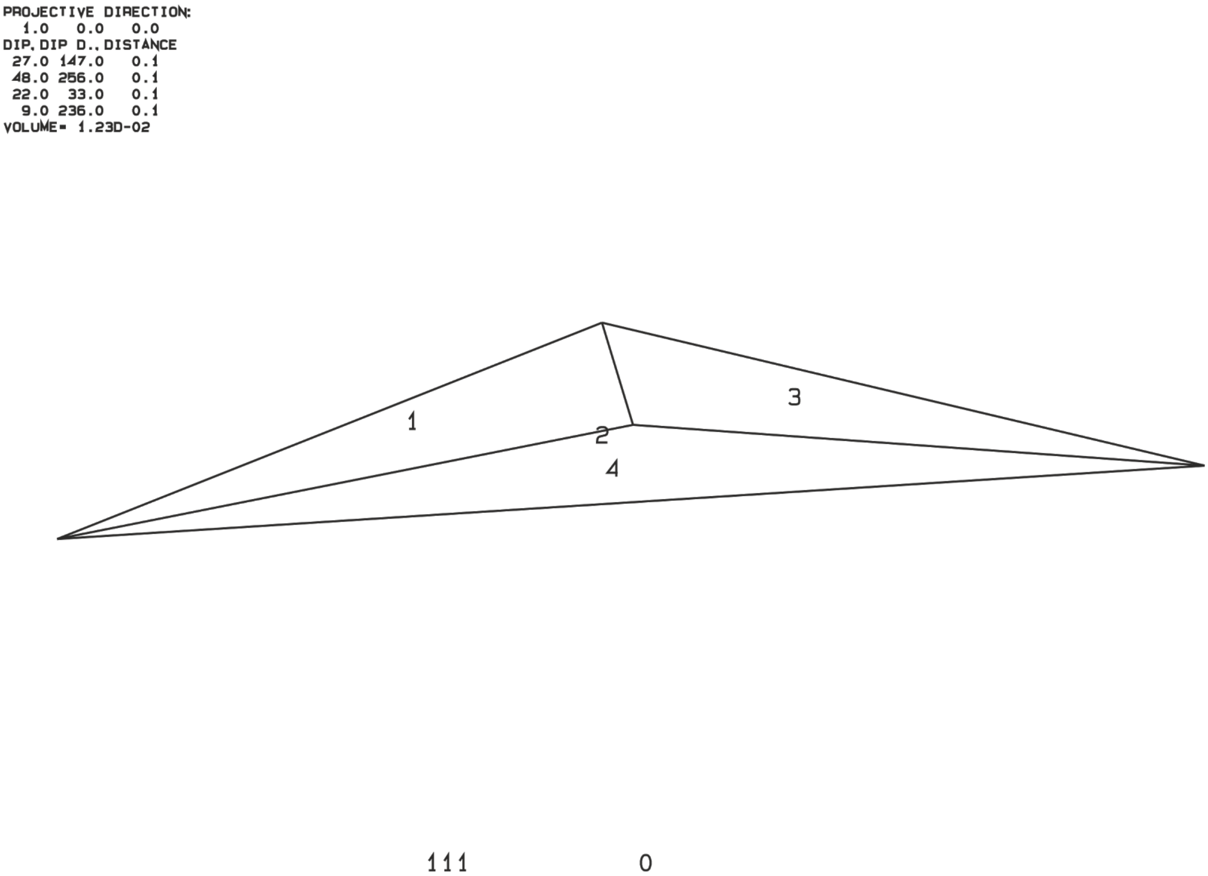

Figure 5.15: Block 64 form and volume original

5.1.16 Block 65

Joint No.	Dip	Dip Direction	Spacing [m]	BP-Code	Volume [m³]
1	44	133	0.72	1111 0	0.0147
2	39	45	0.21		
3	8	281	0.04		
4	82	296	0.85		
5	6	345	0.03		

Table 5.16: Block 65 discontinuity orientations and spacing's, BP-code and volume

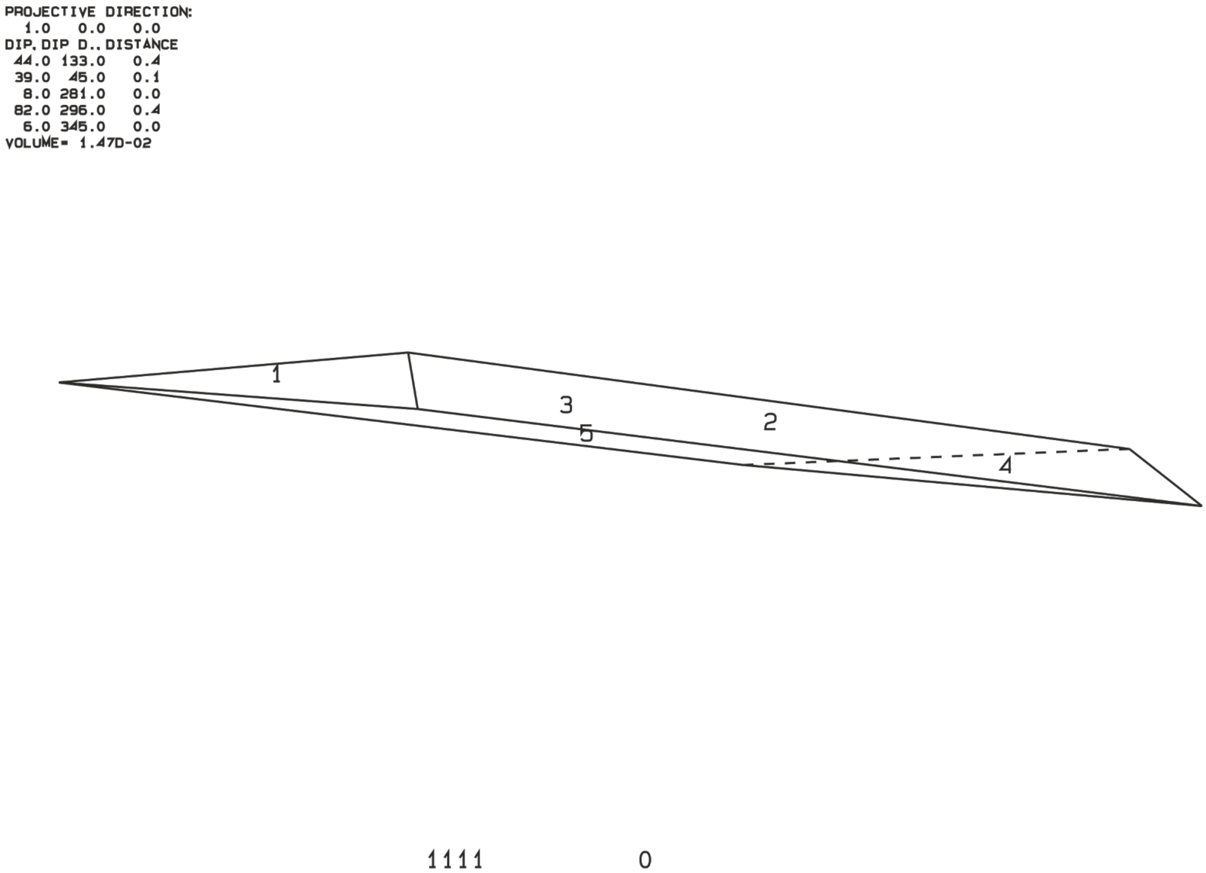

Figure 5.16: Block 65 form and volume original

5.2 Reconstructed Blocks of Area 1

Of the 8 blocks which could be reconstructed, only 5 were removable: 8, 9, 32, 62 and 64. The other 3 blocks once placed into joint sets and simplified free surface orientations were not removable because their JPs were no longer completely within their EPs. Figures 5.17 to 5.45 represent the 8 reconstructed blocks.

5.2.1 Block 8

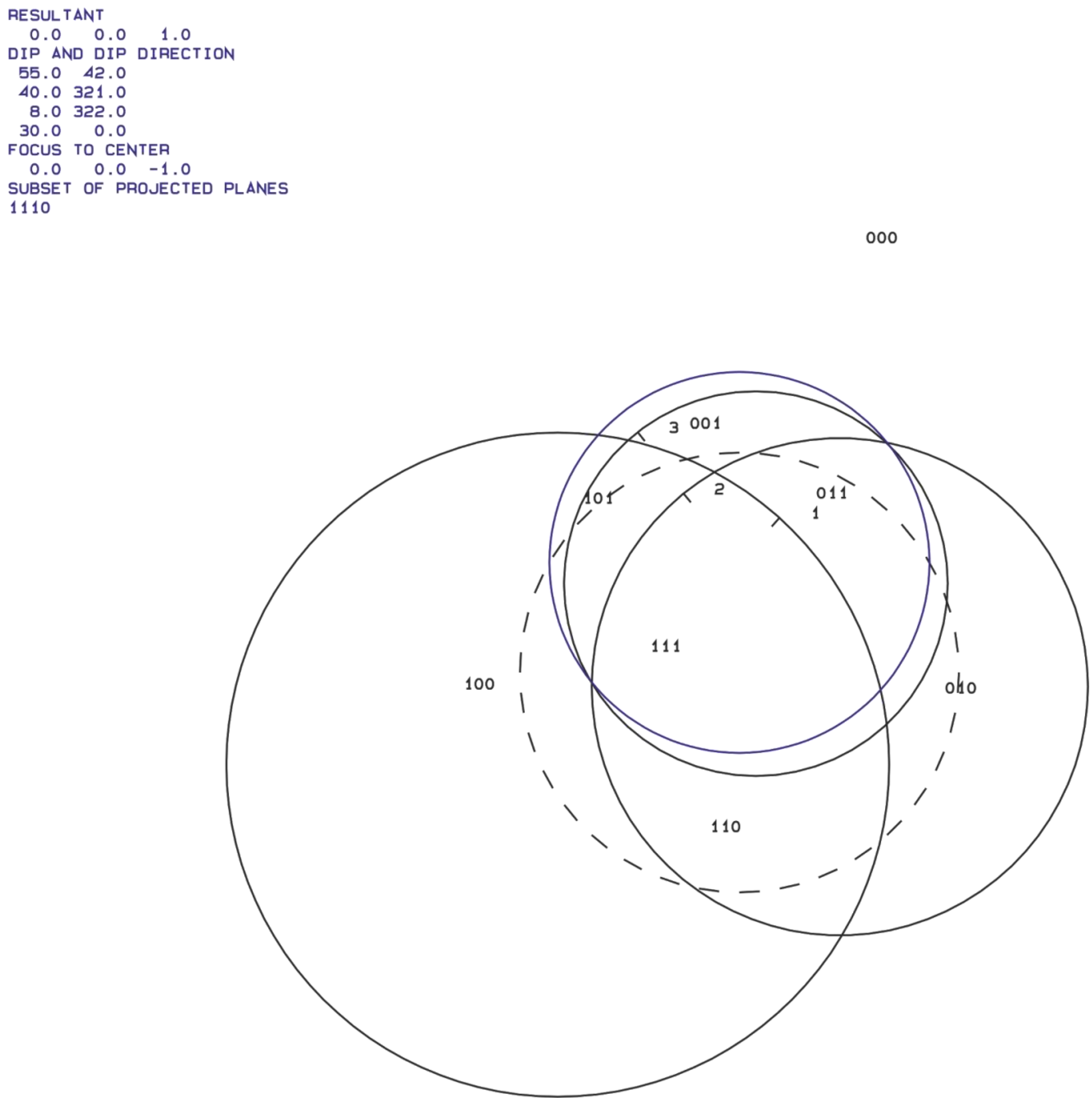

Figure 5.17: Block 8: great circles of discontinuities and free surfaces with JP-Codes: 111

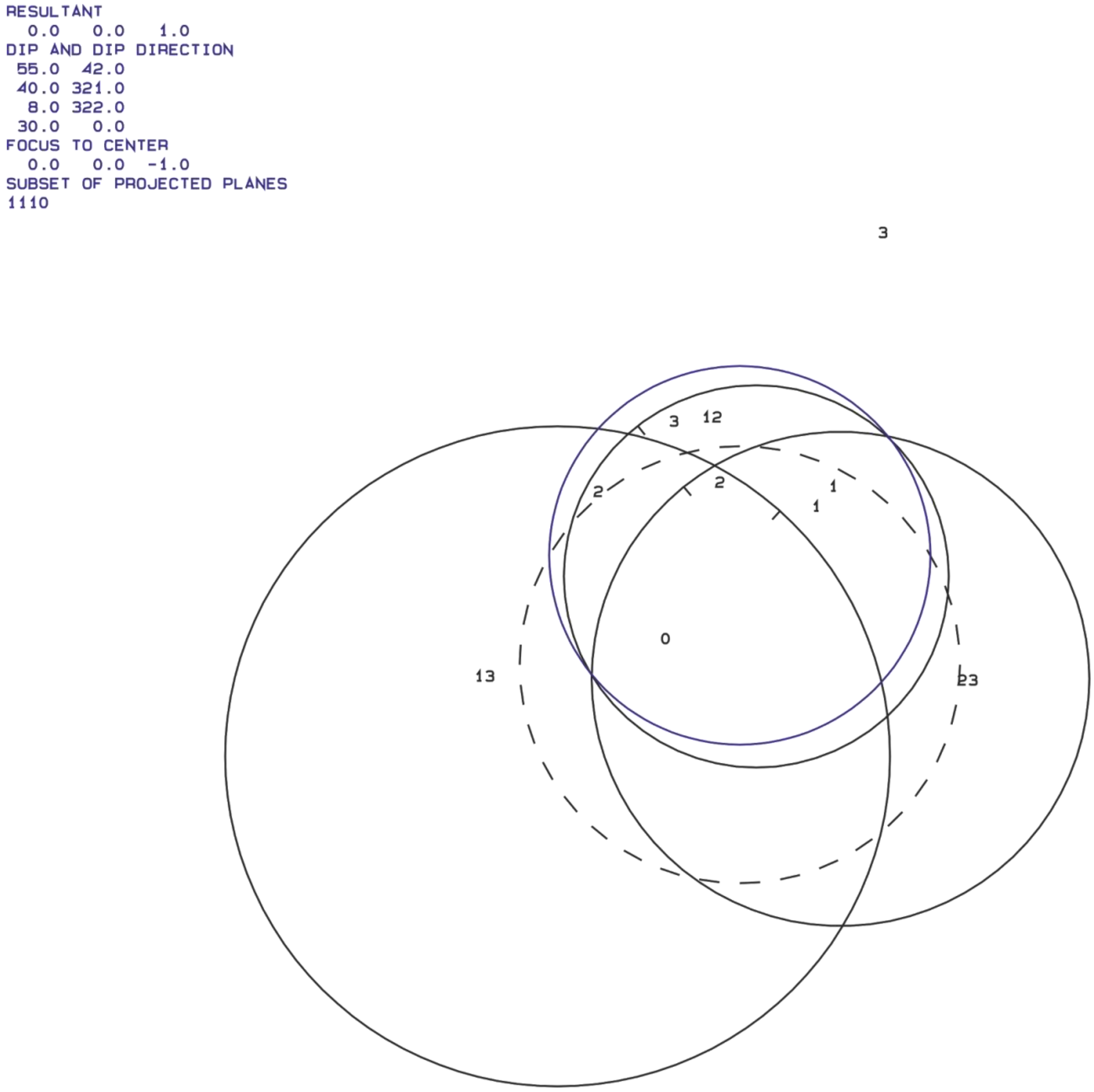

Figure 5.18: Block 8 with the Failure mode 0

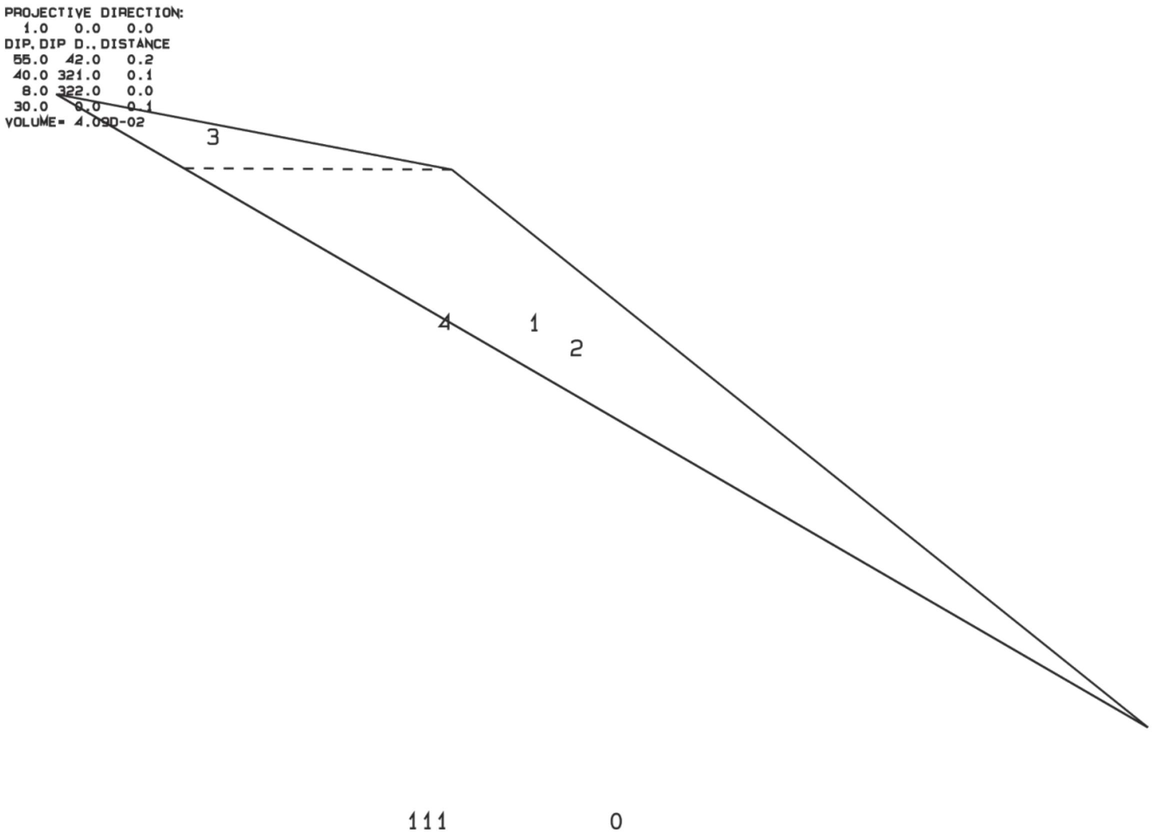

Figure 5.19: Block 8 form and volume: 0.0409m³

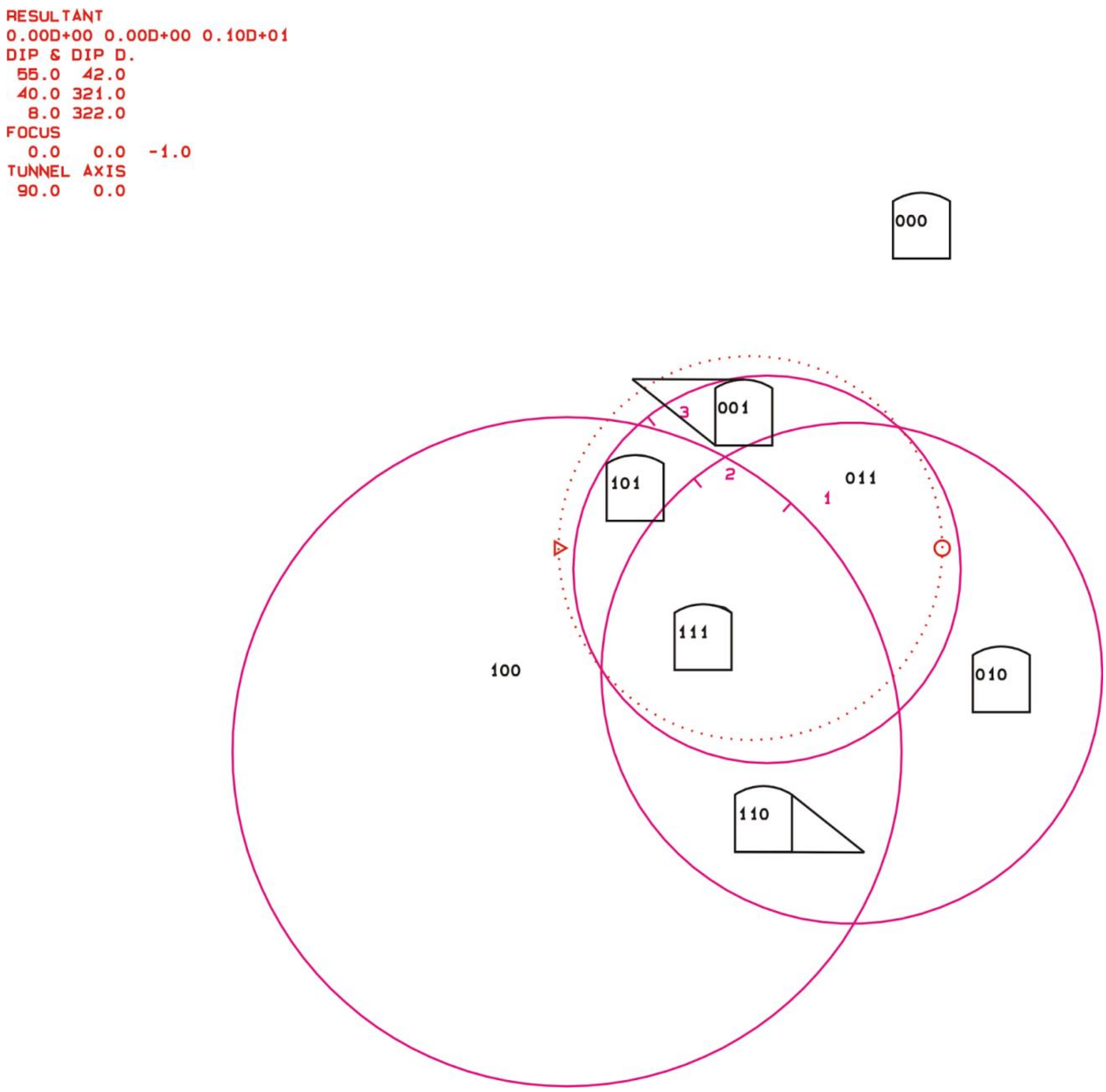

Figure 5.20: Block 8 with JP-Code 111on tunnel cross-section

5.2.2 Block 9

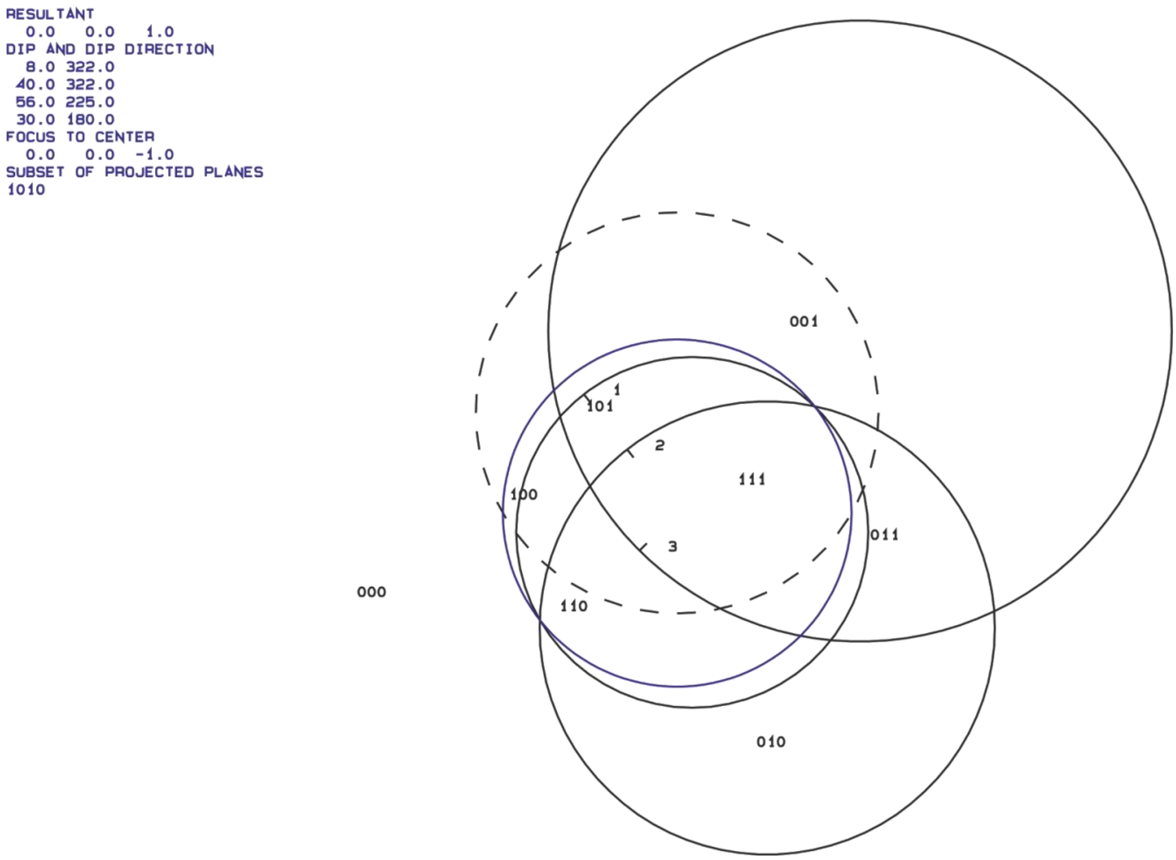

Figure 5.21: Block 9: great circles of discontinuities and free surfaces with JP-Codes: 101

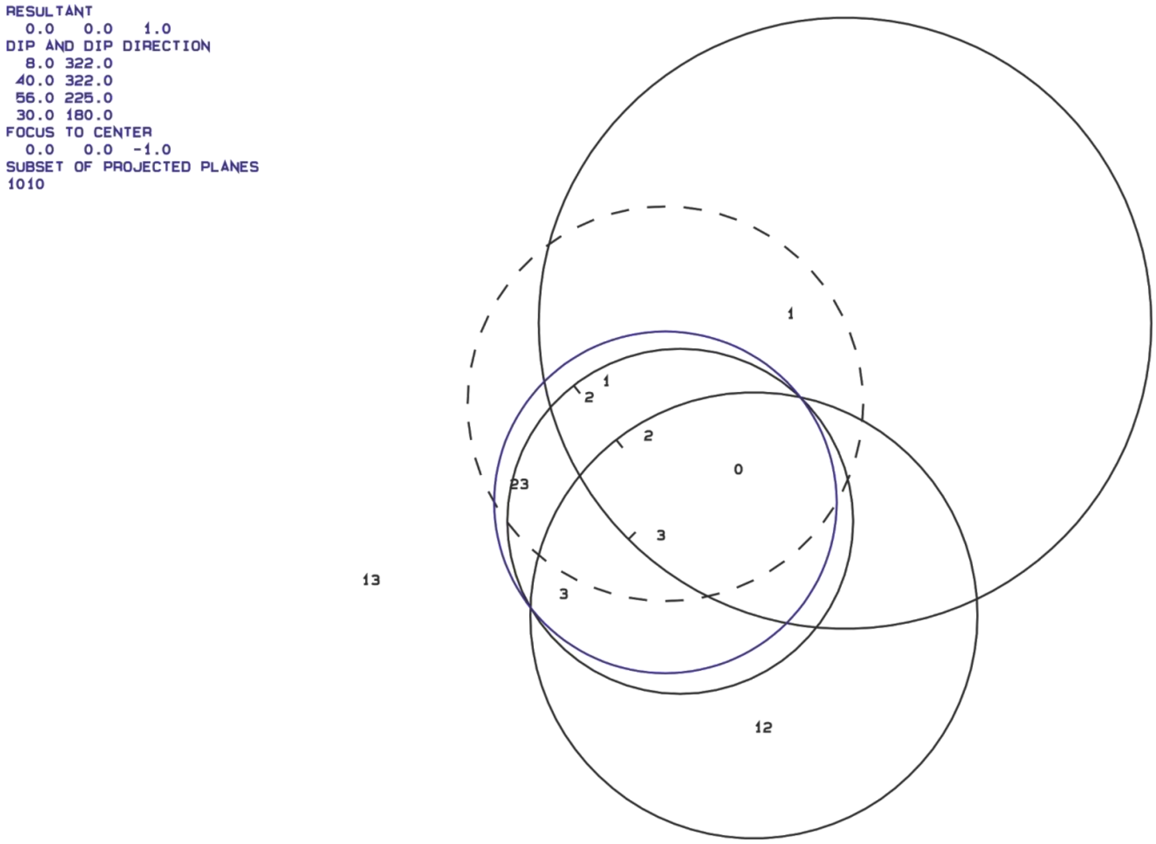

Figure 5.22: Block 9 with the Failure mode 2

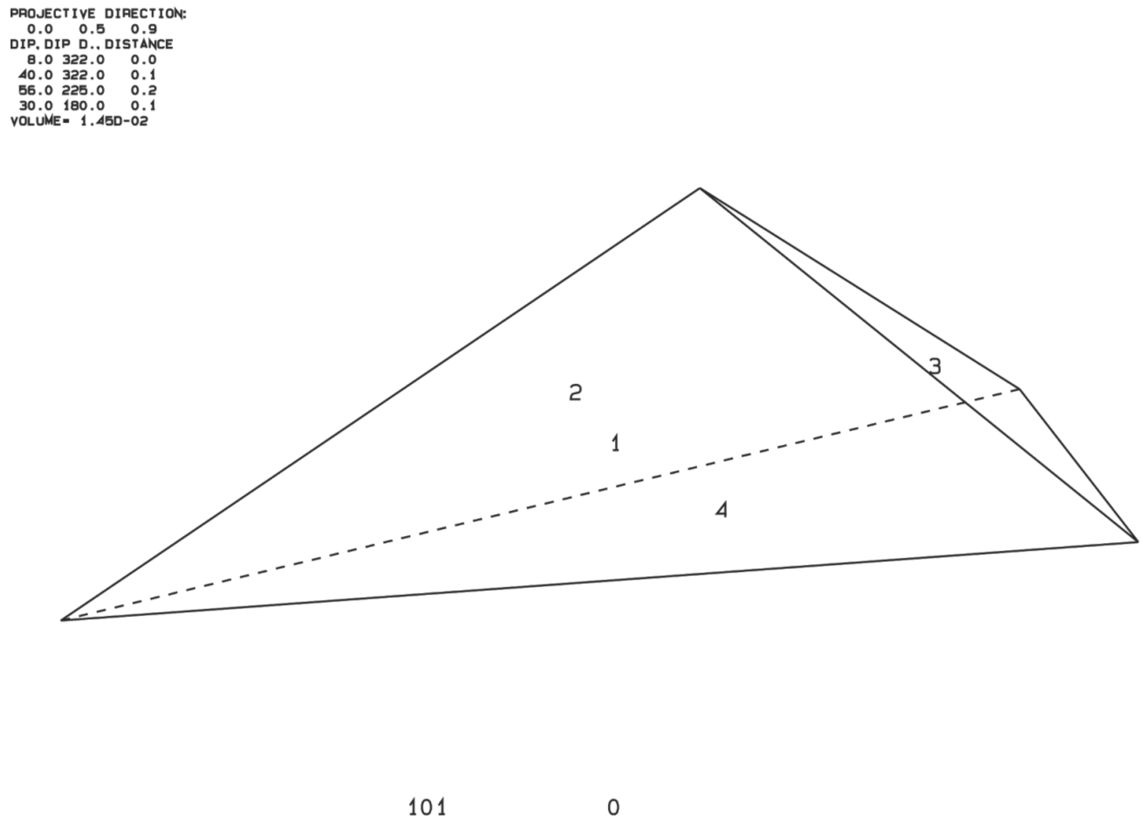

Figure 5.23: Block 9 form and volume: 0.0145m³

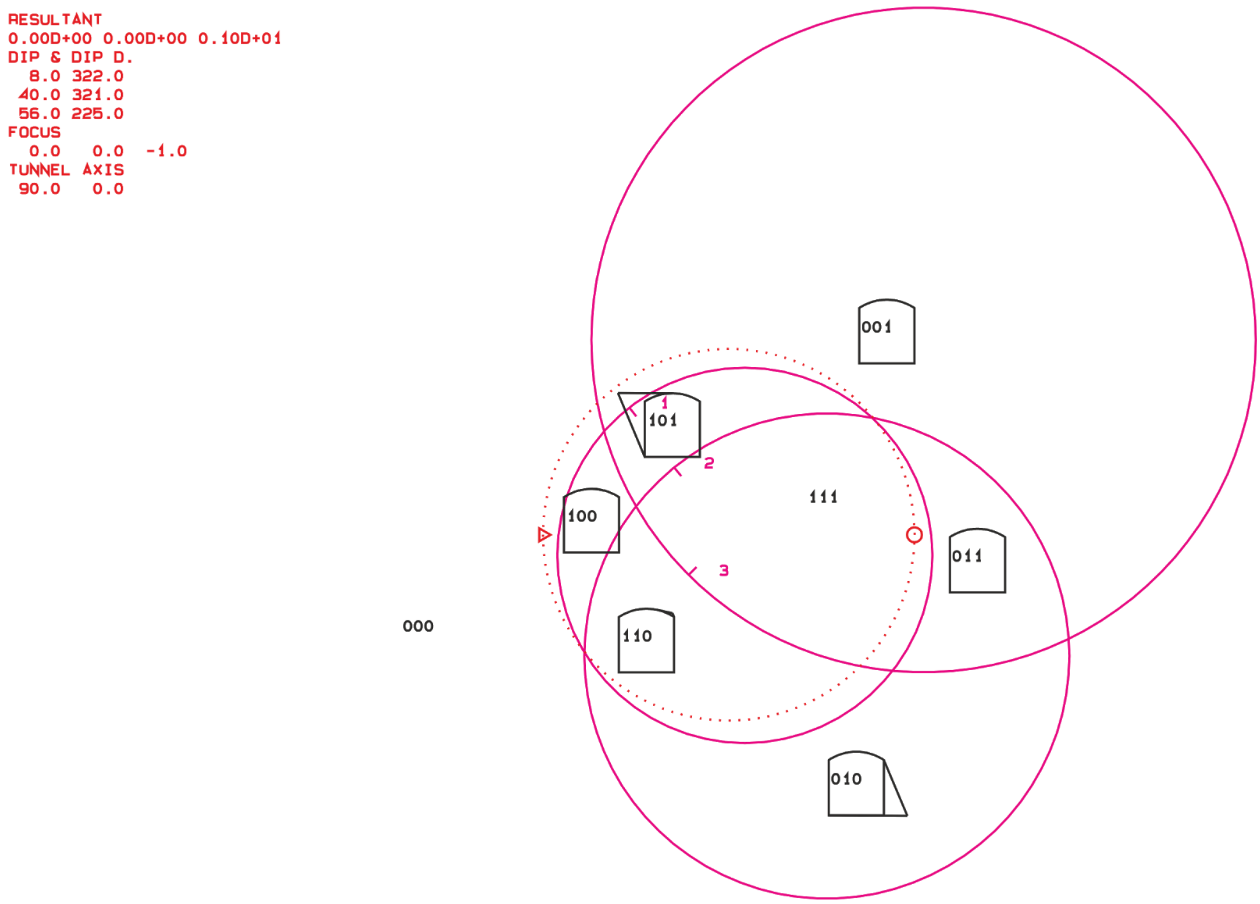

Figure 5.24: Block 9 with JP-Code 101 on tunnel cross-section

5.2.3 Block 32

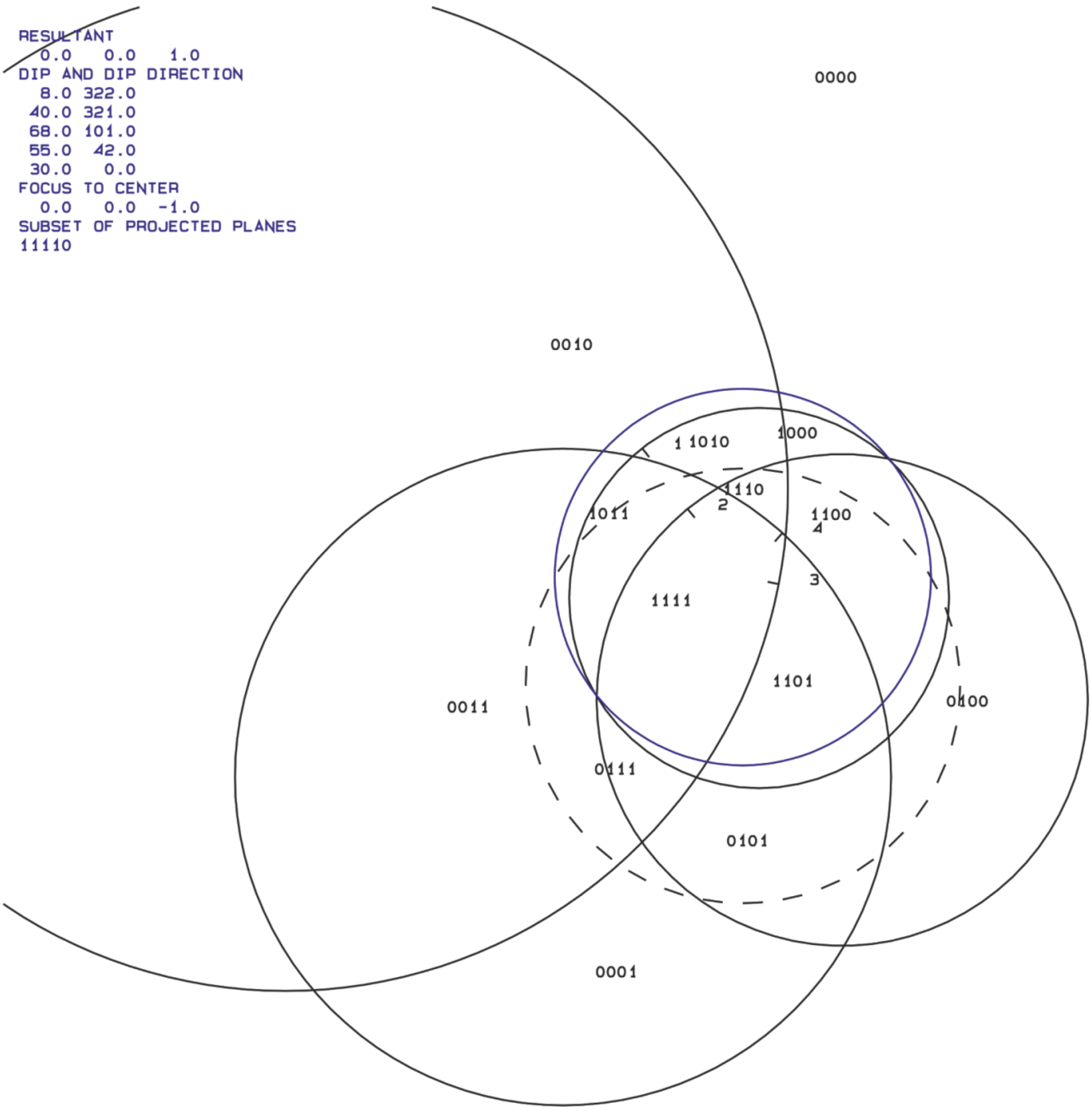

Figure 5.25: Block 32: great circles of discontinuities and free surfaces with JP-Codes: 1111

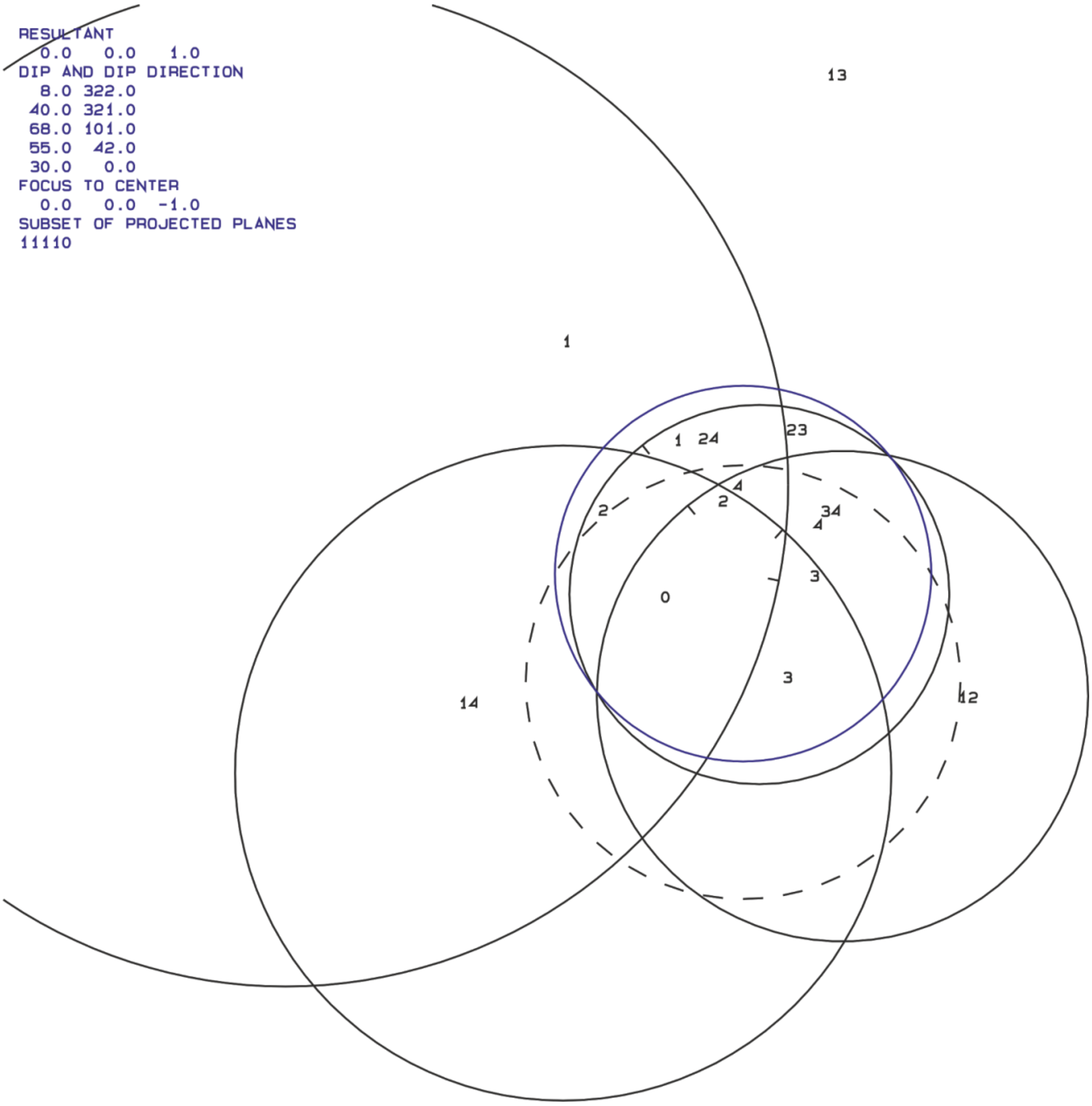

Figure 5.26: Block 32 with the Failure mode 0

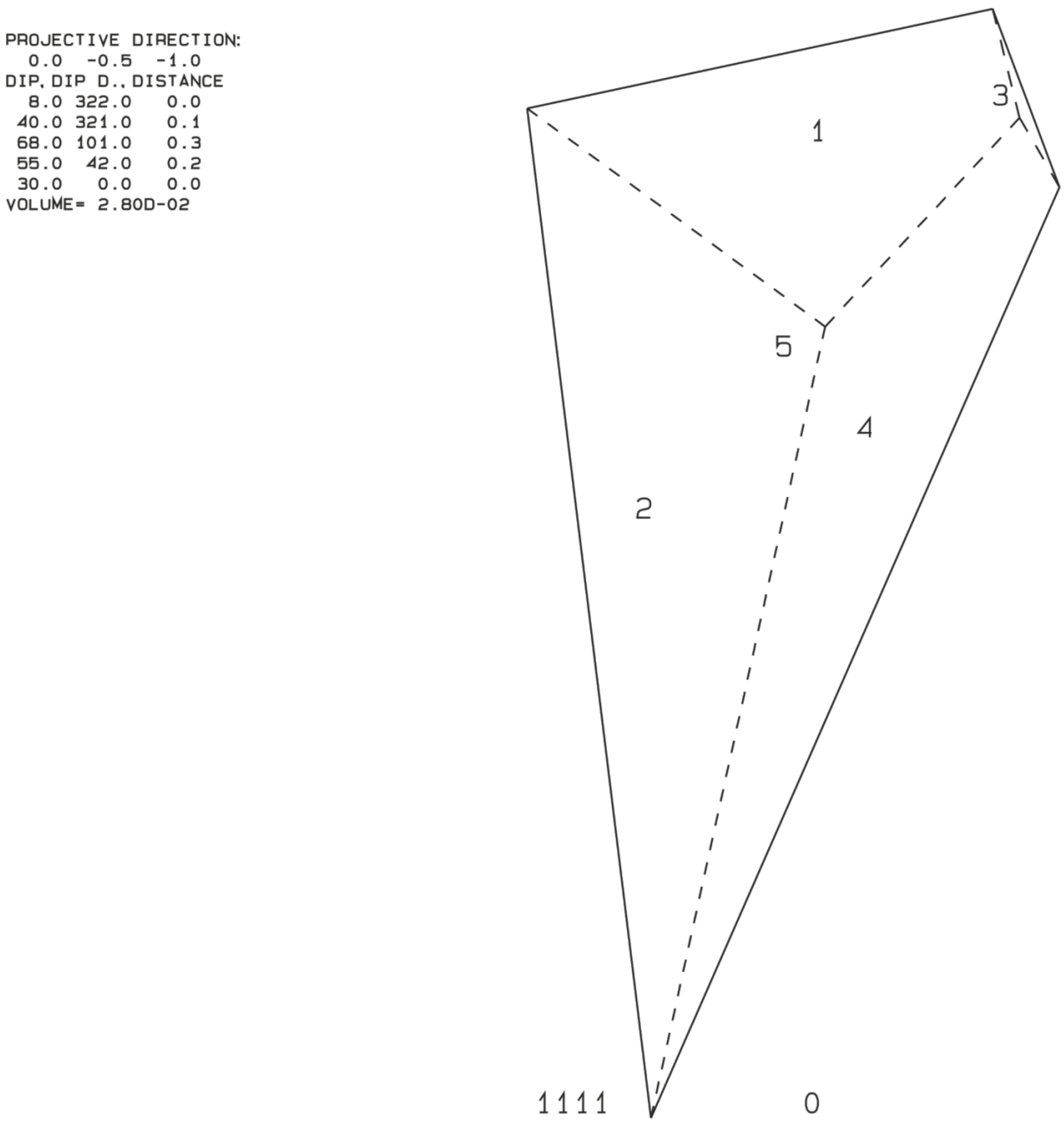

Figure 5.27: Block 32 form and volume 0.0280m³

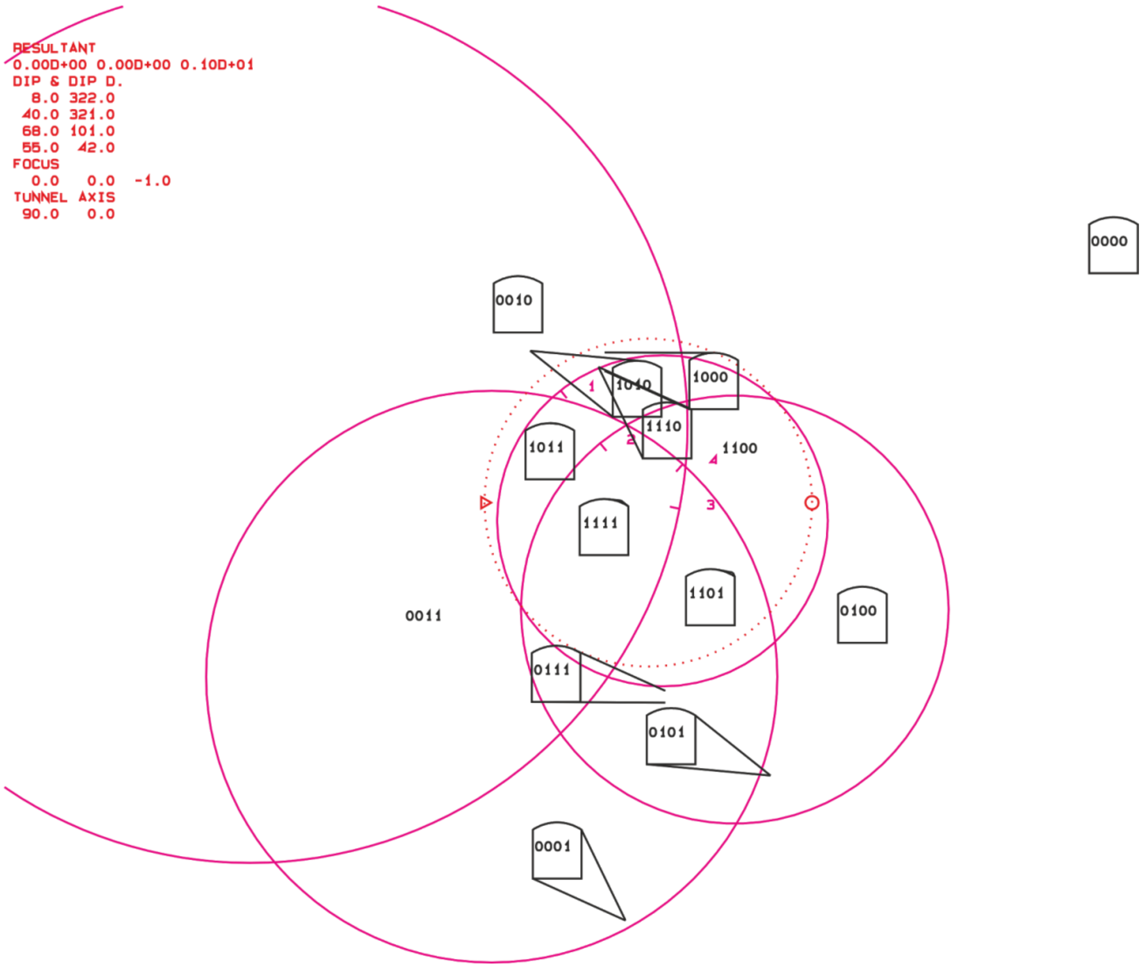

Figure 5.28: Block 32 with JP-Code 1111 on tunnel cross-section

5.2.4 Block 57

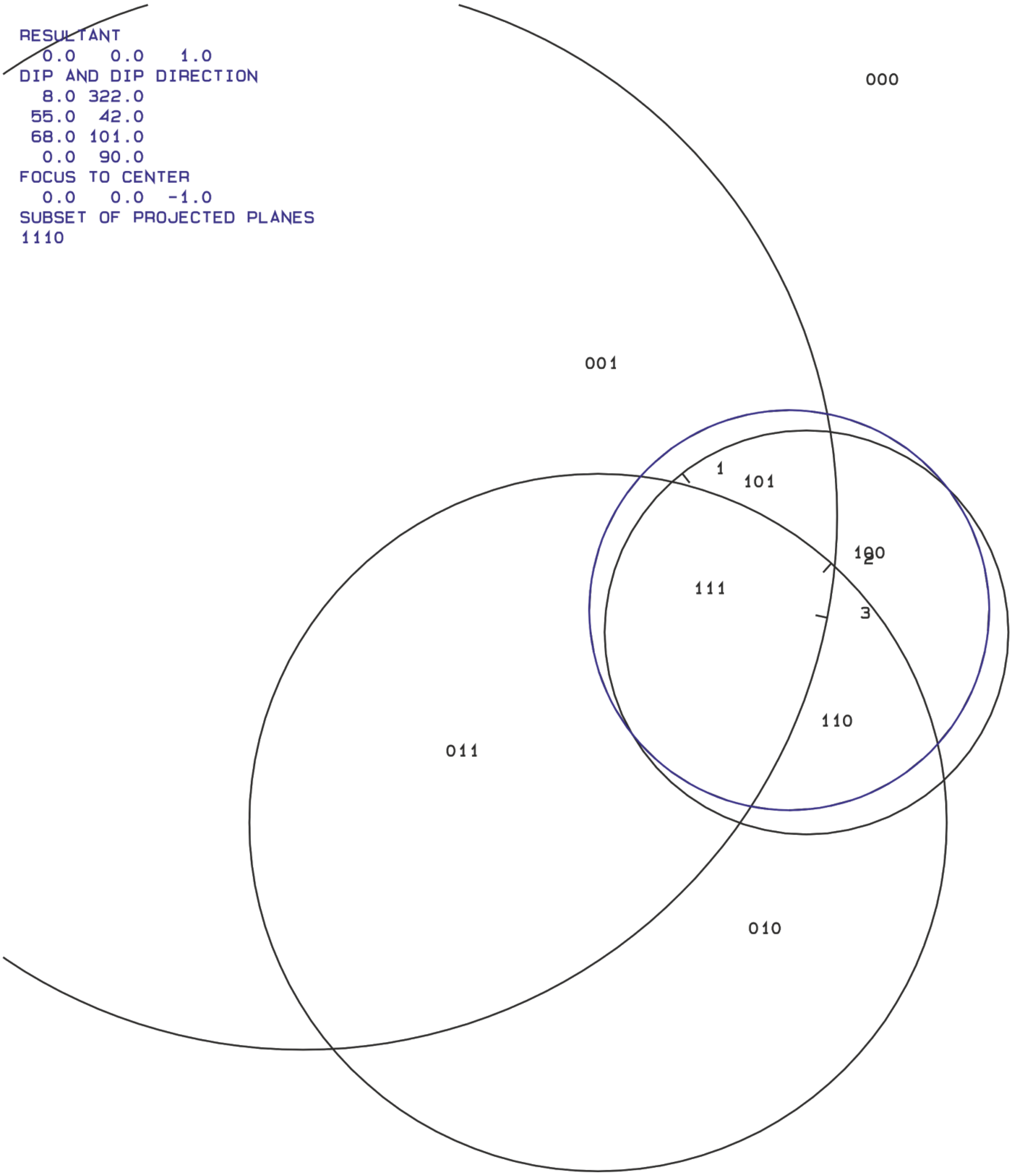

Figure 5.29: Block 57: great circles of discontinuities and free surface with JP-Codes: 111

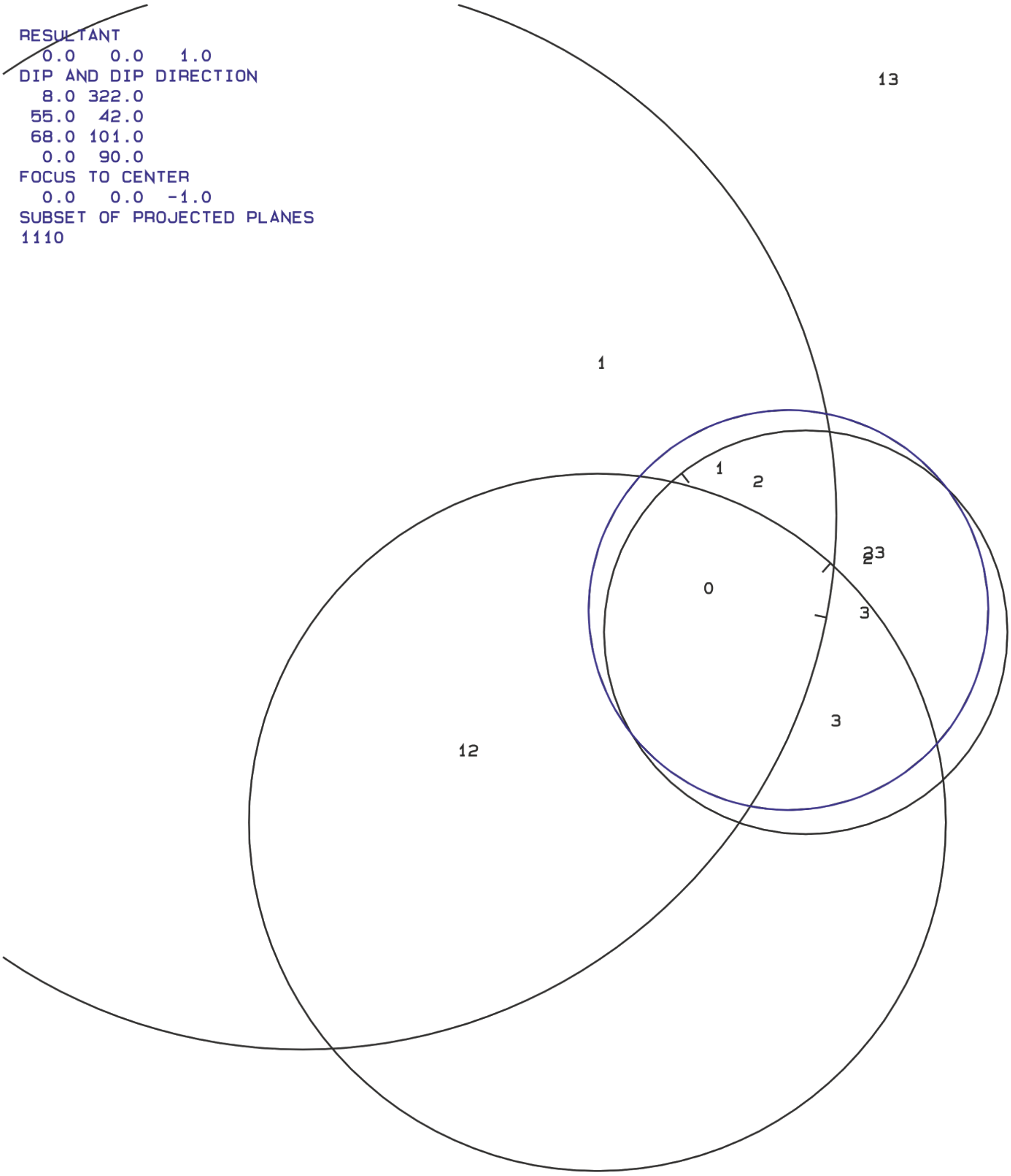

Figure 5.30: Block 57: with failure mode 0

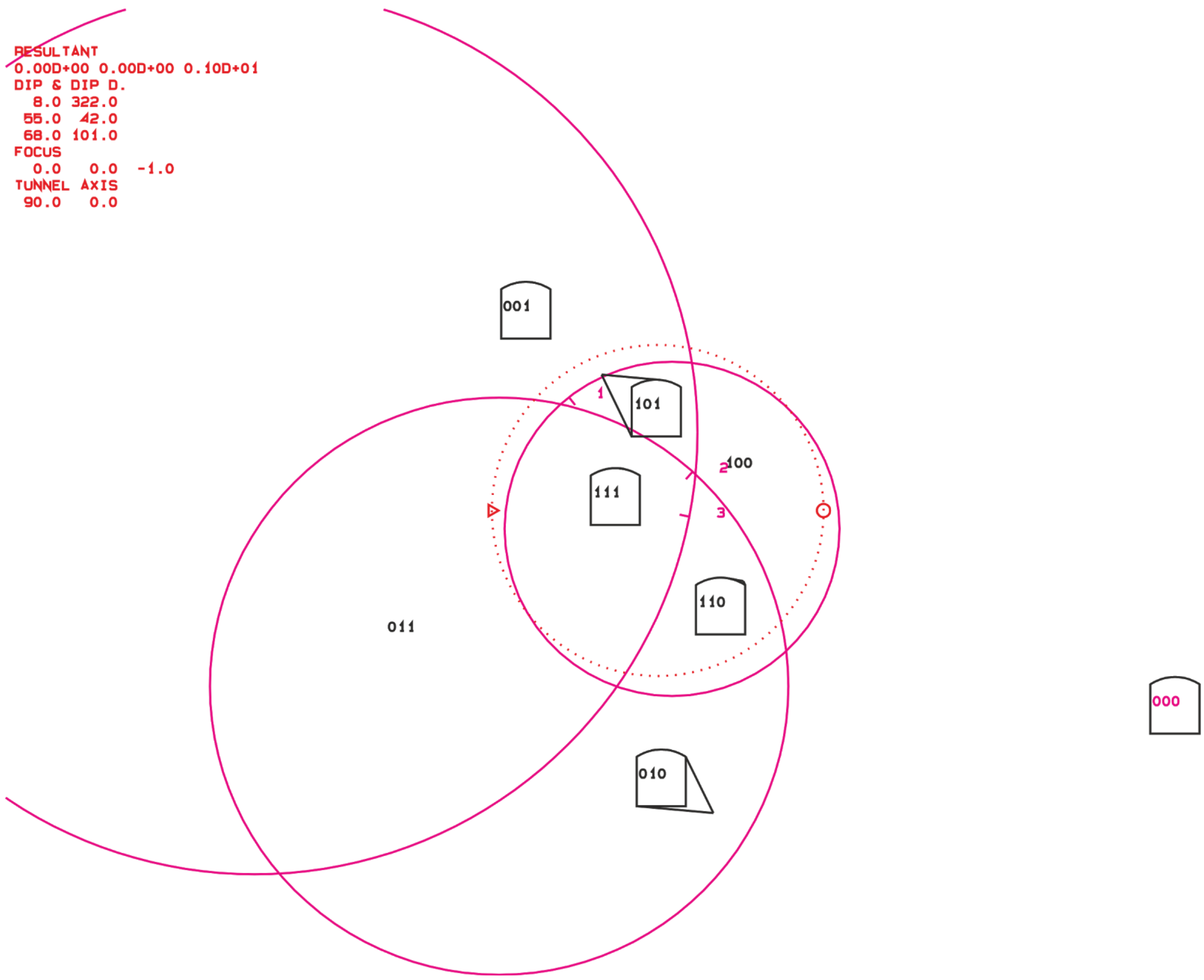

Figure 5.31: Block 57 with JP-Code 111 on tunnel cross-section

5.2.5 Block 58

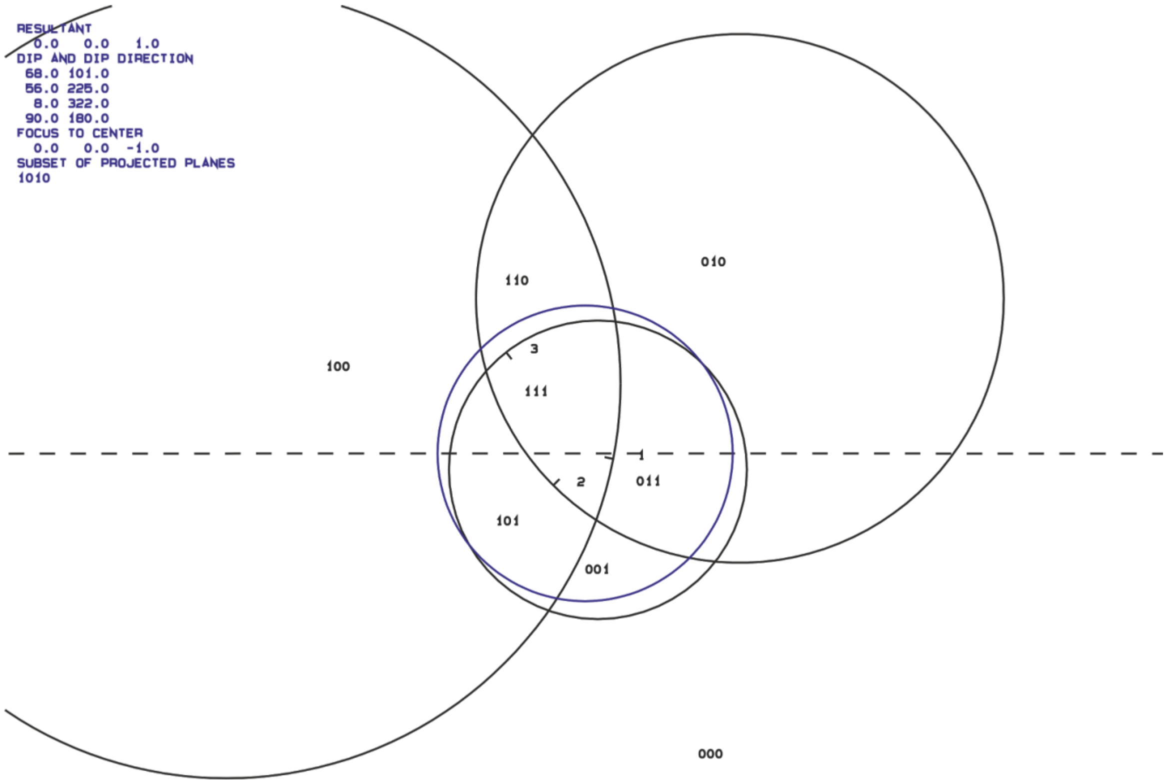

Figure 5.32: Block 58: great circles of discontinuity and free surface with JP-Codes: 101

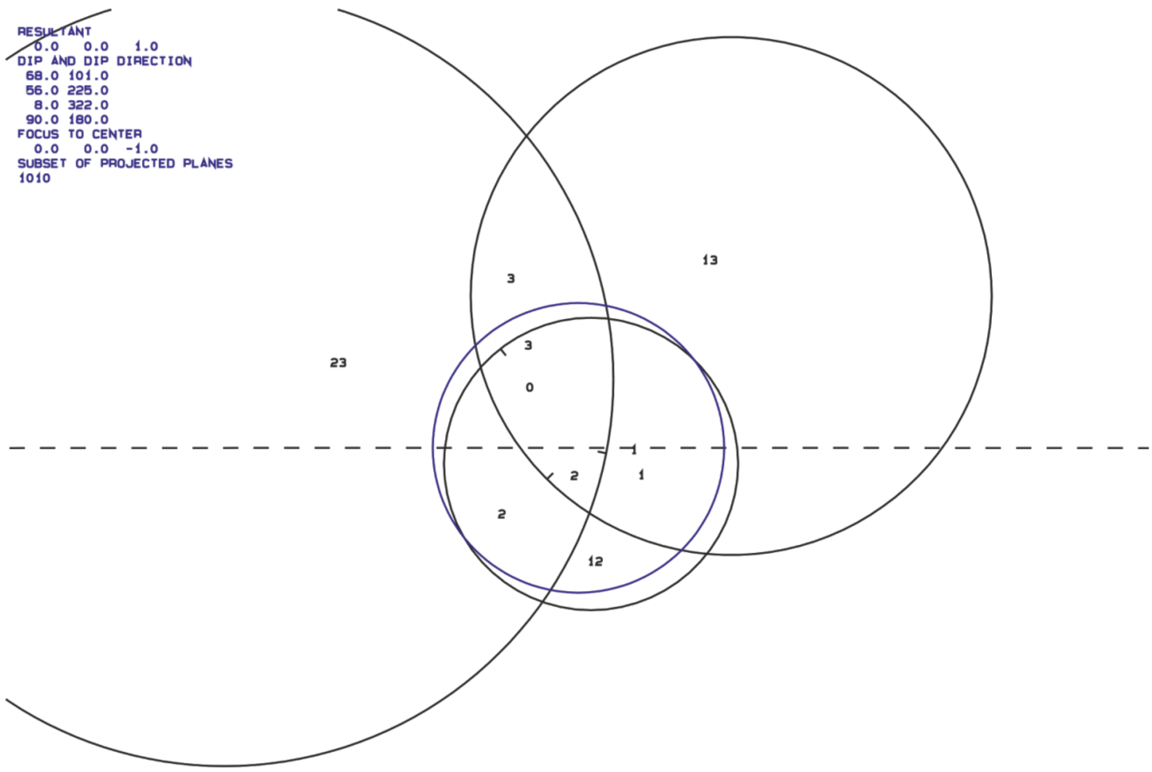

Figure 5.33: Block 58 with failure mode 2

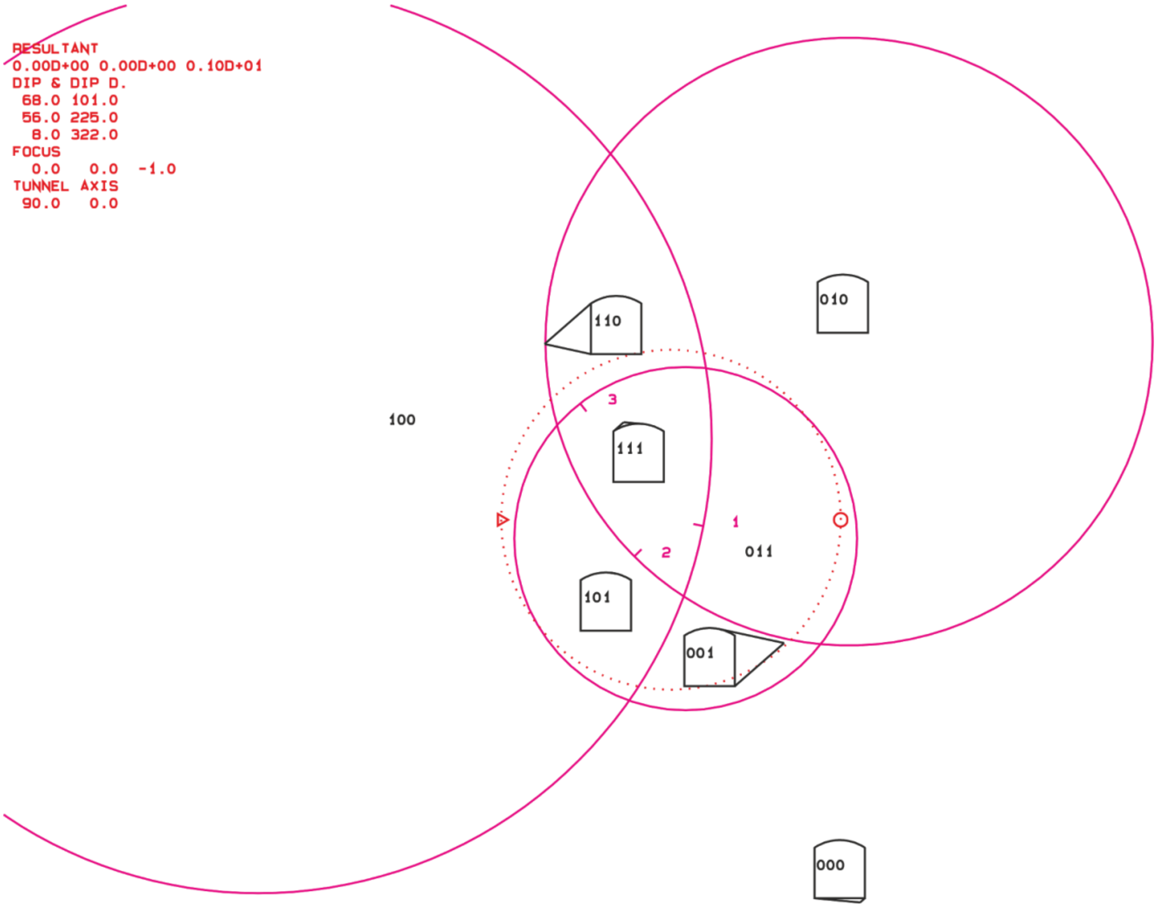

Figure 5.34: Block 58 with JP-Code 101

5.2.6 Block 61

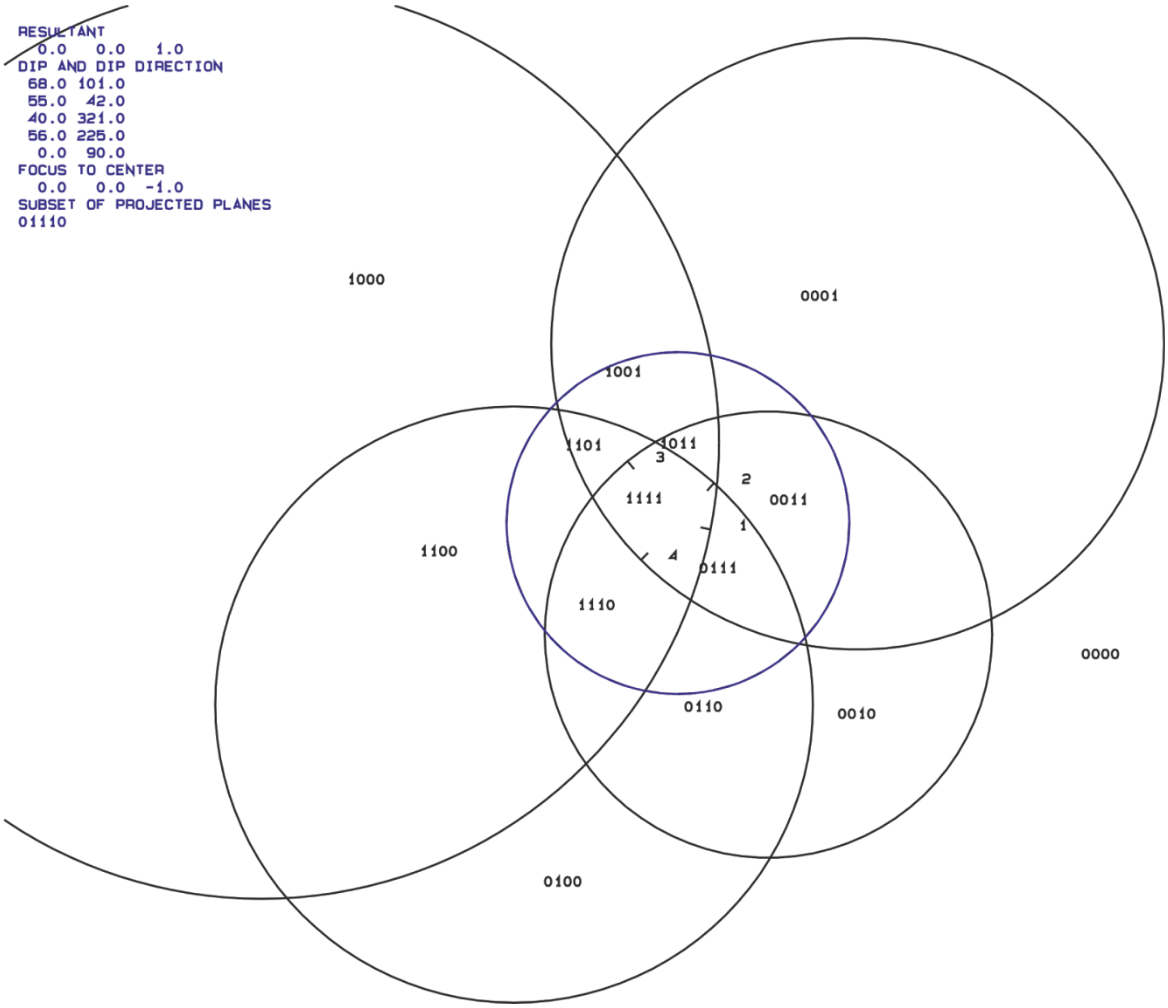

Figure 5.35: Block 61: great circles of discontinuities and free surface with JP-Codes: 0111

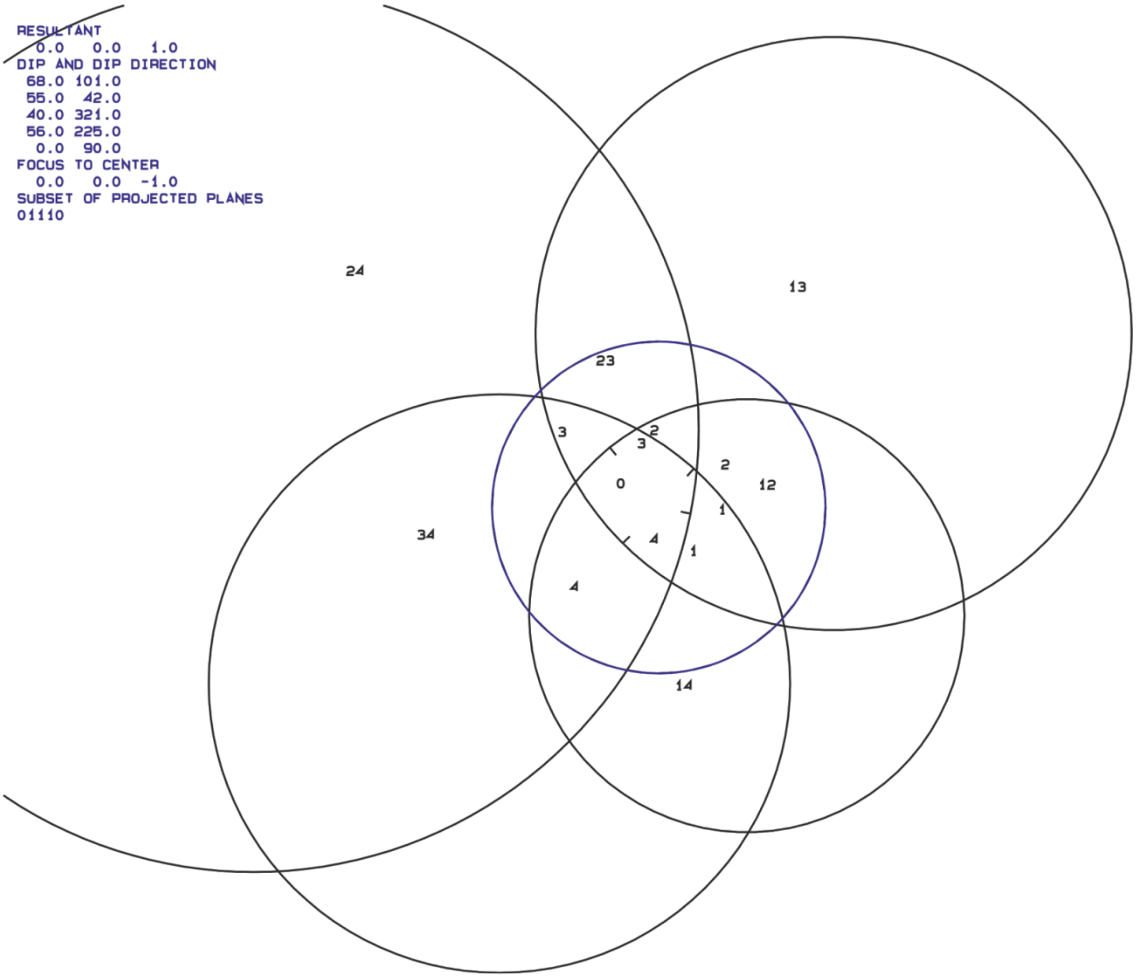

Figure 5.36: Block 61 with failure mode 1

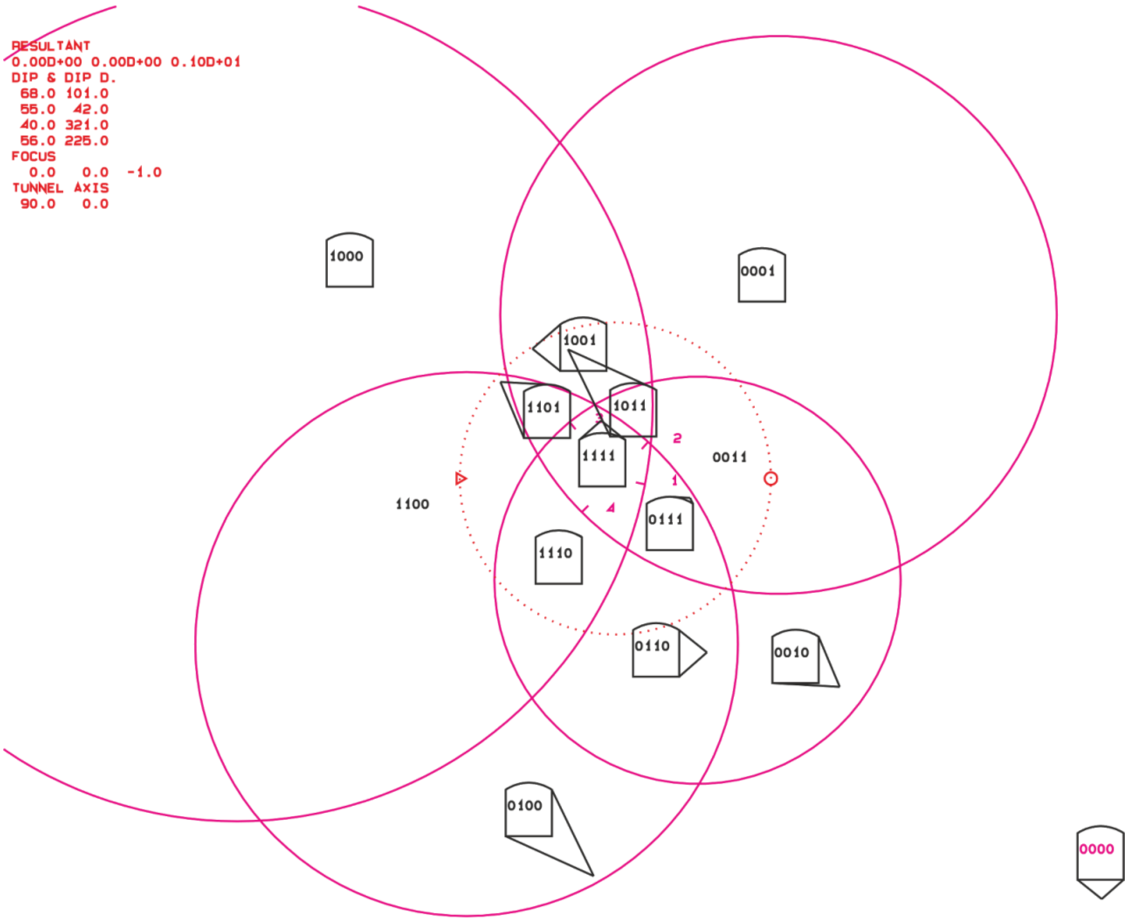

Figure 5.37: Block 61 with JP-Code 0111 on tunnel cross-section

5.2.7 Block 62

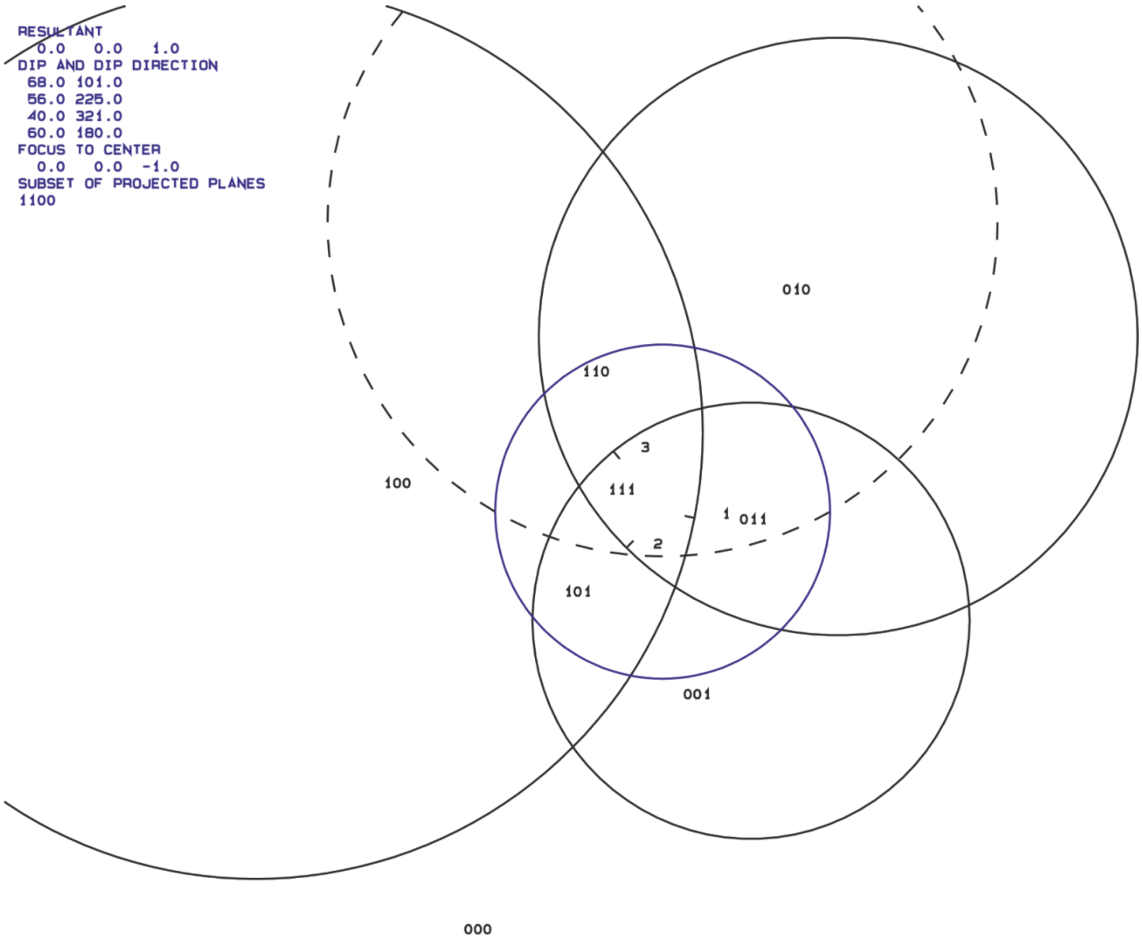

Figure 5.38: Block 62: great circles of discontinuities and free surface with JP-Code: 110

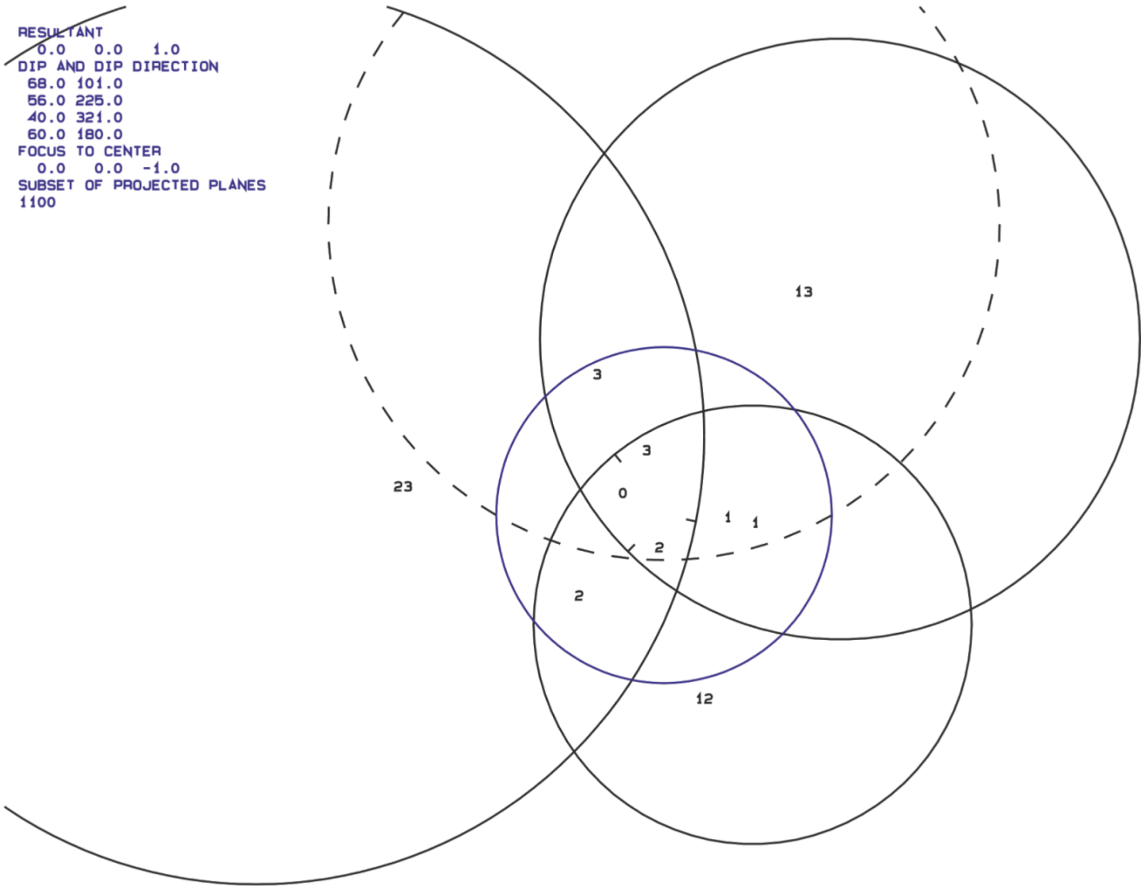

Figure 5.39: Block 62 with failure mode 3

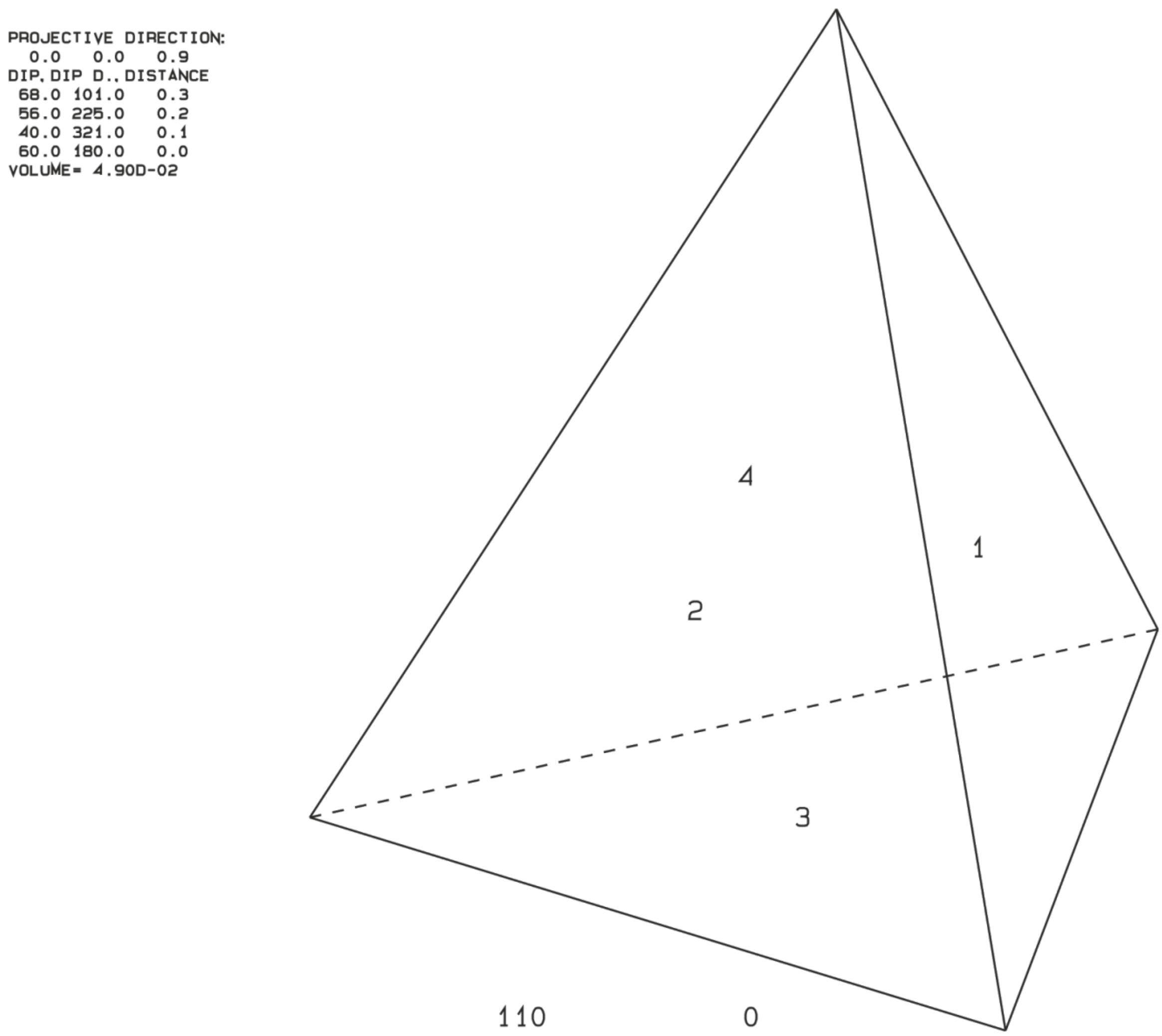

Figure 5.40: Block 62 form and volume 0.0490m³

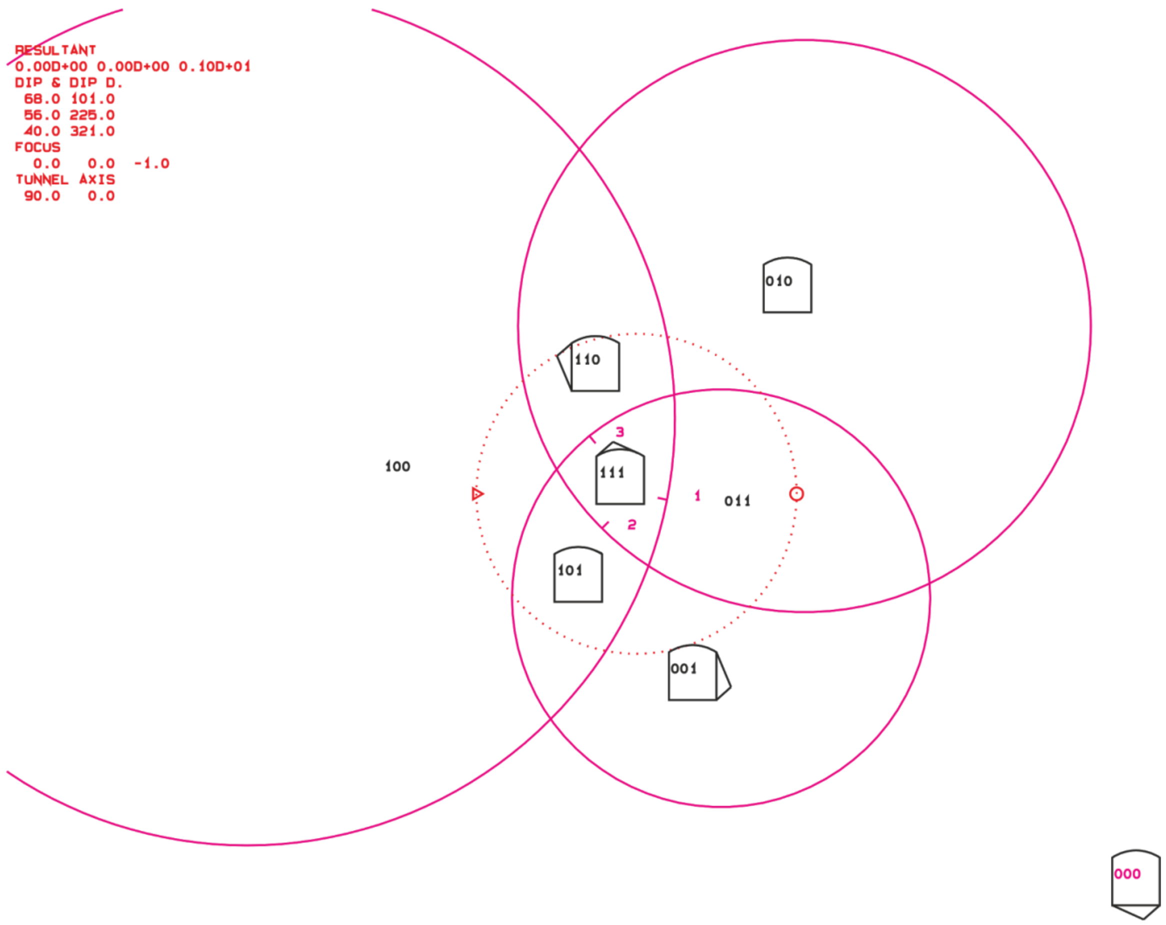

Figure 5.41: Block 62 with JP-Code 110 on tunnel cross-section

5.2.8 Block 64

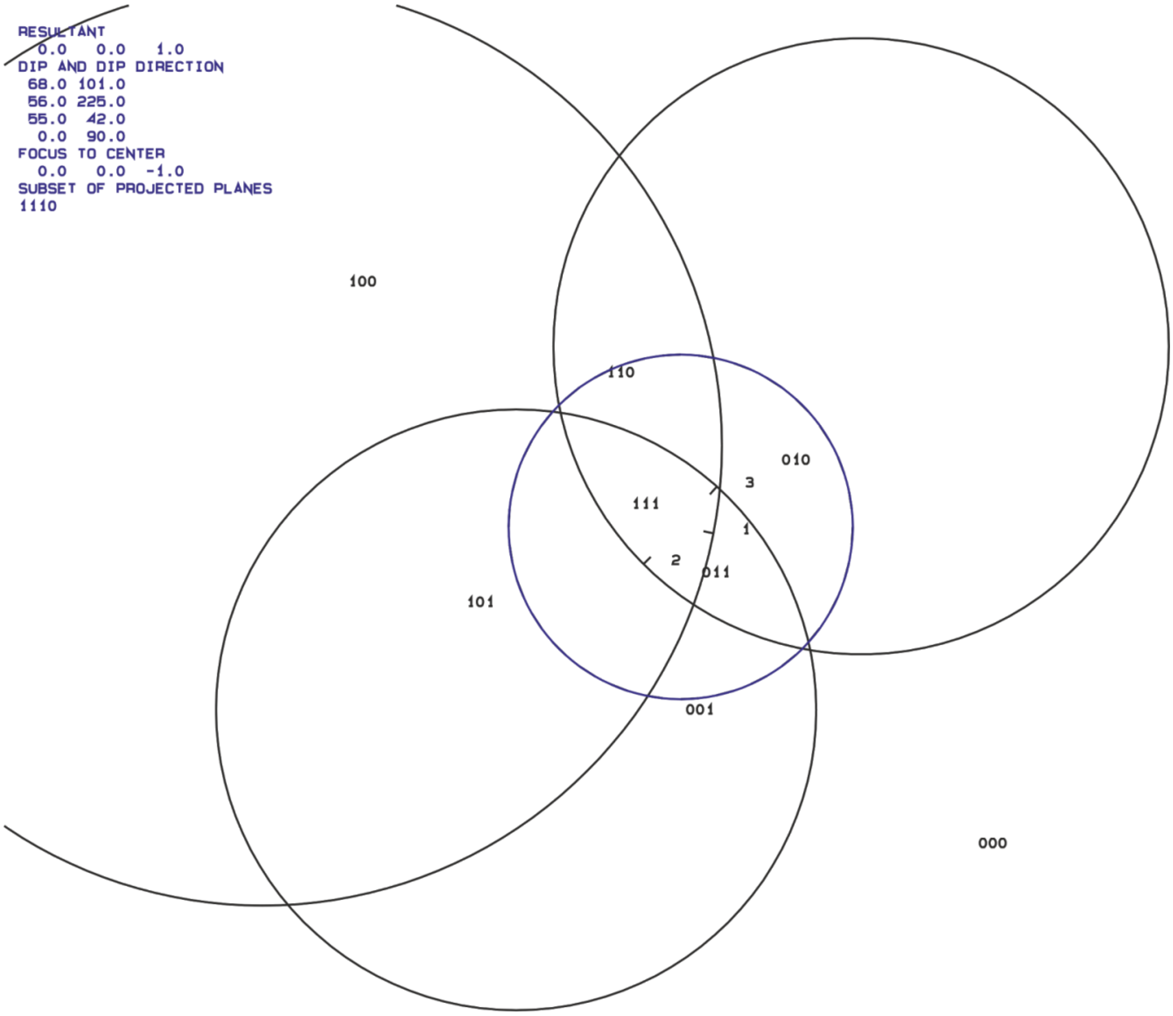

Figure 5.42: Block 64: great circles of discontinuities and free surface with JP-Codes: 111

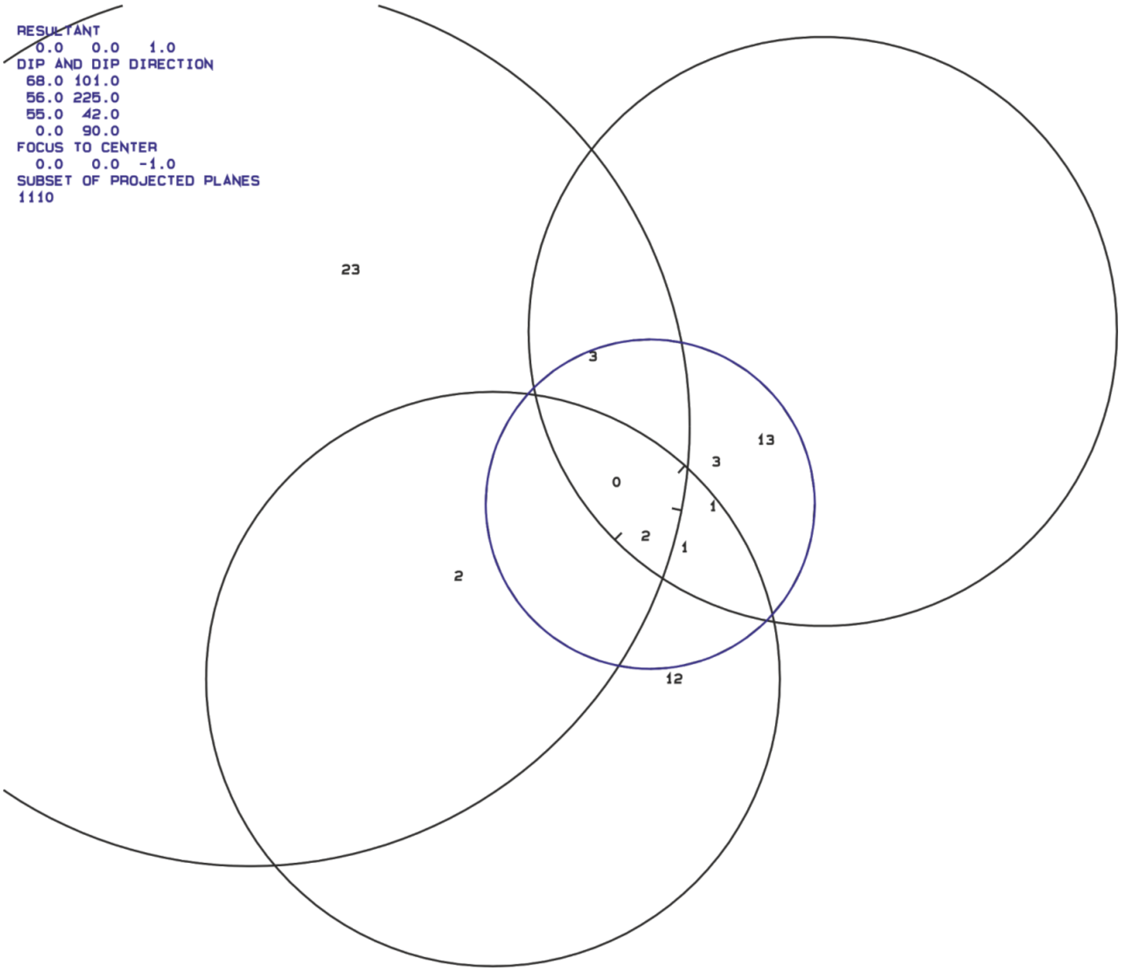

Figure 5.43: Block 64 with failure mode 0

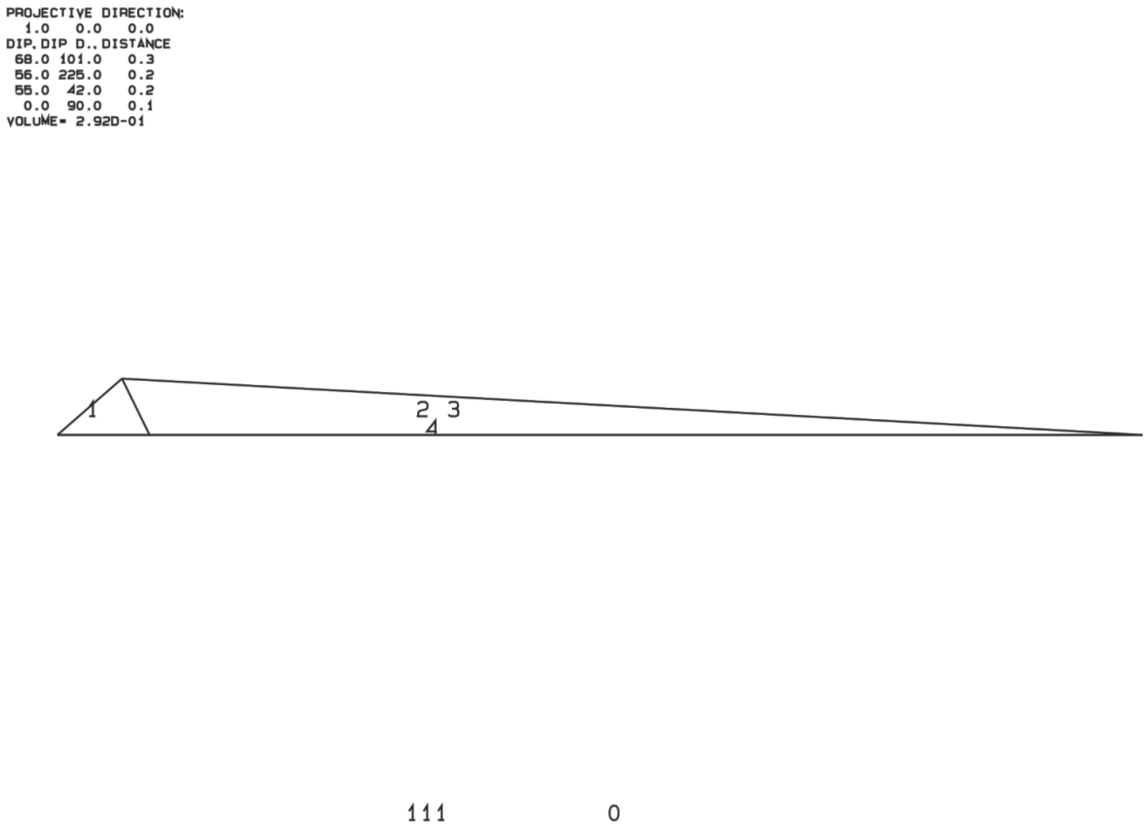

Figure 5.44: Block 64 form and volume 0.0123m³

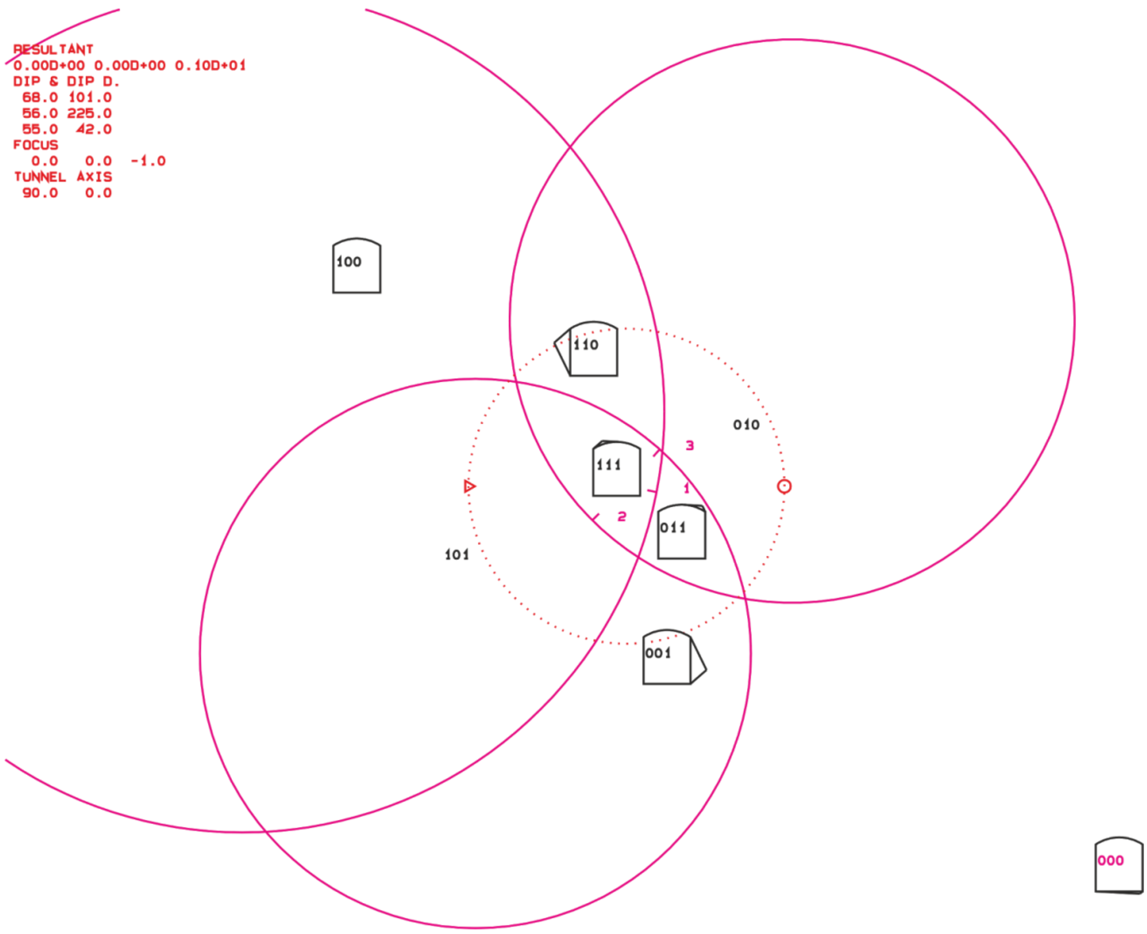

Figure 5.45: Block 64 with JP-Code 111 on tunnel cross-section

5.2.9 Summary of Reconstructed Blocks

In summary, Area 1 consists of 16 previously failed blocks. These blocks were then removed and the dominant joint sets were mapped out and designated. It was established that Area 1 consisted of 5 discontinuity sets (J1, F1, J2, J3 and J4). The previously failed blocks discontinuities were placed into the designated sets. Of the 16 total blocks, those with greater than 5 discontinuity sets could not be reconstructed leaving 14 blocks. Also, any blocks which contained repeated discontinuity sets could not be reconstructed leaving 8 blocks. By this, it is meant that some of the original blocks contained two or more discontinuities which had similar orientations to one of the discontinuity sets. For example, Block 10 contained two discontinuities with similar orientations to J3. Of the 8 blocks which were reconstructed, 3 blocks JPs were no longer completely within their EPs and thus were not potential removable blocks. The 5 blocks which were reconstructed and were potential removable blocks were blocks 8, 9, 32, 62 and 64. Table 5.17 shows the volumes of those blocks from their original calculation and the volume from the set calculation.

Block No.	Original Volume [m^3]	Set Volume [m^3]
8	0.0423	0.0409
9	0.0406	0.0145
32	0.0106	0.0280
62	0.00579	0.0490
64	0.0123	0.292

Table 5.17: Reconstructed blocks showing original volumes and set volumes

With the exception of Block 8, the set block volumes are far different from the original volumes by up to a factor of 10. This may be attributed to the fact that the set volumes constitute an average volume for blocks since the set spacing is fixed. Meanwhile the spacing’s for the original volumes were measured in situ and represent the actual volume of those blocks. The differences in volume may also be attributed to the simplification of the tunnel cross-section. It was assumed that the tunnel surface was planar and was split into 7 orientations. F1 through F7 where F1 =

90/000, F2 = 60/000, F3 = 30/000, F4 = 00/000, F5 = 30/180, F6 = 60/180 and F7 = 90/180.

5.3 Largest Mapped Blocks

The following figures represent the largest mapped in-situ blocks (Figures 5.46 to 5.77).

5.3.1 Block 2

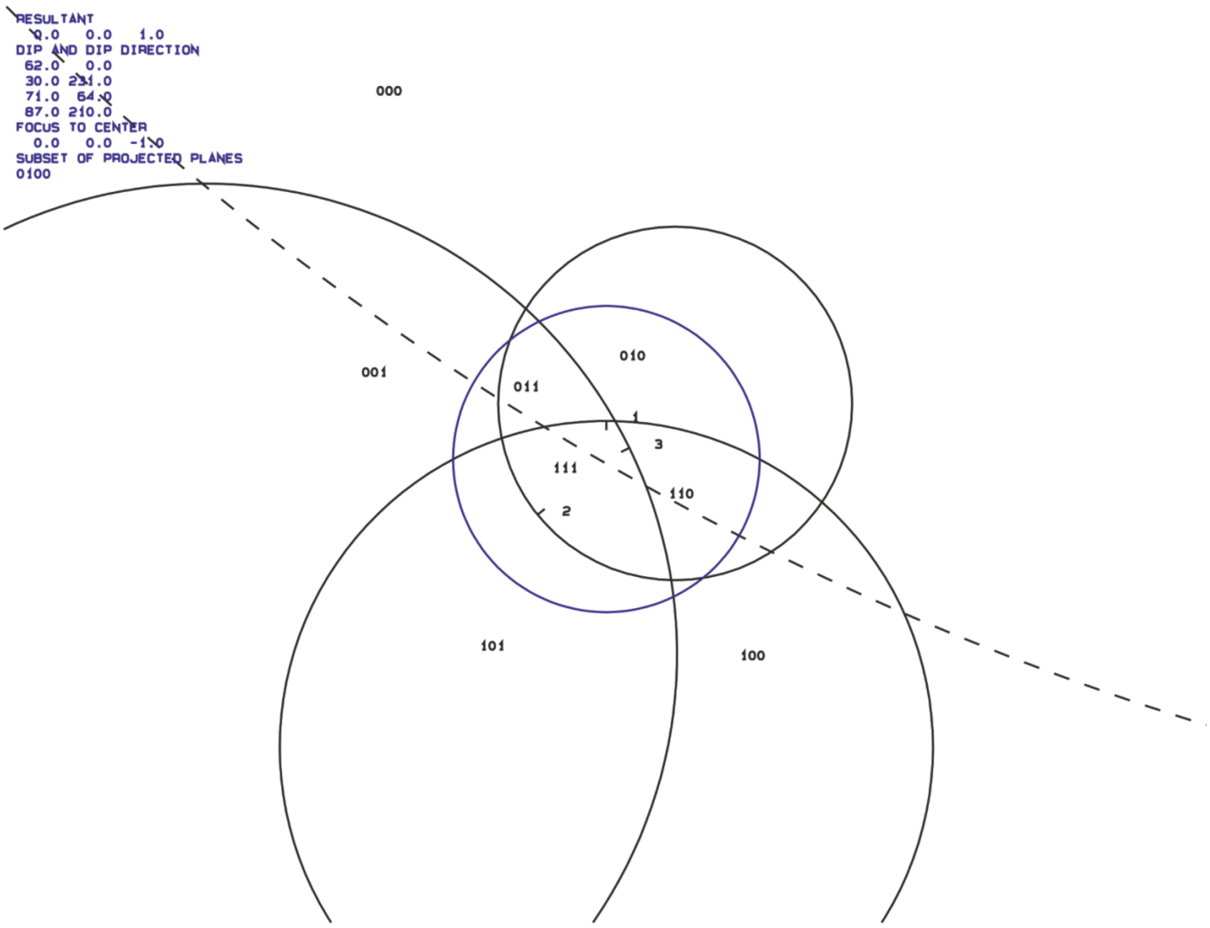

Figure 5.46: Block 2: great circles of discontinuities and free surface with JP-Codes: 010

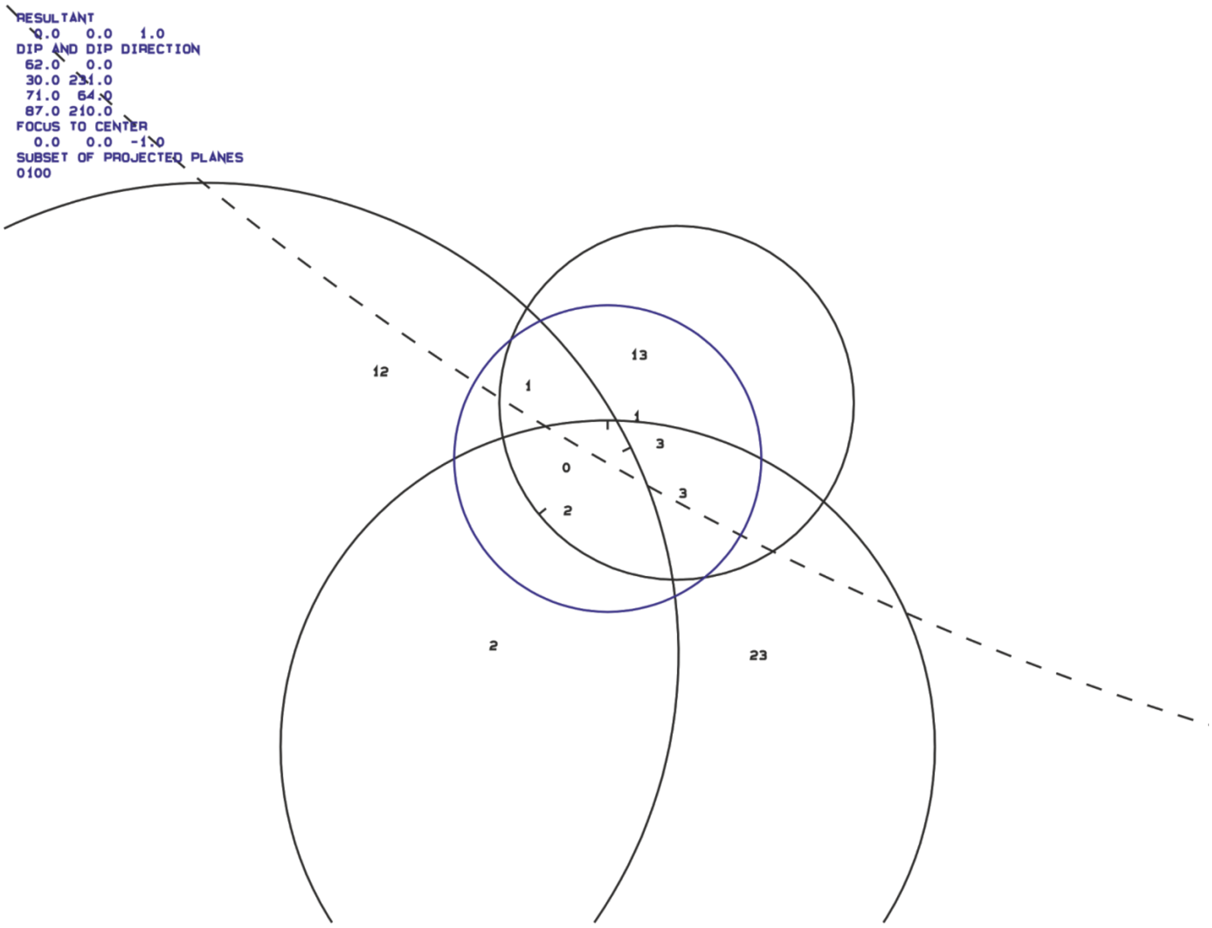

Figure 5.47: Block 2 with failure mode 13

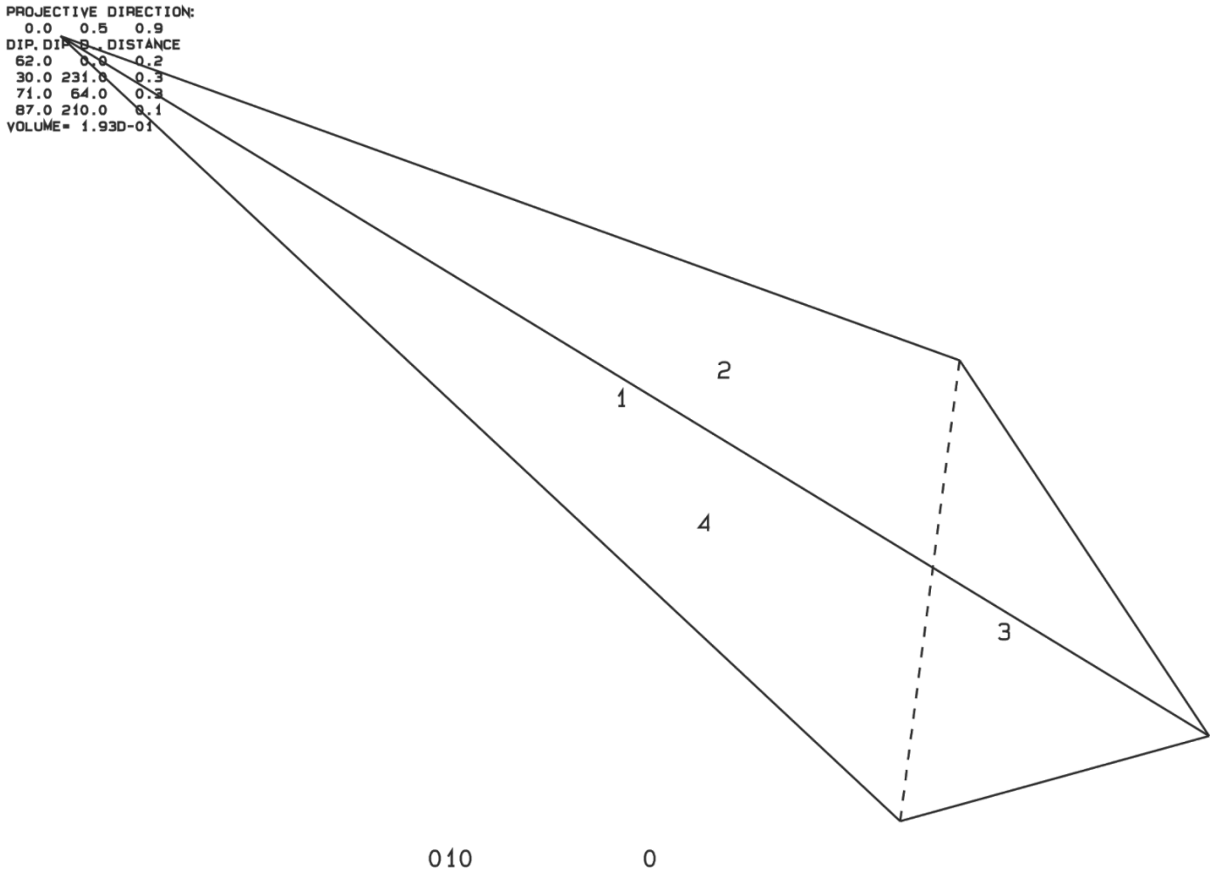

Figure 5.48: Block 2 form and volume 0.193m³

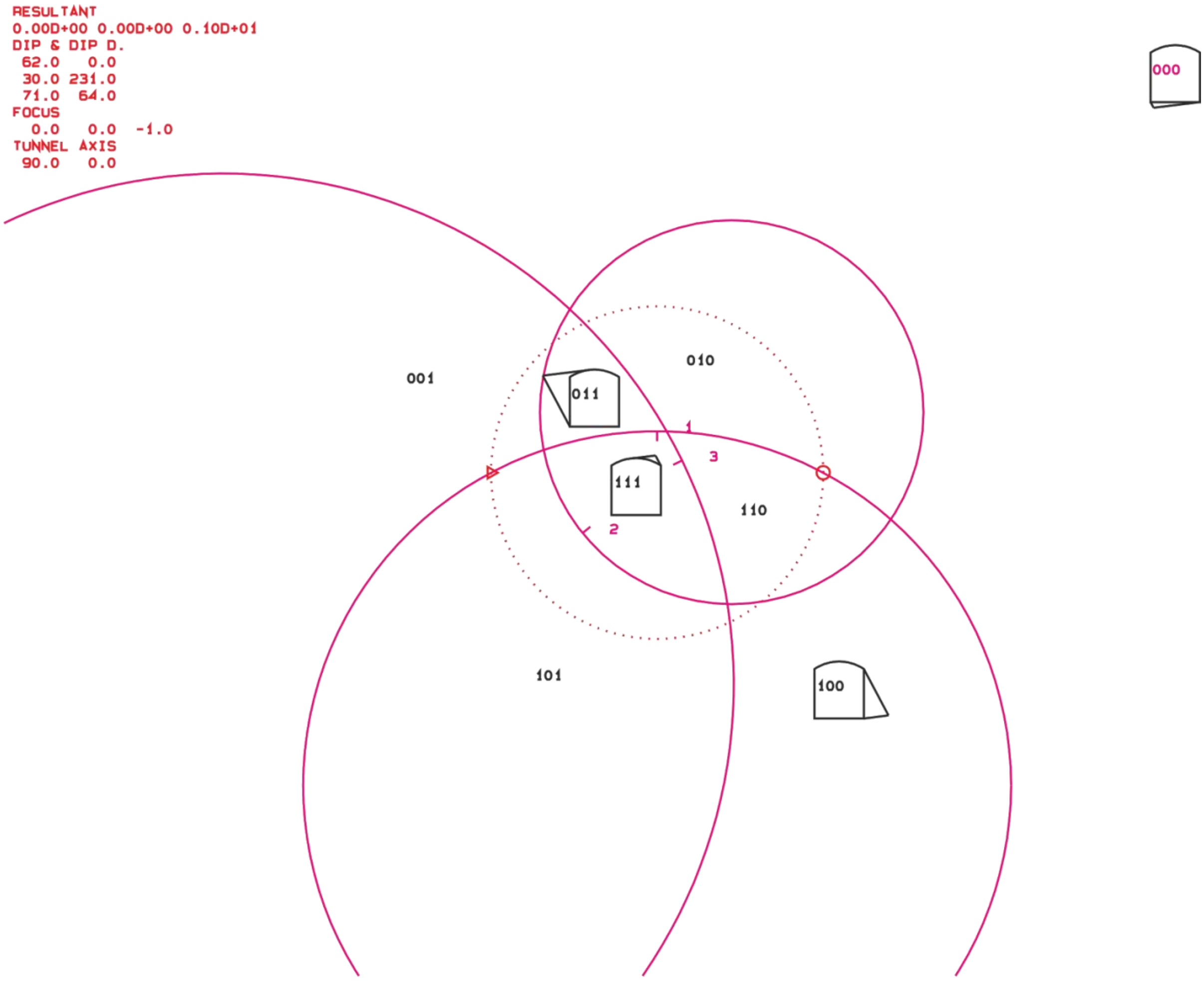

Figure 5.49: Block 2 with JP-Code 010 not shown on tunnel cross-section

5.3.2 Block 5

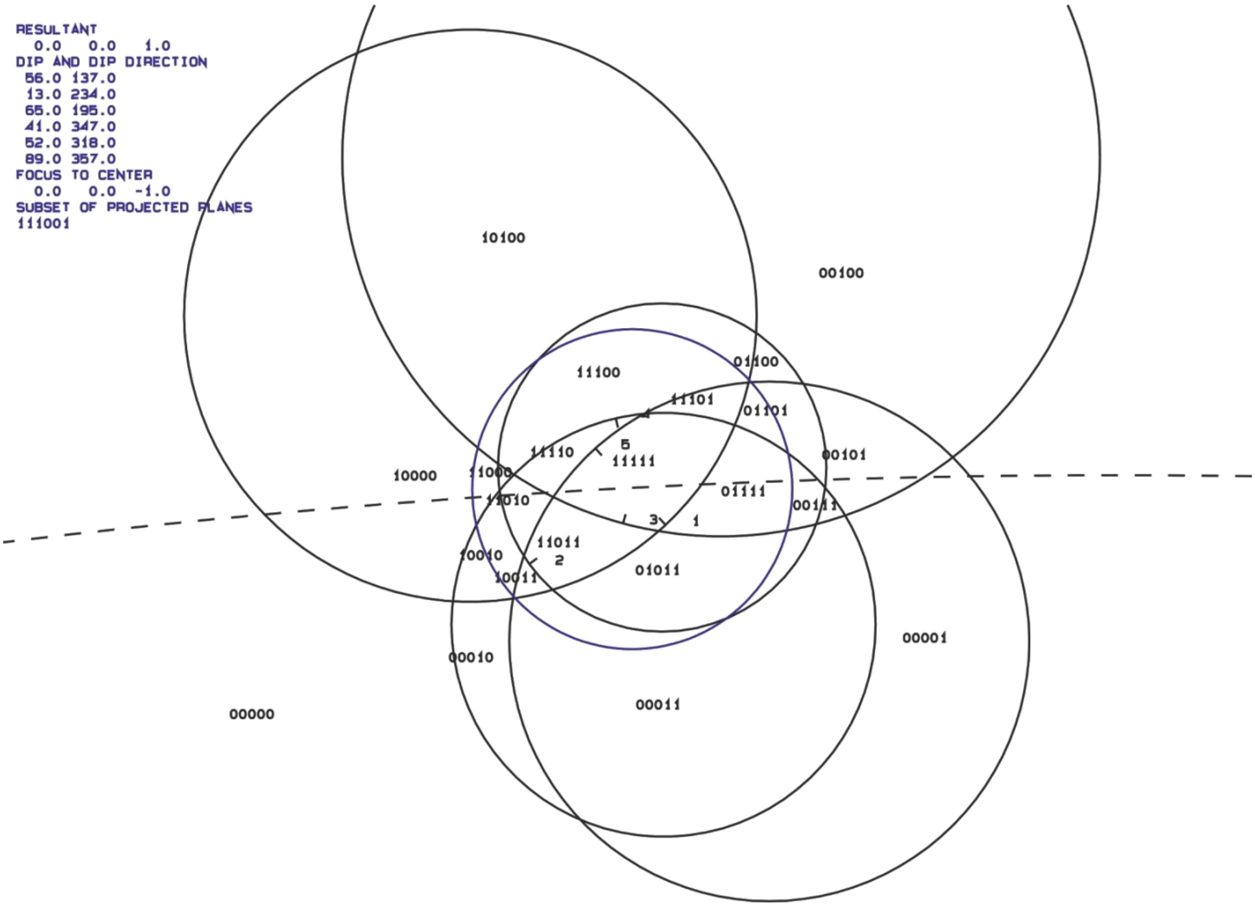

Figure 5.50: Block 5: great circles of discontinuities and free surface with JP-Codes: 11100

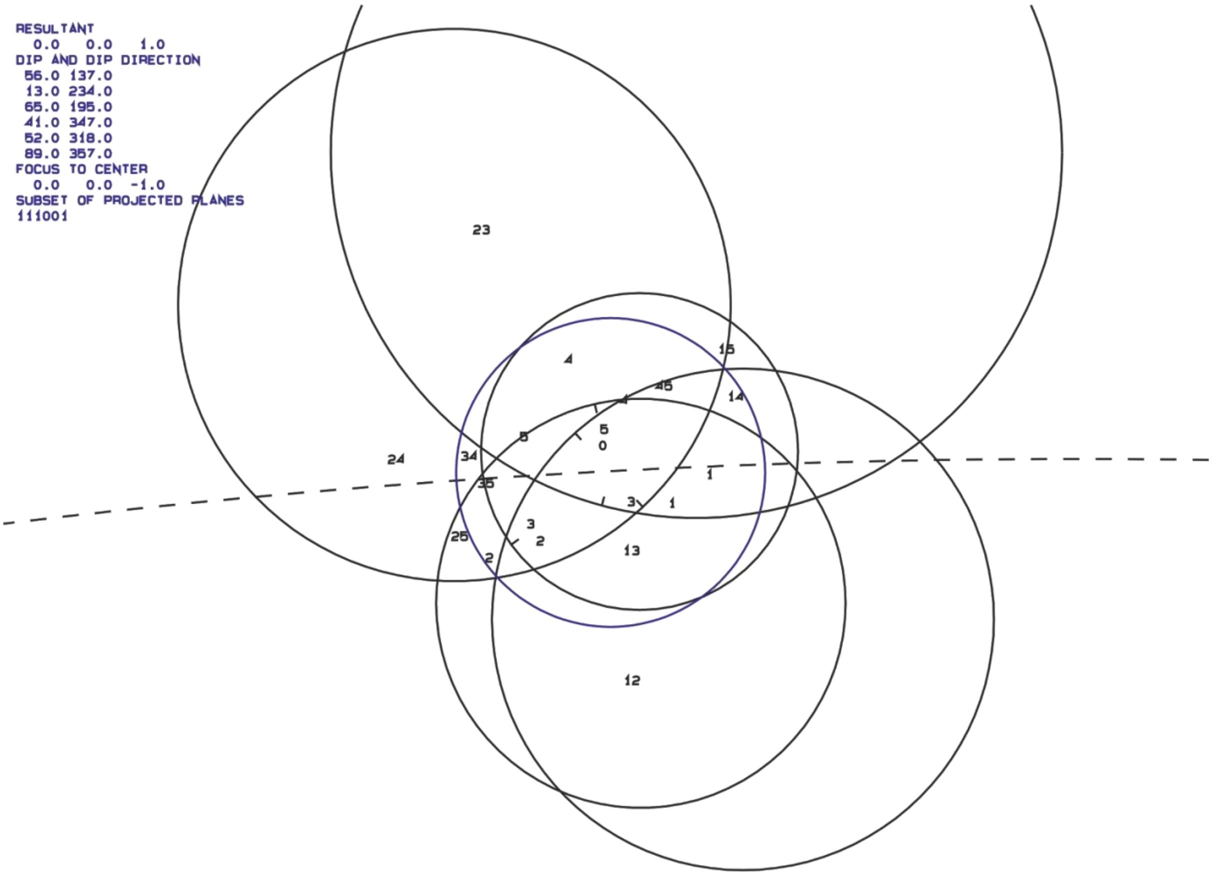

Figure 5.51: Block 5 with failure mode 4

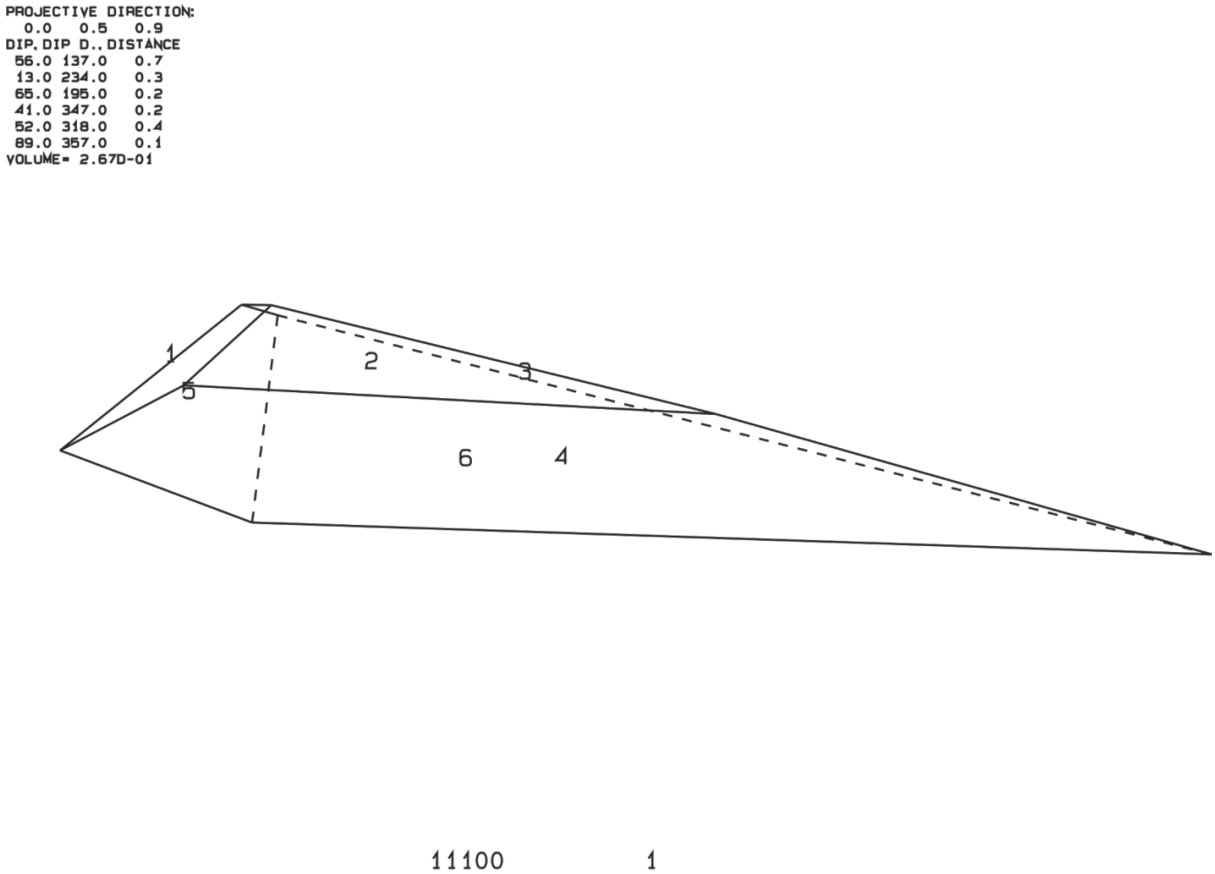

Figure 5.52: Block 5 form and volume 0.267m³

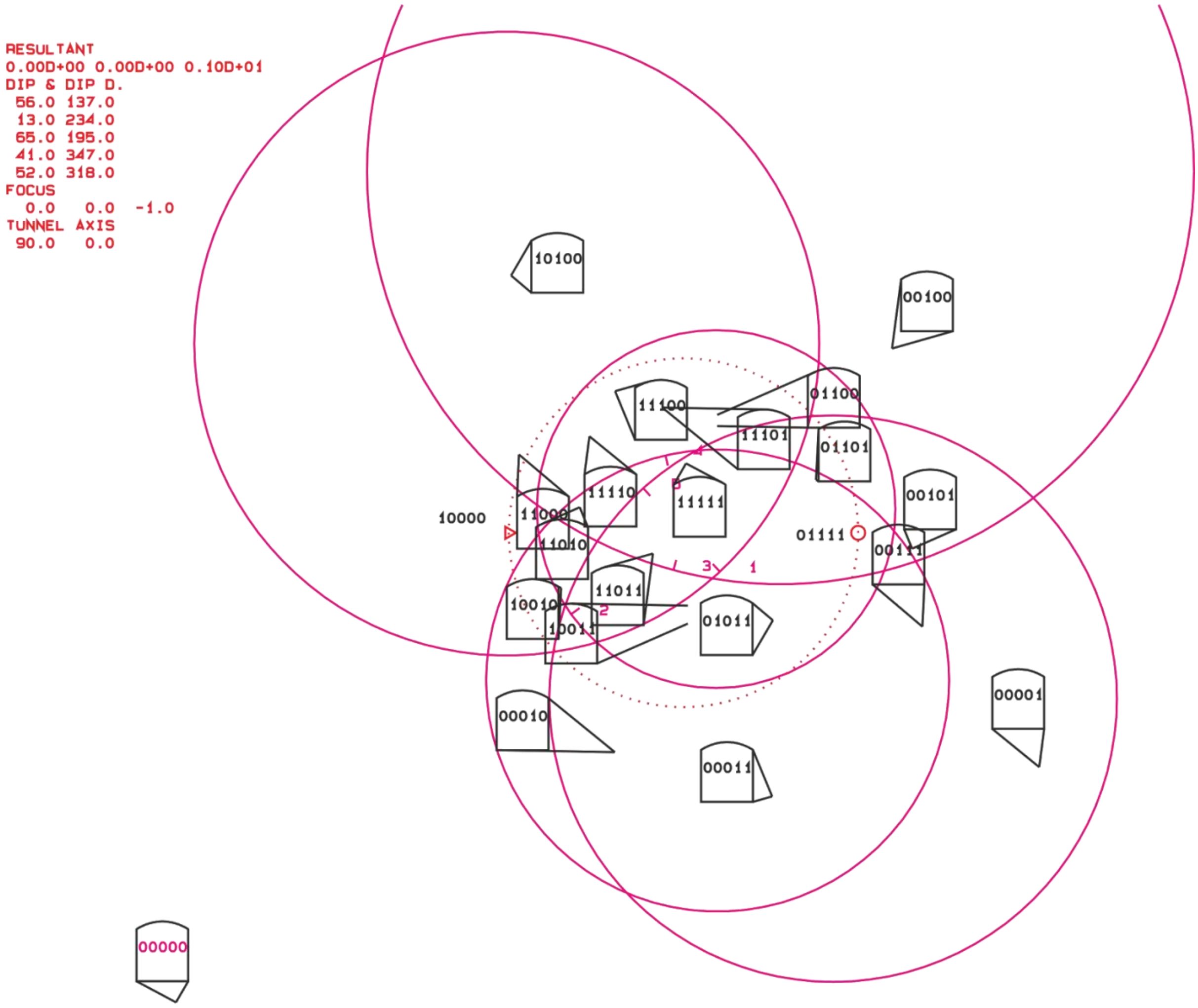

Figure 5.53: Block 5 with JP-Code 11100 on tunnel cross-section

5.3.3 Block 12

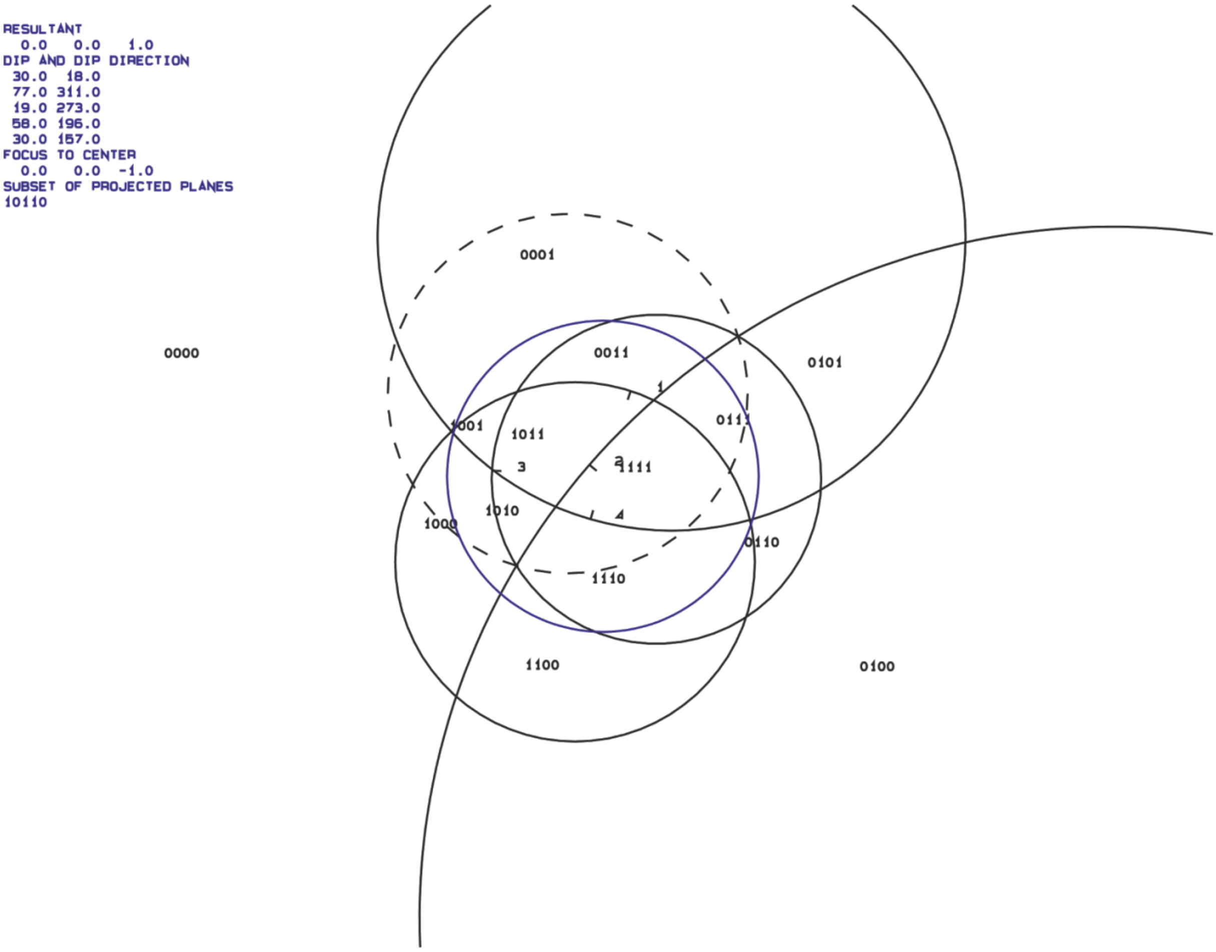

Figure 5.54: Block 12: great circles of discontinuities and free surface with JP-Codes: 1011

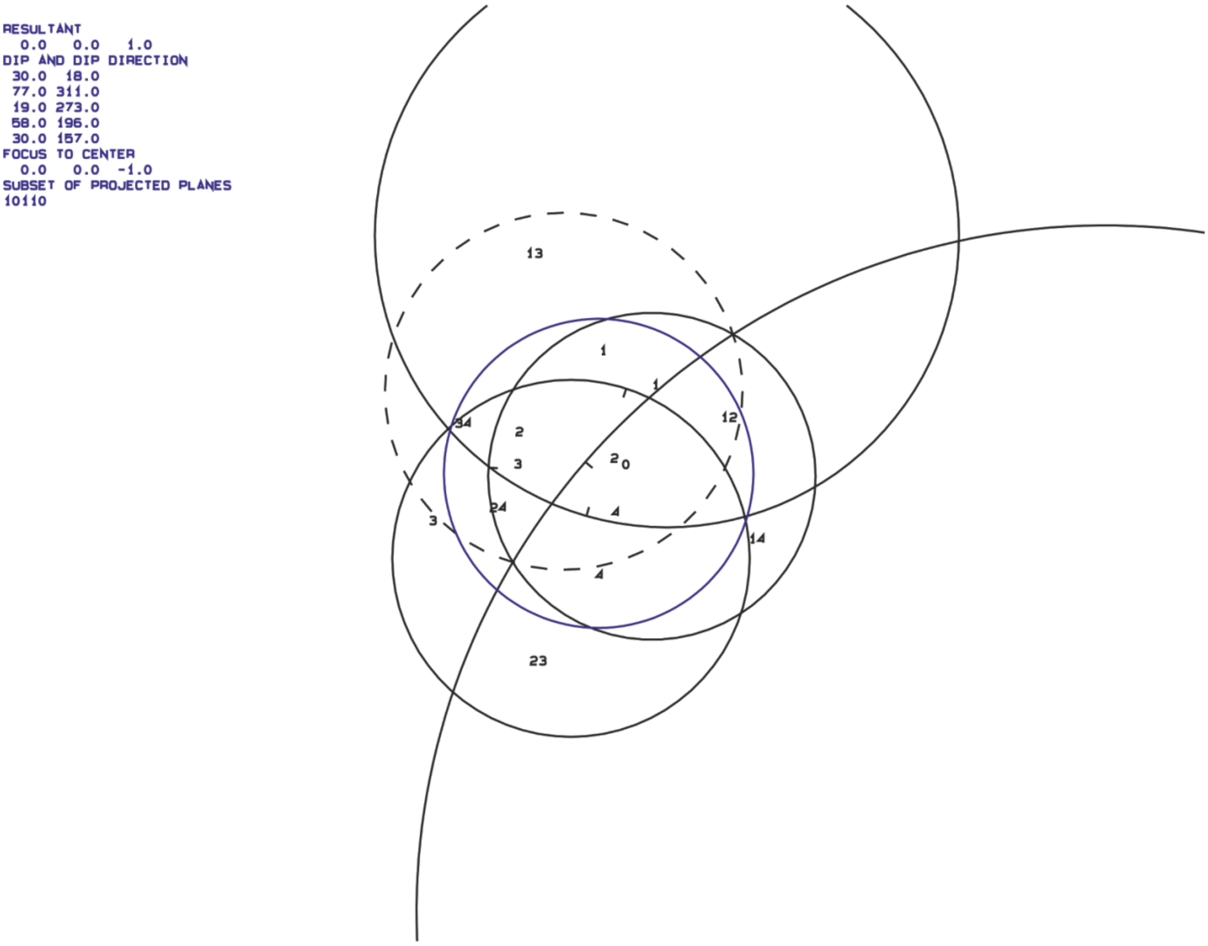

Figure 5.55: Block 12 with failure mode 2

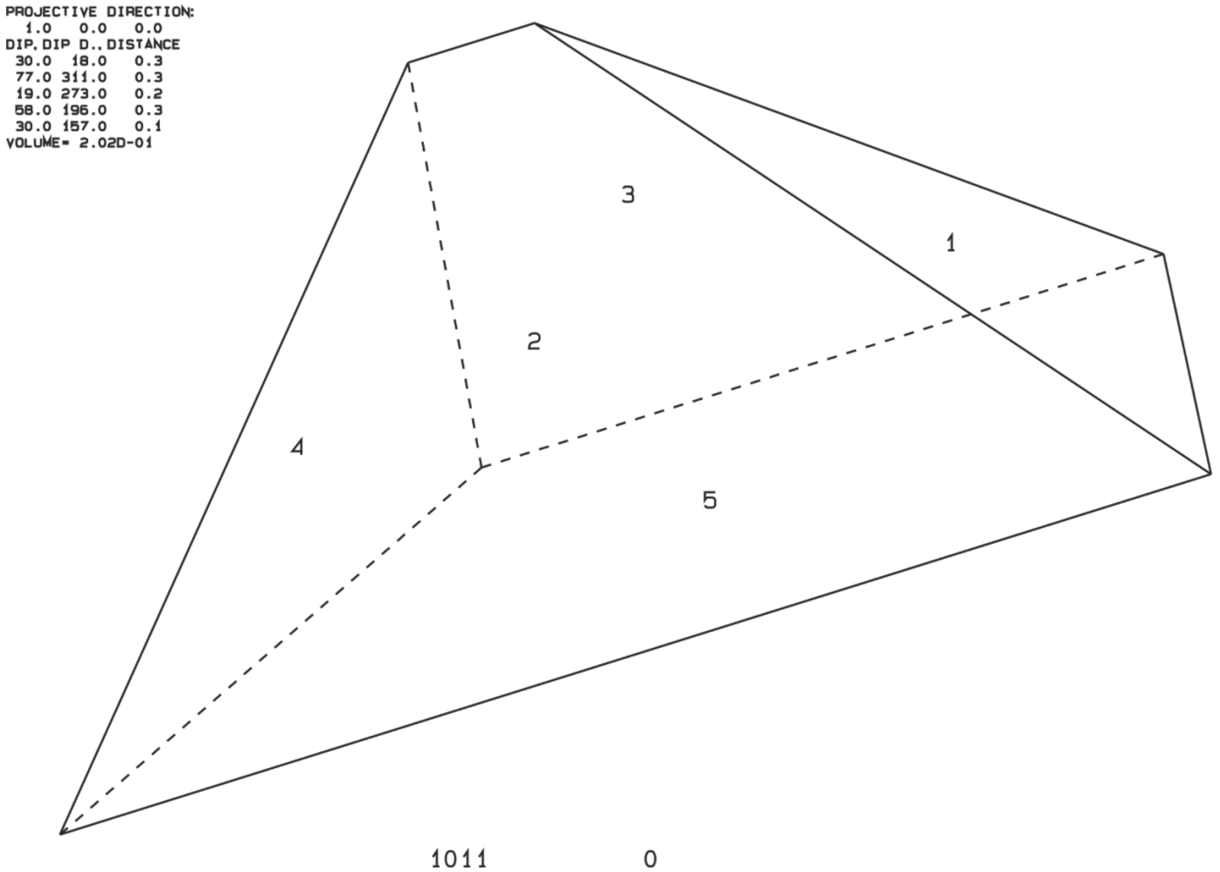

Figure 5.56: Block 12 form and volume 0.202m³

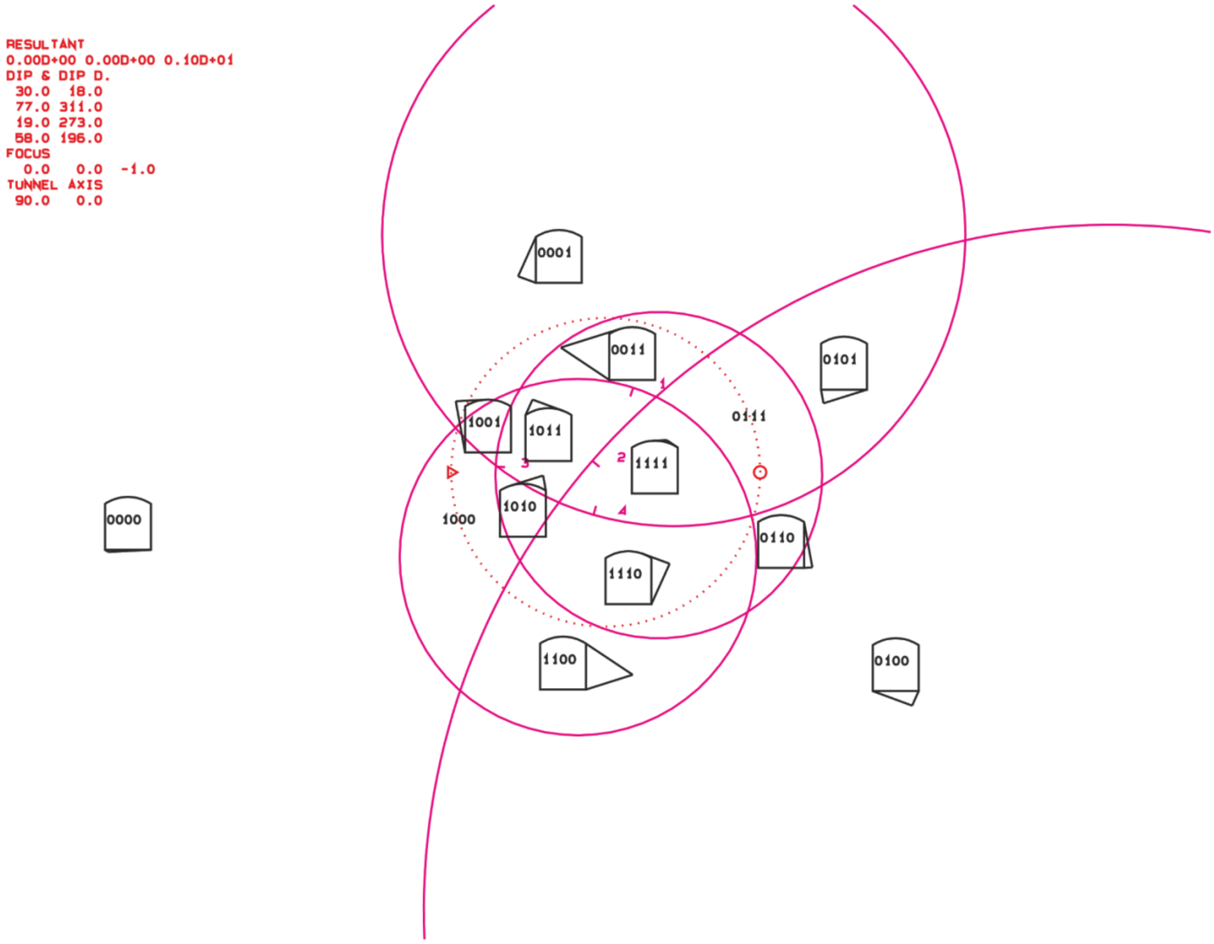

Figure 5.57: Block 12 with JP-Code 1011 on tunnel cross-section

5.3.4 Block 18

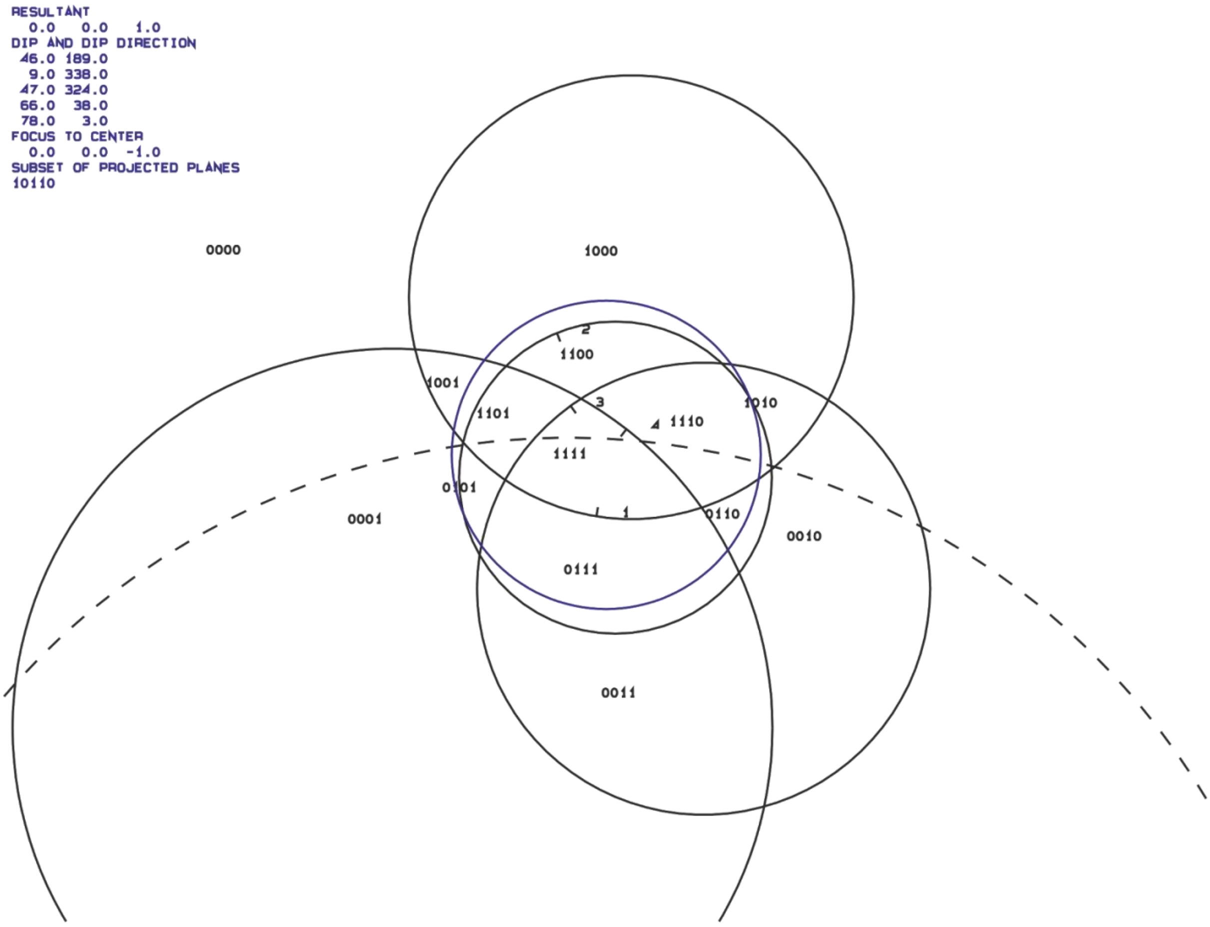

Figure 5.58: Block 18: great circles of discontinuities and free surface (dashed) with JP-Codes: 1011

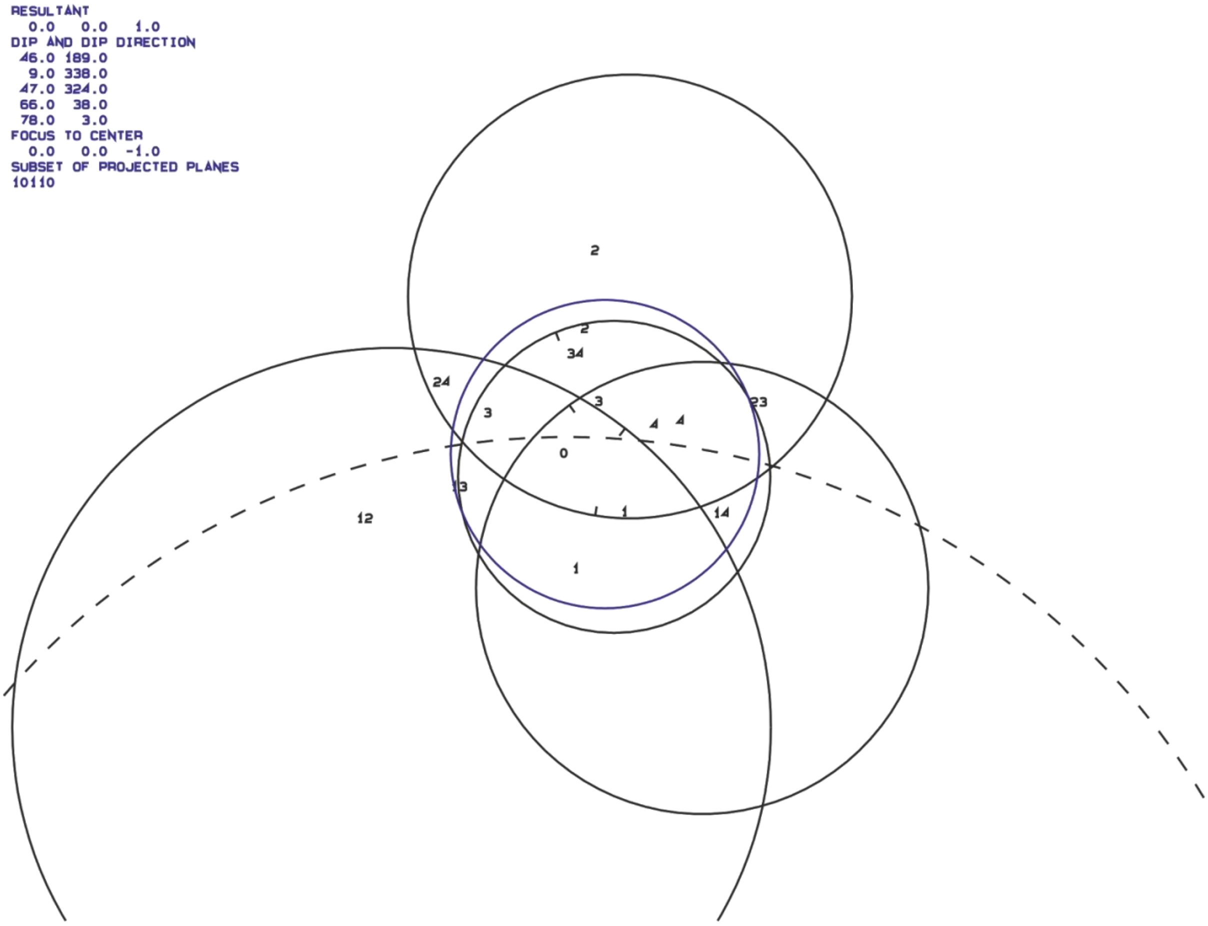

Figure 5.59: Block 18 with failure mode 24

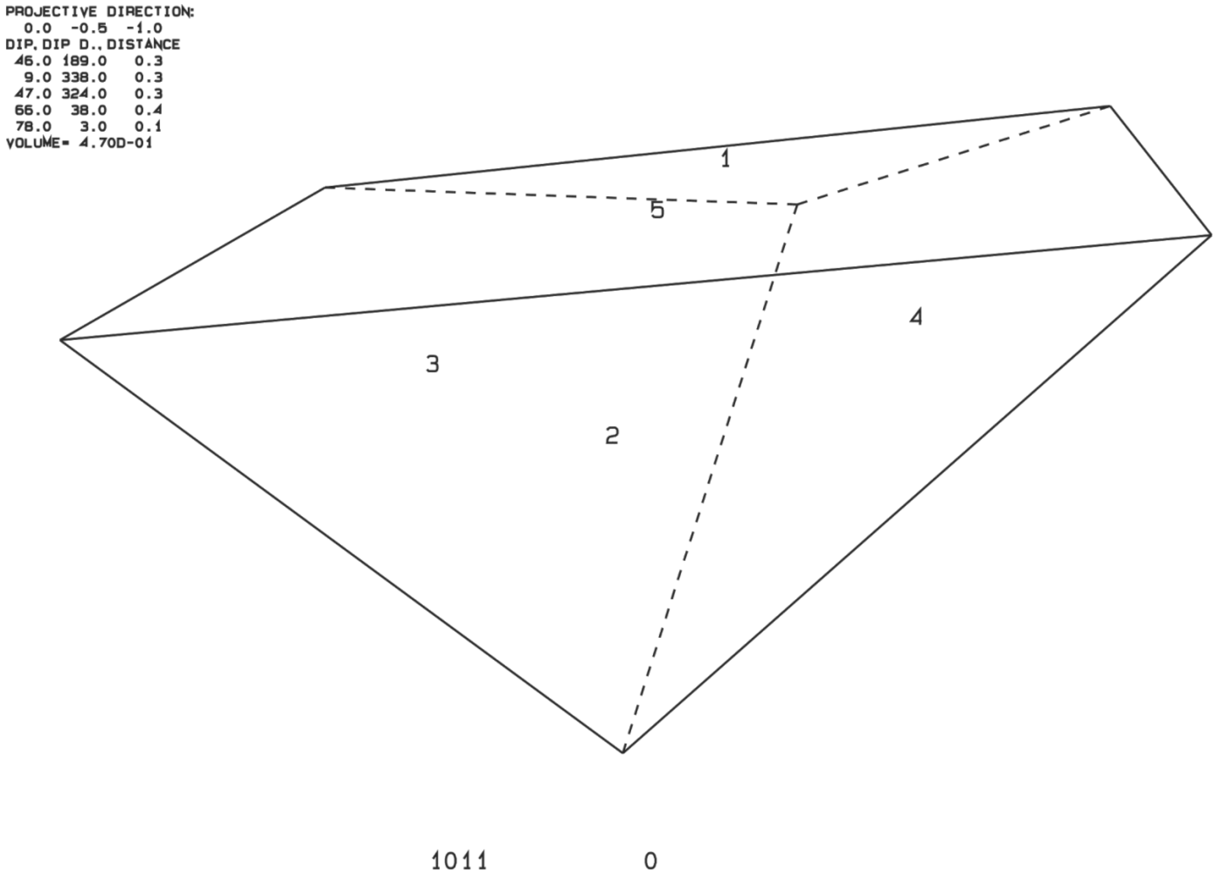

Figure 5.60: Block 18 form and volume 0.470m³

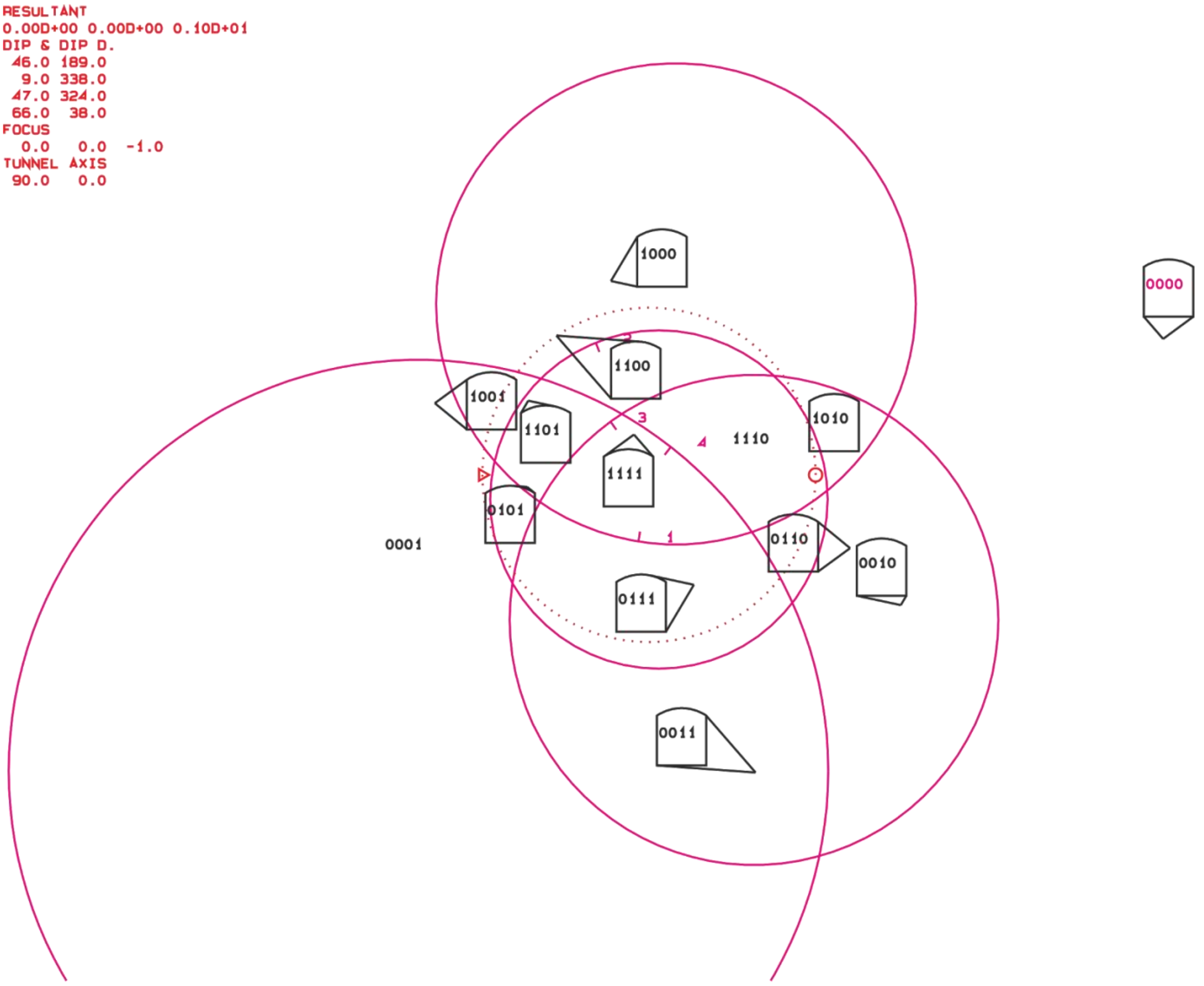

Figure 5.61: Block 18 with JP-Code 1011 on tunnel cross-section

5.3.5 Block 20

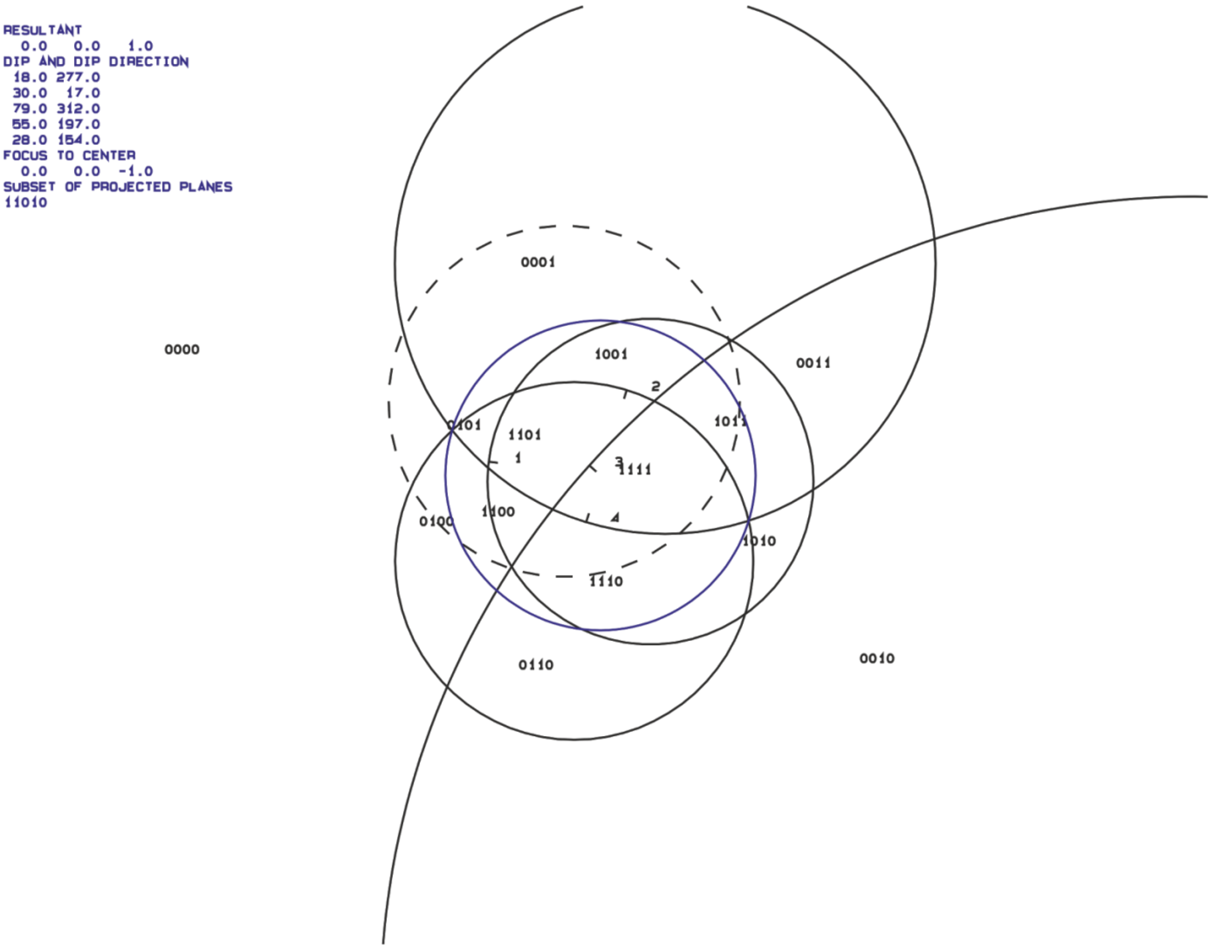

Figure 5.62: Block 20: great circles of discontinuities and free surface (dashed) with JP-Codes: 1101

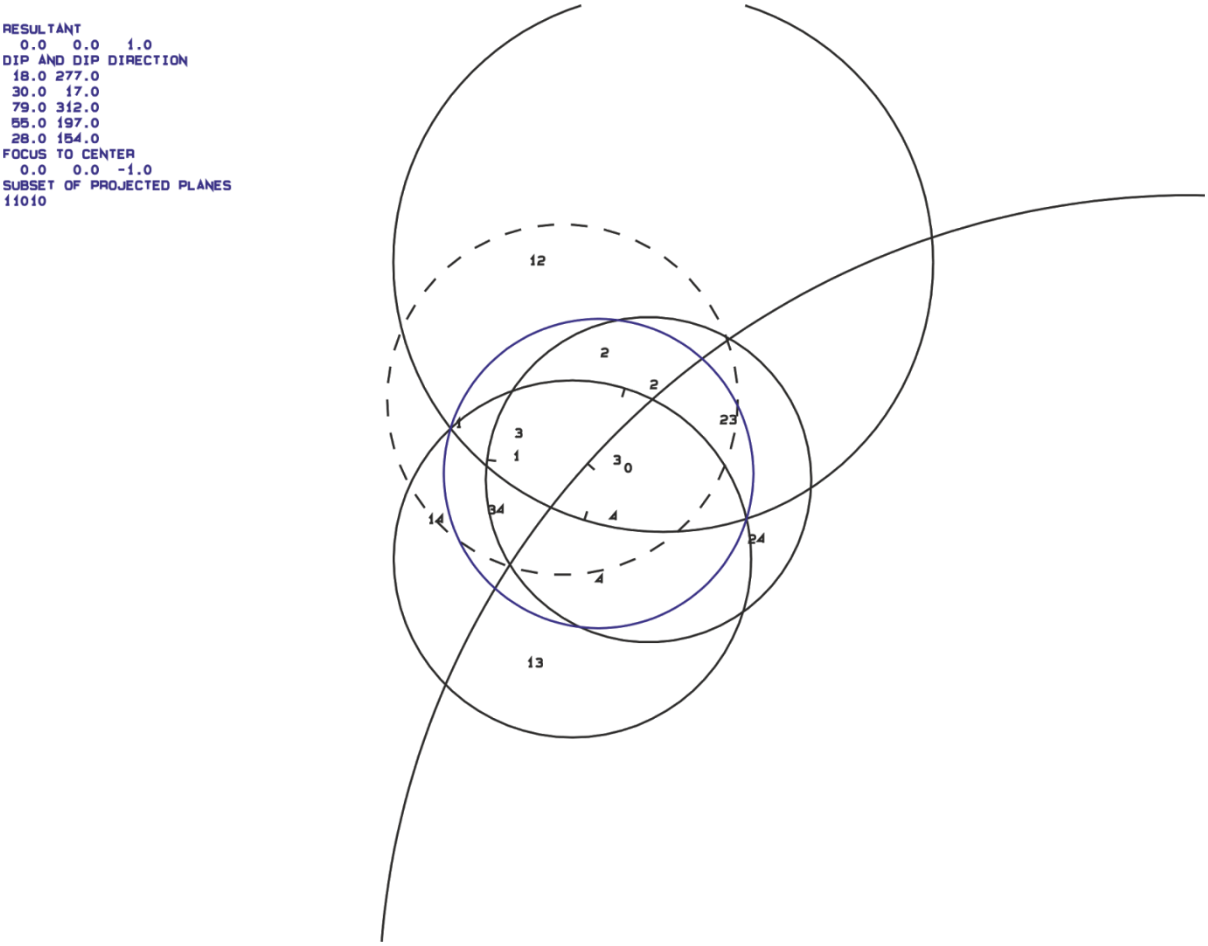

Figure 5.63: Block 20 with failure mode 3

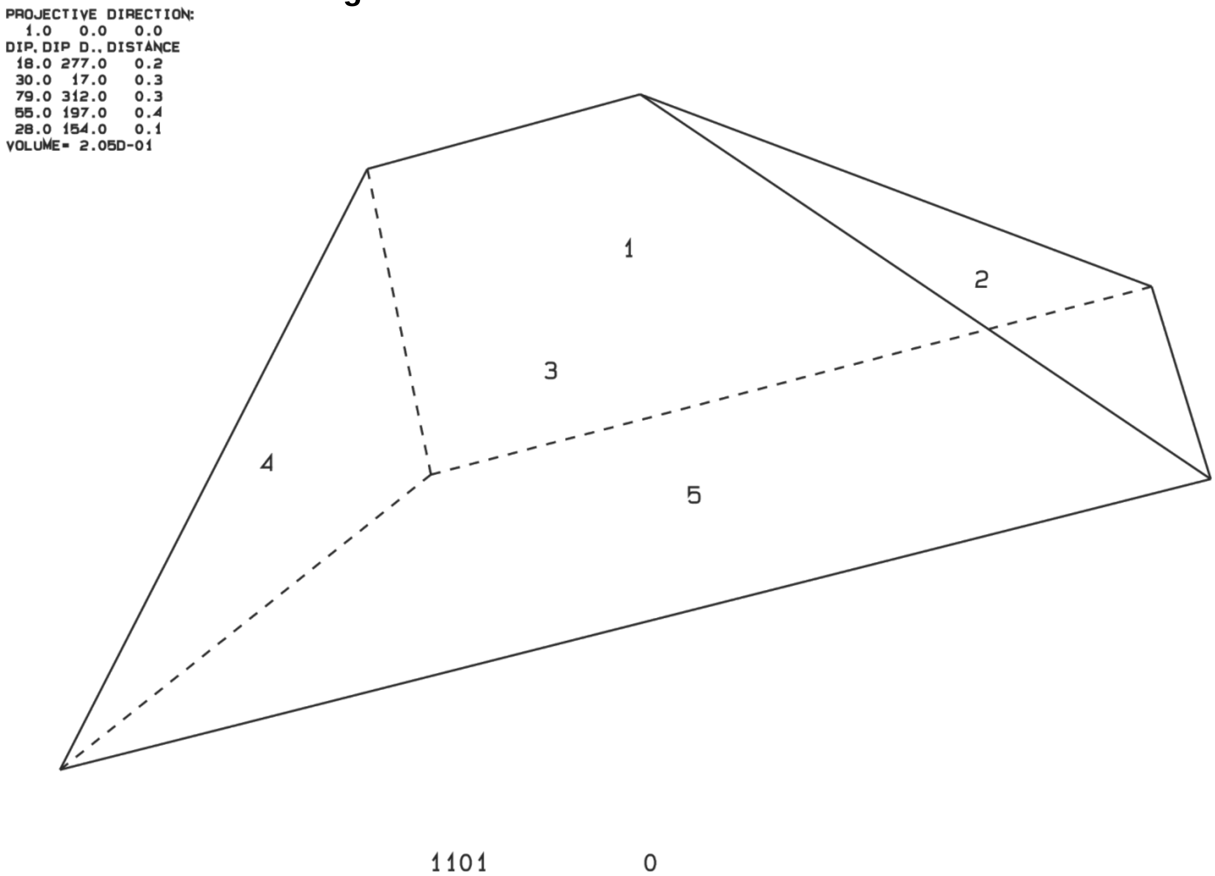

Figure 5.64: Block 20 form and volume 0.205m³

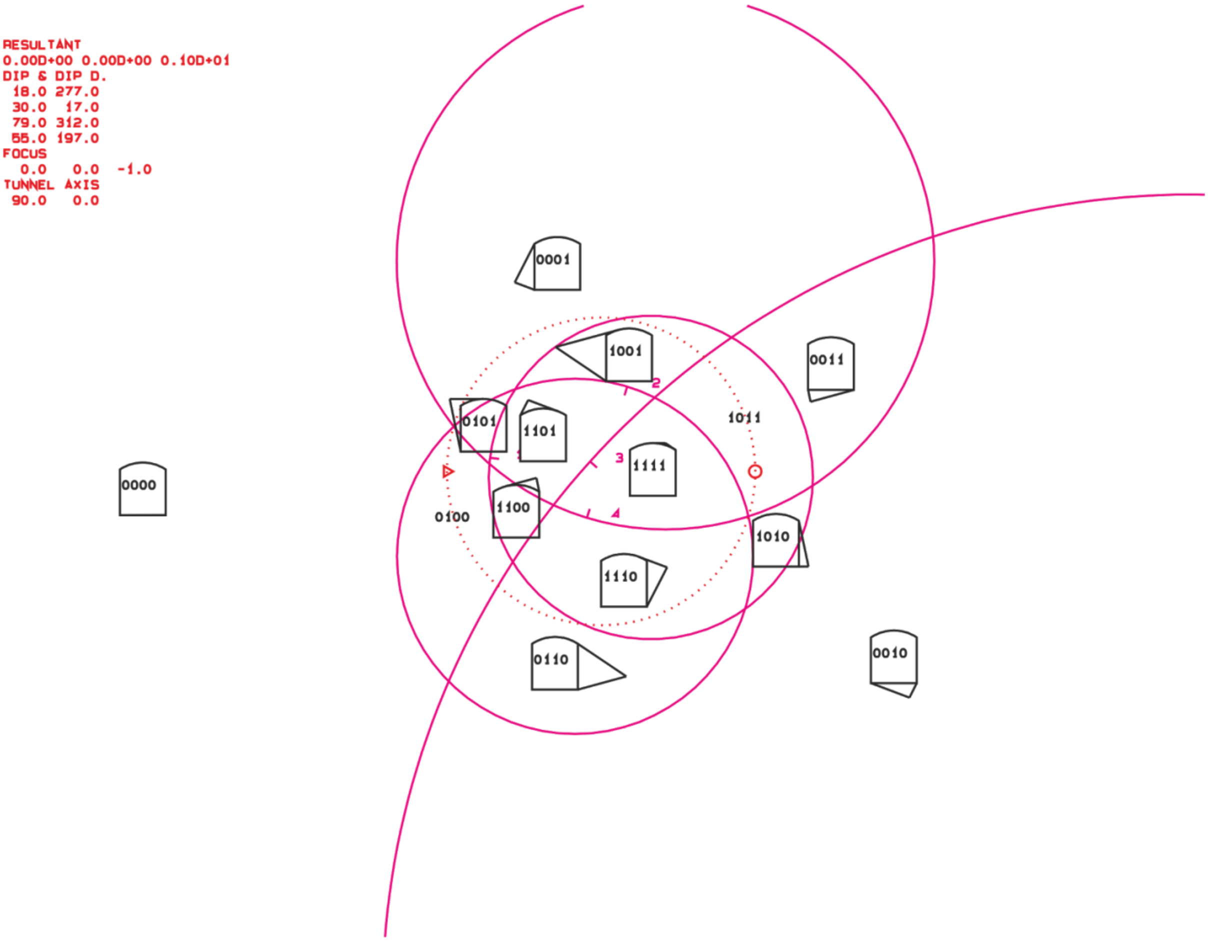

Figure 5.65: Block 20 with JP-Code 1101 on tunnel cross-section

5.3.6 Block 31

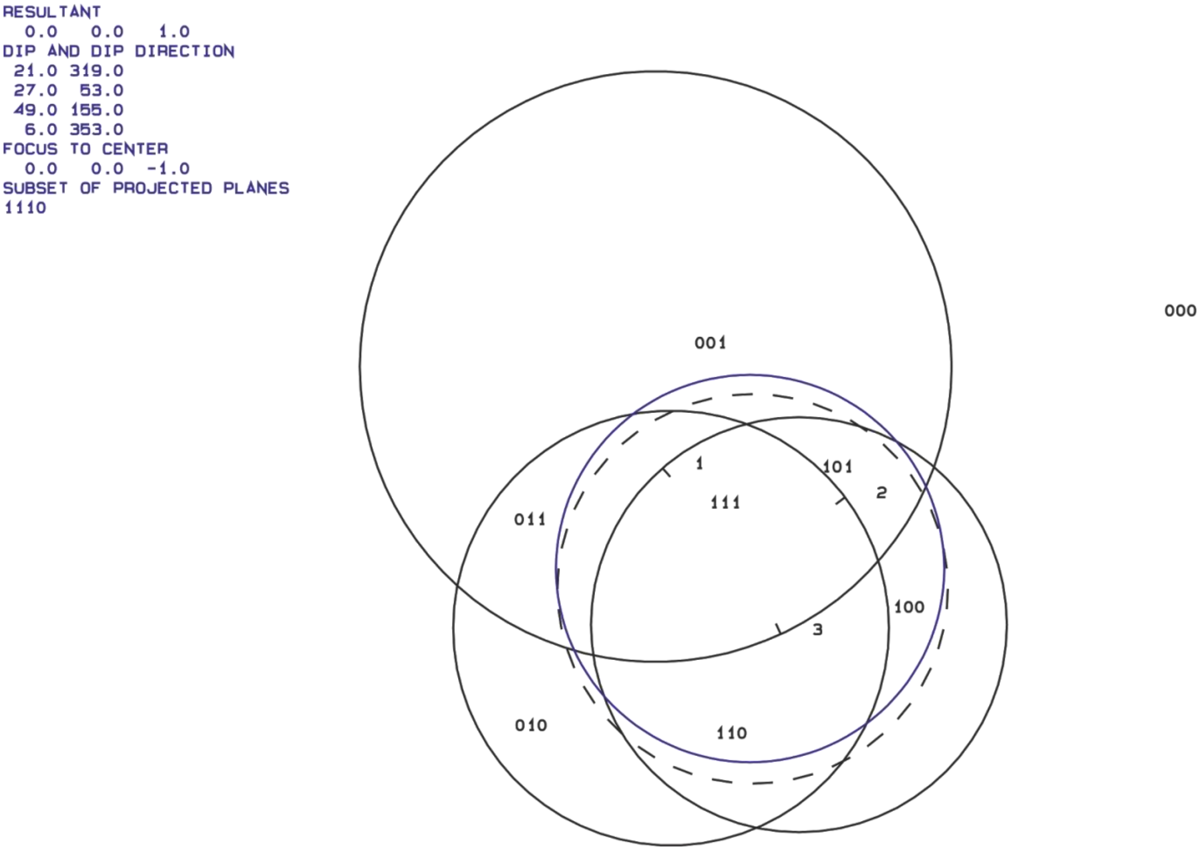

Figure 5.66: Block 31: great circles of discontinuities and free surface (dashed) with JP-Codes: 111

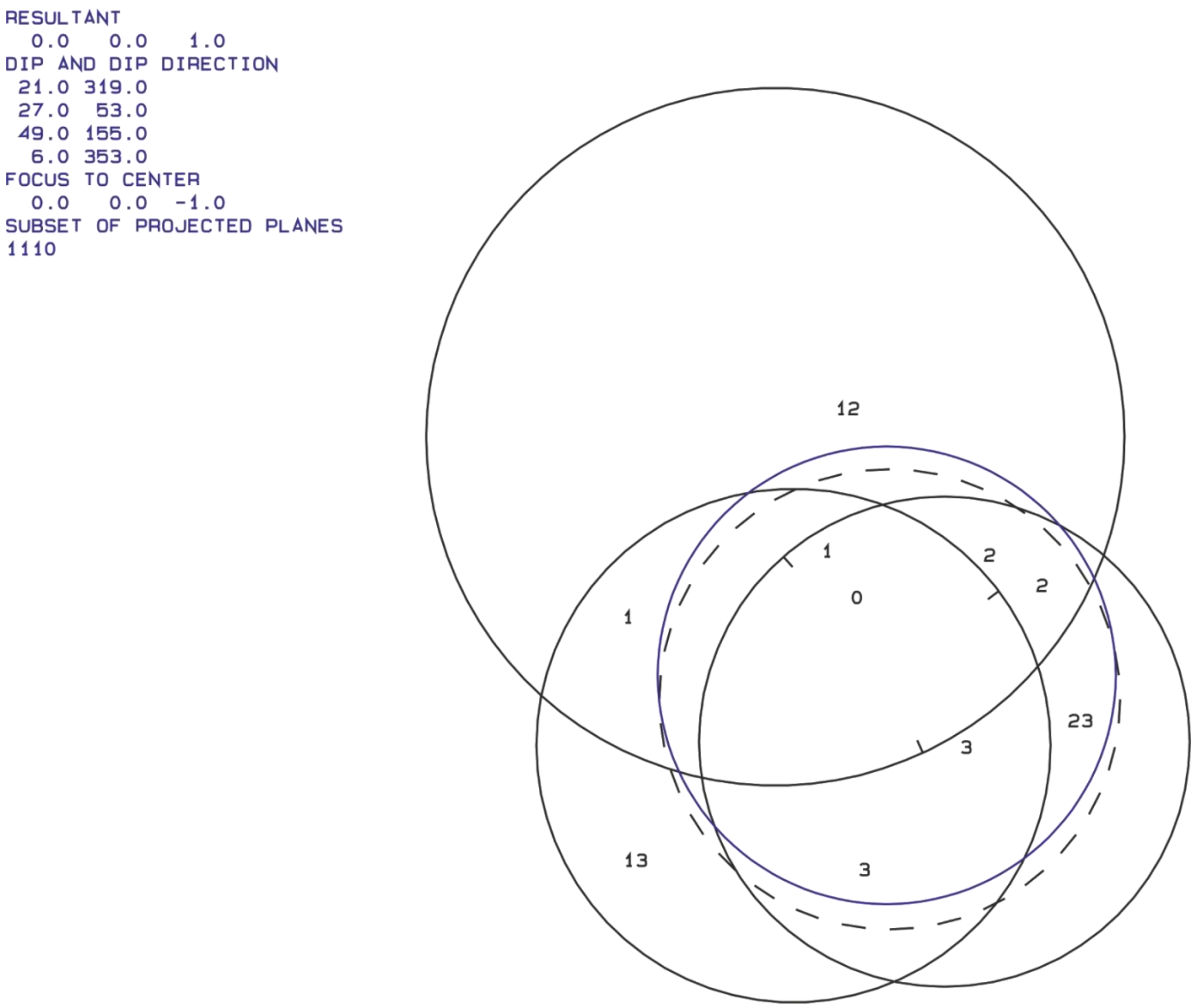

Figure 5.67: Block 31 with failure mode 0

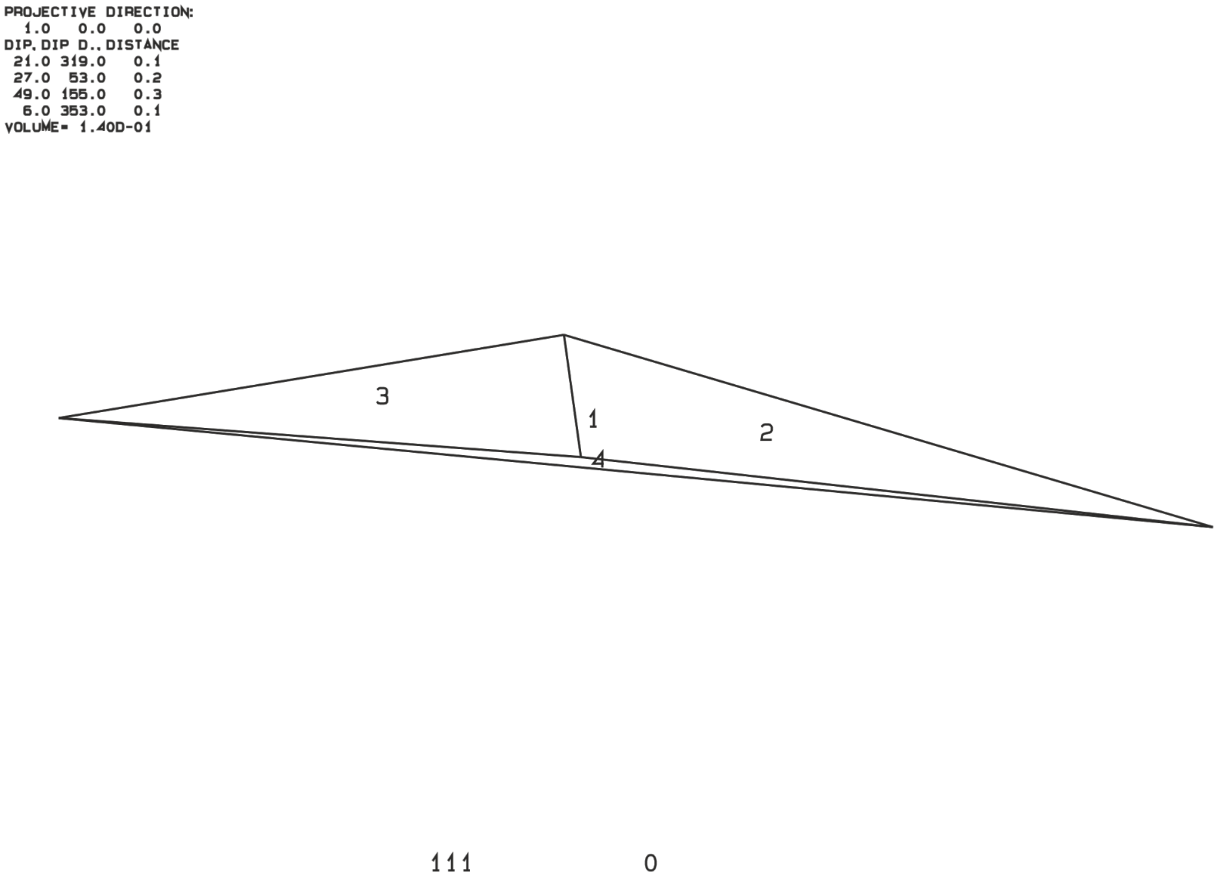

Figure 5.68: Block 31 form and volume 0.140m³

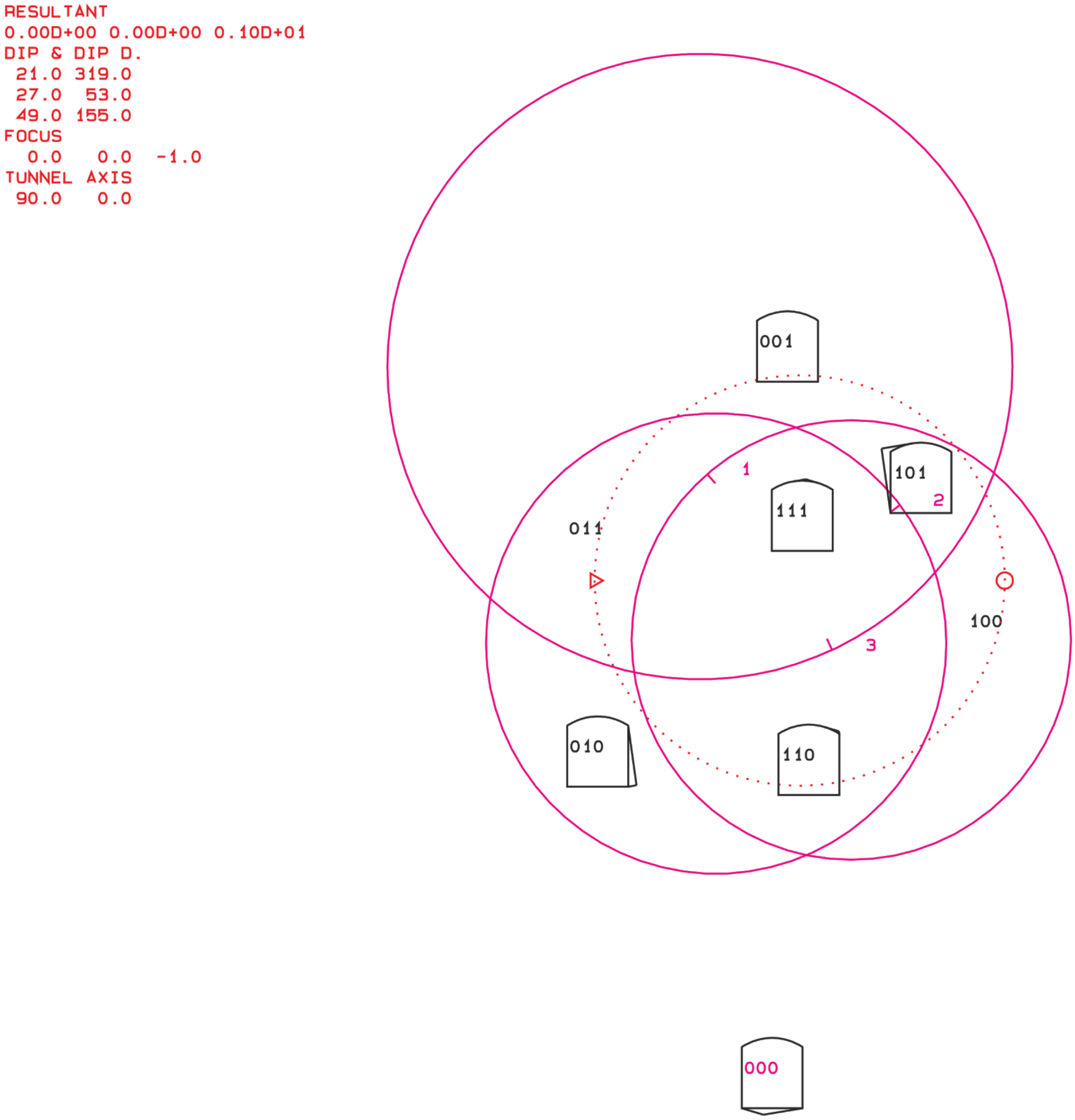

Figure 5.69: Block 31 with JP-Code 111 on tunnel cross-section

5.3.7 Block 68

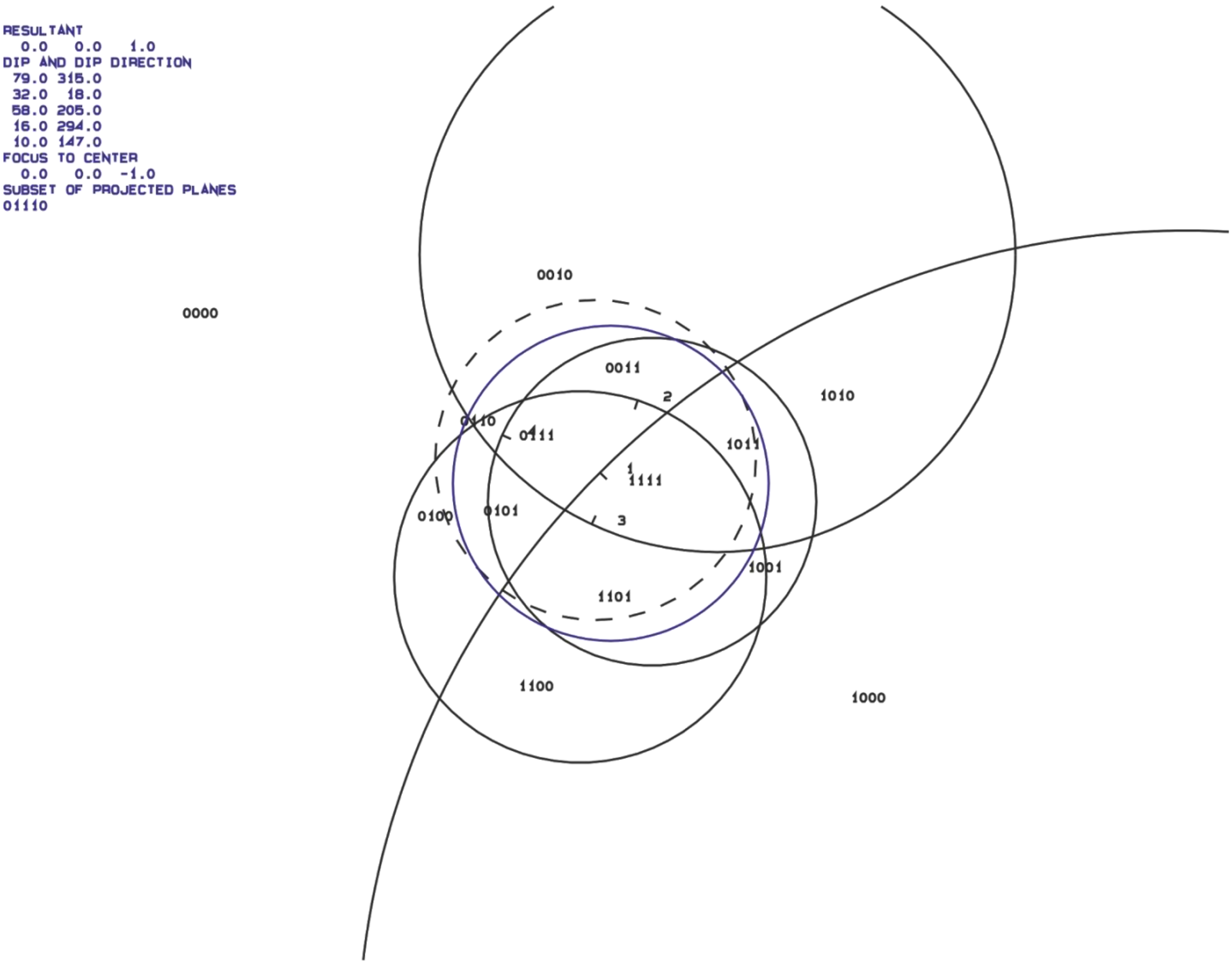

Figure 5.70: Block 68: great circles of discontinuities and free surface (dashed) with JP-Codes: 0111

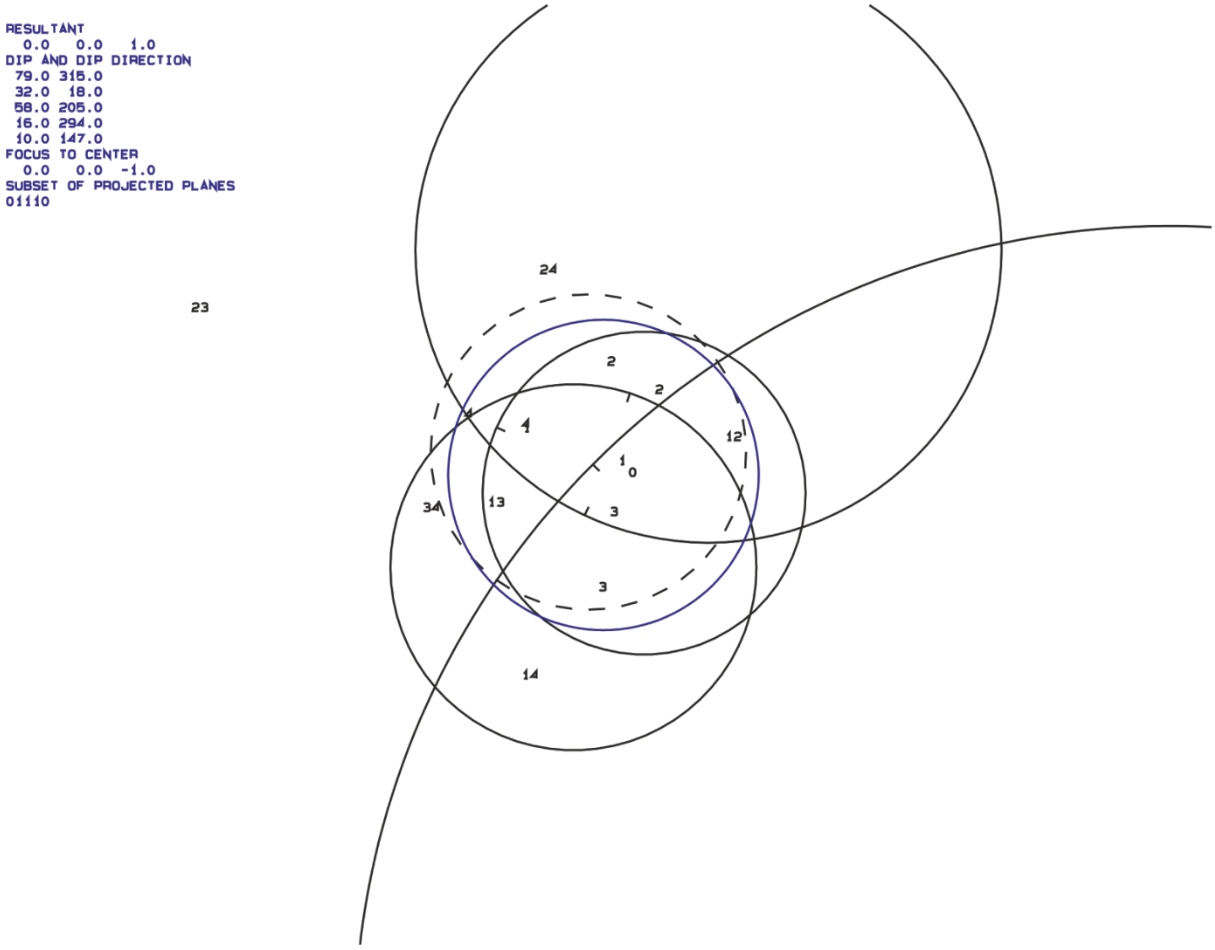

Figure 5.71: Block 68 with failure mode 1

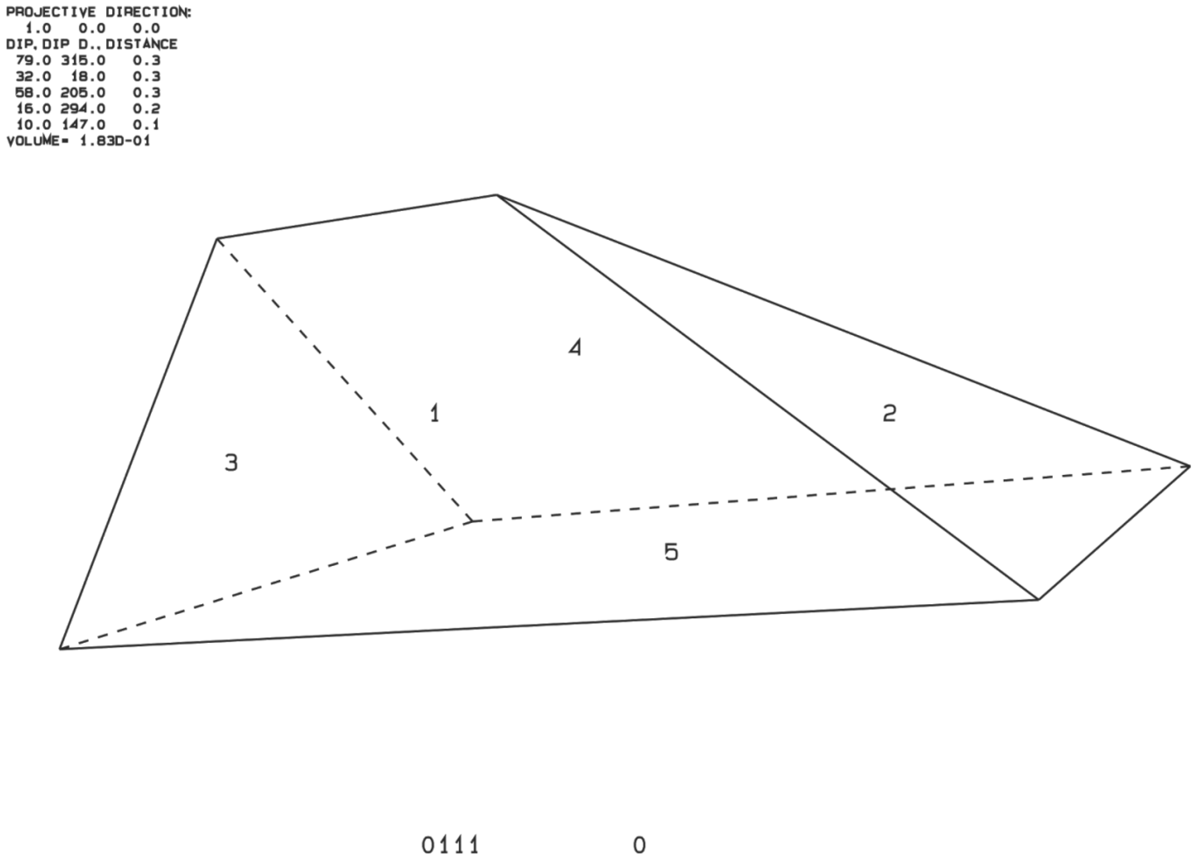

Figure 5.72: Block 64 form and volume 0.183m³

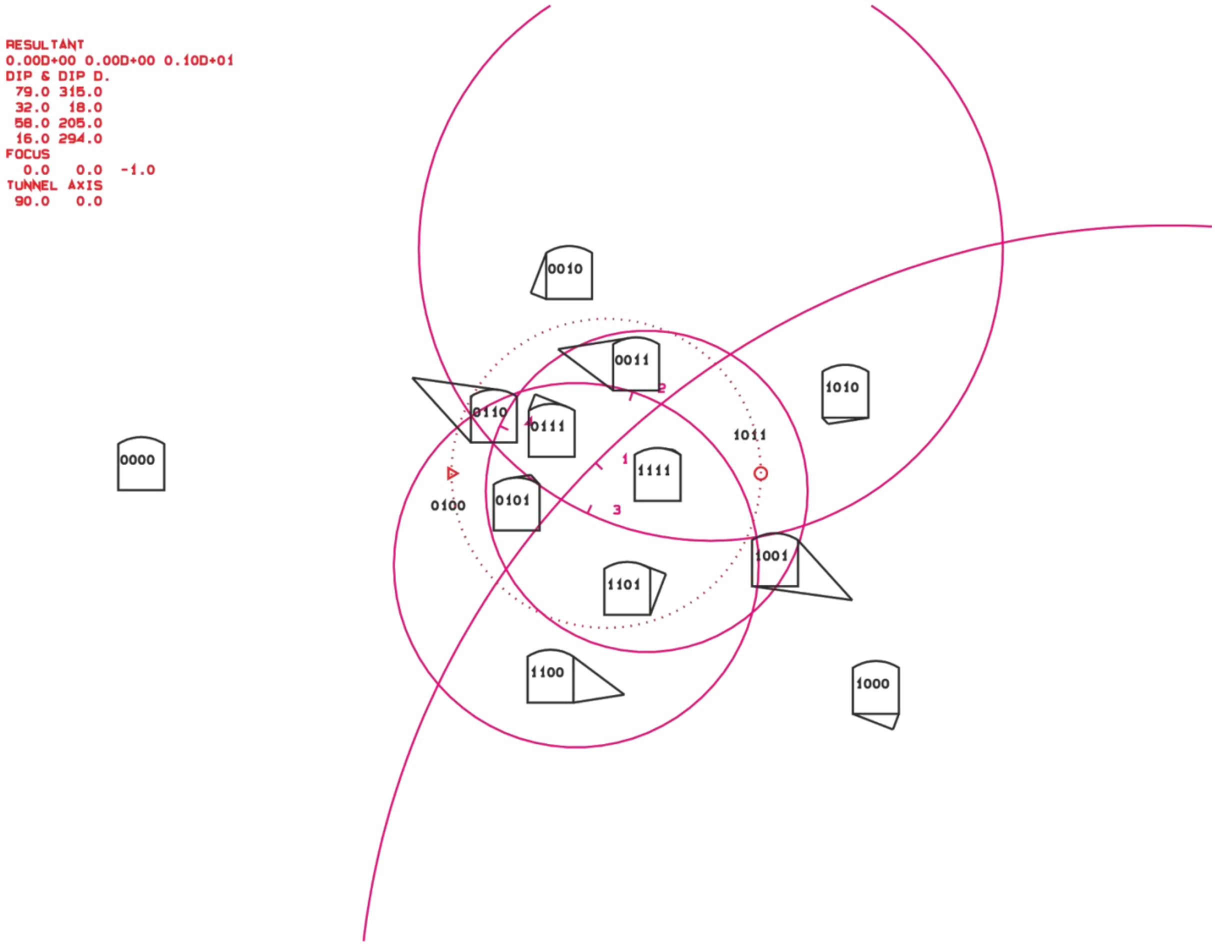

Figure 5.73: Block 68 with JP-Code 0111 on tunnel cross-section

5.3.8 Block 81

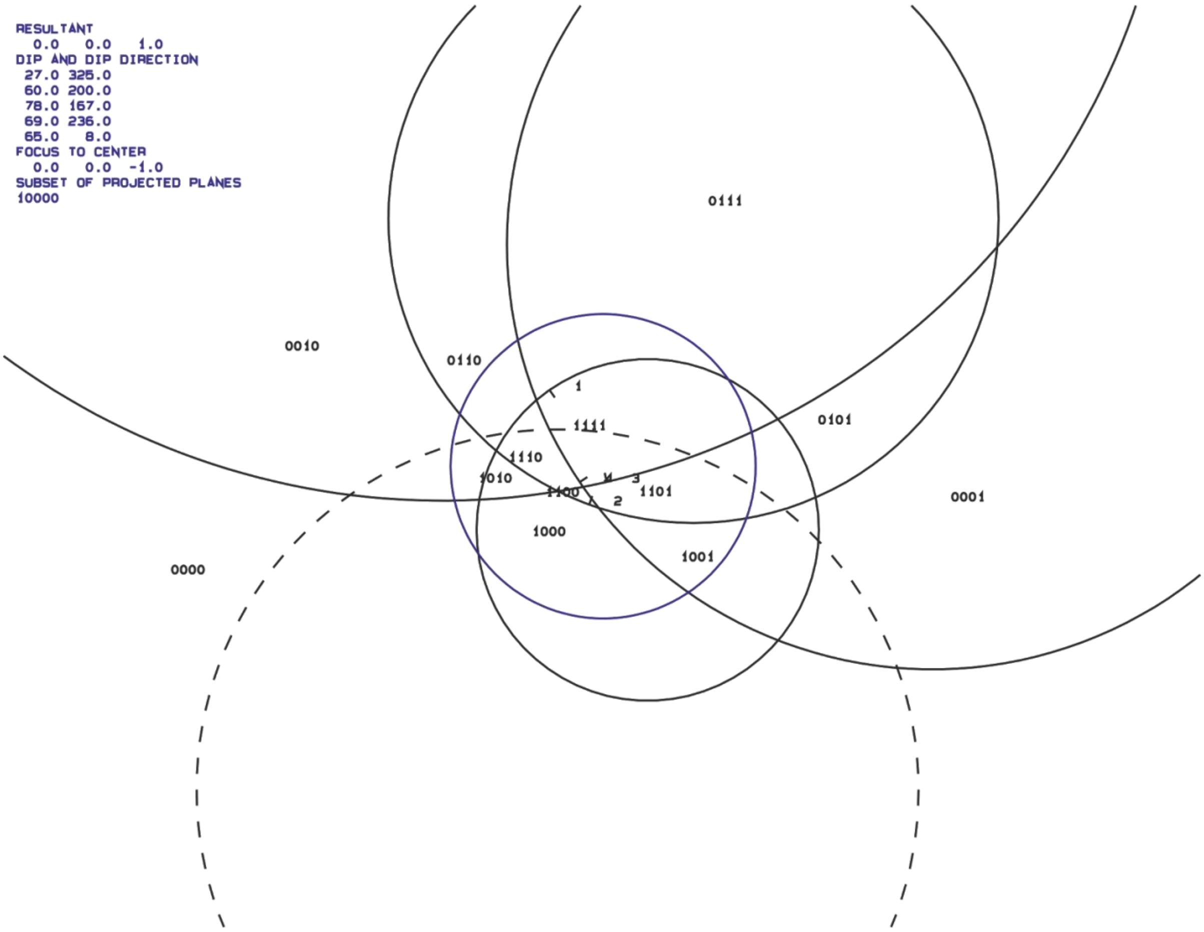

Figure 5.74: Block 81: great circles of discontinuities and free surface (dashed) with JP-Codes: 1000

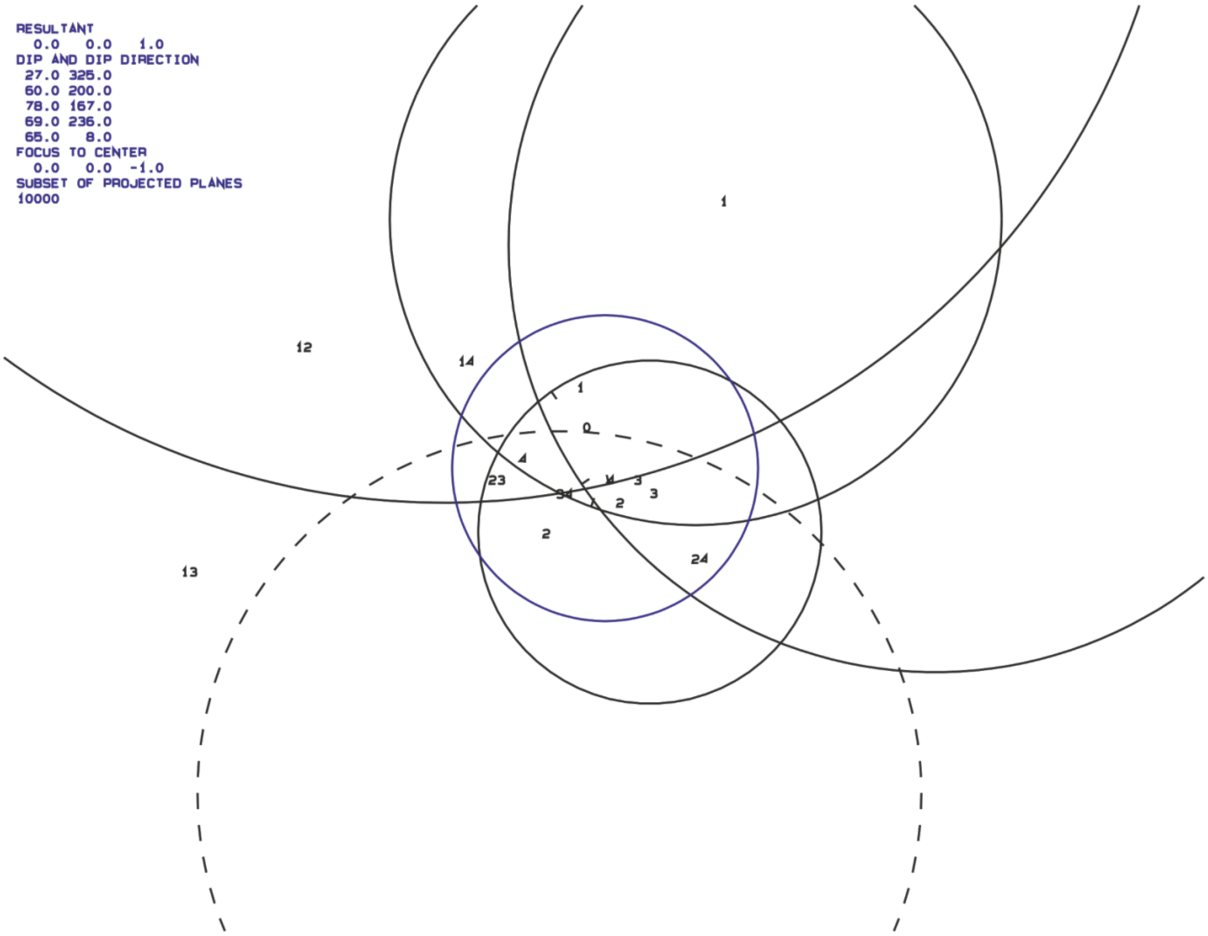

Figure 5.75: Block 81 with failure mode 2

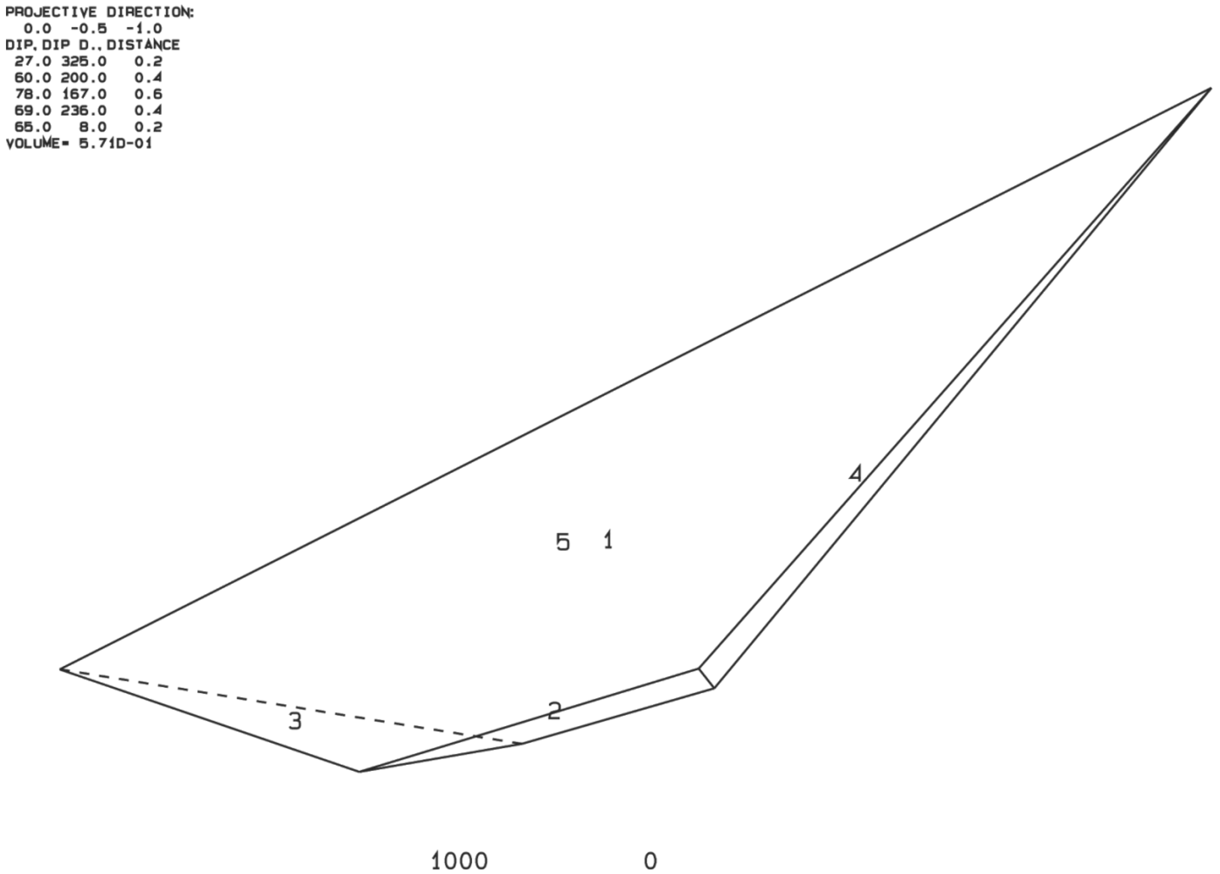

Figure 5.76: Block 81 form and volume 0.0.571m³

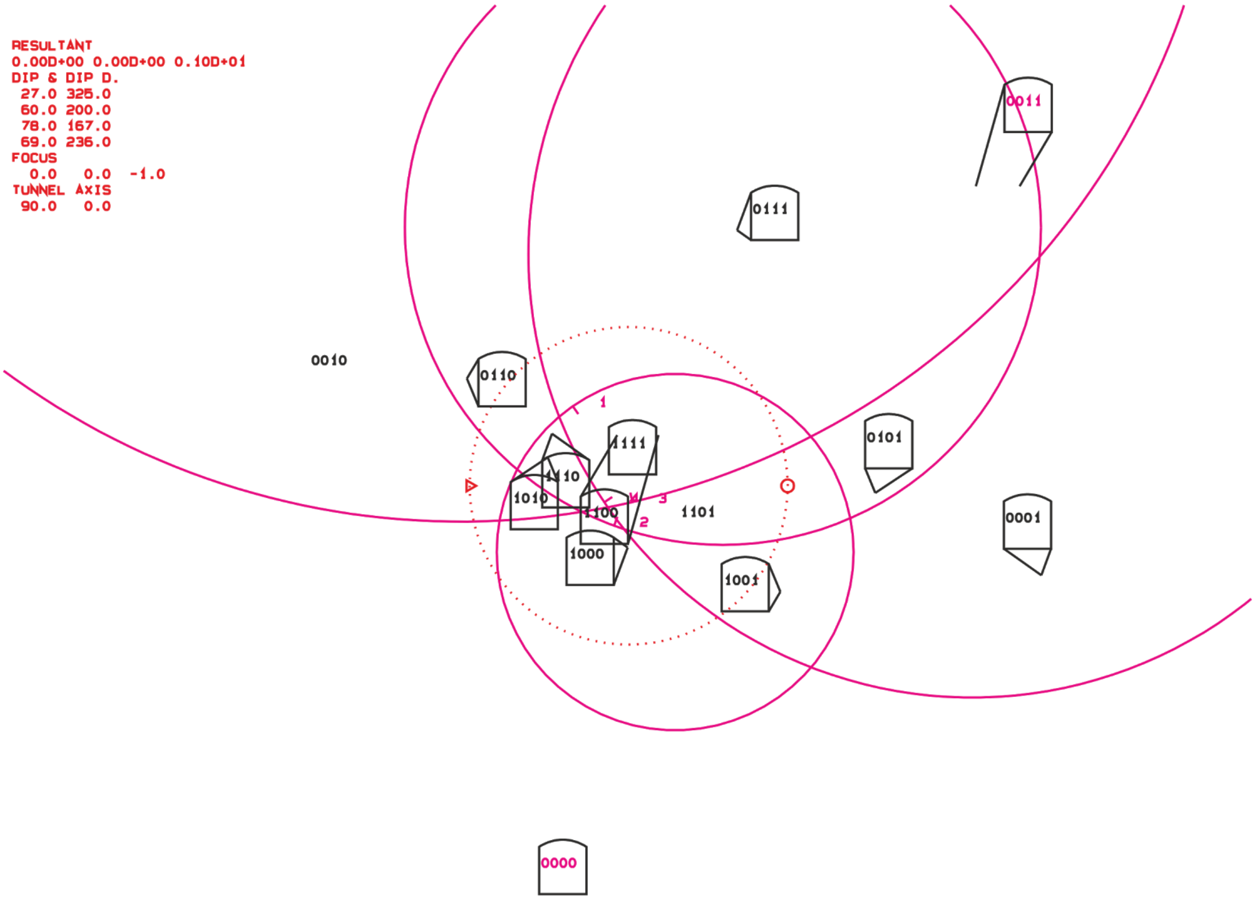

Figure 5.77: Block 81 on tunnel cross-section with JP-Code 1000

6 Conclusion

The following section summarises the outcome of this study.

6.1 Reproduction of In-situ Failed Blocks Using Block Theory

While reconstructing the in-situ failed blocks using Block Theory software several problems became apparent. Block Theory utilises several assumptions in order to simplify rock mass characteristics. By simplifying the fracture network by placing discontinuities of similar orientations into sets and assigning average spacing's to these sets by creating a scanline, Block Theory is able to identify potentially unstable Blocks and calculate their volumes. During this study it became apparent that by this simplification many of the in-situ failed blocks were identified as safe blocks according to Block Theory. Placing discontinuities into sets without considering termination or random fractures as well as simplifying the excavation surfaces without consideration of over- and under breaks, several previously failed block's Joint Pyramids no longer occurred entirely within their Excavation Pyramids. Furthermore, the use of average spacing's for sets resulted in block volumes that were different than the in-situ measured blocks by several orders of magnitude. Scanlines are able to calculate average normal spacing's of individual discontinuity sets, but a range should be considered in order to end up with a range of possible block volumes.

Inspection of smaller segments within the Raabstollen adit of the Arzberg identified the importance of separating a rock mass into several areas of similar geological structure. Bieniawksi's Rock Mass Rating is separated into individual units of homogeneous geological structure that change with the presence of a fault, a change in lithology or deformation. Block Theory should be applied similarly.

6.2 Largest Identified In-situ Blocks

Looking at the size-distribution of the 81 mapped in-situ failed blocks it was apparent that a small portion were significantly larger than the others. 8 of the 81 blocks (~10%) have volumes an order of magnitude larger than the remaining 73 blocks. Further inspection of these blocks showed that they were not constrained to a particular segment of the adit, nor the cross-section. Additionally, the blocks were not constrained by the number of discontinuity surfaces that they were made up of. Four of the largest blocks were tetrahedrons, three had 5 sides and one had 6 sides. A potential explanation for these blocks being larger than the others is the orientation at which the discontinuities occur relative to the orientation and shape of the excavation opening. The majority of these blocks contained two or more discontinuities which had strikes at acute angles to the tunnel excavation. These types of discontinuities outcropped with large surface areas and resulted in blocks with greater volume. This reiterates the effect the orientation of tunnel excavation has on block size.

6.3 The Future of Terrestrial LiDAR for Fracture Network Modelling

The use of terrestrial LiDAR is an invaluable tool for visualising the interaction between 3D outcrop geomorphology and fracture networks especially in dangerous and hard to reach areas. Although acquiring data can occur rapidly, the post-processing portion is often incredibly time consuming and perhaps not economical for excavation projects. Liu and Kieffer explain the need for robust algorithms to make post-processing more efficient and standardisation of these procedures (Kieffer & Liu, 2012). A certain amount of headway has been made towards the automation of identifying fracture networks. Liu and Kaufmann's HSV-coloured 3D rock structure is a method identifying discontinuities of similar orientation rapidly and being able to group them into sets (Liu & Kaufmann, 2015). Buckley et al. stressed error propagation throughout the workflow as a major issue with laser scanning which would be minimized through standardisation of steps involved (Buckley et al., 2008). Terrestrial LiDAR is the future of rapid rock mass characterisation and the identification of removable blocks in excavations and slopes.

References

Abbas, S.M. and Konietzky, H. (2016): Rock Mass Classification Systems.

Barton, N.R., Lien, R. and Lunde, J. (1974). Engineering classification of rock masses for the design of tunnel support. Rock Mech. 6(4), 189-239.

Bieniawski, Z.T. (1989): Engineering rock mass classifications. New York: Wiley.

Buckley, S.J., Howell, J.A., Enge, H.D. and Kurz, T.H. (2008): Terrestrial laser scanning in geology: data acquisition, processing and accuracy considerations. Journal of the Geological Society, London, Vol. 165, pp. 625 - 638.

Cai, M., Kaiser, P.K., Uno, H., Tasaka, Y. and Minami, M. (2004): Estimation of rock mass deformation modulus and strength of jointed hard rock masses using the GSI system. International Journal of Rock Mechanics & Mining Sciences 41, 3 - 19.

Deere, D.U. (1989): Rock quality designation (RQD) after 20 years. U.S. Army Corps Engrs Contract Report GL-89-1. Vicksburg, MS: Waterways Experimental Station.

Deere, D.U., Hendron, A.J., Patton, F.D. and Cording, E.J. (1967): Design of surface and near surface construction in rock. In Failure and breakage of rock, proc. 8th U.S. symp. rock mech., (ed. C. Fairhurst), 237-302. New York: Soc. Min. Engrs, Am. Inst. Min. Metall. Petrolm Engrs.

Ebner, F. & Hubmann, B. & Weber L. (2000): Die Rannach- und Schöckeldecke des Grazer Paläozoikums. - Mitteilungen der Gesellschaft der Geologie und Bergbaustudenten in Österreich, 44: 1-44, Wien.

Gasser, D., Stüwe, K. & Fritz, H. (2010): Internal structural geometry of the Paleozoic of Graz. International Journal of Earth Sciences, 99(5): 1067-1081, Berlin.

Goodman, R.E. (1989): Introduction to Rock Mechanics 2nd Edition. John Wiley and Sons.

Goodman, R.E. and Shi, G. (1985): Block Theory and its application to rock mechanics. Prentice- Hall International Series in Civil Engineering and Engineering Mechanics. 338p

Liu, Q. (2012): Modelling in Engineering Geology; Lecture Notes GEO.941; Technical University of Graz; Master curriculum.

Liu, Q. (2014): Rock Mass Characterization; Lecture Notes GEO.841; Technical University of Graz; Master curriculum.

Liu, Q. and Kaufmann, V. (2015): Integrated assessment of cliff rockfall hazards by mens of rock structure modelling applied to TLS data: New developments. In Eurock 2015 & 64th Geomechanics Colloquium. ÖGG.

Liu, Q. and Kieffer, D.S. (2012): Digital tunnel mapping using terrestrial LiDAR - a case study. In ISRM International Symposium, 28 - 30 May, 2012. Stockholm, Sweden.

Palmstrom A. (1995): RMi – a rock mass characterization system for rock engineering purposes. PhD thesis, University of Oslo, Department of Geology, 400 p.

Palmstrom, A. (1996): Characterizing rock masses by the RMi for Use in Practical Rock Engineering. Tunneling and Underground Space Technology, Vol. 11, No. 2, pp. 175 - 188.

Palmstrom, A. (2005): Measurements of and correlations between block size and rock quality designation (RQD). Tunnelling and Underground Space Technology 20, 362 - 377.

RiSCAN PRO (2005): version 1.2.0sp1. RIEGL LMS.

Weber, L. (2005): Die silberführende Blei-Zinkerzlagerstätte von Arzberg (Oststeiermark). Joannea Geologie und Paläontologie, 7: 9-23, Graz.